Investigation of the Optical and Electrical Properties of Plasma Polymerized Pyrrole-N,N,3,5 Tetramethylaniline Composite Thin Films

Mohammad Mostofa Kamal

Student : PhD Program
Roll: P04031404P
Session: April 2003

Department of Physics
Bangladesh University of Engineering and Technology (BUET)
December, 2010

Investigation of the Optical and Electrical Properties of Plasma Polymerized Pyrrole-N,N,3,5 Tetramethylaniline Composite Thin Films

A Dissertation submitted to the Department of Physics
Bangladesh University of Engineering and Technology
in partial fulfillment of the requirements for the degree of

Doctor of Philosophy
in
Physics

Mohammad Mostofa Kamal

Student : PhD Program
Roll: P04031404P
Session: April 2003

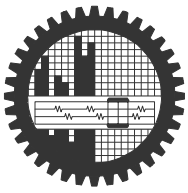

Department of Physics
Bangladesh University of Engineering and Technology (BUET)
December, 2010

Abstract

A capacitively coupled parallel plate glow discharge reactor has been used to deposit plasma polymerized pyrrole (PPPy), plasma polymerized N,N,3,5 tetramethylaniline (PPTMA) and plasma polymerized pyrrole-N,N,3,5 tetramethylaniline (PPPy-PPTMA) bilayer composite thin films on to glass substrates at room temperature. To deposit single-layer PPPy and PPTMA thin films, the deposition parameters such as flow-rate, power, vacuum order, etc. were kept almost same for all samples, but deposition time was varied to grow thin films with different thicknesses, so that the comparison of the results could be made for various plasma polymerized thin films. On the other hand, to deposit the bilayer composite films, pyrrole-monomer has been used as the parent-material and N,N,3,5 tetramethylaniline monomer has been deposited in different deposition time ratios after the pyrrole films were formed. The structural analyses by Fourier transform infrared (FTIR) spectroscopy have indicated that the monomer has undergone re-organization and the ring structure is retained during the plasma polymerization of PPPy and PPTMA thin films, and the bilayer composite thin films contain the characteristics of both of its components. From DTA and TGA traces it is observed that the weight loss in PPPy-PPTMA bilayer composite thin films is much higher than those of its component thin films even at relatively lower temperature. This behavior suggests PPPy-PPTMA bilayer composite thin films are less thermally stable and less breakdown thermal energy is needed for bilayer structure to dissociate the bonds than those of its components. From the UV-Visible absorption spectra, it is observed that both the allowed direct transition (E_{qd}) and allowed indirect transition (E_{qi}) energy gaps are decreased with the decrease of the thickness for all types of thin films, which is an indication of decreasing the resistivity and increasing the conductivity of the thin film of lower thicknesses. Moreover, it is also observed that the energy gaps of the PPPy-PPTMA bilayer composite thin films are higher compared to those of the PPPy and PPTMA thin films which indicates a higher electrical resistivity of the bilayer thin films than those of its component films. The change in the resistivity suggests a probable change in physical properties during the formation of the plasma polymerized thin films and the result is interpreted in terms of oxidation, inhomogeneties and irregularities in the complex polymer-polymer interface of the bilayer composite structure. In the study of the direct current conduction mechanism in PPPy-PPTMA bilayer composite thin films of different composition and different thicknesses the current density – voltage (J-V) characteristics indicate an increase in conductivity of

bilayer thin films as the proportion of PPTMA is increased in the films. It is also observed that the conductivity of the bilayer composite thin film is reduced compared to its component thin films. This result is consistent with the previous result that the higher values of the optical band gaps were observed for bilayer composite thin films as compared to its component thin films. It is seen that in the low voltage region, the current conduction obeys Ohm's law while the charge transport phenomenon appears to be the space charge limited in the higher voltage regions. The free charge carrier density, the mobility and the trap density has been calculated from the J-V characteristics and it is found that the SCLC is trap-mediated. From the study of ac electrical properties the variation of the dielectric constant ε' and dielectric loss factor ε'' with the frequency shows electrical relaxation properties which is related with multi-component contribution of polarizability of the polar materials; e.g. interfacial or space charge polarization, orientational polarization of molecular chain, α-relaxation process, etc. The ac conductivity, σ_{ac} , is observed to be increased with the frequency which is attributed to the relaxations caused by the motion of electrons or atoms, which could involve hopping between equilibrium sites; and it is therefore concluded that, the ac conduction mechanism is due to the hopping of carriers.

Table of Contents

List of Figures

Chapter 1

None

Chapter 2

Chapter 3

Chapter 4

Chapter 5

Chapter 6

Chapter 7

List of Tables

Chapter 1

None

Chapter 2

Chapter 3

None

Chapter 4

Chapter 5

Chapter 6

Chapter 7

None

Nomenclature

A	Area
ABS	Absorbance
AC/ac	Alternating Current
Al	Aluminum
B	Tauc Parameter
CC	Capacitively Coupled
d	Sample Thickness
DC/dc	Direct Current
DTA	Differential Thermal Analysis
EA	Elemental Analysis
E_{qd}	Direct Transition Energy Gap
E_{qi}	Indirect Transition Energy Gap
f	Frequency
FTIR	Fourier Transform Infrared
h	Planck's Constant
I	Current
I	Intensity of Radiation
IR	Infrared
J	Current Density
k	Boltzmanan Constant
K	Extinction Coefficient
LB	Langmuir-Blodgett
MHz	Mega Hertz
MIM	Metal-Insulator-Metal
N	Free Charge Carriers' Density
N_t	Trap Density
PECVD	Plasma Enhanced Chemical Vapor Deposition
PF	Poole-Frenkel
PPTMA	Plasma Polymerized N,N,3,5 Tetramethylaniline
PPPy	Plasma Polymerized Pyrrole
PPPy-PPTMA	Plasma-Polymerized Pyrrole- N,N,3,5 Tetramethylaniline
PVD	Physical Vapour Deposition
rf	Radio Frequency

SCLC	Space Charge Limited Current
SEM	Scanning Electron Microscopy
T_g	Glass Transition Temperature
T_m	Melting Point
tanδ	Loss tangent
TGA	Thermogravimetric Analysis
TSDC	Thermally Stimulated Depolarization Current
UV-vis	Ultraviolet-Visible
V	Voltage
XPS	X-ray Photoelectric Spectroscopy
α	Absorption Coefficient
λ	Wavelength
λ_{max}	Peak Absorption Wavelength
ΔE	Activation Energy
σ_{ac}	AC Electrical Conductivity
ε'	Dielectric Constant
ε''	Dielectric Loss Factor
ε_o	Permittivity of Free Space
μ	Mobility of the Charge Carrier
ν	Frequency
σ_{ac}	ac Conductivity
σ_{dc}	dc Conductivity
θ	Trapping Factor

Candidate's Declaration

It is hereby declared that this thesis or any part of it has not submitted elsewhere for the award of any degree or diploma.

Mohammad Mostofa Kamal
Candidate

Dedicated To

Late Meherunnessa Ahmed, my mother
Late Muhammad Ahmadul Haq, my father
Late Kaniz Shireen Ahmed, my sister
Late Muhammad Enamul Haq, my brother

you left me alone in a painful world
sleep in peace
I'm still bearing your memory and dream.

Acknowledgements

First of all, I would like to express my deep sense of gratitude and profound respect to my research advisor Professor Dr. Md. Abu Hashan Bhuiyan, Department of Physics, Bangladesh University of Engineering and Technology (BUET), for his indispensable guidance, generous help, special care and constant encouragement throughout the long period of my research work. I would like to thank him from the deepest point of my heart for contributing to a very rewarding graduate research experience; knowing him has improved me as a researcher and as a person.

The opportunity to work in the Department of Physics, BUET, was really a unique experience that was rewarding personally, professionally and socially. I would also like to thank the members of the doctoral committee Professor Dr. Nazma Zaman, Professor Dr. Jiban Podder, Professor Dr. Md. Feroz Alam Khan, Professor Dr. A. K. M. Akther Hossain of Department of Physics, BUET and Professor Dr. Md. Tafazzal Hussain of Department of Physics, University of Dhaka for not only their valuable time but also for contributing to my technical knowledge and entrepreneurial spirit during the progress of my research work.

I am thankful to the Head and my teachers in the Department of Physics, BUET for their keen interest and encouragement during my research work. Thanks are also due to all the employees of the Department of Physics for their nice cooperation.

I would like to express my heartiest gratitude to the authority of the Independent University, Bangladesh (IUB) for permitting me to do Ph. D at BUET and for generous support to continue my research work. My special thanks go to the Vice Chancellor of IUB, Professor Bazlul Mobin Chowdhury and to the Director, School of Engineering and Computer Science, Professor Mohammed Anwer for their continous support and inspiration to complete the degree. Many thanks to my colleagues, specially to Mr. Farhad Alam, Ms. Rifat Ara Rouf, Mr. Subrata Kumar Dey, Mr. Noor Nabi and Mr. Nazmul Kabir for giving me valuable inspiration.

I am thankful to Dr. A. Gafur, Senior Engineer, PP & PDC, and the authority of the Bangladesh Council for Scientific and Industrial Research (BCSIR), Dhaka, for giving me the opportunity to do the IR, UV-visible, and DTA/TGA analyses.

Many thanks go to the thin films research group members of the Department of Physics, BUET, past and present, for their advice, help and cooperation. I must appreciate the opportunity to learn and work in such a highly interactive, cutting-edge research environment. The foundational research concepts and professional development opportunities afforded to the students in the research group are truly invaluable. Very special thanks to Mr. Sunirmal Majumder, my ‘dada’, for his immeasurable support and continuous encouragement to finish the experimental work. Mr. Rama Bijoy Sarker, Ms. Hasina Akhter, Mr. Masud Reza, Ms. Rummana Matin, Ms. Tamanna Afroze, Mr. Md. Jellur Rahman, Mr. Md. Ali Ashraf – thank you very much for making everyday unique and interesting along my research journey

I would like to thank my family and friends for their unconditional and unwavering support, interest and understanding throughout the years of my work and studies. I would like to express my indebtedness to my wife Sharmeen Akhter Jharna for keeping me free from almost all the family affairs during the work. Special thanks for my mother, sisters and brothers; my mother-in-law and father-in-law and in laws family. Finally, a heartfelt thanks is also dedicated to my friends Mr. G M Anowar and Mr. Golam Mohiuddin who took an interest in my work, you have no idea how personally rewarding it was to discuss my ideas and work with you. Last but not the least, I must thank to Shattik, my loving son, the little angel. He has grown up without getting enough time from his father but without making any complain about it. Thanks baba, thanks a lot my little angel, I wish your prosperous and successful life.

Chapter 1

Introduction

This introductory chapter reviews the earlier research works on different properties of plasma polymerized thin films and discusses the objectives of the thesis and the thesis layout.

1.1 Introduction

Plasma polymerization is an important technique to fabricate thin polymer films from a variety of organic and organometallic starting materials. Thin films that are deposited by using plasma polymerization technique have functional properties suitable for a wide range of modern applications, because the molecular structures of the thin films obtained are different from the starting materials. The change in the molecular structures of the plasma polymerized thin films occurs, since they are formed with fragmented molecules under ions and electron collisions with high energy [1, 2].

It was known for many years that some organic compounds form solid deposits in plasma generated by some kind of electrical discharge. In most cases, however, the deposits were recognized as by-products of phenomena associated with electric discharge, consequently, little attention was paid either to the properties of these materials (undesirable by-products) or to the process as a means of forming useful materials. This undesirable deposit however had extremely important characteristics that are sought after in the modern technology of coating that is, (i) excellent adhesion to substrate materials and (ii) strong resistance to most chemicals. To explain the reaction mechanism of these materials, many investigators discussed the effects of discharge conditions such as polymerization time, monomer's properties, pressure, discharge current, and discharge power and substrate temperature on the polymerization rate [1].

At these early stages of discovery, the concept of polymers was not well developed, and obviously these processes had never been considered to be polymerization, that is, plasma polymerization or glow discharge polymerization. Only since the 1960s has the formation of materials in plasma been recognized as a means of synthesizing polymers, and the process, when used to make a special coating on metals, has been referred to as plasma polymerization or glow discharge polymerization.

Plasma polymerization today is gaining recognition as an important process for the formation of entirely new kind of materials. The materials obtained by plasma polymerization are significantly different from conventional polymers and also different from most inorganic materials. Hence plasma polymerization should be considered as a method of forming new types of materials rather than a method of preparing conventional polymers. It is an attractive technique, using which it is possible to modify the surface properties of a substrate, while retaining the transparency and bulk properties of the substrate materials. Furthermore, it is a solvent-free, fast and versatile process [1, 3, 4]. Plasma polymerization process covers a wide interdisciplinary area of physics, chemistry, science of interfaces and materials science and so on. Thus plasma polymerization is a versatile technique for the deposition of films with functional properties suitable for a wide range of modern applications [1].

Material preparation and processing have received significant attention in the academic and industrial research community and have become one of the most active areas of research in the development of science and technology in last few decades. Especially, organic thin films have received a great deal of interest due to their interesting applications in the fields of mechanics, electronics and optics. Some special properties lead the thin films to have different characteristics from bulk materials. For example, thin films are not fully dense, have under stress and different defect structures from bulk, quasi-two dimensional (very thin films) etc. Furthermore the thin films are strongly influenced by surface and interface effects which would change their electrical, magnetic, optical, thermal and mechanical properties from that of the bulk materials. The wide applications of thin films include chemical, physical and biological sensors, electronic and electrical conductors and insulator, electrical barriers, diffusion barriers, magnetic sensors, gas sensors, optics-anti-reflection coatings, corrosion protection, wear resistance, microelectronic devices, nonlinear optical devices, molecular devices, coatings for chemical fibers and films, passivation of semiconductors, surface hardening of tool, spaceship components, etc [1, 5-7]. Therefore, it is of interest to develop polymer thin films of high quality for a variety of industrial applications. As a consequence, the study of the structural, optical and electrical properties of organic polymer thin films received special attention of the scientist as potential materials.

In the thin film technology, plasma polymerization has been widely accepted and is preferred owing to the desirable features of the thin films it yields, because the thin films produced in this process are pinhole-free and highly cross-linked and therefore are insoluble, thermally stable, chemically inert and mechanically tough. Furthermore such films are often highly coherent and adherent to a variety of substrates including conventional polymer, glass and metal surfaces [8, 9]. Due to these excellent properties they have been undertaken very actively in the last few decades for a variety of applications such as protective coatings, membranes, biomedical materials, electronic and optical devices, adhesion promoters, anticorrosive surfaces, humidity sensors, electrical resistors, scratch resistant coatings, optical filters, protective coatings, chemical barrier coatings, etc. Metallized surfaces of synthetic materials can be protected against corrosion with a thin polymer layer deposited by plasma polymerization. The processes can be customized to produce hydrophobic or hydrophilic (antifogging effect) coatings. Scratch resistant coatings have been successfully applied on optical lenses. By appropriate plasma surface treatment, new properties such as optical reflection, adhesion, friction coefficient, surface energy (wettability and water repellency), permeability, surface conductivity and biocompatibility of conventional polymers can be obtained. The generation of multilayer/composite materials also has a wide variety of applications, e.g., in biocompatible materials, in the modification of surfaces, in protective coverings of metals, in the design of complex materials, etc [10].

This thesis describes the preparation and discusses the structural, thermal, optical and electrical properties of plasma polymerized pyrrole-*N,N,3,5* tetramethylaniline (PPPy-PPTMA) bilayer composite thin films with different composition and different deposition time ratio and compares with those of its component thin films. It is to be noted that derivatives of aniline and pyrrole are very well known organic materials. Different properties of plasma polymerized thin film of these organic materials have been reported by many investigators. These two materials are chosen to prepare and to characterize the bilayer composite thin film because it is usually observed that the bilayer composite thin films give rise to different properties than the thin films prepared by individual monomers.

1.2 Review of Earlier Research Works

Various properties of plasma polymerized thin films such as structural, physical, chemical, optical and electrical properties have been investigated and have been appeared in the literatures. The development of scientific interest in different technological application of these thin films has drawn much attention of the researchers.

A cursory survey of the literature concerning plasma polymerization reveals that due to the complexity of plasma the bulk of the research has been concentrated on establishing the dependence of the macroscopic and spectroscopic properties of the product on the major process variables e.g. power, monomer type, gas flow rate, pressure etc. Different models have been proposed for the plasma polymerization based on ions, electrons and neutrals which are extensively reviewed [11]. Amongst these models, Poll et al. [12] discussed the role of ion bombardment and pointed to a competition between etching and deposition processes in plasma polymerization in the same domain. Yasuda proposed the CAP (Competition-Ablation-Polymerization) mechanism for glow discharge polymerization [1] and identified two regimes of plasma polymerization in which the mechanisms differ dramatically i.e. the monomer-deficient plasma and the energy-deficient plasma. Indeed the composite plasma process parameter W/F_M (where W is the discharge power and F_M is the mass flow rate of monomer) has shown to be very efficient to control the chemical structure of the polymer. At relatively low input energy level (energy-deficient region) plasma polymer obtained is characterized by a chemical structure and the properties are found to be almost similar to those of conventional polymers. By increasing W/F_M (monomer-deficient region), due to the relatively high energy of the impinging particles, the deposited material is characterized by a short range order combined with a high cross-linking density.

Before characterization one needs to known the chemical species of the plasma polymers and their chemical combinations. Yasuda et al. [13] and Westwood et al. [14] did significantly important investigations on the elemental compositions and empirical formulae of repeating units of plasma polymers produced from a variety of organic compounds using various kinds

of plasma reactors. They observed two trends in the plasma polymers namely: (i) the deficiency of hydrogen and halogens which are attached to the carbon in the monomers, and (ii) the incorporation of oxygen in the polymers even though the monomers do not contain oxygen. They have also determined the empirical formulae of repeating units of plasma polymerized films. Having these observations, they concluded that the incorporation of oxygen is as consequence of the post plasma reaction of trapped free radicals with ambient oxygen.

The structural, optical and electrical behaviors of plasma polymerized thin films have been widely studied. It is known that Infrared (IR) spectroscopic analysis, x-ray photoelectron spectroscopy (XPS), x-ray diffraction (XRD), scanning electron microscopy (SEM), atomic force microscopy (AFM), elemental analysis (EA), etc provide information about the chemical structure of the materials. Differential thermal analyses (DTA) and thermogravimetric analyses (TGA) provide information about thermal behavior of the plasma polymers. For optical characterization of plasma polymerized thin films e.g. to determine the presence, nature and extent of conjugation in materials, impurity states, optical energy gaps, direct and indirect transitions, refractive index and extinction coefficients etc ultraviolet visible (UV-vis) spectroscopic methods are being frequently used by many investigators. For electrical characterization, the direct current (dc) and alternating current (ac) electrical properties are widely studied.

Most plasma polymers are new kinds of materials existing in the form of a highly cross-linked and highly branched three-dimensional network. IR spectroscopic analysis provides information about the structure of plasma polymers. Reflecting the valuable extent of fragmentation and for rearrangement of atoms and legends during the process of polymer formation in plasma, to obtain a clear picture on the chemical composition Jesch et al. [15] studied the Fourier transform infrared (FTIR) spectra of plasma polymers formed from pentane, ethylene, butadiene, benzene, styrene and naphthalene. On the basis of the structures, analyzed by FTIR spectroscopy, they concluded that whether the monomer was aromatic or olefinic or fully saturated, the plasma polymer was highly branched and cross-linked and contains identifiable saturation.

Akther and Bhuiyan [16] studied the structural and optical properties of plasma polymerized N, N, 3, 5 tetramethylaniline (PPTMA) thin film. The structural analysis from FTIR spectroscopy revealed that the PPTMA thin films contain more conjugation as compared to the TMA monomer which modifies on heat treatment. The π-π* transition in PPTMA thin film indicated the presence of an increased degree of conjugation in the resulting films. From the UV-vis absorption spectra, allowed direct transition (E_{qd}) and indirect transition (E_{qi}) energy gap are determined and it is seen that while E_{qd} increases a little, E_{qi} decreases, on heat treatment of PPTMA. The calculated value of Tauc's parameter B for the entire sample indicated an increase in structural order/conjugation in PPTMA thin films on heat treatment.

It is then concluded that PPTMA thin film with conjugation can be produced by plasma polymerization and the structural order can be improved by heat treatment. The allowed direct and indirect transition energy gaps are also modified when the samples are heat treated.

Chowdhury and Bhuiyan [2] investigated the optical properties and chemical structure of plasma polymerized diphenyl (PPDP) thin films. The IR spectroscopic analyses have revealed that the structure of PPDP thin films is not structurally the same as that of the monomer diphenyl and cyclization / aggregation by conjugation occurs in the PPDP structure on heat treatment which is partially relieved on aging. They have concluded that the band gap is not affected appreciably by heat treatment whereas it is modified on aging. The values of E_{qd} and E_{qi} were also found to be changed slightly due to heat treatment but appreciably due to aging. Bhuiyan et al. [17] calculated the optical band gaps of plasma polymerized acrylonitrilc thin films from absorption edge maxima and found that the band gap was modified on doping in contrast to the behavior of inorganic semiconductors, where band gap remains unaffected on doping.

Kumar et al. [18] studied the structural, optical and electrical characteristics of plasma polymerized pyrrole (PPPy) and iodine-doped PPPy prepared using an inductively coupled plasma reactor and found that due to iodine doping the surface morphology of the PPPy film becomes smoother and an increase in the connectivity and continuity between the blocks of polymer chains provided an increase in conductivity. Based on the FTIR spectra, they reported that the ring structure was retained during plasma polymerization and a chemical structure was also proposed for the PPPy film. An analysis of the electronic spectra provided the band gap energies of 1.3 and 0.8 eV for the undoped and doped PPPy films, respectively. From conduction studies they concluded that the conductivity of PPPy film depends upon the number of extrinsic carriers and the conduction current varied with field direction and the nature of the electrode metals, and the conduction mechanism in the undoped PPPy film was reported to be a Schottky-type mechanism.

Structural, electrical, and optical of insitu PPPy and iodine-doped PPPy have been investigated by Rajan et al. [19]. A comparative study of the FTIR spectra of the monomer and PPPy gives information that the ring structure is retained during plasma polymerization. Iodine doping considerably increases the conductivity of the polymer film and decreases the optical band gap energy.

PPPy thin films were simultaneously deposited by Eufinger et al. [20] on stainless steel metallic substrates attached to the cathode and anode from a parallel-plate dc reactor and comparative characterizations were done using cyclic voltammetry, reflection-absorption infrared (RAIR) and UV-vis spectroscopy. Substantial differences were found between the structures of these films, although their overall compositions were very similar. The films on the anode appeared to be less crosslinked and contained less unsaturation and conjugation than the films on the cathode.

Ion et al. [21] investigated on the radiation-induced and electrochemical modification of polypyrrole film by incorporating of large electro-active organic molecules and found that a sensitive modification of polypyrrole film with methylene blue could be achieved by radiation-induced method as a new and innovative method. The evidence of the new film was proved by UV-vis and IR spectroscopies. The cyclic voltammogram, for the prepared modified electrode, is accompanied by a color change from blue green to a transparent film. The new film has a strong stability due to the interaction between the methylene blue and the polymer chain of polypyrrole. The observed effects are explained in a model in which the concurrent positive ion bombardment plays an important role in modifying the structure of a growing plasma-polymerized film. The new proposed method for film preparation, however, could have applications in optoelectronics.

Pure and iodine-doped polyaniline thin films were prepared and characterized by Mathai et al. [22] using ac plasma polymerization technique. The structural analyses of pure and iodine-doped polyaniline thin films are carried out by FTIR spectroscopy, which revealed that the aromatic ring and the infrared absorption features of the monomer aniline were retained in the plasma polymerized aniline. The most probable mechanism of polymerization of aniline is due to hydrogen abstraction. Optical band gaps of iodine doped plasma polymerized aniline thin films were evaluated from UV-vis absorption data, which showed a drastic reduction. However, it is observed that the band gap has increased almost to the undoped value upon heat treatment. In the in situ doped polyaniline thin films, the band gap first reduces and heat treatment only slightly increases the band gap. Subsequent heating does not change the band gaps.

Sajeev et al. [23] prepared pristine and iodine doped polyaniline thin films by ac and radio frequency (rf) plasma polymerization techniques separately and compared their optical and electrical properties. The structural properties of these films were evaluated by FTIR spectroscopy and the optical band gap was estimated from UV-vis measurements. Comparative studies on the structural, optical and electrical properties showed that the optical band gap of the polyaniline thin films prepared by rf and ac plasma polymerization techniques differ considerably and the band gap was further reduced by in situ doping of iodine. The electrical conductivity measurements on these films show a higher value of electrical conductivity in the case of rf plasma polymerized thin films compared to the ac plasma polymerized films.

Prabhakar et al. [24] investigated polyaniline thin films prepared by an inductively coupled pulsed-plasma reactor on several substrates positioned at various distances from the center of the rf coil. The samples were characterized by FTIR, cyclic voltammetry and microscopic techniques. Impedance spectroscopy was used to determine the electrical characteristics of three-layer structures with polyaniline as the middle layer between top and bottom metal electrodes. FTIR results indicated that the chemical composition and structure of the films

were very dependent on the substrate's position with respect to the rf coil, there being considerably less aromatic character closer to the coil. The electrochemical behavior of the films in acidic electrolytes was similar to that of small molecule aniline oxidation products; the number of peaks in the cyclic voltammograms varied with the substrate. SEM indicated that as the films became thicker, they developed nodules atop a somewhat smoother underlayer. Results from transmission electron microscopy and optical birefringence suggested that the films were not completely homogeneous.

Polylinalool thin films were fabricated using rf plasma polymerization by Bazaka et al. [25]. All films were found to be smooth, defect-free surfaces with average roughness of 0.44 nm. The FTIR analysis of the polymer showed a notable reduction in –OH moiety and complete dissociation of C=C unsaturation compared to the monomer, and presence of a ketone band absent from the spectrum of the monomer. Polylinalool were characterized by chain branching and a large quantity of short polymer chains. Films were optically transparent, with refractive index and extinction coefficient of 1.55 and 0.001 (at 500 nm) respectively, indicating a potential application as an encapsulating (protective) coating for circuit boards. The optical band gap was calculated to be 2.82 eV, which is in the semiconducting energy gap region.

Xiao et al. [26] investigated the plasma polymerized nitriles by FTIR, UV-visible, XPS, AFM and revealed that the plasma synthesis conditions affected the chemical structure, surface composition, morphology and property of the plasma deposited films. A high retention of the aromatic ring structure of the starting monomer in the deposited plasma films was obtained when a low discharge power was used during film formation. A red shift in the maximum absorption wavelength was observed. The AFM measurement showed that the film with quite smooth surface could be grown under a relatively low discharge power.

The characterization of plasma polymerized allylamine films was done by Lejeune et al. [27]. The FTIR spectroscopy, XPS and ellipsometry study revealed that the microstructure had a strong dependence on the deposition power. A power transition at about 30W had been identified outlining two deposition modes in agreement with a growth model developed for carbon nitride thin films. Films deposited with a power inferior to 30 W conserve a lot of the initial microstructural properties of allylamine precursor i.e. high-NH_2 content and a low cross-linking of the deposited chains. With a power superior to 30 W, due to collision effects at the surface of the growing film, the microstructure becomes more disordered and more compact.

The plasma polymerization of 4-phenylbenzonitrile (PPBPCN) was carried out by Zhao et al. [28] to synthesize a novel conjugated polynitrile thin film with a better optical property. The structure, compositions and morphology of the PPBPCN thin films were investigated by FTIR, XPS and AFM, and were observed that the plasma synthesis conditions affected the chemical structure, surface composition, morphology and properties of the plasma deposited

conjugated polynitrile films. A fine, homogenous PPBPCN film with a large p-conjugated system and a high retention of the aromatic ring structure of the starting monomer in the deposited plasma films is obtained when a low discharge power of 30 W was used during film formation. A high discharge power of 50 W brings about more severe molecular (aromatic ring) fragmentation. Moreover, for the first time, the as-grown conjugated polynitrile thin films show a blue emission with a relatively high intensity at about 470 nm. It was, however suggested that the conjugated PPBPCN thin films might be applied to LED and photodiode on device performance.

Saloum [29] studied on silicon organic thin films prepared by rf hollow cathode plasma chemical vapor deposition system, from hexamethyldisilazane (HMDSN) as the source compound, under different plasma conditions, namely feed gas and applied rf power. The feed gas has been changed from argon to nitrogen, and the power has been varied between 100 W and 300 W in N_2/HMDSN plasma. The plasma active species (electrons, ion flux rate, and UV radiation) contributing to the films growth mechanisms have been identified by electrical probes and optical emission spectroscopic analysis. The films have been investigated for their thickness and deposition rate, using quartz crystal microbalance, and sensing properties relating to humidity and gas (NH_3, CO_2 and O_2) sorptive investigations, using the piezoelectric effect of quartz crystals of the quartz crystal microbalance. The effect of the different plasma conditions on the plasma phase characteristics and deposited thin films properties, as well as the correlations between deposition rate and plasma characteristics and between sorptive properties, water contact angles and thin films surface morphology were reported.

Bae et al. [30] deposited plasma polymerized organic thin films on Si and glass substrates by plasma-enhanced chemical vapor deposition (PECVD) method using methylcyclohexane and ethyl-cyclohexane as organic precursors. The structural and optical properties of the films were investigated by FTIR and UV-vis spectroscopy. It was observed that as the plasma power was increased, the main IR absorption peak intensity of thin films was increased while the transmittance of the UV-vis spectra was decreased. The increase of absorption peak intensity with increasing the rf power can be explained with either the increase of carbon contents or the scattered reflection caused by plasma bombardment. The optical band gap of the films also has a decreasing tendency with increasing rf power.

PECVD method has been used by Grant et al. [31] to grow homo-polymerized films, co-polymerized films, and multi-layered films on a variety of substrates and characterized by using SEM, FTIR, variable-angle spectroscopic ellipsometry and XPS. The use of polymers as linear optical materials were proposed and rates of deposition and refractive indices were measured and these information were used to design and fabricate photonic structures. They, however, finally concluded that that plasma polymerization using PECVD is an easy method to fabricate multi-layered homo-polymerized and co-polymerized films of known optical thicknesses for photonic applications.

Kouta et al. [32] reported the effect of the discharge conditions on the structure and electrical conductivity of the PPPy films. Comparative studies of the IR, EA and UV-vis observations showed that some pyrrole rings were remained in the PPPy films prepared with 10 and 20 W discharge power, whereas almost all the pyrrole rings were cleaved in the PPPy films prepared with 50 and 100 W discharge power.

Zhang et al. [33] prepared hydrophobia plasma polymer films from perflurohexane and octafluorotoluene and hydrophilic plasma polymer film from acrylic acid. Using in-situ laser Interferometer, FTIR and contact angle measurements, the deposition rate was correlated with the precursor structure, the deposition parameters and the plasma film structure. The results indicated that the deposition relied not only on the deposition power but also on the structure of the precursors to a large extent.

The plasma polymerized thiophene thin films were characterized by Kim et al. [34] using UV-visible spectroscopy, XRD and AFM. An increase in the energy band gap from 3.78 to 4.02 eV with increasing rf power was observed from UV-visible spectra. The refractive index of thin films was also found to be increased as the plasma power was increased. The XRD and AFM results showed that the as-grown films have some oriented structures.

Silverstein et al. [35] investigated on the synthesis, the dependence of molecular structure and properties on the polymerization conditions of plasma polymerized thiophene (PPTh). They found that the transparent polymerized thiophene films depend on the carrier gas used (if any) and on the plasma power.

Plasma polymerization of hexamethyldisiloxane (HMDSO) in presence of different carrier gases was carried out using an inductively coupled electrode-less glow discharge by Fang et al. [36] and was found that the monomer HMDSO were polymerized at different rates from low to high for the carrier gases in the order H_2, He, N_2, Ar and O_2. Different analysis indicated that the polymer deposition rate and the structures of products were mainly dependent on molecular fragmentation, which varied with carrier gas and imposed rf power.

The DTA trace heat capacities, transition temperatures and hence the nature of phase transitions can be determined. Using TGA investigation water content, amount of volatile components and of ash content can be detected. The kinetic parameters, such as activation energy, frequency factor can also be calculated from TGA. Varma [37] calculated the melting points, and the values of latent heats of fusion of a good number of organic solid using DTA. Lewis and Edstrom [38] have used DTA to categorize the high temperature behavior of polynuclear aromatic, which is either thermally reactive or inactive. They have observed that the thermally reactive aromatic species possesses sufficient reactivity at an atmospheric pressure system to undergo a condensation sequence in the liquid phase and yield a measurable amount of polymerized carbonaceous residue at 1023 K. The thermally inactive compounds have sufficient stability so that such condensation reactions do not occur prior to complete volatilization.

The dc electrical conduction mechanisms and ac electrical dielectric properties of various plasma polymerized organic thin films have also been studied by many researchers. Akther and Bhuiyan [39, 40] studied the electrical conduction mechanism in PPTMA thin films. The *J-V* characteristics of PPTMA with Al contacts at different temperatures show an ohmic behavior at the lower applied voltage region and space charge limited conduction (SCLC) dominated by exponential trap distribution at the higher voltage region. The activation energy (ΔE) values indicated that there is a transition in the conduction process from a hopping process to a distinct energy level process from lower to higher temperature region.

Valaski et al. [41, 42] investigated on the influence of electrode material and film thickness on charge transport properties of electrodeposited polypyrrole (PPy) thin films. They found that the film morphology, roughness and electrical conductivity are strongly influenced by the choice of substrate and the choice of electrode materials played a quite important role in specifying the resistivity as well as the conductivity [41]. The selection of metals with high work function values imposes an increase in the mobility and the positive free carrier concentration of semiconductor at thermodynamic equilibrium and consequently, in its electrical conductivity. They also observed that the films with different electrode materials show different properties. Au/PPy/Ni configuration showed only ohmic conduction behavior; on the other hand, TO/PPy/Ni and Au/PPy/Al configuration showed ohmic behavior in the lower voltage region but SCL conduction mechanism in higher voltages. In the study on the influence of the film thickness [42] on the conductivity, they found that different conduction mechanisms were shown by the films of different thickness. When PPy film thickness was increased (~above 300nm) the charge transport tends to be space charge limited, but for smaller thickness ($d \leq 300$ nm) of the films, the charge transport was limited by thermoionic emission. The charge mobility was also found to be increased for the smaller thickness. It was also reported that the film morphology was highly thickness dependent. The morphology was found to be better (lower roughness) for smaller thickness.

The preparation and characterization of ac PPPy thin films has been studied by Joseph John et al. [43]. The electrical conductivity studies of the aluminium/ polymer/ aluminium structure have been carried out and a SCLC mechanism is identified as the most probable conduction mechanism in those polymer films. The electrical conductivity showed an enhanched value in the iodine doped sample. The reduction of optical band gap by iodine doping is correlated with the observed conductivity results.

Sajeev et al. [44] studied on the carrier transport mechanism of polyaniline (PA) thin films prepared by rf plasma polymerization. The mechanism of electrical conduction and carrier mobility of PA thin films for different temperatures were examined using the Al-PA-Al structure. It was found that the mechanism of carrier transport in these films was space charge limited conduction. The J-V studies on an asymmetric electrode configuration using indium tin oxide (ITO) as the base electrode and Al as the upper electrode (ITO-PA-Al structure) showed a diode-like behavior with a considerable rectification ratio.

The influence of temperature and humidity on the electric conductivity of polyaniline (PAn) and polypyrrole (PPy) thin films synthesized by plasma and doped with iodine (PAn/I and PPy/I, respectively) were studied by Morales et al. [45]. The polymers showed the characteristic of ohmic conduction mechanism via electrons. However, the conductivity was found to be much lower than that presented by the polymers obtained by traditional chemical oxidation. To study the temperature dependence of the conductivity the polymers were submitted to heating–cooling cycles. In the heating step of the cycles, the polymers with greater humidity contents did not have the behavior proposed in the Arrhenius model because the loss of water molecules affected the shape of the curve. During the cooling step, the plots showed good agreement with the Arrhenius model. These behaviors suggested that in the absence of humidity, the electric conductivity was dominated by 1-D conducting character of the polymeric systems. The activation energy of PPy/I had an average value of (1.16± 0.1) eV and was found to be independent of the reaction time, whereas PAn/I presented different activation energies that depended on the reaction time and evolved from 0.5 to 1.2 eV, possibly because of structural and conformational changes in the polymeric network. All the activation energies were below 2 eV, placing these polymers in the semiconductor regime. The XRD diffraction analysis, however, showed that PAn/I suffered structural modifications after the heating–cooling cycles, whereas PPy/I remained almost without changes.

The plasma polymerized tetraethylorthosilicate (PPTEOS) thin films were deposited by Zaman and Bhuiyan [46] on to glass substrates at room temperature by a parallel plate capacitively coupled glow discharge reactor. The J–V characteristics of PPTEOS thin films of different thicknesses have been studied at different temperatures in the voltage region from 0.2 to 15 V. In the *J-V* curves two slopes were observed – one in the lower voltage region and another in the higher voltage region. The voltage dependence of current density at the higher voltage region indicates that the mechanism of conduction in PPTEOS thin films is space charge limited conduction. The carrier mobility, the free carrier density and the total trap density were calculated from the observed data. The activation energies are estimated to be about (0.13 ± 0.05) and (0.46 ± 0.07) eV in the lower and higher temperature regions respectively for an applied voltage of 2 V and (0.09 ± 0.03) and (0.43 ± 0.10) eV in the lower and higher temperature regions respectively for an applied voltage of 14 V. The conduction in PPTEOS may be dominated by hopping of carriers between the localized states at the low temperature and thermally excited carriers from energy levels within the band gap in the vicinity of high temperature.

The electric conductivity, activation energy and morphology of polythiophene synthesized by rf resistive plasmas were studied by Olayo et al. [47]. It was reported that the continuous collisions of particles in the plasma had induced the polymerization of thiophene but also broke some of the monomer molecules producing complex polymers with thiophene rings and aliphatic hydrocarbon segments. These multidirectional chemical reactions were more

marked at longer reaction times in which the morphology of the polymers evolved from smooth surfaces, at low exposure time, to spherical particles with diameter in the 300-1000 nm interval. Between both morphologies, some bubbles were observed to be formed on the surface. The intrinsic conductivity of plasma polymers of thiophene synthesized in this way varied in the range of 10-10 to 10-8 S/m. However, the conductivity resulted very sensitive to the water content in the polymers, which produced variations of up to 5 magnitude orders. The activation energy of the intrinsic conductivity was between 0.56 and 1.41 eV, increasing with the reaction time.

Nadzlin et al. [48] prepared organic films by rf plasma chemical vapor deposition using naphthalene (naph), propane (prop), and naphthalene mixed propane (naph-prop). From the study on the optical and electrical properties of the films, they found that all of the samples showed broadband emission of photoluminescence. The conductivity of the mixed film (naph-prop sample) was found to be larger than that of the single monomer film (naph and prop samples) and showed SCLC behavior for the conduction mechanism at the higher voltage region.

The electronic conductivity of bilayer aniline-pyrrole thin films has been studied by Morales et al [10]. The results that they obtained indicated that the plasma technique was capable of forming chemically bonded layered polymers with several possible combinations. It is observed that the synthesis of the bilayer PAn/I–PPy/I polymers by plasma allows controlling the thickness of each layer, creating the possibility of having thin films of different materials chemically bonded at the interface by a complex mechanism of layers that join and separate in several areas. They also found that, the bilayer aniline–pyrrole polymers had greater electric conductivity at room temperature than that shown by the separate homopolymers.

Shukla and Gaur [49] investigated the electrical conduction in solution-grown polymethylmethacrylate (PMMA), polyvinylidenefluoride (PVDF) and PMMA-PVDF double-layered samples in the metal-polymer-metal sandwich configuration at different fields and temperatures with a constant sample-thickness of about 50 μm. They observed certain effects which lead to a large burst of current immediately after the application of field in double-layered samples. An attempt was made to identify the nature of the current by comparing the observed dependence on electric field, electrode material and temperature with the respective characteristic features of the existing theories on electrical conduction. The observed linear current-voltage characteristics of the electrical conduction was interpreted as PF mechanism in PMMA and PVDF samples, whereas, the non-linear behavior of current-voltage measurements in PMMA-PVDF double-layered samples was interpreted as the SCLC mechanism. It was also observed that the conductivity of the polymer films increased on formation of their double-layer laminates, because that the polymer-polymer interface act as charge carrier trapping centers and provides links between the polymer molecules in the amorphous region.

The attention in glow discharge polymerized thin films as possible dielectric materials triggered academic interest in the polymerization process as well. Goodman's [50] work in this field inspired several investigators to characterize the polymerization process and polymers produced from organic monomers. At the very beginning of emergence of plasma polymerization, only electrical and more often dielectric properties of plasma polymerized films were investigated.

Chowdhury and Bhuiyan [51] investigated the dielectric relaxation behavior of the as-deposited and heat treated plasma polymerized Diphenyl (PPDP) thin films in an Al/PPDP/Al configuration over the frequency range from 10^{-1} to 10^{6} Hz and temperature range from 223 to 423 K. It was observed that the ac conductivity was more dependent on temperature in the low frequency region than in the high frequency region and dielectric constant was found to be dependent on frequency above 303 and 343 K in the as deposited and heat treated PPDP respectively. For different relaxation processes, the activation energies were estimated to be about 0.45 and 0.67 eV for the as deposited and 1.35 eV for heat treated PPDP. The dielectric data analysis showed the existence of distribution of relaxation time in these materials.

El-Nahass et al. [52] investigated the dependence of the dc and ac electrical conductivity and ac dielectric properties on the temperature and on the frequency of thermally deposited N-(p-dimethylaminobenzylidene)-p-nitroaniline (DBN) thin films. The dc conductivity showed an increasing rate of thermally activated carrier hopping with increasing temperature. The obtained experimental results of ac conductivity showed that the correlated barrier hopping model is the appropriate mechanism for the electron transport in the DBN film. Both the dielectric constant and dielectric loss were observed to decrease with increasing frequency.

Dielectric constant and conduction current of polyimides thin/ultrathin films of thicknesses 80–2000 nm were measured by Liang et al. [53] using a small electrode system. It was observed that the dielectric constant was decreased with decreasing film thickness, but the conduction current was found to be increased. Using IR reflection absorption spectroscopy, they found that the polyimide chains are oriented parallel to the electrodes. The dependence of the dielectric constants on film thickness was explained by the orientation of polymer chains.

Saravanan et al. [54] investigated on the low dielectric constant thin films based on rf plasma polymerized aniline. The FTIR studies have revealed that the aromatic ring is retained in the polyaniline, thereby increasing the thermal stability. They measured dielectric constant and ac conductivity in the frequency range 100 Hz -1 MHz and the temperature range 300 -373 K and found that the dielectric constant is considerably low in the high frequency range.

Their dielectric properties of rf plasma polymerized pyrrole (PPPy) thin film were studied in the frequency range from 1 kHz to 1 MHz at various temperatures from 303 to 423 K by Sakthi Kumar and Yoshida [55]. The large increase in the capacitance at low frequency region indicated the possibility of an interfacial polarization mechanism prevailing in that region. They reported that the PPPy thin films have high dielectric constant with small variations against frequency and temperature, low dielectric losses, chemical inertness and also stability against environment and therefore these films could be considered as an ideal dielectric material.

Polyaniline thin films were prepared by using ac plasma polymerization technique and characterized by Joseph Mathai et al. [56]. Capacitance, dielectric loss, dielectric constant and ac conductivity of those films were investigated in the frequency range from 100 Hz to 1MHz and in the temperature range from 300 to 373 K. Capacitance and dielectric loss were observed to be decreased with frequency and increased with temperature. The ac conductivity $\sigma(\omega)$ was found to vary as ω^{-1}. Annealing of polyaniline thin films in high vacuum at 373 K for 1 hour reduced the dielectric loss.

Ram et al. [57] did the dielectric measurements of polymeraldine salt in an Al-polymeraldine salt-Al configuration as functions of frequency and temperature. The analysis showed that the movement of charge carriers under the influence of an electric field gives rise to the space charge phenomenon, leading to interfacial polarization. A shift of Cole-Cole plot with increasing temperature was observed which indicated the presence of multiple relaxations. The relaxation phenomenon was attributed to the damping of dipole oscillators originating due to the application of external electric field. The mobility of charge carriers was calculated using the approximation to space charge theories.

The dielectric properties from a set of molybdenum (Mo) containing diamond like carbon (DLC) films deposited using electron cyclotron resonance chemical vapor deposition (ECR – CVD) were investigated by Huang et al [58]. It is shown that the film permittivity can be greatly increased by the introduction of Mo. There is a drastic reduction in the permittivity at frequencies of up to 10 kHz. The ac conductivity exhibits three characteristic regions in the frequency range investigated: constant, liner and super liner regions. The high ε'' and $\tan\delta$ at low frequencies resulted from the high dc conductivity of the films. The relaxation polarizations in the film are responsible for the peaks of ε'' and $\tan\delta$. For the film with high Mo content, the permittivity is frequency dependent at low temperature. However, for the high frequency of 1 MHz, the film permittivity is weakly Mo dependent at the temperature below 145 K. The relaxation time was observed to decrease with increasing Mo content in the films at room temperature. The effect of voltage on the permittivity of the films is insignificant at frequencies above 10 kHz. Finally, it was concluded that the films have a potential application in microwave devices.

Frequency and temperature dependence of dielectric constant ε' and dielectric loss ε'' in pure polyester resin and polymer composites with various types of glass fiber were studied by Akram et al. [59] in the frequency range 330 Hz - 3 MHz and in the temperature range 25-150°C. The experimental results show that ε' and ε'' increased with the addition of glass fiber in polyester resin. The value of ε' was found to be decreased with increasing frequency, which indicated that the major contribution to the polarization comes from orientation polarization. Dielectric loss peaks were also observed in the composite materials at high temperature due to T_g of polyester. The value of ε' increased with increasing temperature, and was due to greater freedom of movement of the dipole molecular chains within the polyester at high temperature.

The relationship between chemical structure and dielectric properties of plasma-enhanced chemical vapor deposited carbon-based polymer thin films prepared from two precursors, benzene and octafluorocyclobutane was studied by Jiang et al. [60]. Two different monomer feed locations, directly in the plasma zone or in the downstream (DS) region and two different pressures, 80 Pa (high pressure) or 6.7 Pa (low pressure), were used. The dielectric constant (ε_r) and dielectric loss (tan δ) of the films were investigated over a range of frequencies up to 1 MHz and the dielectric strength (breakdown voltage) was characterized by the current-voltage method. Spectroscopic ellipsometry was performed to determine the film thickness and refractive index. Good dielectric properties were exhibited, as PP-benzene films formed in the high pressure, DS region showed a dielectric strength of 610 V/μm, a ε_r of 3.07, and a tan δ of 7.0×10^{-3} at 1 kHz. The PECVD processing pressure had a significant effect on final film structure and the film's physical density had a strong impact on dielectric breakdown strength. It was also reported that the residual oxygen content in the PP-benzene films significantly affected the frequency dependences of the dielectric constant and loss.

It is followed from the reported literatures that an interest could be grown on the study of different properties of multi-layer thin films for their versatile applications. Although there is much interest on the study of multilayer thin films, reports on the structural, optical and electrical properties on such films are less abundant in the literature. It is in this context, a systematic study on the structural, optical and electrical properties of PPPy-PPTMA bilayer composite thin films with different composition and different deposition time ratio is undertaken. This thesis describes not only the preparation and characterization of PPPy-PPTMA bilayer composite thin films but also those issues of its component thin films; i.e., PPPy and PPTMA. The structural characterization of the thin films would be done by using FTIR spectroscopic analysis, thermal behavior would be studied by DTA and TGA, optical properties would be characterized by UV-vis spectroscopy and electrical characterization would be carried on by studying dc and ac electrical measurements.

1.3 Objectives of the Thesis

The field of plasma polymerization and the polymer produced in plasma is one of the fastest growing areas of material science and technology. Among the various plasma polymerization processes the glow discharge is by far the most important and widely used one. The technique and the polymer produced have thus drawn much attention of the scientist, technologists and industrialists.

The materials produced in glow discharge have got high resistivity, high dielectric breakdown strength and cost effectiveness and have also got many other advantageous characteristics. Their advantageous and typical characteristics make the material to be utilized in various disciplines such as, in dielectric, electronic, optical, biomedical devices, etc.

The aim of the present research is to prepare and to investigate the different properties of the plasma polymerized pyrrole-N,N,3,5 tetramethylaniline (PPPy-PPTMA) bilayer composite thin films. It is already mentioned in the preceding section that the derivatives of aniline and pyrrole are very well known organic materials and different properties of plasma polymerized thin film of these organic materials have been reported by many investigators. These two materials are chosen to prepare and to characterize the bilayer composite thin film because it is usually observed that the bilayer / multilayer / composite thin films give rise to different properties than the thin films prepared by individual monomers. It is also to be noted that the reports on the structural, optical and electrical properties on bilayer/multi-layer composite thin films are less abundant in the literature. Moreover versatile applications of the multi-layer thin films have drawn attention on the study of their different properties. It is in this context, a systematic study on the structural, optical and electrical properties of PPPy-PPTMA bilayer composite thin films with different composition and different deposition time ratio is undertaken. The PPPy and PPTMA thin films, however, would be deposited at different deposition condition such as different power, different flow rate, etc to find the optimum condition for good sample deposition. The PPPy-PPTMA bilayer thin films would be deposited by changing the deposition time ratio of PPPy and PPTMA where pyrrole-monomer would be used as the mother-material and N,N,3,5 tetramethylaniline monomer would be deposited in different deposition time ratios after the pyrrole films were formed. The structural and physical properties of the deposited bilayer thin films would be investigated and would be compared with those of the PPPy and PPTMA thin films by using the following ways.

(a) Structural Investigations

- To investigate the structure of the organic thin films by Fourier transform infrared (FTIR) spectroscopy.

- To investigate the thermal degradation / transformations by differential thermal analysis (DTA) and thermogravimetric analysis (TGA)

(b) Optical Properties

- To study optical properties using UV-visible spectroscopy and to determine the absorption co-efficient, extinction co-efficient, direct and indirect transition band gaps of the thin films.

(c) Electrical Properties

- Direct Current (dc) J-V characteristics; thermally activated conduction process and isothermal discharging current, etc.

- Alternating current (ac) dielectric relaxation process, dielectric loss and loss tangent, ac conductivity, etc.

An analysis of the results would be done using existing theories to understand the structural, optical and electrical behavior of the thin films and also to understand their relations. Finally, the suitability of thin films in electrical, electronic and/or optical devices would be evaluated.

1.4 Thesis Layout

Chapter 1 is the introductory chapter begins with a general introduction followed by a review of the earlier research works on the plasma polymerized thin films and the objectives of the thesis.

Chapter 2 discusses the fundamental aspects of plasma, polymers, their classification and general properties, plasma polymerization mechanism, different reactors geometries for plasma polymerization, different types of glow discharge, advantages and disadvantages of plasma polymers, applications of plasma polymerized thin films, theory of solids etc.

Chapter 3 describes the experimental details related with the structural, optical and electrical characterization of plasma polymerized thin films which includes the descriptions of monomers and substrate materials, capacitively coupled glow discharge plasma polymerization set up for polymer formation, the thickness measurement method, contact electrode deposition technique for electrical measurement etc.

Chapter 4 describes the existing theories for structural characterization of plasma polymerized thin films, e.g. the theory of FTIR, TGA, DTA etc and the corresponding experimental results are also discussed.

The existing theories for optical characterization of plasma polymerized thin films are described in Chapter 5 and the corresponding experimental results e.g. optical absorption, absorption coefficient, extinction coefficient, direct and indirect energy band etc are also discussed.

Chapter 6 describes the existing theories of direct current electrical conduction in plasma polymerized thin films, and discusses the corresponding experimental results, e.g. J-V characteristics, Conduction mechanism, temperature dependent conductivity etc.

Chapter 7 describes the existing theories of alternating current electrical conduction in plasma polymerized thin films, and discusses the corresponding experimental results e.g. frequency and temperature dependence of ac conductivity and dielectric constants, dielectric relaxation, dielectric loss, Cole-Cole plots etc.

Finally the thesis is folded up with conclusions and suggestions for future work in chapter 8.

References

[1] Yasuda, H., *Plasma Polymerization*, Academic Press; New York, 1985.

[2] Chowdhury, F.-U.-Z., and Bhuiyan, A. H., *An investigation of the optical properties of plasma-polymerized Diphenyl thin films*, Thin Solid Films, 306, 69-74, 2000.

[3] Bell, A. T., and Shen, M., (Eds.), *Plasma Polymerization*, American Chemical Society, Washington, D.C., 1979.

[4] d' Agostino, R., Ed.; *Plasma deposition, treatment, and etching of polymers*, Academic Press: Boston, 1990.

[5] Chermisinoff, N. P., *Handbook of Polymer Science and Technology*, Vol. 4 Marcel Dekker Inc., New York, 1989.

[6] Biederman, H., and Osada, Y., *Plasma Chemistry of Polymers*, Advance in Polymer Science, Berlin, 1990.

[7] Morita, S. and Hattori, S., *Applications of Plasma Polymers,* in "Plasma Deposition, Treatment, and Etching of Polymers"; R d'Agostino, (Ed.), Academic Press, San Diego, CA, 1990.

[8] Evsyukov, S. E., Gautheron, F., Hoffken, H. W., Born, K., *Synthesis, X-ray structure, and polymerization of 1-Vinyl-3-cyanomethylimidazolium Chloride*, J. Appl. Polym. Sci., 82, 499-509, 2001.

[9] Moser, E. M., Faller, C., Pietrzko, S. , Eggimann, F., *Modeling the functional performance of plasma polymerized thin films*, Thin Solid Films, 355-356, 49-54, 1999.

[10] Morales, J., Olayo, M. G., Cruz, G. J., Olayo, R., *Synthesis by plasma and characterization of bilayer aniline–pyrrole thin films doped with iodine* J. Poly. Sci. Polym. Phys., 40, 1850-1856, 2002.

[11] Morosoff, N., in *An Introduction to Polymerization, Plasma Deposition, Treatment and Etching of Polymers*, Edited by R. d'Agostino, Academic Press, Inc., Boston, 1990.

[12] Poll, H.U., Arzt, M., and Wickleder, K.H., Eur. Polym. J. 12, 505, 1976.

[13] Yasuda, H., Bumgarner, M. O., Marsh, H. C., Morosoff, N., *Plasma polymerization of some organic compounds and properties of the polymers*, J. Polym. Sci. Polym. Chem., 14, 195-224, 1976.

[14] Westwood, A. R., Eur. Polym. J., 7, 377, 1971.

[15] Jesch, J. , Bloor, J. E., Kronick, P. C., J. Polym. Sci., 14, 1487, 1966.

[16] Akther, H. and Bhuiyan, A. H., *Infrared and ultra violet-visible spectroscopic investigation of plasma polymerized N,N,3,5 -tetramethylaniline thin films*, Thin Solid Films 474, 14-18, 2005.

[17] Bhuiyan, A. H., Rajopadhye, N.R., Bhoraskar, S.V., *A few electronic properties of thin films of plasma-polymerized acrylonitrile* , Thin Solid Films, 161, 187-195, 1988.

[18] Sakthi Kumar, D., Kenji Nakamura, Satoko Nishiyama, Shigeru Ishii, Hiromichi Noguchi, Kunihiro Kashiwagi, and Yasuhiko Yoshida; *Optical and electrical characterization of plasma polymerized pyrrole films* J. Appl. Phys., 93, 2705-2711, 2003.

[19] John Rajan, K., and Sakthi Kumar, D., *Structural, electrical, and optical studies of plasma-polymerized and iodine-doped poly pyrrole*, J. Appl. Polym. Sci., 83, 1856-1859, 2002.

[20] Eufinger, S.,. Van Ooij, W. J, Ridgway, H., *DC plasma-polymerization of pyrrole: comparison of films formed on anode and cathode*, J. Appl. Polym. Sci., 61, 1503 -1514, 1996.

[21] Ion, R. M., Scarlat, F., and. Niculescu, V. I. R., *Methylene-Blue Modified Polypyrrole Film Electrode for Optoelectronic Applications*, Journal of Optoelectronics and Advanced Materials 5, 109 -114, 2003.

[22] Joseph Mathai, C., Saravanan, S., Anantharaman, M. R., Venkitachalam, S., and Jayalekshmi, S., *Effect of iodine doping on the band gap of plasma polymerized aniline thin films*, J. Phys. D: Appl. Phys. 35, 2206 – 2210, 2002.

[23] Sajeev, U. S., Joseph Mathai, C., Saravanan, S., Rajeev R. Ashokan, Venkatachalam, S., Anantharaman, M. R., *On the optical and electrical properties of rf and a.c. plasma polymerized aniline thin films*, Bull. Mater. Sci., 29, 159-163, 2006.

[24] Tamirisa Prabhakar, A., Liddell KNona, C., Pedrow Patrick, D., Osman Mohamed, A., *Pulsed-Plasma-Polymerized Aniline Thin Films* , J. Appl. Polym. Sci. 93, 1317-1325, 2004.

[25] Kateryna Bazaka, Mohan V. Jacob, Robert A. Shanks, *Fabrication and Characterization of RF Plasma Polymerized Thin Films from 3,7-Dimethyl-1,6-octadien-3-ol Electronic and Biomaterial Applications*, Advanced Materials Research 123-125, 323-326, 2010.

[26] Xiao, H., Xiongyan Zhao, Uddin, A-., and Lee, C.B., *Preparation, characterization and electronic and optical properties of plasma-polymerized nitrites*, Thin Solid Films 477, 51-57, 2005.

[27] Michaël Lejeune, Frédéric Brétagnol, Giacomo Ceccone, Pascal Colpo, François Rossi; *Microstructural evolution of allylamine polymerized plasma films*, Surface & Coatings Technology 200, 5902-5907, 2006.

[28] Zhao Xiong-Yan, Wang Ming-Zhu, and Xiao Jun; *Deposition of plasma conjugated polynitrile thin films and their optical properties*, European Polym. J. 42, 2161-2167, 2006.

[29] Saloum, S., Alkhaled, B., *Growth Rate and Sensing Properties of Plasma Deposited Silicon Organic Thin Films from Hexamethyldisilazane Compound*, ACTA PHYSICA POLONICA A 3, 484-489, 2010.

[30] Bae, I.-S., Jung, C. -K., Cho, S. J., Song, Y.-H., Boo, J.-H., *A comparative study of plasma polymerised organic thin films on their electrical and optical properties*, J. Alloys and Compounds, 449, 393-396, 2008.

[31] John T. Grant , Jiang, H., O'Neill, K., Eyink, K., Johnson, W. E., Johnson, E. M., Tullis, S., Tomlin, D. W., Fleitz, P., Bunning, T. J., *The characterization of polymer thin films grown by plasma polymerization*, MTAEC 38, 3, 2004.

[32] Kouta Hosono, Ichiro Mastubaia, Norimitsu Murayama, Woosuck Shin and Noriya Izu; *Effects of discharge power on the structure and electrical properties of plasma polymerized polypyrrole films*, Mater, Lett. 58, 1374, 2004.

[33] Zhang, J., Ooij, W. V., France, P., Datta, S., Radomyselkiy, A., and Xie, H., *Investigation of deposition rate and structure of pulse DC plasma polymers*, Thin Solid Films 390, 123-129, 2001.

[34] Kim, M.C., Cho, S.H., Han, J. G., Hong, B.Y., Kim, Y.J., Yang, S. H., and Boo, J. H, *High-rate deposition of plasma polymerized thin films using PECVD method and characterization of their optical properties*, Surf. Coat. Technol. 169-170, 595-599, 2003.

[35] Silverstein, M. S., Visoly-Fisher, I., *Plasma Polymerized thiophene : molecular structure and electrical properties*, Polymer 43, 11-20, 2000.

[36] Fang Jianglin, Chen Hong, and Yu Xuhai; *Studies on Plasma Polymerization of Hexamethyldisiloxane in the presence of Different Carrier Gases*, J. Appl. Polym. Sci. 80, 1434 -1438, 2001.

[37] Varma, M. C. P. , J. Appl. Chem., 8, 117, 1958.

[38] Lewis, I.C., and Edstrom, T., Proc. Fifth Carbon Conf., Pergamon press, London, 413, 1962.

[39] Akther, H. and Bhuiyan, A. H., *Space charge limited conduction in plasma polymerized N,N,3,5 tetramethylaniline thin films,* Thin Solid Films 488, 93-97, 2005.

[40] Akther, H. and Bhuiyan, A. H., *Electrical and optical properties of plasma polymerized N,N,3,5, -tetramethylaniline thin films*, New J. Phys. 7, 173, 2005.

[41] Valaski, R., Ayoub, S., Micaroni, L., Hümmelgen, I. A., *Influence of electrode material on charge transport properties of polypyrrole thin films*, Thin Solid Films 388, 171-176, 2001.

[42] Valaski, R., Ayoub, S., Micaroni, L., Hümmelgen, I. A., *Influence of thin thickness on charge transport of electrodeposited polypyrrole thin films*, Thin Solid Films, 415, 206-210, 2002.

[43] Joseph John, Sajeev Sivraman, Jayalekhmy, S., Anantharaman, M. R., *Investigations on the mechanism of carrier transport in plasma polymerized pyrrole thin films*, Journal of Physics and Chemistry of Solids, 71, 935-939, 2010.

[44] Sajeev Sivaraman and AnantharamaN, M. R., *Derermination of charge carrier transport in radio frequency plasma polymerized aniline thin films*, J. Phys. D; Appl. Phys. 43, 1-5, 2010.

[45] Morales, J., Olayo, M. G., Cruz, G. J., Castillo-Ortega, M. M., and Olayo, R., *Electronic conductivity of pyrrole and aniline thin films polymerized by plasma*, J. Appl. Polym. Sci., 38, 3247-3255, 2000.

[46] Zaman, M., and Bhuiyan, A. H., *Direct current electrical conduction mechanism in plasma polymerized thin films of tetraethylorthosilicate*, Thin Solid Films, 517, 5431-5434, 2009.

[47] Ma. Guadalupe Olayo, Guillermo J. Cruz, Salvador López, Juan Morales, and Roberto Olayo; *Conductivity and Activation Energy in Polymers Synthesized by Plasmas of Thiophene*, J. Mex. Chem. Soc. 54, 18-23, 2010.

[48] Tengku Nadzlin Bin Tengku Ibrahim, Kunihiko Tanaka, and Hisao Uchiki; *Optical and electrical properties of organic films prepared by RF plasma chemical vapor deposition using mixed naphthalene and propane source*, Japanese J. Appl. Phys., 47, 794-796, 2008.

[49] Prashant Shukla and Gaur, M. S., *Investigation of electrical conduction mechanism in double- layered polymeric system*, J. Appl. Polym. Sci, 114, 222-230, 2009.

[50] Goodman, J., J. Polymer. Sci. , Lett. Ed., 44 (144), 551-552, 1960.

[51] Chowdhury, F.-U.-Z., and Bhuiyan, A. H., *Dielectric properties of plasma polymerized diphenyl thin films*, Thin Solid Films 370, 78-84, 2000.

[52] El-Nahass, M. M., Zeyada, H. M., El-Samanoudy, M. M., El-Menyawy, E. M., *Electrical conduction mechanisms and dielectric properties of thermally evaporated N-(p-dimethylaminobenzyllidene)-p-nitroaniline thin films*, J. Phys. Condens Mat., 18, 5163-5173, 2006.

[53] Liang, T., Makita, Y., Kimura, S., *Effect of film thickness on the electrical properties of polyimide thin films*, Polymer 42, 4867-4872, 2001.

[54] Saravanan, S., Joseph Mathai, C., Venkatachalam, S., and Anantharaman, M. R., *Low k thin films based on rf plasma-polymerized aniline*, New J. Phys. 6, 64, 2004.

[55] Sakthi Kumar, D., and Yasuhika Yoshida, *Dielectric properties of plasma polymerized pyrrole thin film capacitors*, Surf. Coat. Technol, 169-170, 600-603, 2003.

[56] Joseph Mathai C., Saravanan, S., Anantharaman, M. R., Venkitachalam, S., and Jayalekshmi, S., *Characterization of low dielectric constant polyaniline thin film synthesized by ac plasma polymerization technique*, J. Phys. D: Appl. Phys. 35, 240-245, 2002.

[57] Ram, M. K., Annapoorni, S., Panday, S. S., and Malhotra, B. D., *Dielectric relaxation in thin conducting polyaniline films*, Polymer, 39, 3399-3404, 1998.

[58] Huang, Q. F., Yoon Rusli, S. F., Zhang, Q., and Ahn, J., *Dielectric properties of molybdenum-containing diamond-like carbon films deposited using electron cyclotron resonance chemical vapor deposition*, Thin Solid Films 409 211-219, 2002.

[59] Muhammad Akram, Athar Javed, Tasneem Zahra Rizvi, *Dielectric Properties of Industrial Polymer Composite Materials*, Turk J. Phys., 29, 355- 362, 2005.

[60] Hao Jiang, Lianggou Hong, Venkatasubramanianc, N., John T. Granc, Kurt Eyink, Kevin Wiacek, Sandra Fries-Carr, Jesse Enlow, Timothy J. Bunning; *The relationship between chemical structure and dielectric properties of plasma-enhanced chemical vapor deposited polymer thin films*, Thin Solid Films 515, 3513-3520, 2007.

Chapter 2

Fundamental Aspects of Plasma, Polymer and Plasma Polymerization

Fundamental aspects of plasma, polymer, and plasma polymerization would be discussed in this chapter

2.1 Introduction

Plasma polymerization is an important technique for fabricating thin polymer films from almost any organic or inorganic gas. Through plasma polymerization, a very thin (<10 nm), uniform, pinhole-free, highly resistive, highly adherent, chemically inert and flawless film with a high cross-link density, low solubility, and unusually high thermal stability can be obtained in a solvent-free process. It is a unique and rather unconventional thin film technology which yields polymers having properties completely different from those of conventional polymers. Since the plasma polymer (PP) films have cross-linked structure and have good chemical and physical stability, these are used in the areas where mechanical, thermal, and electrical strengths are necessary [1-3].

2.2 The Polymers

2.2.1 Introduction : Origin of Polymer Science

Polymers (or macromolecules) are very large molecules made up of smaller units, called monomers or repeating units, covalently bonded together in any conceivable pattern. The word polymer was derived from the classical Greek words “poly” meaning “many” and “mers” meaning “parts”. The molecules of the polymers usually exist in the form of long chains and each chain consists of a large number of small molecules. The chains may be linear, branched or cross-linked [4]. The shape of the building block monomer unit and the degree of cross-linking are the main factors affecting the polymer chain structure. The properties of polymers are strongly influenced by details of chain structure. Simple examples of a polymer chain are shown in Figure 2.1 (a) and (b). Polymer chains may contain of the order 10^3-10^5 monomer units [4]. The end groups’ effect on the properties of the bulk material is very small.

Polymers are thought to be colloidal substances i.e., glue-like material; which refuse to crystallize and exhibit high viscosity in solution and diffuse slowly in liquids. Thus these materials are different from crystalloids substances consisting of small particles that can diffuse in liquids easily when in solutions. The specific molecular structure (chainlike structure) of polymeric materials is responsible for their intriguing mechanical properties.

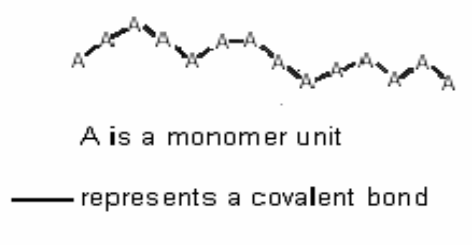

Figure 2.1 (a) A Simple Polymer Chain

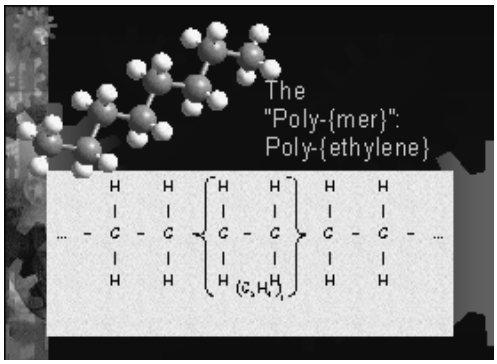

Figure 2.1 (b) A Polymer Chain of polyethylene

Certain polymers available in nature are protein, cellulose, silk etc. while many others including polystyrene, polyethylene and nylon are produced only by synthesis. Natural polymers such as proteins, nucleic acids and cellulose serve us as food, clothes, medicine and many other useful materials [5]. They are also found in many forms such as horns of animals, tortoise shell, shellac (from the *lac* beetle), rosin (from pine trees), asphalt, and tar from distillation of organic materials. One of the most useful of the natural polymers was rubber, obtained from the sap of the *hevea* tree.

The first synthetic polymer, a phenol-formaldehyde polymer, was introduced under the name “Bakelite”, by Leo Baekeland in 1909. Its original use was to make billiard balls. Rayon, the first synthetic fiber was developed as a replacement for silk in 1911. Ever since a huge variety of synthetic polymers have been manufactured and find application in almost every area of the modern world.

Polymer science was born in the great industrial laboratories of the world of the need to make and understand new kinds of plastics, rubber, adhesives, fibers, and coatings. Only much later polymer science came to academic life. Despite the importance of polymers, details of their molecular structure remained a mystery until 1922, when Hermann Staudinger proposed the correct structure model of polymer molecules [6]. Perhaps because of its origins, polymer science tends to be more interdisciplinary than most sciences; combining chemistry, chemical engineering, materials, and other fields as well. However, the scientists of that day realized that they did not understand many of the relationships between the chemical structures and the physical properties that resulted. The research that ensued forms the basis for physical polymer science. Many polymers crystallize, and the size, shape, and organization of the crystallites depend on how the polymer was crystallized. Other polymers are amorphous, often because their chains are too irregular to permit regular packing. The onset of chain molecular motion heralds the glass transition and softening of the polymer from the glassy (plastic) state to the rubbery state. Mechanical behavior includes such basic aspects as modulus, stress relaxation, and elongation to break. Each of these is relatable to the polymer’s basic molecular structure and history.

2.2.2 Different Types of Polymers

Depending on the different functional groups and structures in the field of macromolecules, polymers are classified in various ways listed below

- **Origin :** Natural, Semi synthetic, Synthetic.
- **Chemical Structure :** Homochain (single, double, triple bonds), Heterochain.
- **Line Structure :** Linear, Branched, Cross-linked.
- **Monomer Arrangement :** Copolymers (two different repeating units in their chain), Ter polymers (three chemically different repeating units)
- **Thermal Processing Behavior :** Thermoplastic, Thermosetting plastic
- **Polymerization Mechanism :** Adition (step growth), Condensation (chain growth)
- **Tacticity :** Isotactic, Syndiotactic, Atactic
- **Structure :** Non- crystalline (amorphous) , Semi-crystalline, Crystalline.

2.2.2.1 Natural Polymers

Living organisms make many polymers, nature's best. Natural polymers are those already existing in the universe from time immemorial. Most such natural polymers strongly resemble step-polymerized materials. However, living organisms make their polymers enzymatically, the structure ultimately being controlled by DNA, itself a polymer. Natural polymers such as proteins, nucleic acids and cellulose serve us as food, clothes, medicine and many other useful materials. They are also found in many forms such as horns of animals, tortoise shell, shellac, rosin, asphalt, and tar from distillation of organic materials

Natural polymers are sometimes referred as natural products or renewable resources. Wool and silk are both proteins. All proteins are actually copolymers of polyamide-2 (or nylon-2, old terminology). As made by plants and animals, however, the copolymers are highly ordered, and they have monodisperse molecular weights, meaning that all the chains have the same molecular weights. Cellulose and starch are both polysaccharides, being composed of chains of glucose-based rings but bonded differently. Natural rubber, the hydrocarbon polyisoprene, more closely resembles chain polymerized materials.

2.2.2.2 Synthetic Polymers

The first synthetic polymer was introduced under the name "Bakelite", by Leo Baekeland in 1909. Rayon, the first synthetic fiber was developed as a replacement for silk in 1911. Ever since a huge variety of synthetic polymers have been manufactured. At initial stage the synthesis was aimed at making substitutes for the natural macro molecules rubber and silk; but a vast technology has grown up, that now produces hundreds of substances that have no natural counterparts. Synthetic macromolecular compounds include elastomers, fibers

and plastics. Elastomers have the particular kind of elasticity of rubber. Fibers are long, thin and thread like. They have great strength along the length of the fibers that characterizes cotton, silk and wool. Plastics can be extruded as sheets or pipes, painted on surfaces or molded to from countless objects. In the search by the early organic chemists for pure compounds in high yields, many polymeric substances were discovered. The concept extending the structure to very high molecular weights by continued condensation was understood. Other condensation polymers were prepared in succeeding decades.

2.2.2.3 Homochain Polymers and Heterochain Polymers

In the case of polyethylene the backbones of the molecular chains are built up by carbon (C) atoms. However, this is not always the case. In some polymers the backbones are constructed by atoms of another element, or even by atoms of several elements. For example the molecular chains of polydimethylsiloxane are constructed by silicon (Si) and oxygen O atoms. If the backbone is formed by atoms of one single element, the polymer is called a homochain polymer. If the backbone is formed by atoms of two or more elements, the polymer is called heterochain polymer [7].

2.2.2.4 Linear, Branched and Cross-linked Polymers

The classification of polymers is also done according to their architecture which can vary in different ways. In Figure 2.2 three possible molecule architectures are depicted.

A linear polymer consists of a long chain of monomers. A branched polymer has branches covalently attached to the main chain. Cross-linked polymers have monomers of one chain covalently bonded with monomers of another chain. Cross-linking results in a three-dimensional network; the whole polymer is a giant macromolecule. Elastomers are loosely cross-linked networks while thermosets are densely cross-linked networks. Elastomers, however, are rubbery polymer that can be stretched easily to several times their unstretched length and which rapidly returns to their original dimensions when the applied stress is released.

Polymers are also classified as linear (one-dimensional) and three-dimensional. Linear polymers are substances composed of linear molecules. Linear molecules are also called polymer chain. Polymers composed of molecules linked together by chemical bonds (cross bond), so that a three dimensional space network is formed, are said to be three dimensional. If the cross bonds are so few and far between that the lengths of linear polymer molecules contain a great number of molecular units, the three-dimensional polymers are additionally called cross linked and the lengths are called network chains. Linear polymers are soluble, able to form true solutions and can exist in the liquid state. Three dimensional polymers are infusible and insoluble; they can only swell in the solvent, absorbing a limited amount of it and retaining, in the main, the properties of solids.

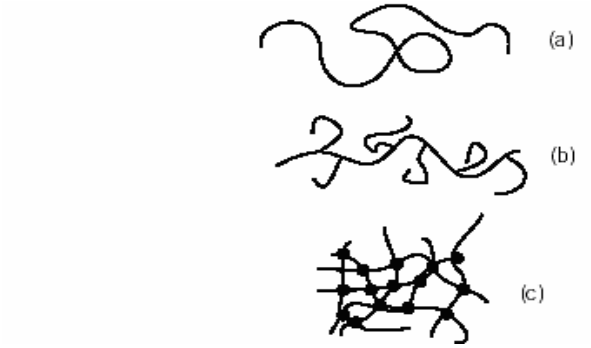

Figure 2.2 Types of molecular configuration (a) Linear chain (b) Branched molecule and (c) Cross-linked network

2.2.2.5 Homopolymer and Copolymer

Another classification of polymers is based on the chemical type of the monomers. Homopolymers consist of monomers of the same type; copolymers have different repeating units. Furthermore, depending on the arrangement of the types of monomers in the polymer chain, we have the following classification:

- In *random* copolymers two or more different repeating units are distributed randomly.
- *Alternating* copolymers are made of alternating sequences of the different monomers
- In *block* copolymers long sequences of a monomer are followed by long sequences of another monomer
- *Graft* copolymers consist of a chain made from one type of monomers with branches of another type.

Figure 2.3 is a presentation of homopolymer and different types of copolymer.

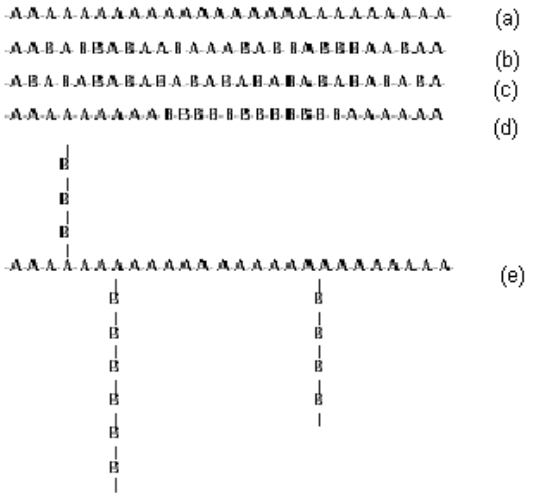

Figure 2.3 (a) Homopolymer (b) Random copolymer (c) Alternating Copolymer (d) Block copolymer (e) Graft copolymer

2.2.2.6 Thermoplastics and Thermosetting Plastics

Polymers are also divided into two categories according to their thermal processing behavior: Thermoplastics and Thermosetting Plastics. Thermoplastics, such as polyethylene, nylon and polystyrene are mixture of molecules and can be heated up to liquid state and be remoulded. Thermosetting plastics such as vulcanized rubber and epoxy resin have highly cross-linked molecular structures, that is, all molecules are chemically bonded together to form a percolating network. If thermosetting plastics are heated up they will decompose before becoming liquids.

Molecules in a thermoplastic are held together by relatively weak intermolecular forces so that the material softens when exposed to heat and then return to its original condition when cooled. Thermoplastic polymers can be repeatedly softened by heating and then solidified by cooling. Most linear and slightly branched polymers are thermoplastic. A thermosetting plastic or thermoset, on the other hand, solidifies or sets irreversibly when heated, and can not be reshaped by heating. Thermosets usually are 3-dimensional networked polymers and are formed by the condensation polymerization process. These polymers posses a high degree of cross-linking between polymer chain, which restrict the motion of the chain and lead to a rigid material. Figure 2.4 shows the structures of thermoplastic and thermosetting plastic.

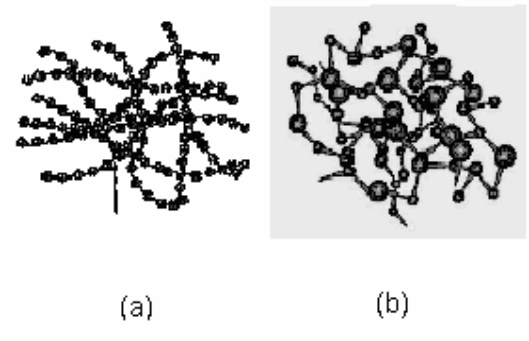

Figure 2.4 Structure of (a) thermoplastic and (b) thermosetting plastic

2.2.2.7 Crystalline and Amorphous States of Polymer

The most important properties in polymer usually result from the fact that how the atoms and chains are linked together in space. The morphology of most polymers is semi-crystalline consisting of both crystalline and amorphous regions i.e., they form mixtures of small crystals and amorphous material and melt over a range of temperature instead of at a single melting point. The crystalline material shows a high degree of order formed by folding and stacking of the polymer chains and the atoms are arranged in a regular three-dimensional

array in this type of solids. There is a basic unit, called the unit cell, which is repeated throughout the structure in all three dimensions. Crystalline solids have a well-defined transition melting point. The reason for having a well-defined melting point is that crystalline molecules are bound by similar forces: the energy needed to break the bonds is the same. Polymer chains are very long; it is very difficult for the chains to fit into a perfect crystalline arrangement. Amorphous materials are materials whose molecules have no regular order structure. Glass is an example of this structure; the forces binding the molecules together will vary. Thus the material will not have a well-defined melting temperature. These materials go through a glass transition state with an average temperature Tg [8]. An amorphous solid is formed when the chains have little orientation throughout the bulk polymer. The glass transition temperature is the point at which the polymer hardens into an amorphous solid. This term is used because the amorphous solid has properties similar to glass.

In the crystallization process, it has been observed that relatively short chains organize themselves into crystalline structures more readily than longer molecules. Therefore, the degree of polymerization (DP) is an important factor in determining the crystallinity of a polymer. Polymers with a high DP have difficulty organizing into layers because they tend to become tangled. The cooling rate also influences the amount of crystallinity. Slow cooling provides time for greater amounts of crystallization to occur. Fast rates, on the other hand, such as rapid quenches, yield highly amorphous materials. The crystalline region of polymer forms what are called *lamellae* and a group of lamellae can then form spherulites [7-10]. Lamellae are large parallel chains of polymers molecules. Lamellae formations achieve a very high degree of crystallization surrounded by amorphous region. The amorphous region contains most of the physical and chemical impurities.

2.3 From Little Molecules to Big Molecules

The behavior of polymers represents a continuation of the behavior of smaller molecules at the limit of very high molecular weight. As a simple example, consider the normal alkane hydrocarbon series. These compounds have the general structure H{—CH_2—}$_n$H, where the number of — CH_2— groups, *n*, is allowed to increase up to several thousand.

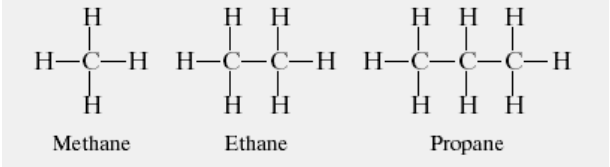

At room temperature, the first four members of the series are gases. *n*-Pentane boils at 36.1°C and is a low-viscosity liquid. As the molecular weight of the series increases, the viscosity of the members increases. Although commercial gasolines contain many branched-chain materials and aromatics as well as straight-chain alkanes, the viscosity of gasoline is

markedly lower than that of kerosene, motor oil, and grease because of its lower average chain length.

These latter materials are usually mixtures of several molecular species, although they are easily separable and identifiable. This point is important because most polymers are also “mixtures”; that is, they have a molecular weight distribution. In high polymers, however, it becomes difficult to separate each of the molecular species, and people talk about molecular weight averages.

Compositions of normal alkanes averaging more than about 20 to 25 carbon atoms are crystalline at room temperature. These are simple solids known as wax. It must be emphasized that at up to 50 carbon atoms the material is far from being polymeric in the ordinary sense of the term.

2.4 Cross-link in Polymers

Highly cross-linked structure is the most significant property of plasma polymers to distinguish it from the conventional polymers. Cross-linking in polymer means, in addition to the bonds which hold monomers together in a polymer chain, many polymers form bonds between neighboring chains. These bonds can be formed directly between the neighboring chains, or two chains may bond to a third common molecule. Though not as strong or rigid as the bonds within the chain, these cross-links have an important effect on the polymer. Polymers with a high enough degree of cross-linking have "memory." When the polymer is stretched, the cross-links prevent the individual chains from sliding past each other. The chains may straighten out, but once the stress is removed they return to their original position and the object returns to its original shape.

2.5 Major Polymer Transitions

Crystallization is an example of a first-order transition, in this case liquid to solid. Most small molecules crystallize, an example being water to ice; this transition is very familiar. A less classical transition is the glass–rubber transition in polymers. The major polymer transitions are presented in Figure 2.5.

At the glass transition temperature, T_g, the amorphous portions of a polymer soften. The most familiar example is ordinary window glass, which softens and flows at elevated temperatures. Yet glass is not crystalline, but rather it is an amorphous solid. It should be pointed out that many polymers are totally amorphous. Carried out under ideal conditions, the glass transition is a type of second-order transition. The basis for the glass transition is the onset of coordinated molecular motion is the polymer chain. At low temperatures, only vibrational motions are possible, and the polymer is hard and glassy (Figure 2.5, region 1).

In the glass transition region, region 2, the polymer softens, the modulus drops three orders of magnitude, and the material becomes rubbery. Regions 3, 4, and 5 are called the rubbery plateau, the rubbery flow, and the viscous flow regions, respectively.

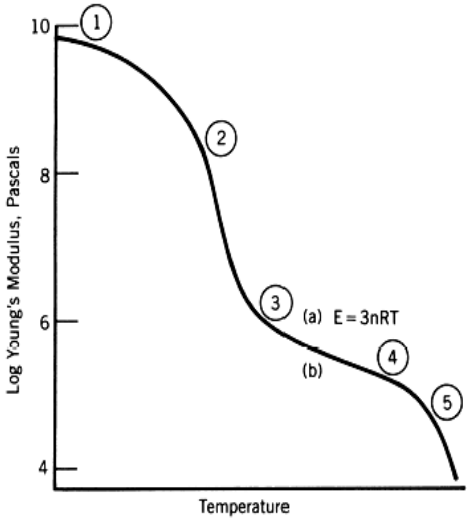

Figure 2.5 Idealized modulus–temperature behavior of an amorphous polymer.

2.6 Plasma

Fundamentally, Plasma is a gas, which is partially ionized, either through heating or through photo-ionization, and is composed of electrons, ions, photons and various neutral species at many different levels of excitation [11] and which has a low enough density to behave classically. There being approximately the same density of positive charges as of negative in plasma. In point of fact it is not necessary for both groups of charge carriers to be mobile for the system to display plasma characteristics; one group can be stationary, as for example, are the positive lattice ions of a metallic solid. For plasma to display plasma characteristics, however the average distances, between the plasma charged particles must be very much smaller than the physical dimensions of the total plasma.

The classical definition of plasma limits the term, to an appreciably ionized gas or vapor that conducts neutral fluids *hot* and viscous. The modern definition is less restrictive, plasma simply connoting a more or less ionized gas. The plasma created by electric glow discharge is often called low temperature plasma or *cold* plasma (low electron density plasma) to distinguish it from hot plasma (high electron density or fully ionized plasma).

Plasmas can be generated in a variety of ways depending on the application such as combustion flames, electrical discharges, controlled nuclear reactions, shocks and other means. Plasma generation devices include low-pressure electrical discharges or glow

discharge (direct current and alternating current), Penning plasma discharges, microwave-generated plasma devices, radio frequency (rf) capacitive discharges, and rf inductively coupled (IC) plasma devices.

The technique of most interest is the glow discharge. In glow discharge system, plasmas are produced when energy is transferred by an electric field to free electrons within a low-pressure environment. The free electrons collide with molecules and any other surfaces exposed to the plasma [12]. Through inelastic electron collisions with molecules, more electrons, ions, free radicals, and molecules in excited states are generated, and this results in the plasma state. Plasmas produced by this technique are called non-equilibrium or cold plasmas in contradiction to equilibrium plasmas created by arcs or plasma jets. The term non-equilibrium means that there is no thermal equilibrium between electrons and other neutral species and ions. The ambient temperature of plasma in a plasma polymerization reaction however is generally in the vicinity of 380 to 400 K and remains reasonably constant after a steady-state condition is established.

Equations (2.1-a) and (2.1-b) show how radicals can be formed in a noble gas or oxygen plasma. Cold gas oxygen plasmas contain species such as O+, O-, O_2+, O, and O_3, as well as ionized ozone and metastably-excited O_2 and free electrons. Each of the energetic fragments is very reactive with other fragments, and any surfaces exposed to the plasma, mostly via free radical chemistry. Plasma pretreatments using non-polymerizable gases remove carbonaceous contaminants from a surface while simultaneously altering substrate chemistry in other ways [13].

Helium: $He \rightarrow h\nu + He + He^{+} + e$ (2.1-a)

Oxygen: $O_2 \rightarrow O_2^{*} + O + O_2^{+} + O^{+} + e^{-}$ (2.1-b)

Table 2.1 lists typical bond dissociation energies for various organic and inorganic species. In glow discharges, electrons typically have bombardment energies of 20 eV or less (Table 2.2), which is enough energy to break most covalent bonds. In low-pressure cold plasmas, electrons do not achieve thermodynamic equilibrium with gas molecules, and thus the temperature of the plasma remains close to ambient. This important feature allows plasma polymerization to be carried out without thermal degradation of reactants or products [1].

The analyses of plasmas are far harder to model than solids, liquids and gasses because they act in a self-consistent manner. The separation of electrons and ions produce electric fields and the motion of electrons and ions produce both electric and magnetic fields. The electric fields then tend to accelerate plasmas to very high energies while the magnetic fields tend to guide the electrons.

Table 2.1 Typical bond dissociation energies [11].

Bond	Dissociation Energy (eV)
C-C	3.61
C=C	6.35
C=C (π bond)	2.74
C-H	4.3
C-N	3.17
C=N	9.26
C-O	3.74
C=O	7.78
C-F	5.35
C-Cl	3.52
N-H	4.04
O-H	4.83
O-O	1.52

Table 2.2 Energy available in a glow discharge [14].

Species	Energy (eV)
Electrons	0-20
Ions	0-2
Metastables	0-20
UV/Visible	3-40

Based on the relative temperatures of the electrons ions and neutrals, plasmas are classified as thermal or non-thermal. Thermal plasmas have electrons and the heavy particles at the same temperature i.e. they are in thermal equilibrium with each pother. Non-thermal plasmas, on the other hand, have the ions and neutrals at a much lower temperature (ambient temperature) whereas electrons are much 'hotter'. Plasma is sometime referred to as being hot if it is nearly fully ionized or cold if only a small fraction (for example 1 %) of the gas molecules is ionized. Even in 'cold' plasma the electron temperature is still typically several thousand degrees. Plasmas utilized in plasma technology (technological plasmas) are usually cold in this sense.

Since thermal decomposition breaks interatomic bonds before ionizing, most terrestrial plasmas begin as gases. In fact, plasma is sometimes defined as a gas that is sufficiently ionized to exhibit plasma-like behavior. Note that plasma-like behavior ensues after a remarkably small fraction of the gas has undergone ionization. Thus, fractionally ionized gases exhibit most of the exotic phenomena characteristic of fully ionized gases. Plasmas resulting from ionization of neutral gases generally contain equal numbers of positive and

negative charge carriers. In this situation, the oppositely charged fluids are strongly coupled, and tend to electrically neutralize one another on macroscopic length-scales. Such plasmas are termed quasi-neutral ("quasi" because the small deviations from exact neutrality have important dynamical consequences for certain types of plasma mode). Strongly non-neutral plasmas, which may even contain charges of only one sign, occur primarily in laboratory experiments: their equilibrium depends on the existence of intense magnetic fields, about which the charged fluid rotates. It is sometimes remarked that 95% of the universe consists of plasma. In earlier epochs of the universe, everything was plasma. In the present epoch, stars, nebulae, and even interstellar space, are filled with plasma. The solar system is also permeated with plasma, in the form of the solar wind, and the Earth is completely surrounded by plasma trapped within its magnetic field.

2.7 Plasma Polymerization

2.7.1 Introduction

Plasma polymerization refers to the formation of polymeric materials under the influence of plasma. Because the most practical means of carrying out plasma polymerization involves the use of an electric glow discharge in a vacuum. The term glow discharge polymerization has been used, in every practical sense, synonymously with plasma polymerization [2], although plasma polymerization can be carried out by means of other than glow discharge.

Unlike conventional polymerization, most of the reactions in plasma polymerization are one-step reactions between two reactive species. Some other reactions are between an activated species and a molecule, which are essentially the same as the propagation reaction of the conventional addition polymerization. Such reactions can proceed in a chain mechanism if the reacting molecule has the appropriate molecular structure. However, even in such cases the formation of polymerization is because of the very low ceiling-temperature of addition polymerization in vacuum.

In the polymerization process the gaseous monomers, stimulated through plasma, condense on freely selectable substrates, as high cross-linked layers. Condition for this process is the presence of chain-producing atoms, such as carbon, silicium or sulfur, in the working gas. As the monomer molecules in plasma, for the most part, become shattered into reactive particles, there remain at most, only partially preserved chemical structures of the output gases in the product, which results in cross-linked and disordered structure (Figure 2.6). Structural preservation and cross-linking gradients can be controlled through process parameters, such as pressure, working gas-flow and applied electrical output; so that one can also construct so called gradient layers; i.e with increasing degree of crosslinking over the thickness.

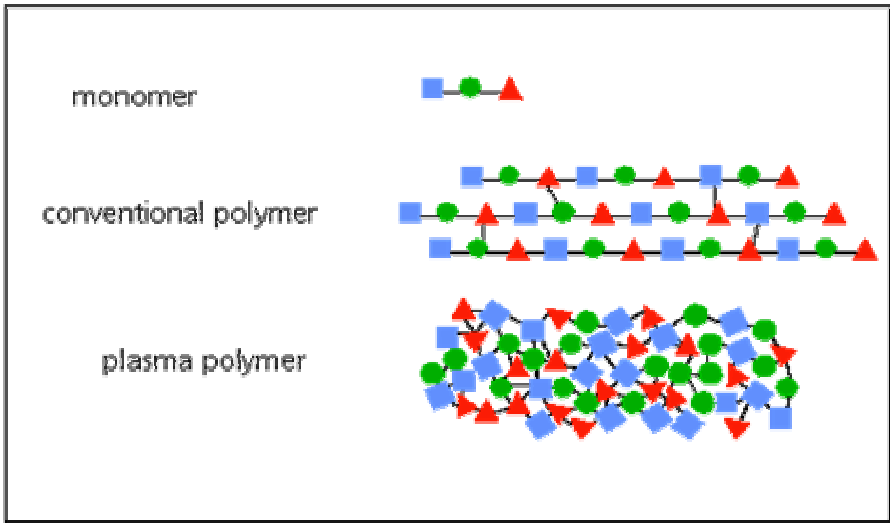

Figure 2.6 Polymer produced by conventional polymerization and plasma polymerization

Plasma polymerization is usually initiated and generated in the vapor phase during the plasma process and sometimes the materials deposition process in this method is called plasma enhanced chemical vapor deposition (PECVD). As polymerization proceeds, the growing polymer can not remain in the vapor phase and diffuse to a surface. Reactive species in the gas phase such as ions and free radicals, may simultaneously interact with surfaces inside the plasma reactor that have been activated by the impact of the glow discharge to form ions or free radicals from the surface molecules of substrates.

However, the advantages of PECVD are as follows :

- Plasma enhances the kinetics of the chemical reactions by ionization and the dissociation of the reactive molecules. In plasma the kinetic obstacles can be overcome without increasing the temperature to unacceptably high value.
- The starting feed gases used may not contain the type of functional groups normally associated with conventional polymerization.
- The PECVD is an environmental benign technology and the coating is often highly coherent and adherent. The polymerization may be achieved without using solvent.
- Plasma polymer coating can be easily adjusted and by repeating the same processing, the multilayer coating can be achieved.
- Through careful control of the polymerization parameters, it is possible to tailor the films with respect to specific chemical functionality, thickness, and other chemical and physical properties.

2.7.2 Different Geometries of Reactors

The plasma polymers are strictly system dependent, and therefore it is important to discuss different types of plasma reactor geometry. The most widely used reactor configurations for plasma polymerization can be broadly divided into three classes, namely, reactors with internal electrodes, reactors with external electrodes and reactors without electrodes.

2.7.2.1 Reactors with Internal Electrodes

Reactors with internal electrodes have different names, e.g., bed, parallel plates, planar, etc. Their main features are power supply, vacuum chamber, electrode, and eventually one or more substrate holders. Among the internal electrode arrangement, a bell-jar type reactor with parallel plate metal electrodes is most frequently used, by using ac (1 – 50 KHz) and rf fields for plasma excitation. The vacuum chamber can be made either of glass or of conducting materials, such as metal, to better shield from external sources. Pump-out is usually is at the base of the bell-jar. Monomer injection may be at the base or at some other convenient position over the electrodes or through the centre of upper electrode. The electrodes may be oriented horizontally or vertically.

Figure 2.7 shows different types of reactors. For a dc or low frequency discharges, internal electrodes are required. A common set up is to place circular or square electrodes in a bell-jar. If the electrodes diameter is relatively large and they are placed relatively close together a large zone of uniform electric field is created. For this reason this geometry is favored for industrial applications.

2.7.2.2 Reactors without Electrodes

The name electrode-less reactor implies that no impurities can be sputtered off and incorporated into the growing films. In these reactors, microwave power systems characterized by tubular or pyrex reactors and by a resonant cavity coupled with power supply in the GHz region (typically 2.45 GHz). The plasma is generated in the resonant cavity and the polymer is generally collected outside the glow region.

2.7.2.3 Reactors with External Electrodes

External electrode reactors can be either capacitively or inductively coupled; power is transmitted from the power supply to the gas by a capacitor and coil respectively. Insulating tubular reactors are usually utilized (glass, quartz or alumina for reactor materials). Inductively coupled tubular reactors, when operating at low pressure (<< 1 torr), are not uniformly coupled to the power supply; however, coupling uniformly increases with the increasing working pressure.

At sufficiently high frequencies, the electrodes may be placed outside the reactor vessel ("electrode-less glow discharge"). Such electrodes may be curved to match a cylindrical vessel and create an electric field perpendicular to the cylindrical axis. Alternatively two cylindrical electrodes may be wrapped around the cylinder to create an electric field roughly parallel to it. Finally, a coil may be wrapped around the cylinder with an electric field between the ends of the coil exciting the glow discharge. This arrangement is known as inductively coupling.

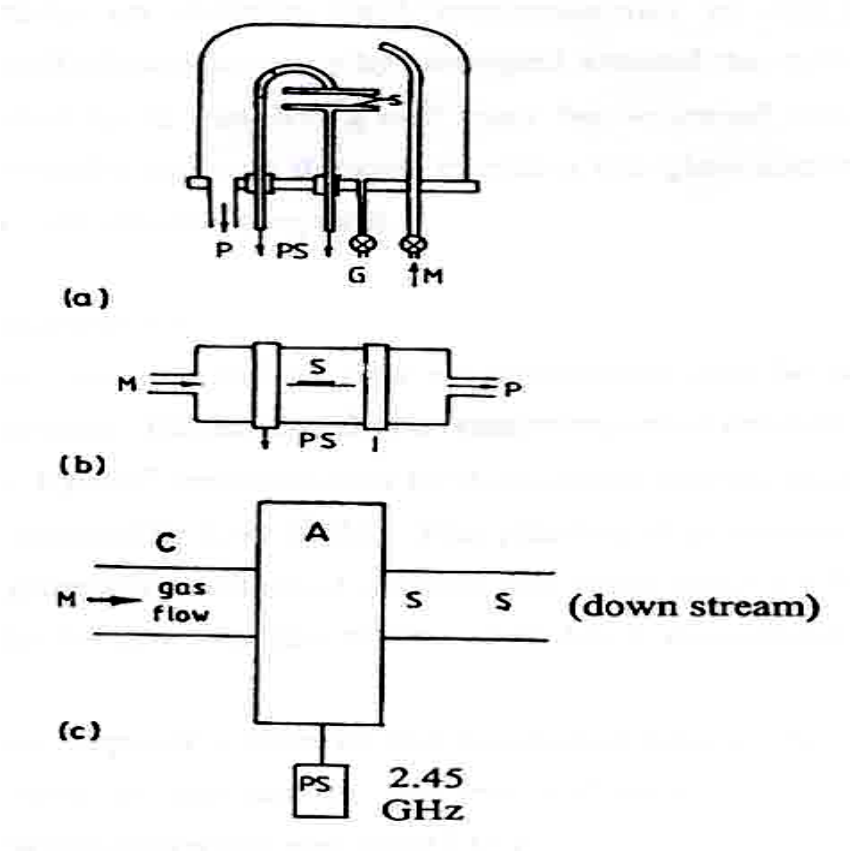

Figure 2.7 Different types of Reactors (a) Reactors with internal electrodes (b) Reactors without electrodes and (c) Reactors with external electrodes and

2.7.3 Different Types of Glow Discharge

The dc/ac glow discharge in organic gas results in the production of a large number of species. These species are energetic neutrals and neutral fragments of parent monomer molecules in ground of excited states. Depending on the discharge condition, both ions and neutrals vary in their molecular weight arising from collisions with electrons. These electrons causes discharge typically, and have average energy of 5-10eV, which is more than sufficient to break the chemical bonds that are usually having binding energies within 3-9 eV. Generally, free radicals are considered the most important species for plasma polymerization.

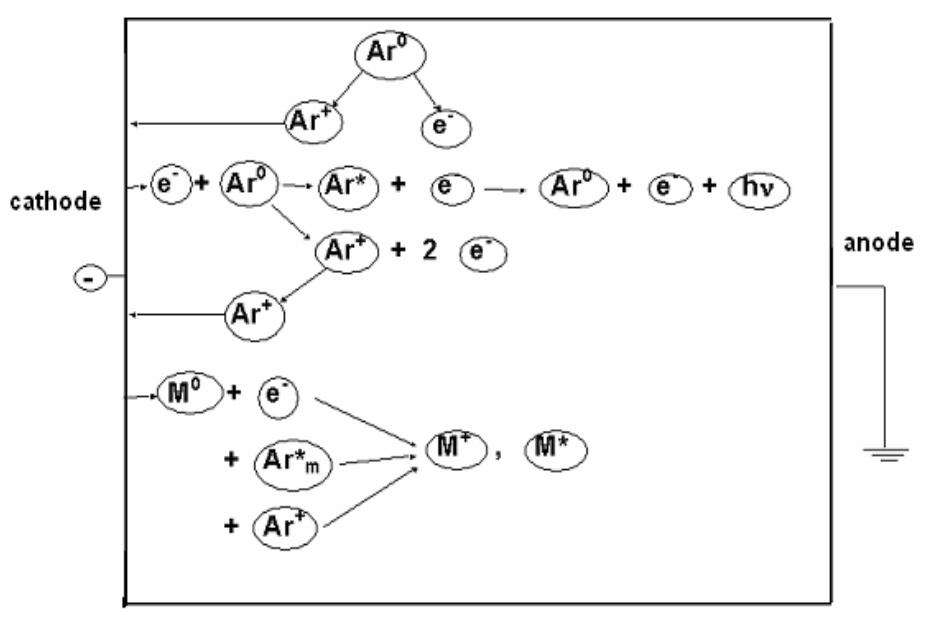

Figure 2.8 Schematic representation of the basic processes in a glow discharge.

A glow discharge is a kind of plasma i.e., an ionized gas consisting of equal concentrations of positive and negative charges and a large number of neutral species. In the simplest case, it is formed by applying a potential difference (of a few 100 V to a few kV) between two electrodes that are inserted in a cell (or that form the walls of the cell). The cell is filled with a gas (an inert gas or a reactive gas) at a pressure ranging from a few mtorr to atmospheric pressure. Due to the potential difference, electrons that are emitted from the cathode and give rise to collisions with the gas atoms or molecules (excitation, ionization, dissociation). The excitation collisions give rise to excited species, which can decay to lower levels by the emission of light. This process is responsible for the characteristic name of the "glow discharge". The ionization collisions create ion-electron pairs. The ions are accelerated toward the cathode, where they release secondary electrons. These electrons are accelerated away from the cathode and can give rise to more ionization collisions. In its simplest way, the combination of secondary electron emission at the cathode and ionization in the gas, gives rise to self-sustained plasma.The character of the gas discharge critically depends on the frequency or modulation of the current.

2.7.3.1 Direct Current Glow Discharge

A glow discharge can be established if a gaseous phase of any bifunctional or polyfunctional compounds between two electrodes are subjected to the influence of dc electric field under low pressure. For a dc glow discharge, the mechanism involves the bombardment of the electron with positive ions resulting in the generation of secondary electrons. These in turn are accelerated away from the cathode until they have gained enough energy to ionize a

molecule or atom by inelastic collision. Such ionization produces additional electrons and ions. An electron can transfer essentially all its energy to an atom or molecule by inelastic collision, but very little by elastic collision. This is a consequence of the fact that the mass of electron is almost negligible relative to the mass of atom or molecule.

2.7.3.2 Alternating Current Glow Discharge

If the gaseous phase of monomer is subjected to an alternating electric field, the glow discharge is also achieved. But, the mechanism of glow discharge is changed with the frequency. At low frequencies (e.g., 50 Hz), the glow discharge polymerization is simply as the form of dc glow discharge. With increasing frequency, the motion of ions can no longer follow the periodic changes in the field. When the frequency of the applied voltage is more than a few kHz, positive ions become immobile and the positive space charge is partially retained from one half-cycle to the next (this helps the discharge to reinitiate). An increase of the frequency in to MHz region causes no significant displacement of either electrons or positive ions and losses of charged species from diffusion and recombination processes are replaced by electron-impact ionization of neutral gas molecules in the discharge volume. This type of discharge is called radio frequency (rf) glow discharge (100 kHz – 30 MHz). However, at frequencies above 500 kHz, the motion of ions is lost to the walls and electrodes within the production region of the glow discharge chamber. The mechanism, by which the electrons pick up sufficient energy to cause bond dissociation or ionization, involves random collision of electrons with gas molecules, and the electron picks up an increment of energy with each collision. It is well known that, a free electron in vacuum under the action of an alternating electric field oscillates with its velocity 90° out of phase with the field and thus obtains energy, on the average, from the applied field. The electron can gain energy from the field only as a consequence of elastic collision with the gas atoms; the electric field converts the random motion of electrons to ordered oscillatory motion. Because of its interaction with the oscillatory electric field, the electron gains energy on each collision until it acquires enough energy to be able to make an inelastic collision with a gas atom. Some fraction of these inelastic collisions results in ionization.

2.7.4 Working Principle of Plasma Polymerization

Plasma polymerization process usually takes place in low temperature plasma, which is generated by glow electrical discharges operated in a molecular gas under low pressure. The energy transfer from electrons to gas molecules leads to the formation of a host of chemically reactive species such as radicals and ions, which along with photons cause a variety of plasma-chemical reactions. Plasma polymerization is an ultra-thin film processing technology and covers very important subject area that can be recognized as comprising the vacuum deposition of covalently bonded materials.

In plasma polymerization process the monomer gas is pumped into a vacuum chamber where it is polymerized by plasma to form a thin, clear coating. The monomer starts out as a liquid. It is converted to a gas in an evaporator and is pumped into a vacuum chamber. A glow discharge initiates polymerization. Plasma polymerization occurs due to the dissociation of covalent bonds in gas phase molecules, and subsequent reactions between gas phase species and surfaces result in the deposition of polymeric materials. Dissociation results from interactions between monomer and energetic species, such as ions, electrons, photons, and excited neutrals created in the glow discharge. The generation of reactive species which take part in the deposition of polymeric films under vacuum can be achieved by the interactions of monomer and energetic species or by thermolysis of monomer.

The energetic species can cause considerable fragmentation of the original monomer. The activated fragments are recombined, sometimes accompanying rearrangement, and the molecules grow to large molecular weight ones in a gas phase or at the surface of the substrate. The process is done in a low pressure, low temperature plasma. This means the temperature in the chamber never really rises above room temperature. Plasma polymerization is essentially a PECVD process. It refers to the deposition of polymer films through plasma dissociation and to the excitation of an organic monomer gas and subsequent deposition and polymerization of the excited species on the surface of the substrate

2.7.5 Growth Mechanism

The study of plasma polymerization kinetics is commonly employed to elucidate polymerization mechanism. With this background a comparison of the polymer formation rates of various monomers by plasma polymerization would provide an overview of the kind of reaction mechanism responsible for plasma polymerization.

In plasma polymerization *generation* of free radicals and atoms are occurred, at first, by collisions of electrons and ions with monomer molecules, or by dissociation of monomers absorbed on the surface of the sample. Secondly, *propagation* of the formation of polymeric chain which can take place both in the gas phase (by adding radical atoms to other radicals or molecules) and on the deposited polymer film (by interaction of the surface free radicals with either gas phase or absorbed monomers). Finally, *termination* can also take place in the gas phase or at the polymer surface, by similar process as in the propagation step, but ending either with the final product or with a closed polymer chain. The individual steps and reaction that occur in plasma polymerization generally depends on the system.

The probable chain growth polymerization is represented by :

$$M_n^* + M \rightarrow M_{n+1}^*$$

where M_n^* is the reactive chain carrying species and M is the monomer molecules. The rapid step-growth mechanism is very likely to be the reaction in plasma polymerization and this reaction is expressed as :

$$[M_m^* + M_n^* \rightarrow M_{m+n}^*] \times N$$

where N represents the number of repetitions of similar reactions. In this case, the reaction occurs between molecules.

If *M* is a difunctional reactive species the overall polymerization is represented by

$$n^* M^* \rightarrow^* (M_n)^*$$

On the other hand if the reactive species are monofunctional (M*), such as free radical R*, the reaction is given by

$$M_m^* + M_n^* \rightarrow M_{m+n}$$

which is essentially a termination process, that occurs in free radical polymerization and does not contribute without additional elementary steps. Yasuda and Lamaze pointed out that the reactivation of the product of an elementary reaction was bound to occur in plasma.

The overall polymerization mechanism based on the rapid step growth principle is shown in Figure 2.9.

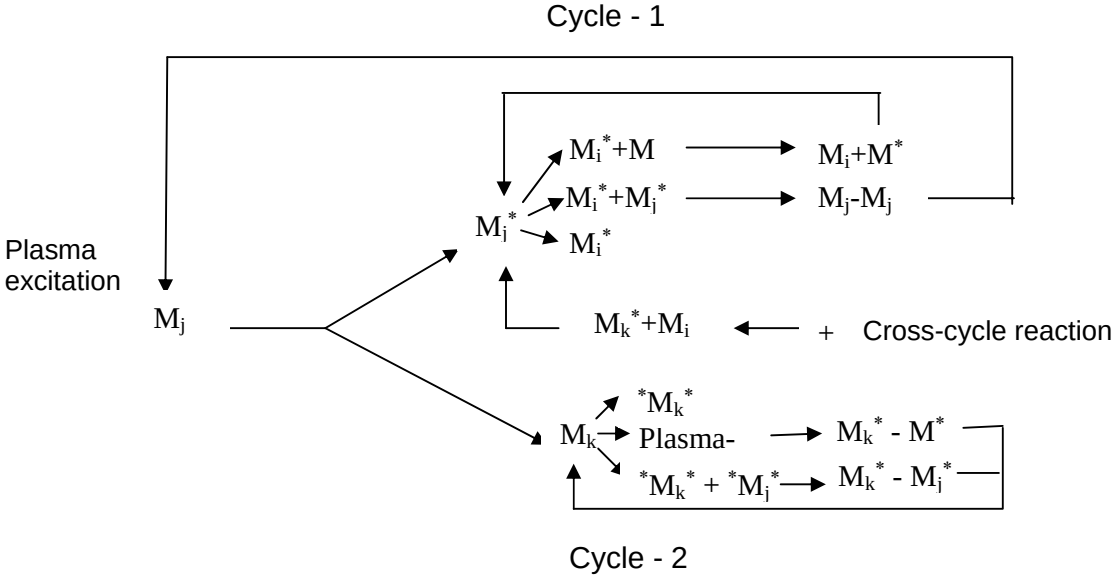

Figure 2.9 Schematic representation of step-growth mechanism in plasma polymerization.

In the Figure 2.9, M_x refers to a neutral species, M* is the monofunctional activated species and *M* is the difunctional, The subscripts i, j, k indicate the difference in the size of species involved. Cycle I is via the repeated activation of the reaction products from monofunctional activated species, and cycle II is that of difunctional. The species participating in the rapid step growth polymerization can be mono- or multifunctional (radical, cation, cation-radical, diradical, etc).

2.7.6 Deposition of Plasma Polymerized Thin Film

The deposition of thin films on solid substrates by the plasma polymerization process has been practiced for over two decades [1, 11, 15]. The characteristics of the plasma-formed films (adhesion, mechanical properties, extent of crosslinking, etc) are dictated by the choice of kinetic formation parameters such as power input, plasma pressure, and reaction time [16]. The plasma polymerization of simple organic monomers (e.g. hydrocarbons) produces films that are highly cross-linked, pinhole-free, thermally and chemically stable, and very adherent. Furthermore, plasma polymerized (PP) films can be prepared from monomers that cannot be polymerized by conventional chemical techniques (e.g. methane, ethane, saturated hydrocarbons, organo-metallics) [17].

Free radicals are formed in plasmas by bond breakage that occurs upon the absorption of energy generated in the plasma. Through inelastic collisions, monomers are fragmented into activated species or into their constituent atoms. The activated fragments are recombined and rearranged by a rapid step growth mechanism, and deposition occurs due to a loss of kinetic energy upon collision of the activated species with the substrates or walls of the reactor. The loss of kinetic energy is due either to a chemical reaction of the species or increased molecular weight [11]. The activated species for film formation come from the gas phase, but the actual film formation proceeds at the substrate surface. Deposited species containing unpaired electrons are highly unstable, and the molecules become highly reactive at the surface of exposed substrates. The repetition of activation/fragmentation and recombination leads to film formation. This concept is significantly different than the mechanism of conventional polymerization. Additionally, any gases in a reaction vessel (e.g. nitrogen and oxygen) may be activated into their corresponding radicals and may be incorporated into the films by radical recombination reactions [18]. Consequently, polymers formed in plasmas generally have complex, highly crosslinked structures due to the large number of reaction pathways available during plasma excitation [19]. Carrier gases assist deposition by increasing ionization and ion energies in the plasma and subimplantation at the surface. The fragmentation of hydrocarbon starting materials in a plasma is best represented by two types of reactions: the elimination of hydrogen and C-C bond scission. Figure 2.10 shows the predominant sources of free radicals for hydrocarbons exposed to a plasma.

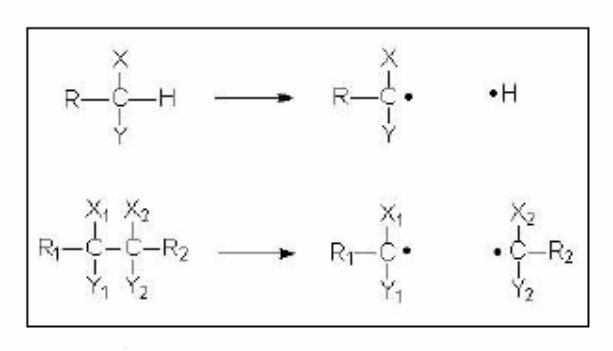

Figure 2.10 Hydrogen elimination and C-C bond scission of hydrocarbons exposed to a plasma.

While most ionization requires energy greater than 10 eV, the dissociation of a molecule requires less energy. For example, the energy required to dissociate a C-C bond is 3.61 eV [11]. In a plasma, the scission of bonds occurs much more frequently than does the formation of ions. Bond scission does not occur as a consequence of the ionization of molecules, but rather it occurs simultaneously with ionization

In spite of the complexity of plasma polymerization processes, the main set of parameters governing a given process may be optimized and then successfully reproduced [20]. Discharge power, flow rate, frequency of excitation, and working pressure are not independent variables and must all be optimized for a particular polymerization process.

The concentration of residual free radicals produced by a plasma decays rapidly when specimens activated by a plasma are exposed to the atmosphere after treatment. The concentration decreases by half in less than a minute due to oxidation of the surface by the atmosphere and the formation of peroxides. If a plasma treated surface is left under vacuum, residual free radicals are active for considerably longer, and are available to react with any reactive species introduced into the chamber.

Plasma polymerization mechanisms can be distinguished by the type of monomer used in the polymerization process. If the monomer is unsaturated, the plasma may induce polymerization by creating reactive species in the electrical discharge, and the molecular weight then increases by a more conventional step-growth fashion. In the plasma polymerization of saturated carbon compounds, the monomer is fragmented by the plasma into reactive species that recombine and condense on the substrate surface. These polymers, because of the smaller size of the activated species, are very different in structure and stoichiometry than conventionally formed polymers [21].

It is generally accepted that very little polymerization occurs in the gas phase, where the monomer is fragmented. Instead, energetic species reach the substrate surface and are converted to highly energetic neutral species. The most stable species deposit onto the substrate and form a number of three-dimensional islands that usually have very different

chemistry from the precursor. Surface migration of atoms to these islands causes them to grow, and continued growth results in the islands coalescing to form an interconnected network of islands [22]. These films are typically highly crosslinked and conjugated [23].

Polymerization rate must be clearly distinguished from deposition rate because they are often very different and involve different mechanisms. The deposition rate of a plasma polymer is dependent on more parameters than the polymerization rate. The deposition rate is dependent upon the chemical composition of the substrate, the topography of the substrate, the geometry of the reactor, the reactivity of the monomer, the flow rate, the working gas pressure, the temperature of the substrate, the power, and the frequency of the power source [24, 25]. The substrate temperature is an important parameter to consider when examining deposition rates; the deposition rate decreased with increasing substrate temperature in most studies [26]. Polymer deposition rate shows a distribution according to substrate position in the reaction chamber because of the heterogeneity of the concentration of active species and monomers in the reaction vessel.

The plasma deposited films, however, have got many advantages, such as :

- **Pinhole-free:** Under common reaction conditions, the plasma films appear to coalesce during formation in to a uniform over-layer, free of void. This continuous barrier structure is suggested by transport studies and electrical studies.
- **Barrier Film:** The pinhole-free and dense, cross-linked nature of these films suggests that they have potential as barrier and protective films, many study bear this out.
- **Unique Substrate :** Plasma deposited polymeric films can be placed upon almost any solid substrate including metals, ceramics and semiconductors. Other surface grafting or surface modification technologies are highly dependent upon the chemical nature of the substrate.
- **Low Leaches :** Due to their highly cross-linked nature, plasma deposited film contains negligible amounts of low molecular weight components that might lead to an adverse biological reaction. In addition, the plasma deposited over-layers can prevent leaching of the molecular weight species from the substrate.
- **Unique Film Chemistry :** The chemical structure of the polymeric over-layer films produced by radio frequency plasma deposition can not be synthesized by conventional organic chemical methods. Complex gas phase molecular rearrangements account for these unique surface chemical compositions.

2.7.7 Competitive Ablation and Polymerization

Two types of polymerization processes may occur during plasma processes: plasma induced polymerization and plasma-state polymerization. Plasma-induced polymerizations occur only with unsaturated monomers and are essentially step-growth polymerizations

initiated by the reactive species contained in the plasma. Plasma-state polymerizations are atomic processes that can only occur in plasma and produce non-polymer-forming byproducts.

When a monomer gas enters the plasma region, it instantly becomes a complex mixture of the original monomer, forming ionized and excited species and fragments, as well as gaseous products that do not participate in the polymerization. When a polymerizable and chemically reactive material is introduced to plasma, particles can be deposited, ablated, and re-deposited if they collide with a solid surface before they are evacuated. The plasma is constantly in contact with the reactor walls, the solid substrate, and the substrate mount, and polymer-forming intermediates and gas by-products originate from these solids, as well. Within a given monomer–reactor system, the total reactor pressure at constant temperature is a function of only the feed flow rate and the pumping rate. However, once plasma is initiated, the situation changes dramatically; the pressure becomes a function of the reactions occurring within the plasma. Extending the definition of ablation to include ablation of the solid phase and fragmentation of the gas-phase species, ablation processes contribute to a pressure increase, while plasma polymerization processes contribute to a pressure decrease. In other words, if polymerization processes dominate, a pressure drop is expected when the plasma is ignited; if ablation processes dominate, a pressure increase is expected.

This type of behavior is an example of the Competitive Ablation and Polymerization (CAP) model of plasma polymerization developed by Yasuda and Hsu [27]. An example of this process occurs during the plasma polymerization of carbonyl sulfide and C_2F_4, among others. Deposition rates for these polymerizations increase rapidly, marked by a pressure decrease, until reaching a distinct maximum (in different power regions for different flow rates), and then begin to decrease rapidly. These observations were rationalized as follows: At a low level of energy input, polymerization is dominant, which results in the deposition rate increasing with increasing power. However, above a certain threshold of energy input, ablation processes become significant enough to contribute to the processes of the system. Ablation processes eventually become dominant, and polymer deposition is severely hindered.

Fluorine and oxygen show a significant tendency to induce ablation during plasma processes [28]. Ablation processes occurring during the plasma polymerization of oxygen- or fluorine-containing compounds are generally attributed to the reactive species of these two elements generated during fragmentation [29]. The effect of the ablation process, which continues to increase with increasing power after the deposition plateau, is to decrease the deposition rate. The CAP model is a phenomenological representation of the atomic (fragmentation) type of deposition that approximates most plasma polymerization processes much better than molecular models based on conventional step-growth polymerization reactions [30]. The CAP model does not apply to all monomers. Methane in the plasma state, for example, only shows a decrease in pressure due to its low ablation rate [20].

Figure 2.11 summarizes the different processes that are competing during plasma polymerization and deposition. Note the many processes in competition that inevitably lead to a very complicated structure being deposited.

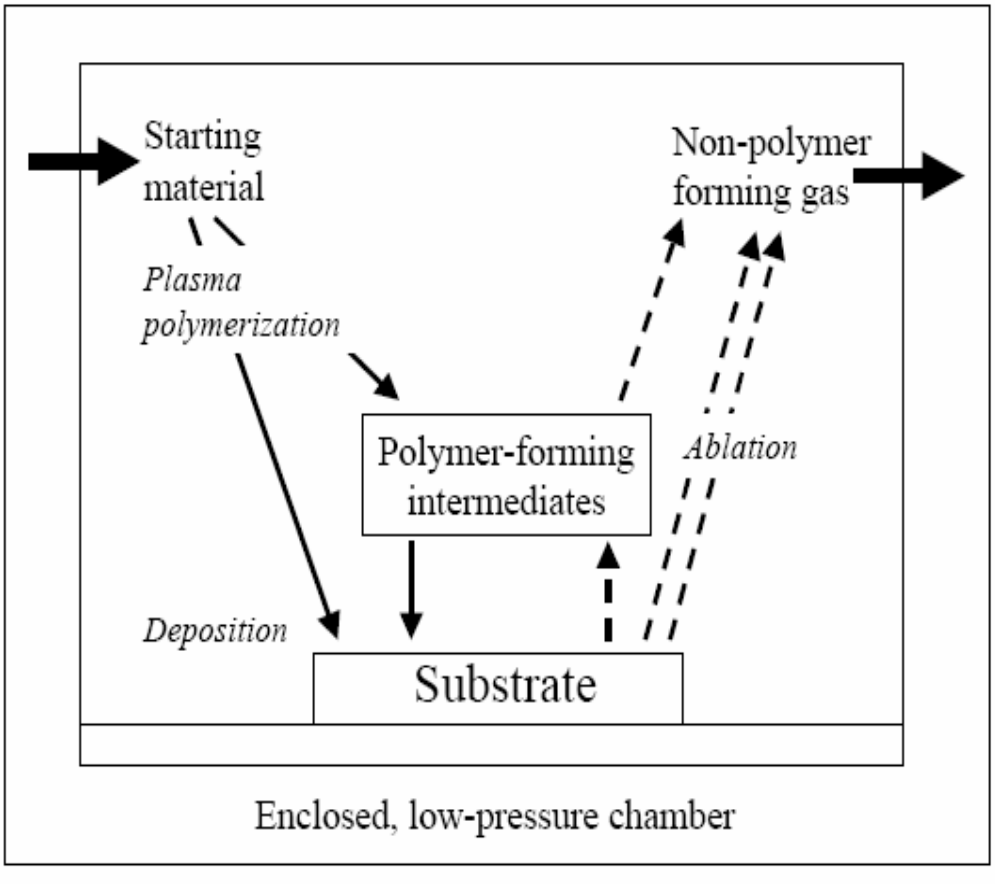

Figure 2.11 Plasma processes occurring during plasma polymerization [30].

It was mentioned that even when the same monomer is used for plasma polymerization at constant operational conditions (flow rate, discharge power, reaction pressure, etc.), polymers with identical chemical composition are never obtained when a different reactor is used or when substrate position is varied [18]. This is a direct result of the CAP processes that occur. Plasma polymerization processes show intense system dependence, owing to the nature of the polymerization and ablation processes that are occurring simultaneously.

2.7.8 Oxidation in Plasma Polymer Films

Most PP films contain trapped free radicals that readily react with atmospheric oxygen and H_2O after deposition [13, 31]. As discussed by Yasuda et al. [32] films with a large density of free radicals are often produced in plasma polymerization. These free radicals can be long lived, surviving for many days and even months after deposition. Consequently, oxygen incorporation into the film most likely arises from post-deposition chemical reactions between

the radicals and oxygen and water vapor molecules from ambient air [31]. In a study by Durrent et al. [33], amorphous hydrogenated and oxygenated carbon films were deposited from C_6H_6/O_2/He/Ar mixtures in an rf plasma deposition system. The presence of C=O absorption bands in the FTIR spectrum of a PP film was interesting in films deposited when the oxygen flow rate was zero, because no O_2 was deliberately introduced into the chamber. These results indicated that, unless oxygen is present in the reaction chamber during a plasma process, the incorporation of oxygen PP films does not occur until it is exposed to the atmosphere.

Figure 2.12 shows a possible oxidation process for organic PP films. The scheme shown is representative; the reactions are not balanced and the figure does not show all of the possible reactants and products.

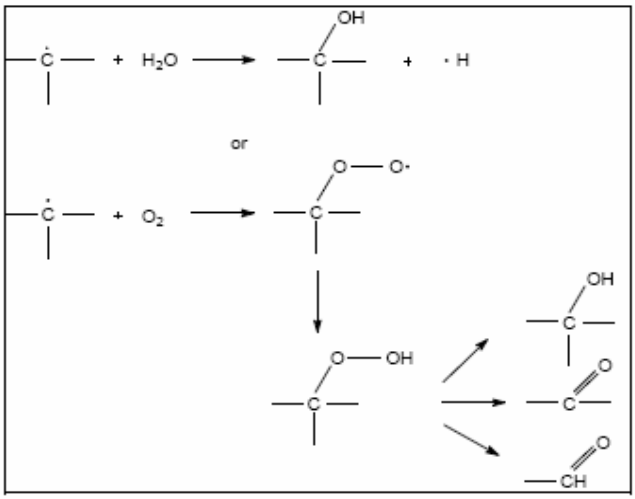

Figure 2.12 Proposed oxidation of free radicals [31].

2.7.9 Adsorption, Adhesion and the Interface

Adsorption theory best explains a variety of adhesion properties, and states that molecular forces arising from primary and secondary interactions are responsible for adhesion [34]. Furthermore, materials adhere because of the interatomic and intermolecular forces that are established between the substrate and the adhesive [35]. Provided there is good interfacial contact, van der Waals interactions (dipole-dipole interactions and induced dipole-dipole interactions), acid-base interactions, or hydrogen bonding should be sufficient for good adhesion. Since molecular energies across an interface decrease drastically with increasing intermolecular distance, this theory stresses intimate molecular contact. The formation of primary bonds across an interface (covalent, ionic, or metallic), termed chemisorption, is also included under this theory.

There is strong evidence favoring the adsorption (and chemisorption) mechanism to explain strong metal-polymer adhesion. Bonding enhancement may result from the creation of chemical groups on the stabilized metal surface that produce covalent linkages or acid-base interactions with the adhesive [36].

Interfacial phenomena have a significant influence on all biological and industrial processes and are of fundamental importance to the science of adhesion. The interface or intrphase can be defined as a transition zone between the surface of a substrate and the bulk of a polymer that is solidified against the substrate. It may also be defined as a region of material whose chemical or physical structures have been modified because of contact between two different phases. Unfortunately, the boundaries of the interface are difficult to define.

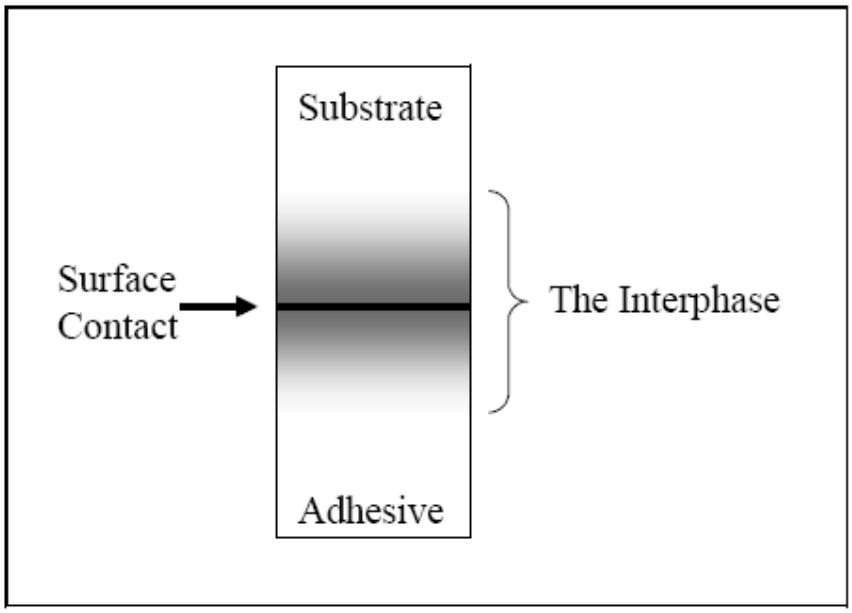

Figure 2.13 The interfacial region [37].

Figure 2.13 shows a typical system where an adhesive and a substrate meet. The interfacial zone is defined by the location of the boundary lines. The boundaries are positioned to include the entire region where there are non-zero gradients in composition or density. Most metal surfaces that have been exposed to the atmosphere are covered with some type of oxide layer [38]. Aluminum metal exposed to the atmosphere contains a thin, tough oxide layer which pacifies the surface and prevents continued oxidation. Formation of the oxide layer involves chemisorption of oxygen on the surface, followed by a chemical reaction to form the oxide [39]. This oxide layer is thin and is covered with low molecular weight organic molecules and water adsorbed from the atmosphere. Adsorbed contaminants are problematic and difficult to completely eliminate because as the surface concentration of contaminants decreases, the binding energy of the remaining contaminants increases.

2.7.10 Advantages and Disadvantages of Plasma Polymerization

Plasma polymerization is a new material preparation process. The material produced by plasma polymerization is vastly different from conventional polymers. The process is a completely dry process and the deposition is flawless. The plasma polymerization is capable of forming an ultra thin, uniform and pinhole free film containing a minimum amount of flaw. No catalytic agent is required to form polymers. The technique is preferred in many cases over conventional polymerization process due to the absence of minimization of undesirable by-products. An important contribution to the field of plasma polymerization is that one needs low cost equipment for laboratory experimentation and plant production.

Advantages

The following discussion also supports the advantages of the technique over conventional polymerization process :

- Hydrocarbons of any classes can be used for production of membranes.
- The films are precipitated at low pressures in a predetermined and controlled atmosphere, which yields non-porous pure films without any trace of moisture.
- There is a strong possibility of preparing films from organic compounds of variety of classes such as saturated, unsaturated, aliphatic, cyclic, aromatic and metalorganic monomers.
- Ability to vary the composition of films by changing the composition of the gaseous phase during deposition.

Disadvantages

The chemistry of plasma deposited material or films on a surface are often not well defined. The apparatus used to produce plasma polymer can be expensive. Finally, contamination may be a problem and are must be exercised to prevent extraneous gases and pump oils from entering the reaction zone.

In spite of the drawbacks, plasma polymerization is far well developed process for many types of modification that simply can not be done by any other technique.

2.7.11 Some Differences between Plasma Polymer and Conventional Polymer

- Polymerization of the monomer to form a polymer or intermediate polymer to be further processed in succeeding steps in conventional polymerization, but plasma polymers are not characterized by repeating units, as is typical for conventional polymers, i.e., it is a one-step process.

- In conventional polymerization, the properties of the polymer are determined by the monomer being used, but the properties of the plasma polymer are not determined by the monomer being used but rather by the plasma parameters.
- Plasma polymers have a higher elastic modulus than the conventional polymers. (May be due to dense cross-linkage of polymer chains).
- Low water vapour or gas permeability and low decay of wettability than the conventional polymers. (Due to cross linking).
- The properties of plasma polymer are much more dependent on the processing factors and morphology than the conventional polymers. For example, properties of plasma polymers are directly or indirectly related to the number of free radicals.
- Internal stress in a plasma polymer is a characteristic property which is not found in most conventional polymers.
- Solvent resistance of plasma polymers is generally higher than the conventional polymers.
- The surface energies of plasma polymers of hydrocarbons are generally higher than those of conventional hydrocarbon polymers due to the presence of oxygen containing groups [2].

2.7.12 Applications of Plasma Polymerized Thin Films

Potential applications of plasma polymerized thin films include adhesive bonding between the substrates and polymers, wettability characteristics, printability of polymers and so on. The use of plasma polymerized films may further benefits from the following significant advantages [17]:

- The starting material does not have to contain the type of functional groups normally associated with conventional polymerization.
- Plasma polymerized films are often highly coherent and adherent to a variety of substrates including conventional polymers, glass, and metal surface.
- Deposition is achieved without the use of solvents (environmentally benign process).
- The thickness of PP films can be easily varied from 20 Å to 1 μm.
- Through careful control of the plasma polymerization parameters, PP films can be tailored to contain specific functional groups.
- PP films can be deposited directly onto an activated substrate without breaking vacuum.
- The films are pinhole-free, uniform and crosslinked.
- The films have very high cross-linking density, and hence very low permeability.
- They are insoluble in solvent due to the highly cross-linked structure.
- PP films are relatively stable at high temperature.
- Multilayer films or films with grading of chemical or physical characteristics are easily made by this process.

Plasma polymerization for the deposition of thin films has achieved significant importance in several fields of applications such as microelectronics, the automobile industries and biomaterials. Of similar interest are plasma surface treatment techniques such as for cleaning, grafting, surface activation, and hydrophilic or hydrophobic finishing.

There are multi-dimensional uses of plasma polymerized materials. Only some potential applications are mentioned as follows:

- **In Optical Systems :** Polymer thin films produced in plasma are rigorously used as anti-reflection coating, anti-dimming coating, improvement of transparency, optical fibre, optical wave guide, laser and optical window, contact lens etc.

- **In Electrical Devices :** as insulator, thin film dielectric and separation membranes for batteries.

- **In Electronic Devices :** as integrated circuit elements. These films are also used as VLSI resists and in non-crystalline semiconductor and non-crystalline fine ceramic etching.

- **In Chemical Processing Systems :** as protective coating, adhesion improvement abrasion resistant coating, anti-creasing and scratching.

- **Biomedical Applications :** Thin films of plasma polymer are used in immobilized enzymes organelles and cells, sustained release of drugs and pesticides, sterilization and pasteurization, artificial kidney, blood vessel, blood bag, anti-clotting.

- **Filters and Membranes :** as reverse osmosis membrane, ion exchange membranes for reaction microprobes membranes for blood sieving, semi-permeable membranes to prepare porosity of any configuration and high cross-linking and for separation of gas mixture. The films prepared in plasma might also be utilized as filter for removal of air borne impurity.

- **In Textile :** Anti-flammability, anti-electrostatic treatment, dying affinity, hydrophilic improvement, water repellence, shrink-proofing.

References

[1] Riccardo d'Agostino (Ed.), *Plasma Deposition, Treatment and Etching of Polymers*, Academic Press, Boston, 1990.

[2] Yasuda, H., *Plasma Polymerization*, Academic Press, Inc, New York, 1985.

[3] Joel R. Fried, *Polymer Science and Technology*, Printic, Hall of India PV. LTD. New Delhi, India, 2002.

[4] Dissado, L. A., and Fothergill, J. C., *Electrical degradation and breakdown in polymers*. P. Peregrinus, London, 1992.

[5] Gauri Shankar Mishra, *Introductory Polymer Chemistry*. New Age International, New Delhi, India, 1993.

[6] Rolf MÄulhaupt, *Hermann Staudinger and the origin of macromolecular chemistry*, Angew. Chem. Int. Ed., 43, 1054, 2004.

[7] IUPAC. *A classification of linear single-strand polymers*, Pure Appl. Chem., 61, 243, 1989.

[8] Fried, J. R., *Polymer science and technology*, Prentice-Hall International Editions, London, 1995.

[9] Anderson, J. C., Leaver, K. D., Rawlings, R. D., and Alexander, J. M., *Material Science*, Third Edition, Chapman and Hall, 1985.

[10] Muccigrosso, J., and Phillips, P. J., *The Morphology of Cross-Linked PE*, IEEE Transactions on Electrical Insulation. EI-13, 172-178, 1978.

[11] Yasuda, H. K., *Plasma Polymerization*; Academic Press: Orlando, FL, 1985.

[12] Suhr, H., *Applications of Non-equilibrium Plasmas to Organic Chemistry* in "Techniques and Applications of Plasma Chemistry Polymers", Hollahan, J. R., and Bell, A. T., Eds.; Wiley and Sons, New York, 1974.

[13] Tsai, Y. M., and Boerio, F. J., J. Appl. Polym. Sci. 70, 1283, 1998.

[14] Clark, D. T., Dilks, A., Shuttleworth, D., *Polymer Surfaces*, Wiley, London, 1978.

[15] *Plasma Polymerization and Plasma Interactions with Polymers*; K. Yasuda, Ed.; Applied Polymer Symposium No. 46; John Wiley & Sons: New York, NY, 1990.

[16] Kay, E., Levenson, L. L., James, W. J., and Auerbach, R. A., J. Vac. Sci. Technol. 16, 359, 1979.

[17] Shi, F., Surf. Coat. Technol. 82, 1, 1996.

[18] Sharma, A. K., and Yasuda, H., J. Adhes., 13, 201, 1982.

[19] Kaplan, S., and Dilks, A., J. Appl. Polym. Sci.: Appl. Polym. Symp. 38, 105, 1984.

[20] Liston, E. M., Martinu, L., and Wertheimer, M. R., In *Plasma Surface Modification of Polymers*, Strobel, M., Lyons, C., and Mittal, K. L., Eds; VSP: The Netherlands, 1994.

[21] Surendran, G., and James, W. J., J. Appl. Polym. Sci.: Appl. Polym. Symp. 38, 75, 1984.

[22] Sun, Z., J. Non-Cryst. Solids, 261, 211, 2000.

[23] Morosoff, N., and Patel, D. L., ACS Poly. Prepr. 27, 82, 1986.

[24] Taylor, C. E., Boerio, F. J., Zeik, D. B., Clarson, S. J., Ward, S. M., and Dickie, R. A., *Proc. 17th Annual Meeting of the Adhesion Society*; Beorio, F., Ed.; The Adhesion Society: Blacksburg, Va., 1994.

[25] Biederman, H., and Slavinska, D., Surf. Coat. Technol. 125, 371, 2000.

[26] Biederman, H., and Osada, Y., *Plasma Polymerization Processes*, Elsevier, Amsterdam, 1992.

[27] Yasuda, H., and Hsu, T., Surf. Sci. 76, 232, 1978.

[28] Kay, E., presented at the *IUPAC International Roundtable on Plasma Polymerization and Plasma Treatment*, Limoges, France, 1977.

[29] Yasuda, H., presented at the *IUPAC International Round table on Plasma Polymerization and Plasma Treatment*, Limoges, France, 1977.

[30] Inagaki, N., *Plasma Surface Modification and Plasma Polymerization*, Technomic Publishing Company: Lancaster, PA, 1996..

[31] Yasuda, H., Marsh, H. C., Bumgarner, M. O., and Morosoff, N., J. Appl. Polym. Sci. 19, 2845, 1975.

[32] Morosoff, N., Crist, B., Bumgarner, M. O., Hsu, T., and Yasuda, H., J. Macromol. Sci. Chem. A10, 451, 1976.

[33] Durrent, S. F., Oliveira, R. T., Castro, S. G. C., Bolivar-Marinez, L. E., Galvao, D. S., and Moraes, M. A. B., J. Vac. Sci. Technol., A 15, 1334, 1997.

[34] Huntsberger, J. R., In *Treatise on Adhesion and Adhesives*, Vol. 1; R.L. Patrick, Ed.; Marcel Dekker: New York, 1967.

[35] Kinloch, A. J., *Adhesion and Adhesives, Science and Technology*; Chapman and Hall: New York, 1987.

[36] Liston, E. M., Martinu, L., and Wertheimer, M. R., in *Plasma Surface Modification of Polymers*, M.Strobel, C. Lyons and K.L. Mittal, Eds; VSP: The Netherlands, 1994.

[37] Sanchez, I. C., in *Physics of Polymer Surfaces and Interface*, Sanchez, I. C., Ed; Butterworth-Heinemann: Boston, 1992.

[38] Buckley, D. H., *Surface Effects in Adhesion, Friction, Wear, and Lubrication*; Elsevier Scientific: New York, 1981.

[39] *Handbook of Adhesives, 3rd ed*.; Skeist, I., Ed.; Chapman and Hall: New York, 1990.

Chapter 3

Materials and Thin Film Preparation

This chapter describes the experimental details related to the structural, optical and electrical characterizations of plasma polymerized thin films which would include the descriptions of monomers and substrate materials, capacitively coupled glow discharge plasma polymerization set up for polymer formation, the thickness measurement method, contact electrode deposition technique for electrical measurement, etc.

3.1 Introduction

This chapter describes the experimental details related to the structural, optical and electrical characterization of plasma polymerized thin films which includes the descriptions of monomers and substrate materials, capacitively coupled glow discharge plasma polymerization set up for polymer formation, the thickness measurement method, contact electrode deposition technique for electrical measurement etc. The experimental details of several methods for characterization of the thin films are also discussed e.g. for structural characterization - FTIR Spectroscopy, DTA, TGA etc; methods for optical characterization - UV-Vis Spectroscopy; method for electrical characterization viz. dc and ac characterizations etc are discussed in detail.

3.2 The Monomers

In this study we have used two types of monomers to prepare plasma polymerized single-layer and bilayer thin films : Pyrrole (Py) and N,N,3,5 Tetramethylaniline (TMA).

The monomer pyrrole was collected from Aldrich-Chemie D-7924, Steinheim, Germany. Pyrrole is a heterocyclic, organic compound, a five-membered ring, the molecules of which contain a ring of four carbon atoms and one nitrogen. Its chemical formula is C_4H_5N. The simplest member of the pyrrole family is pyrrole itself, a basic heterocyclic compound; colorless to pale yellow, toxic oil with pungent taste and similar to chloroform odor; insoluble in water; soluble in alcohol, ether, and dilute acids; boils at 403 ± 2^o K; polymerizes in light. Pyrrole ring system is involved in colored products (green pigment, chlorophyll; red, hemoglobin; blue, indigo) in nature. Pyrrole and its derivatives are widely used as an intermediate in synthesis of pharmaceuticals, medicines, agrochemicals, dyes, photographic chemicals, perfumes and other organic compounds. They are also used as catalysts for polymerization process, corrosion inhibitors, preservatives, and as solvents for resins and terpenes. They are used in metallurgical processes and are also useful in the intensive study of transition-metal complex catalyst chemistry for uniform polymerization, luminescence chemistry and spectrophotometric analysis. Many natural coloring materials are derived from pyrrole, including chlorophyll and hemoglobin. Pyrrole has very low basicity compared to amines and other aromatic compounds like pyridine, wherein the ring nitrogen is not bonded to a hydrogen atom. This decreased basicity is attributed to the delocalization of the lone pair of electrons of the nitrogen atom in the aromatic ring. Protonation results in loss of aromaticity, and is, therefore, unfavorable. The chemical structure of the monomer pyrrole is shown in Figure 3.1.

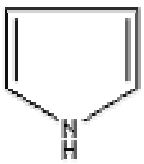

Figure 3.1 The chemical structure of Pyrrole

The monomer N,N,3,5 Tetramethylaniline (TMA) was collected from BDH chemical limited, Germany. Its chemical formula is $(CH_3)_2C_6H_3N(CH_3)_2$. It is a colorful (orange) liquid with boiling point 499 $\pm$ 2^o K. Its density is 0.913 and refractive index is 1.5443. It was used without further purification. TMA contains four methyl groups where two groups are attached to the nitrogen atom. The chemical structure of the monomer is shown in Figure 3.2.

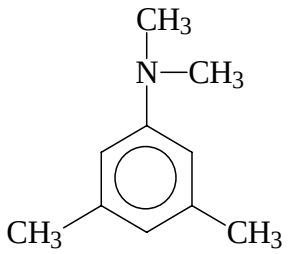

Figure 3.2 The chemical structure of N,N,3,5 tetramethylaniline

3.3 Sample Preparation

The electric field, when applied to the gaseous monomers at low pressures (0.01 to 1 mbar), produces active species that may react to form cross-linked polymer films. In this experiment, air was used as the primary plasma. To deposit single-layer PPPy and PPTMA thin films, the monomer pyrrole and TMA vapor were introduced downstream of the primary air glow discharge through a flowmetre at the flow rate of about $20cm^3$(STP)/min into the glow discharge reactor. Since the boiling point of TMA is about 499 K, therefore in order to deposit good PPTMA films the natural flow of monomer gas during deposition is not suitable. To increase the flow rate the container filled with TMA liquid is heated using a heating mantle. In laboratory plasma polymerized thin films were prepared using a bell-jar type capacitively coupled glow discharge system which will be described in the following sections. The glow discharge chamber was evacuated by a rotary pump and plasma was generated around the substrates, which were kept on the lower electrode, using a step up transformer connected to the electrodes with a power of about 50W at line frequency. Transparent light-yellow colored PPPy and PPTMA of different thickness were deposited onto the glass substrates. The deposition parameters such as flow-rate, power, vacuum order etc were kept almost same for all samples so that the comparison of the results could be made for various plasma polymerized thin films. The deposition-time was varied from 30 min to 80 min to deposit thin films of different thickness.

To deposit the PPPy-PPTMA bilayer composite thin films, pyrrole-monomer has been used as the mother-material and TMA monomer has been deposited in different deposition time ratio after the pyrrole thin films were grown. The deposition time-ratios of PPPy : PPTMA were (50min :10min), (45min :15min), (40min :20min), (35min : 25min) and (30min : 30min). Different time-ratios of the monomer have produced the bilayer thin films with different thicknesses.

3.4 Substrate and Their Cleaning Process

The substrates used were pre-cleaned glass slides (25.4 mm X 76.2 mm X 1.2 mm) from Sail Brand, China, purchased from local market. Electrodes and PPPy, PPTMA and PPPy-PTMA bilayer composite thin films were deposited onto them.

A thoroughly cleaned substrate is a prerequisite for the preparation of films with reproducible properties. Before depositing the films, each substrate was chemically cleaned by acetone and thoroughly rinsed with distilled water then dried in hot air.

3.5 Capacitively Coupled Plasma Polymerization Set-up

A locally fabricated capacitively coupled plasma polymerization system was used in the present work to deposit the samples. A schematic diagram of the plasma polymerization system is shown in Figure 3.3. A glow discharge is a kind of plasma and the plasma polymerization setup has been used enormously in recent years to form various kinds of plasma polymers. Different configuration of polymerization set up cause the sigificant variation of the properties of plasma polymers i.e. the geometry of the reaction chamber, position of the electrodes, nature of input power etc. Plasma polymerization, however, takes place in a glow discharge excited in a monomer gas or vapor, or their mixture with argon, providing thus the dielectric (polymeric) component of the composite [1-4].

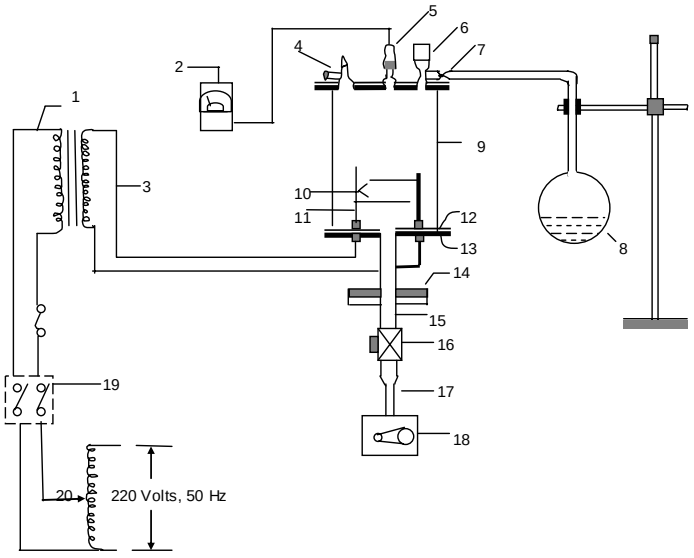

Figure 3.3 Schematic diagram of the plasma polymerization system.

(1 high voltage power supply, 2 pirani gage, 3 high tension leads, 4 gas inlet valve, 5 gauge head, 6 monomer injection valve, 7 flow meter, 8 monomer container, 9 Pyrex glass dome, 10 metal electrodes, 11 electrode stands, 12 gasket, 13, lower flange, 14 bottom flange, 15 brass tube, 16 valve, 17 liquid nitrogen trap, 18 rotary pump, 19 switch and 20 variac).

A photograph of the plasma polymerization system which is used in the laboratory is shown in Figure 3.4.

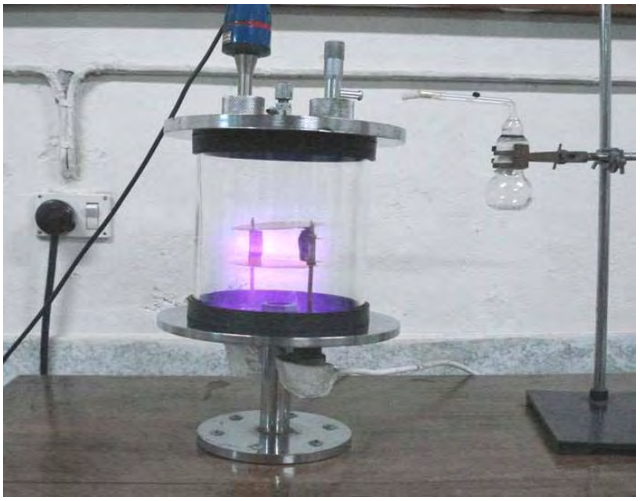

Figure 3.4 Plasma polymerization system in laboratory.

The glow discharge plasma deposition set-up consists of the following components is shown in Figure 3.3 and 3.4.

❖ **Plasma reaction chamber :** The plasma chamber consists of a cylindrical Pyrex glass bell-jar having 0.l5m in inner diameter and 0.18 m in length. The top and bottom edges of the glass bell-jar are covered with two rubber L-shaped (height and base 0.015m, thickness, 0.001 m) gaskets. The cylindrical glass bell jar is placed on the lower flange. The lower flange is well fitted with the diffusion pump by an I joint. The upper flange is placed on the top edge of the bell-jar. The flange is made up of brass having 0.01 m in thickness and 0.25 m in diameter. On the upper flange a laybold pressure gauge head, Edwards high vacuum gas inlet valve and a monomer injection valve are fitted. In the lower flange two highly insulated high voltages feed-through are attached housing screwed copper connectors of 0.01m high and 0.004 m in diameter via Teflon insulation.

❖ **Electrode system :** A capacitively coupled electrode system was used in the present set-up. Two circular stainless steel plates of diameter 0.09 m and thickness of 0.001 m are connected to the high voltage copper connectors. The inter-electrode separation can be changed by moving the electrodes through the electrode stands. After adjusting the distance between the electrodes they are fixed with the stands by means of screws. The substrates were kept on the lower electrode for plasma deposition.

❖ **Pumping unit :** It is used for evacuating the plasma reaction camber. In order to create laboratory plasma, first step is pumping out the air/gas from the plasma chamber. In this system a rotary pump of vacuubrand (Vacuubrand GMBH & Co: Germany) is used.

❖ **Vacuum pressure gauge :** A vacuum pressure gauge head (Laybold AG) and a meter (Thermotron^{TM} 120) of Laybold, Germany, are used to measure inside pressure of the plasma deposition chamber.

❖ **Input power supply for plasma generation :** The input power supply for plasma excitation comprises of a step-up high-tension transformer and a variac. The voltage ratio at the output of the high-tension transformer is about 16 limes that of the output of the variac. The maximum output of the variac is 220 V and that of the transformer is about 3.5 kV with a maximum current of 100 mA. The deposition rate increases with power at first and then becomes independent of power at high power values at constant pressure and flow rate.

❖ **Monomer injecting system :** The monomer injecting system consists of a conical flask of 25 ml capacity and a Pyrex glass tube with capillarity at the end portion. The capillary portion is well fitted with metallic tube of the nozzle of the high vacuum needle valve. The conical flask with its components is fixed by stand-clamp arrangement.

❖ **Supporting frame :** A metal frame of dimension (1.15 m × 0.76 m × 0.09 m) is fabricated with iron angle rods, which can hold the components described above. The upper and lower bases of the frame are made with polished wooden sheets. The wooden parts of the frame are varnished and the metallic parts are painted to keep it rust free. The pumping unit is placed on the lowed base of the frame. On the upper base a suitable hole is made in the wooden sheet so that the bottom flange can be fitted with nut and bolts.

❖ **Flowmeter :** The system pressure of a gas flow is determined by the feed in rate of a gas and the pumping out rate of a vacuum system. The monomer flow rate is determined by a flowmeter. So flowmeters are used in plasma polymerization system to control the monomer deposition rate [1, 5]. In the plasma polymerization set up a flowmeter (Glass Precision Engineering LTD, Meterate, England) is attached between the needle valve and the monomer bottle.

❖ **Liquid Nitrogen trap :** Cold trap, particularly a liquid N_2 trap, acts as a trap pump for different type gas. The liquid N_2 trap system is placed in the fore line of the reactor chamber before the pumping unit in the plasma deposition system. It consists of a cylindrical shape chamber having 6.4 cm diameter and 11.5 cm in length using brass material. The cross-sectional view of the liquid N_2 chamber is shown in Figure 3.5.

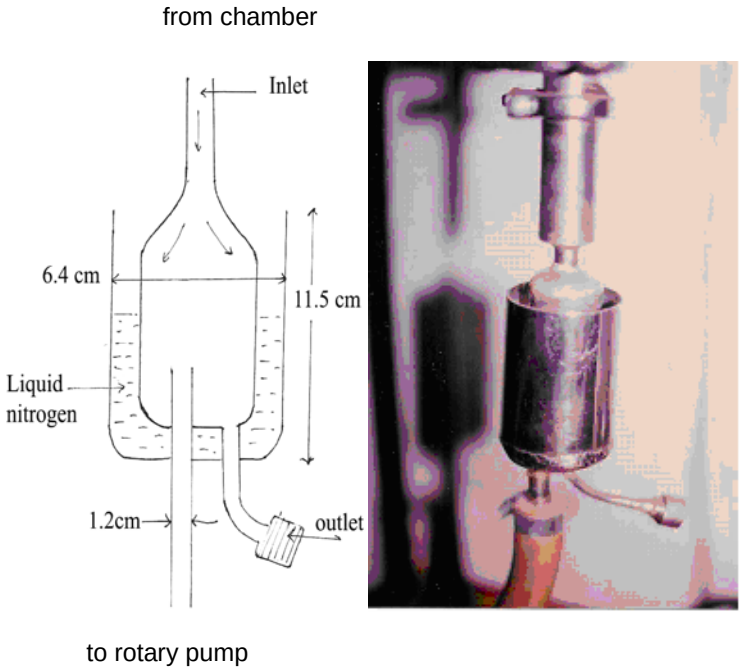

Figure 3.5 The cross-sectional view and photograph of liquid nitrogen trap.

3.6 Generation of Glow Discharge Plasma in the Laboratory

Glow discharges are produced by an applied static or oscillating electric field where energy is transferred to free electrons in vacuum. Inelastic collisions of the energetic free electrons with the gas molecules generate free radicals, ions, and species in electronically excited states. This process also generates more free electrons, which is necessary for a self-sustaining glow [6-8]. The excited species produced are very active and can react with the surfaces of the reactors as well as themselves in the gas phase.

The important feature of glow discharge plasma is the non-equilibrium state of the overall system. In the plasmas considered for the purpose of plasma polymerization, most of the negative charges are electrons and most of the positive charges are ions. Due to large mass difference between electrons and ions, the electrons are very mobile as compared to the nearly stationary positive ions and carry most of the current. Energetic electrons as well as ions, free radicals, and vacuum ultraviolet light can possess energies well in excess of the energy sufficient to break the bonds of typical organic monomer molecules which range from approximately 3 to 10 eV. Some typical energy of plasma species available in glow discharge as well as bond energies encountered at pressure of approximately 0 .01 mbar.

The chamber of the plasma polymerization unit and monomer container is evacuated to about 0.01 mbar. The monomer vapor is then injected to the chamber slowly for some time. A high-tension transformer along with a variac is connected to the feed-through attached to

the lower flange. While increasing the applied voltage, light pink colors monomer plasma is produced across the electrodes at around 0.15-mbar-chamber pressure. Figure 3.7 is the photograph of glow discharge plasma across the electrodes in the capacitively coupled parallel plate discharge chamber.

3.7 Measurement of Thickness of the Thin Films

Thickness is the single most significant film parameter. Any physical quantity related to film thickness can in principle be used to measure the film thickness. It may be measured either by several methods with varying degrees of accuracy. The methods are chosen on the basis of their convenience, simplicity and reliability. Since the film thicknesses are generally of the order of a wavelength of light, various types of optical interference phenomena have been found to be most useful for measurement of film thicknesses. Several of the common methods are

- During Evaporation,
- Multiple-Beam Interferometry, (Tolansky Fezeau fringes method, Fringes of equal chromatic order, Donaldson method etc.)
- Michelson interferometer
- Using a Hysteresis graph and other methods used in film-thickness determination with particular reference to their relative merits and accuracies.

In our system, Multiple-Beam Interferometry technique was employed for the measurement of thickness of the thin films. This technique is described below.

3.7.1 Multiple-Beam Interferometry

This method utilizes the resulting interference effects when two silvered surfaces are brought close together and are subjected to optical radiation. This interference technique, which is of great value in studying surface topology in general, may be applied simply and directly to film-thickness determination. When a wedge of small angle is formed between unsilvered glass plates, which are illuminated by monochromatic light, broad fringes are seen arising from interference between the light beams reflected from the glass on the two sides of the air wedge. At points along the wedge where the path difference is an integral and odd number of wavelengths, bright and dark fringes occur respectively. If the glass surfaces of the plates are coated with highly reflecting layers, one of which is partially transparent, then the reflected fringe system consists of very fine dark lines against a bright background. A schematic diagram of the multiple-beam interferometer along with a typical pattern of Fizeau fringes from a film step is shown in Figure 3.6 and a photograph of the interferometer is presented in Figure 3.7 .

As shown in this figure, the film whose thickness is to be measured is over coated with a silver layer to give a good reflecting surface and a half-silvered microscope slide is laid on

top of the film whose thickness is to be determined, The thickness of the film d can then be determined by the relation

$$d = \frac{\lambda b}{2a} \qquad (3.1)$$

where λ is the wavelength and *b/a* is the fractional discontinuity identified in the figure. In general, the sodium light is used, for which λ = 5893 A°. In practice, several half-silvered slides of varying thickness and therefore of varying transmission are prepared, and one of these is selected for maximum resolution. Accurate determinations of fringe spacing are difficult and time consuming; but a method of image comparison, which considerably improves the ease, and rapidity of measurement has recently been developed. Alternatively, a simple film- thickness gauge utilizing Newton's rings may be developed, which involves no critical adjustment of wedges, etc., and which reduces error in film-thickness determination. In conclusion, it might be mentioned that the Tolansky method of film-thickness measurement is the most widely used and in many respects also the most accurate and satisfactory one [9].

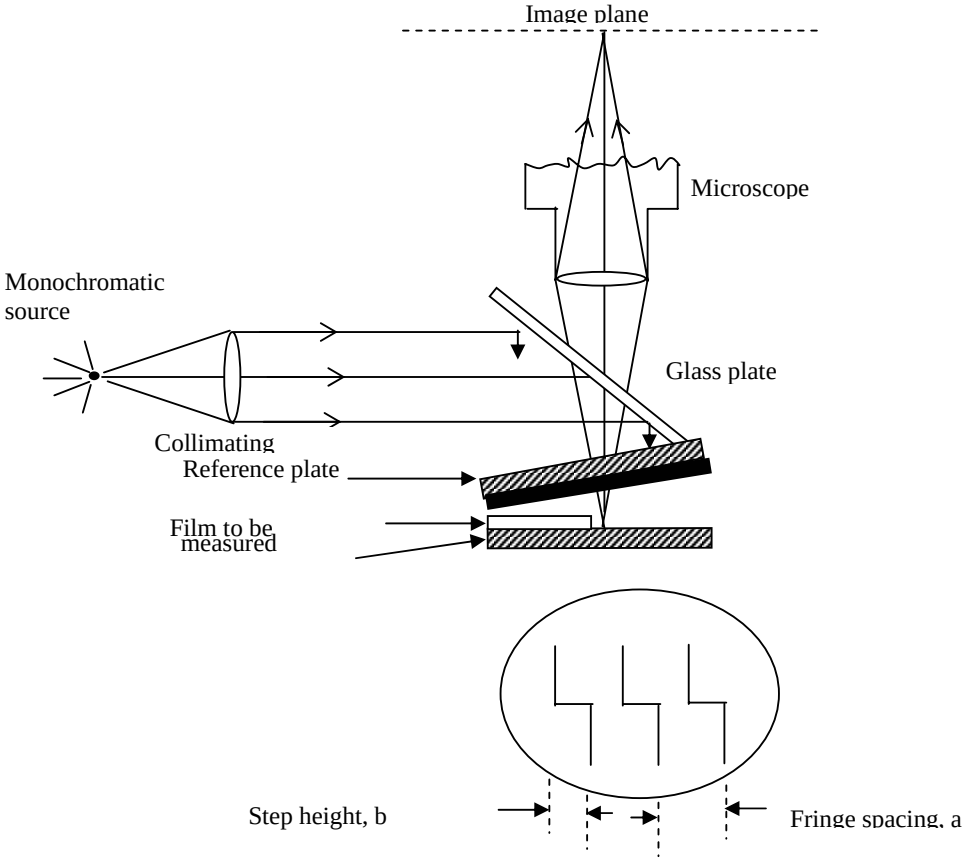

Figure 3.6 Interferometer arrangements for producing reflection Fizeau fringes of equal thickness.

Figure 3.7 Interferometer arrangements in the laboratory

3.8 Experimental Techniques for Characterization of Thin Films

In this work, the plasma polymerized thin films viz. PPPy, PPTMA and PPPy-PPTMA bilayer thin films have been characterized by different experimental methods. The following experimental methods are employed to study different properties of thin films :

- Fourier Transform Infrared (FTIR) Spectroscopy, Differential Thermal Analysis (DTA), Thermogravimetric Analysis (TGA) for structural characterization.
- Ultraviolet-Visible (UV-Vis) Spectroscopy for optical characterization.
- Direct Current (dc) and Alternating Current (ac) measurements for electrical characterization.

The experimental details of the above methods are described below.

3.8.1 Fourier Transform Infrared Spectroscopy

For FTIR studies, the as-grown PPPy, PPTMA and PPPy-PPTMA bilayer thin film were scraped off from the glass substrates in powder form and were mixed with potassium bromide (KBr). This mixture was then pelletized. These pellets of the mixture were used to record the FTIR spectra at room temperature using a double-beam FTIR spectrometer (Shimadzu -IR 470, Shimadzu Corporation, Tokyo, Japan). The strength of an IR absorption spectrum is dependant on the number of molecules in the beam. With a KBr disk the strength will be dependant on the amount and homogeneity of the sample dispersed in the KBr powder. The spectrometer has its repeatability of the transmittance, 0.5%, except the wavenumber range, where the absorption bands of the water vapor exist. All the spectra were recorded in transmittance (%) mode in the wavenumber region 4000-500 cm^{-1}.

The FTIR spectra of the monomers' liquid Pyrrole and TMA were also recorded at room temperature using a double-beam FTIR spectrometer (Shimadzu -IR 470, Shimadzu Corporation, Tokyo, Japan). A drop of each of the respective liquid monomers was placed between two thin KBr pellets to record the IR spectrum of the monomers.

Figure 3.8 The FTIR spectrometer.

3.8.2 Differential Thermal Analysis and Thermogravimetric Analysis

The PPPy, PPTMA and PPPy-PPTMA bilayer thin film films were scrapped off from the substrate to use as the sample for the DTA/TGA investigations. The DTA/TGA scans of PPTMA thin films were taken using a computer controlled TG/DTA 6300 system connected to an EXSTAR 6000 station, Seiko Instruments Inc., Japan. The TG/DTA module uses a horizontal system balance mechanism.

The specifications of the instrument are: sample weight $\leq$ 200mg, Temperature range; room temperature to 1573 K, Heating rate; 0.01°K/min. to 100.00 °K/min., TGA Measuring Range; $\pm$ 200 mg(0.2 μg), DTA Measuring Range; $\pm$ 1000 μV(0.06 μV), Gas flow; $\leq$ 1000m/min.

Figure 3.9 shows the TG/DTA 6300 system.

3.8.3 Ultraviolet-visible Spectroscopy

UV-Vis spectra of as grown PPPy, PPTMA and PPPy-PPTMA thin films on glass substrates were obtained in absorption mode with a spectrophotometer Shimadzu UV-160A (Shimadzu Corporation, Tokyo, Japan) in the wavelength range 200 to 800 nm at room temperature.

UV-Vis spectrum of the Pyrrole and TMA monomer liquids were also obtained in absorption mode with a spectrophotometer Shimadzu UV-160A (Shimadzu Corporation, Tokyo, Japan) in the wavelength range 200 to 800 nm at room temperature.

Figure 3.10 shows a photograph of UV-visible spectrometer (Shimadzu UV-160A) in the laboratory.

(b)

Figure 3.9 The TG/DTA 6300 system

Figure 3.10 The UV-visible spectrometer Shimadzu UV-160A.

3.8.4 Electrical Measurements

3.8.4.1 Electrode materials and Contact Electrodes

Aluminium (Al) (purity of 4N British Chemical Standard) was used for electrode deposition. Al has been reported to have good adhesion with glass slides [9]. Al film has advantage of easy self-healing burn out of flaws in sandwich structure.

For electrical measurements, Al electrodes were deposited on the both sides of the sample, i.e. after the lower electrode was deposited on the thin film, the upper electrode was deposited on the film in a similar manner in the opposite direction of the lower electrode by using an Edward vacuum coating unit E-306A (Edward, UK). The system was evacuated by an oil diffusion pump backed by an oil rotary pump. The chamber could be evacuated to a pressure less than 1.33×10^{-3} Pa. The glass substrates were masked with (0.08 m × 0.08 m × 0.001 m) engraved brass sheet for the electrode deposition.

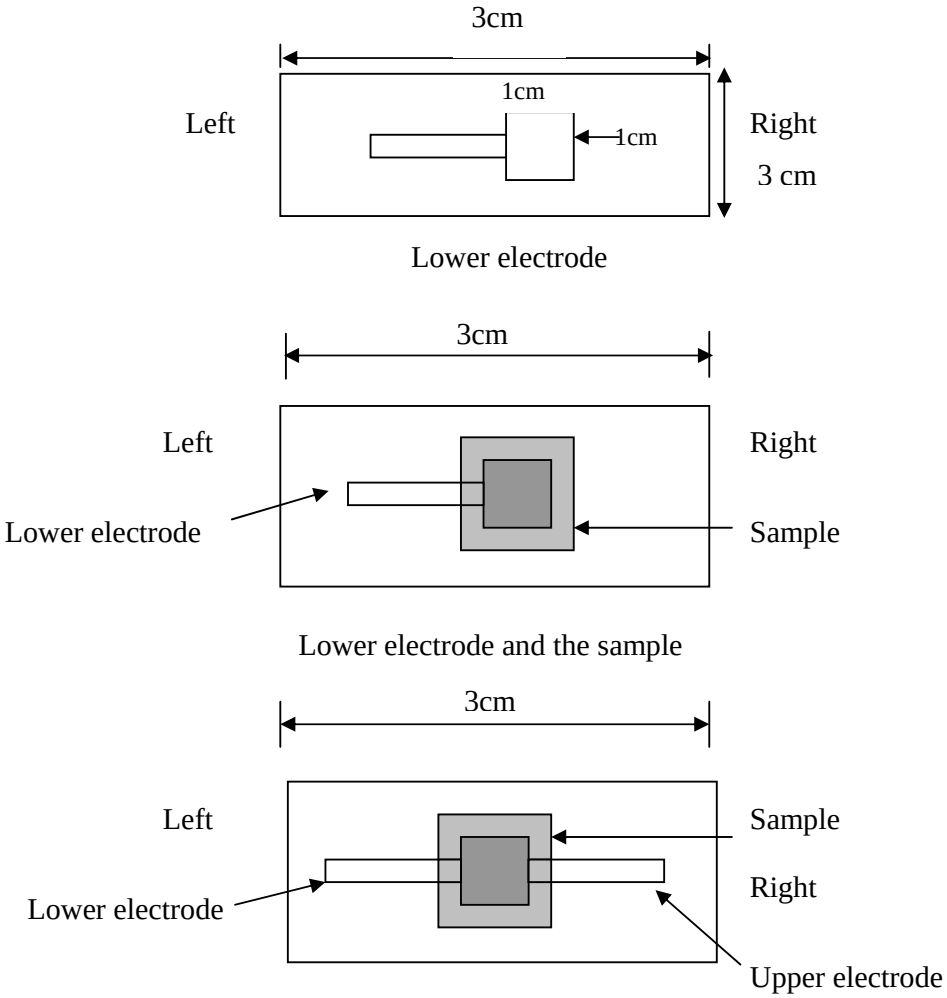

Figure 3.11 The electrode configuration for electrical measurements.

The electrode assembly used in the study is shown in Figure 3.11. The glass substrates with mask were supported by a metal rod 0.1 m above the tungsten filament. For the electrode deposition Al was kept on the tungsten filament. The filament was heated by low-tension power supply of the coating unit. The low-tension power supply was able to produce 100 A current at a potential drop of 10 V. During evacuation of the chamber by diffusion pump, the diffusion unit was cooled by the flow of chilled water and its outlet temperature was not allowed to rise above 305K. When the penning gauge reads about 1.33 x 10^{-3} Pa, the Al on tungsten filament was heated by low-tension power supply until it was melted. The Al was evaporated, thus lower electrode onto the glass slide was deposited. Al coated glass substrates were taken out from the vacuum coating unit and were placed on the middle of the lower electrode of the plasma deposition chamber for thin film deposition under optimum condition.

3.8.4.2 Direct Current Electrical Measurements

The current across the thin films was measured by a high impedance Keithley 614 electrometer and the dc voltage was applied by an Agilent 6545A stabilized dc power supply. The measurements were carried out under dynamic vacuum of about 1.33 Pa to avoid any ambient effect. The block diagram for dc measurements and a photograph of dc measurement set up are shown in Figure 3.12 and Figure 3.13. The thermally activated current or the temperature dependence of current across the thin films was measured at different applied voltages using the above mentioned electrometer. The measurements were performed at different temperatures ranges from 298 to 398 K. For these measurements the samples were heated by a heating coil which was wrapped around the specimen chamber. The temperature was measured by a Chromel-Alumel (Cr-Al) thermocouple placed very close to the sample which was connected to a Keithley 197 A digital microvolt meter (DMV).

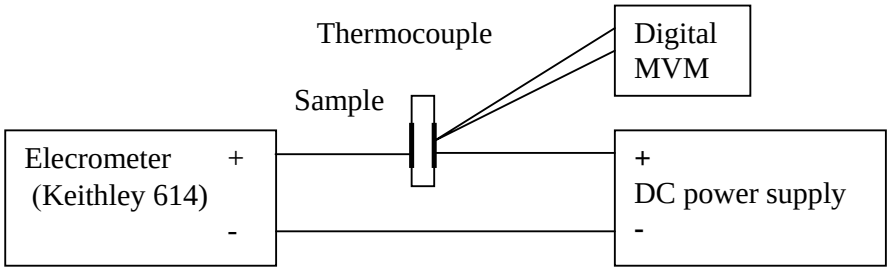

Figure 3.12 A schematic circuit diagram of DC measurements.

Figure 3.13 DC measurement setup in the laboratory.

3.8.4.3 Alternating Current Electrical Measurements

The ac measurement was performed in the frequency range from 100 to 3×10^6 Hz and temperature range 298 - 423 K, by a low frequency (LF) Impedance analyzer, Agilent 4192A, 5 Hz -13 MHz (Agilent Technologies Japan, Ltd. Tokyo, Japan).

The temperature was recorded by a Cr- Al thermocouple placed very close to the sample which was connected to a Keithley 197A digital microvoltmeter (DMV). To avoid oxidation, all measurements were performed in a vacuum of about 1.33 Pa. Photographs of the Impedance analyzer and ac measurement set-up are shown in Figure 3.14.

Figure 3.14 Photographs of the ac electrical measurement set-up.

References

[1] Yasuda H, *Plasma Polymerization*, Academic Press, Inc., New York, 1985.

[2] Chowdhury, F.-U.-Z., Islam, A. B. M. O., and Bhuiyan, A. H., *Chemical analysis of plasma- polymerized diphenyl thin films*, Vacuum, 57, 43-50, 2000.

[3] Anghel, S. D., Frentiu, T., Cordos, E. A., Simon, A., Popescu, A., *Atmospheric pressure capacitively coupled plasma source for the direct analysis of non-conducting solid samples*, J. Anal. At. Spectrom, 14, 541-545, 1999,.

[4] Akther, H., Bhuiyan, A. H., *Space charge limited conduction in plasma polymerized N, N, 3, 5 Tetramethylaniline thin films*, Thin Solid Films 488, 93 -97, 2005.

[5] Akther, H. and Bhuiyan, A. H., *Electrical and Optical properties of plasma polymerized N, N, 3, 5 tetramethylaniline thin films*, New J. Phys. 7, 173, 2005.

[6] Chen, F. F., *Introduction to plasma physics*, Plenum Press, New York, 1974.

[7] Lieberman, M. A., and Lichtenberg, A. J., *Principles of plasma discharges and materials processing*, Wiley, New York, 1994.

[8] Bogaerts, A., and Neyts, E., *Gas discharge plasma and their applications*, Spectrochimica Acta Part B, 57, 609-658, 2002.

[9] Tolansky, S., *Multiple Beam Interferometry of Surfaces and Films*, Clarendon Press, Oxford, l948.

Chapter 4

The Structural Characterization

This chapter describes the existing theories for structural characterization of plasma polymerized thin films, e.g. the theory of FTIR, TGA, DTA etc and the corresponding experimental results are also discussed.

4.1 Introduction

There are several methods for structural characterization of plasma polymerized thin films, e.g. Elemental Analysis (EA), Scanning Electron Microscopy (SEM), Energy Dispersive X-ray (EDX), Infrared Spectroscopy (IR), Differential Thermal Analysis (DTA), Thermogravimetric Analysis (TGA) etc.

The EA is a useful technique for chemical investigation of organic or inorganic materials. The chemical compositions of plasma polymerized materials can be characterized by this technique. The elemental composition of plasma polymerized materials generally differs substantially from that of monomer, which does not usually happen in case of conventional polymers. The investigations dealing with the surface morphology of different polymer materials is done by the method of SEM. EDX is a technique used for identifying the elemental composition of the specimen, or an area of interest thereof. The EDX analysis system works as an integrated feature of a SEM, and can not operate on its own without the latter. Infra-red (IR) spectroscopy is a natural tool for the investigation of molecular structure and bonding and identification of functional groups in organic compounds. The main goal of IR spectroscopic analysis is to determine the chemical functional groups in the sample, but determination of conformations or even investigations of chemical reactions are also possible by using this analysis. The technique of DTA is an important tool to study the structural and phase changes occurring both in solid and in liquid materials during heat treatment. These changes may be due to dehydration, transition from one crystalline form to another, destruction of crystalline structure, oxidation, decomposition etc. Thermo Gravimetric Analysis (TGA) is to measure the mass of a sample as a function of temperature. The method for example can be used to determine water of crystallization, follow degradation of materials, determine reaction kinetics, study oxidation and reduction, or to teach the principles of stoichiometry, formulae and analysis.

In this chapter the theory of FTIR spectroscopy, DTA and TGA would be described and the experimental results would be discussed.

4.2 Theory of Fourier Transform Infrared spectroscopy

4.2.1 Introduction

Infra-red (IR) spectroscopy is a natural tool for the investigation of molecular structure and identification of functional groups in organic compounds. It represents a powerful and flexible experimental technique which provides direct information about the potential energy surface in the vicinity of the equilibrium position, and thus provides a probe of the structural and bonding characteristics.

IR spectroscopy deals with the interaction of infrared light with matter, measures different IR frequencies by a sample positioned in the path of an IR beam and it reveals information about the vibrational states of a molecule. When a beam of electromagnetic radiation of intensity is passed through a substance, it can either be absorbed or transmitted, depending upon its frequency, and the structure of the molecules. The resulting spectrum represents the molecular absorption and transmission, creating a molecular fingerprint of the sample. Like a fingerprint, no two unique molecular structures produce the same infrared spectrum. This makes infrared spectroscopy useful for several types of analyses.

If a transition, however, exists which is related to the frequency of the incident radiation by Planck's law, then the radiation can be absorbed. The type of absorption spectroscopy depends upon the type of transition involved and accordingly the frequency range of the electromagnetic radiation absorbed. If the transition is from one vibrational energy level to another, then the radiation is from the infrared portion of the electromagnetic spectrum and the technique is known as infrared spectroscopy [1, 2].

The portion of the infrared region most useful for analysis of organic compounds is not immediately adjacent to the visible spectrum, but is that having a wavelength range from 2,500 to 16,000 nm, with a corresponding frequency range from 1.9×10^{13} to 1.2×10^{14} Hz. Photon energies associated with this part of the infrared radiation are not large enough to excite electrons, but may induce vibrational excitation of covalently bonded atoms and groups. Any structural change like addition substitution, of groups or atoms in a molecule affects the relative mode of vibration of the group.

Intensity and spectral position of IR absorptions allow the identification of structural elements of molecule. The main goal of IR spectroscopic analysis is to determine the chemical functional groups in the sample, but determination of conformations or even investigations of chemical reactions are also possible by using this analysis. A molecule absorbs only those frequencies of IR light that match vibrations that cause a change in the dipole moment of the molecule. In a complicated molecule many fundamental vibrations are possible, but not all are observed. Some motions do not change the dipole moment for the molecule; some are so much alike that they coalesce into one band. Even though an IR spectrum is characteristic for an entire molecule, there are certain groups of atoms in a molecule that gives rise to absorption bands at or near the same wavenumber, ν,(frequency) regardless of the rest of the structure of the molecule. These persistent characteristic bands enable to identify major structural features of the molecule.

Different functional groups absorb characteristic frequencies of IR radiation and this absorption results due to the changes in vibrational and rotational status of the molecules. Actually, a molecule, when exposed to radiation produced by the thermal emission of a hot

source (a source of IR energy), absorbs only at frequencies corresponding to its molecular modes of vibration in the region of the electromagnetic spectrum between visible (red) and short waves (microwaves). These changes in vibrational motion give rise to bands in the vibrational spectrum; each spectral band is characterized by its frequency and amplitude. The absorption frequency depends on the vibrational frequency of the molecules, whereas the absorption intensity depends on how effectively the infrared photon energy can be transferred to the molecule, and this depends on the change in the dipole moment that occurs as a result of molecular vibration. As a consequence, a molecule will absorb infrared light only if the absorption causes a change in the dipole moment. Thus, all compounds except for elemental diatomic gases such as N_2, H_2 and O_2, have infrared spectra and most components present in a flue gas can be analyzed by their characteristic infrared absorption. Furthermore, using various sampling accessories, IR spectrometers can accept a wide range of sample types such as gases, liquids, and solids. Thus, IR spectroscopy is an important and popular tool for structural elucidation and compound identification.

However, It is rarely, if ever, possible to identify an unknown compound by using IR spectroscopy alone. Its principal strengths are:

- It can identify unknown materials
- It can determine the quality or consistency of a sample
- It can determine the amount of components in a mixture
- It is a quick and relatively cheap spectroscopic technique,
- It is useful for identifying certain functional groups in molecules
- An IR spectrum of a given compound is unique and can therefore serve as a *fingerprint* for this compound.

It should be noted, however, that when a spectrum is recorded using a conventional, dispersive IR spectrometer, each data point reveals the transmitted light at the respective frequency. The signal provided by the IR technique, however, contains information about the complete spectrum of the probe. This signal has to be transformed from the *time-domain* into the *frequency-domain* in order to reveal the spectrum. This transformation is called *Fourier transformation* and then the spectroscopic analysis then termed as Fourier Transform Infrared (FTIR) spectroscopy.

4.2.2 Why FTIR?

The IR spectroscopy has been a workhorse technique for materials analysis in the laboratory for over seventy years. An IR spectrum represents a fingerprint of a sample with absorption peaks which correspond to the frequencies of vibrations between the bonds of the atoms making up the material. Because each different material is a unique combination of atoms, no two compounds produce the exact same infrared spectrum. Therefore, IR spectroscopy

can result in a positive identification (qualitative analysis) of every different kind of material. In addition, the size of the peaks in the spectrum is a direct indication of the amount of material present. With modern software algorithms, infrared is an excellent tool for quantitative analysis.

The original infrared instruments were of the dispersive type. These instruments separated the individual frequencies of energy emitted from the infrared source. This was accomplished by the use of a prism or grating. An infrared prism works exactly the same as a visible prism which separates visible light into its colors (frequencies). A grating is a more modern dispersive element which better separates the frequencies of infrared energy. The detector measures the amount of energy at each frequency which has passed through the sample. This results in a spectrum which is a plot of intensity vs. frequency.

The FTIR spectrometry was developed in order to overcome the limitations encountered with dispersive instruments. The main difficulty was the slow scanning process. A method for measuring all of the infrared frequencies simultaneously, rather than individually, was needed. A solution was developed which employed a very simple optical device called an interferometer. The interferometer produces a unique type of signal which has all of the infrared frequencies “encoded” into it. The signal can be measured very quickly, usually on the order of one second or so. Thus, the time element per sample is reduced to a matter of a few seconds rather than several minutes. Most interferometers employ a beamsplitter which takes the incoming infrared beam and divides it into two optical beams. One beam reflects off of a flat mirror which is fixed in place. The other beam reflects off of a flat mirror which is on a mechanism which allows this mirror to move a very short distance (typically a few millimeters) away from the beamsplitter. The two beams reflect off of their respective mirrors and are recombined when they meet back at the beamsplitter. Because the path that one beam travels is a fixed length and the other is constantly changing as its mirror moves, the signal which exits the interferometer is the result of these two beams “interfering” with each other. The resulting signal is called an interferogram which has the unique property that every data point (a function of the moving mirror position) which makes up the signal has information about every infrared frequency which comes from the source. This means that as the interferogram is measured, all frequencies are being measured simultaneously. Thus, the use of the interferometer results in extremely fast measurements. Because the analyst requires a frequency spectrum (a plot of the intensity at each individual frequency) in order to make identification, the measured interferogram signal can not be interpreted directly. A means of “decoding” the individual frequencies is required. This can be accomplished via a well-known mathematical technique called the Fourier transformation. This transformation is performed by the computer which then presents the user with the desired spectral information for analysis.

The FTIR spectroscopy is preferred over dispersive or filter methods of IR spectral analysis for several reasons:

- It is a non-destructive technique
- It provides a precise measurement method which requires no external calibration
- It can increase speed, collecting a scan every second
- It can increase sensitivity – one second scans can be co-added together to ratio out random noise
- It has greater optical throughput
- It is mechanically simple with only one moving part

4.2.3 Infrared Frequency Range and Spectrum Presentation

Infrared radiation spans a section of the electromagnetic spectrum having wave-numbers from roughly 3,000 to 10 cm^{-1}, or wavelengths from 0.78 to 1000 μm. It is bound by the red end of the visible region at high frequencies and the microwave region at low frequencies. IR absorption positions are generally presented as either wave-numbers ($\bar{\nu}$) or wavelengths (λ). Wave-number defines the number of waves per unit length. Thus, wave-numbers are directly proportional to frequency, as well as the energy of the IR absorption. The wave-number unit (cm^{-1}) is more commonly used in modern IR instruments that are linear in the cm^{-1} scale. In the contrast, wavelengths are inversely proportional to frequencies and their associated energy. At present, the recommended unit of wavelength is μm (micrometers). Wave-numbers and wavelengths can be interconverted using the following equation:

$$\bar{\nu}(cm^{-1}) = \frac{1}{\lambda(\mu m)} \times 10^4 \qquad (4.1)$$

IR absorption information is generally presented in the form of a spectrum with wavelength or wavenumber as the x-axis and absorption intensity or percent transmittance as the y-axis. Transmittance, *T*, is the ratio of radiant power transmitted by the sample (*I*) to the radiant power incident on the sample (I_0). Absorbance (*A*) is the logarithm to the base 10 of the reciprocal of the transmittance (*T*).

$$A = \log_{10}(1/T) = \log_{10}(I_0 / I\ ) \qquad (4.2)$$

The transmittance spectra provide better contrast between intensities of strong and weak bands because transmittance ranges from 0 to 100% *T* whereas absorbance ranges from infinity to zero. The analyst should be aware that the same sample will give quite different profiles for the IR spectrum, which is linear in wave-number, and the IR plot, which is linear in wavelength. It will appear as if some IR bands have been contracted or expanded.

The IR region is commonly divided into three smaller areas: near IR, mid IR, and far IR.

	Near IR	Mid IR	Far IR
Wavenumber (cm^{-1})	13000 – 4000	4000 – 200	200 – 10
Wavelength (μm)	0.78 – 2.5	2.5 – 50	50 – 1000

The region of most interest for chemical analysis is the mid-infrared region (4,000 cm^{-1} to 400 cm^{-1}) which corresponds to changes in vibrational energies within molecules. The far infrared region (400 cm^{-1} to 10 cm^{-1}) is useful for molecules containing heavy atoms such as inorganic compounds but requires rather specialized experimental techniques. The far- and near IR are not frequently employed because only skeletal and secondary vibrations (overtones) occur in these regions producing spectra that are difficult to interpret.

In particular, the energy of most molecular vibrational modes corresponds to that of the IR part of the electromagnetic spectrum, that is, between around 650 cm^{-1} and 4000 cm^{-1}. However, in practice, the analysis and assignment of spectral features is difficult, and correspondingly, attention is focused instead upon characteristic functional groups and the associated familiar bands. This though, neglects a great deal of the information contained within the IR spectrum.

4.2.4 Infrared Absorption

At temperatures above absolute zero, all the atoms in molecules are in continuous vibration with respect to each other. When the frequency of a specific vibration is equal to the frequency of the IR radiation directed on the molecule, the molecule absorbs the radiation.

The total number of observed absorption bands is generally different from the total number of fundamental vibrations. It is reduced because some modes are not IR active and a single frequency can cause more than one mode of motion to occur. Conversely, additional bands are generated by the appearance of overtones (integral multiples of the fundamental absorption frequencies), combinations of fundamental frequencies, differences of fundamental frequencies, coupling interactions of two fundamental absorption frequencies, and coupling interactions between fundamental vibrations and overtones or combination bands (Fermi resonance). The intensities of overtone, combination, and difference bands are less than those of the fundamental bands. The combination and blending of all the factors thus create a unique IR spectrum for each compound.

IR radiation does not have enough energy to induce electronic transitions as seen with UV. Absorption of IR is restricted to compounds with small energy differences in the possible vibrational and rotational states.

For a molecule to absorb IR, the vibrations or rotations within a molecule must cause a net change in the dipole moment of the molecule. The alternating electrical field of the radiation (remember that electromagnetic radiation consists of an oscillating electrical field and an oscillating magnetic field, perpendicular to each other) interacts with fluctuations in the dipole moment of the molecule. If the frequency of the radiation matches the vibrational frequency of the molecule then radiation will be absorbed, causing a change in the amplitude of molecular vibration.

The simplest treatment of IR absorption in molecular systems is a semi-classical treatment. Essentially, classical electromagnetism requires that, if a system is to absorb radiation, that it do so by virtue of periodic changes in its electric dipole moment. The frequency of the dipole oscillations must be equal to the frequency of the incident radiation for absorption to occur.

The dipole moment is a vector quantity, thus, absorption may occur provided that at least one component of the dipole moment can oscillate at the incident frequency. Of course, as a molecule vibrates, the dipole moment will oscillate at the frequency of the molecular oscillations, as the dipole moment is a function of the nuclear coordinates. In the harmonic approximation used throughout this work, any molecular vibration may be expressed as a sum over normal modes; thus, the dipole moment may only oscillate at these normal mode frequencies, and radiation may only be absorbed at these normal mode frequencies. However, selection rules may ensure that certain normal modes are so-called “silent" modes, *i.e.* they do not absorb radiation.

4.2.5 Molecular Vibrations

The energy of a molecule consists of translational, rotational, vibrational and electronic energy

$$E = E_{electronic}+E_{vibrational}+E_{rotational}+E_{translational} \quad (4.3)$$

Translation energy of a molecule is associated with the movement of the molecule as a whole, for example in a gas. Rotational energy is related to the rotation of the molecule, whereas vibrational energy is associated with the vibration of atoms within the molecule. Finally, electronic energy is related to the energy of the molecule's electrons.

Like radiant energy, the energy of a molecule is quantized too and a molecule can exist only in certain discrete energy levels. Within an electronic energy level a molecule has many possible vibrational energy levels. To raise the electronic energy state of a molecule from the ground state to the excited state will cost more energy than to raise the vibrational energy state.

Organic functional groups differ from one another both in the strength of the bonds, and in the masses of the atoms involved. Molecules are flexible, moving collections of atoms. The atoms in a molecule are constantly oscillating around average positions. Bond lengths and bond angles are continuously changing due to this vibration. A molecule absorbs infrared radiation when the vibration of the atoms in the molecule produces an oscillating electric field with the same frequency as the frequency of incident IR "light". All of the motions can be described in terms of two types of molecular vibrations. One type of the vibration, a stretch, produces a change of bond length. A stretch is a rhythmic movement along the line between the atoms so that the interatomic distance is either increasing or decreasing. The second type of vibration, a bend, results in a change in bond angle. These are also sometimes called scissoring, rocking etc motions. Each of these two main types of vibration can have variations. A stretch can be symmetric or asymmetric. Bending can occur in the plane of the molecule or out of the plane; it can be scissoring, like blades of a pair of scissors, or rocking, where two atoms move in the same direction.

The vibrational energy of a molecule is not determined by the orbit of an electron but by the shape of the molecule, the masses of the atoms and, eventually by the associated vibronic coupling. For example, simple diatomic molecules have only one bond allowing only stretching vibrations. More complex molecules may have many bonds, and vibrations can be conjugated. The atoms in a CH_2 group, commonly found in organic compounds, can vibrate in six different ways: symmetrical and antisymmetrical stretching, scissoring, rocking, wagging and twisting.

The major types of molecular vibrations are stretching and bending. The various types of vibrations are illustrated in Figure 4.2.1, Figure 4.2.2 and Figure 4.2.3. Infrared radiation is absorbed and the associated energy is converted into these types of motions. The absorption involves discrete, quantized energy levels. However, the individual vibrational motion is usually accompanied by other rotational motions. These combinations lead to the absorption bands, not the discrete lines, commonly observed in the mid IR region.

Stretching: Change in inter-atomic distance along bond axis

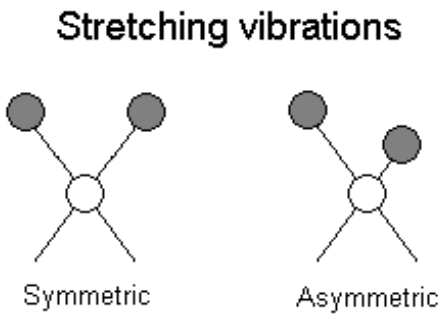

Figure 4.2.1 Stretching vibrations

Bending: Change in angle between two bonds. There are four types of bend:

- Rocking
- Scissoring
- Wagging
- Twisting

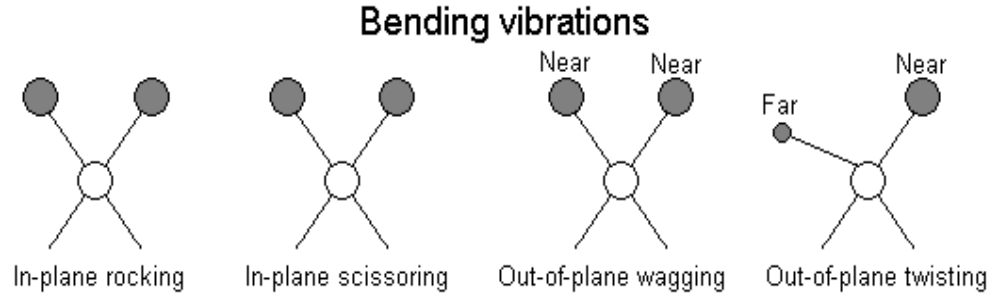

Figure 4.2.2 Bending vibrations

In general, a polyatomic molecule with n atoms has 3*n* – 6 distinct vibrations. Each of these vibrations has an associated set of quantum states and in IR spectroscopy the IR radiation induces a jump from the ground (lowest) to the first excited quantum state. Although approximate, each vibration in a molecule can be associated with motion in a particular group. Clearly, even for simple molecules, a description of the vibrations is quite complicated and this complexity rapidly increases as the size of the molecule increases. Fortunately, as we will see, it is almost never necessary to be able to picture all the molecular vibrations for IR spectroscopy to be useful.

4.2.5.1 Vibrational coupling

In addition to the vibrations mentioned above, interaction between vibrations can occur (*coupling*) if the vibrating bonds are joined to a single, central atom. Vibrational coupling is influenced by a number of factors;

- Strong coupling of stretching vibrations occurs when there is a common atom between the two vibrating bonds
- Coupling of bending vibrations occurs when there is a common bond between vibrating groups
- Coupling between a stretching vibration and a bending vibration occurs if the stretching bond is one side of an angle varied by bending vibration
- Coupling is greatest when the coupled groups have approximately equal energies
- No coupling is seen between groups separated by two or more bonds

4.2.5.2 Some General Trends

- Stretching frequencies are higher than corresponding bending frequencies. (It is easier to bend a bond than to stretch or compress it.)

- Bonds to hydrogen have higher stretching frequencies than those to heavier atoms.
- Triple bonds have higher stretching frequencies than corresponding double bonds, which in turn have higher frequencies than single bonds (Except for bonds to hydrogen).

4.2.6 The Fingerprint Region

The fact that there are many different vibrations even within relatively simple molecules means that the infrared spectrum of a compound usually contains a large number or peaks, many of which will be impossible to confidently assign to vibration of a particular group. Particularly notable is the complex pattern of peaks below 1500 cm^{-1} which are very difficult to assign. However, this complexity has an important advantage in that it can serve as a *fingerprint* for a given compound. Consequently, by referring to known spectra, the region can be used to identify a compound.

4.3 Interpretation of Spectra

To obtain a more detailed interpretation of an IR spectrum, two types of analysis are usually done : Qualitative and Quantitative analysis.

4.3.1 Qualitative Analysis

The combination of the fundamental vibrations or rotations of various functional groups and the subtle interactions of these functional groups with other atoms of the molecule results in the unique, generally complex IR spectrum for each individual compound. IR spectroscopy is mainly used in two ways: structural elucidation and compound identification.

4.3.1.1 Structural Elucidation

Because of complex interactions of atoms within the molecule, IR absorption of the functional groups may vary over a wide range. However, it has been found that many functional groups give characteristic IR absorption at specific, narrow frequency ranges regardless of their relationship with the rest of the molecule.

Multiple functional groups may absorb at one particular frequency range, but a functional group often gives rise to multiple-characteristic absorption. Thus, the spectral interpretations should not be confined to one or two bands and the whole spectrum should be examined.

For systematic evaluation, the IR spectrum is commonly divided into three regions :

- The Functional Group Region, 4000 to 1300 cm^{-1}
- The appearance of strong absorption bands in the region of 4000 to 2500 cm^{-1} usually comes from stretching vibrations between hydrogen and some other atoms with a mass of 19 or less.
- The O-H and N-H stretching frequencies fall in the 3700 to 2500 cm^{-1} region, with various intensities.

4.3.1.2 Compound Identification

Since the IR spectrum of every molecule is unique, one of the most positive identification methods of an organic compound is to find a reference IR spectrum that matches that of the unknown compound. Therefore, to obtain a more detailed interpretation of an IR spectrum it is necessary to refer to correlation charts and tables of infrared data. A large number of reference spectra for vapor and condensed phases are available in printed and electronic formats. The spectral libraries compiled by Sadtler and Aldrich are some of the most popular collections. In addition, spectral databases are often compiled according to application areas such as forensics, biochemicals, and polymers. Computerized search programs can facilitate the matching process.

However, there are many different tables available for reference and a brief summary is given below for some of the main groups.

When assigning peaks to specific groups in the infrared region it is usually the stretching vibrations which are most useful. Broadly speaking, these can be divided into four regions:

- 3700 – 2500 cm^{-1} → Single bonds to hydrogen
- 2300 – 2000 cm^{-1} → Triple bonds
- 1900 –1500 cm^{-1} → Double bonds
- 1400 – 650 cm^{-1} → Single bonds (other than hydrogen)

It should also be noted that the region 1650 – 650 cm^{-1} contains peaks due to bending vibrations but it is rarely possible to assign a specific peak to a specific group.

In many cases where exact match to the spectrum of an unknown material cannot be found, these programs usually list the reference compounds that match the unknown spectrum most closely. This information is useful in narrowing the search. When it is combined with the data from other analysis such as NMR or mass spectrometry, a positive identification or high-confidence level tentative identification can often be achieved.

In Table 4.3.1a more detail lists of bonds and their corresponding peaks are listed.

Table 4.3.1 : Some Characteristics bonds and their corresponding peaks in the IR spectra.

Type of Bonds	**Bond**	**Wavenumber (cm^{-1})**	**Notes**
Single Bonds to Hydrogen	C–H	3000 – 2850	Saturated alkanes, limited value as most organic compounds contain C-H
	=C–H	3100 – 3000	Unsaturated alkene or aromatic
	≡C–H	3300	Terminal Alkyne
	O=C–H	2800 and 2700	Aldehyde, two weak peaks
	O–H O–H (free)	340 – 3000 ~3600	Alcohols and Phenols. If hydrogen bonding present peak will be broad 3000-2500 (*e.g.* carboxylic acids)
	N–H	3450 – 3100	Amines: Primary - several peaks, Secondary - one peak, tertiary - no peaks
Double Bonds	C=O	1840 – 1800 & 1780 – 1740	Anhydrides
	C=O	1815 – 1760	Acyl halides
	C=O	1750 – 1715	Esters
	C=O	1740 – 1680	Aldehydes
	C=O	1725 – 1665	Ketones
	C=O	1720 – 1670	Carboxylic acids
	C=O	1690 – 1630	Amides
	C=C	1675 – 1600	Often weak
	C=N	1690 – 1630	Often difficult to assign
	N=O	1560 – 1510 & 1370 – 1330	Nitro compounds
Triple Bonds	C≡C	2260 – 2120	Alkynes, bands are weak
	C≡N	2260 – 2220	Nitriles
Single Bonds (not to Hydrogen)	C–C	Variable	No diagnostic value
	C–O, C–N	1400 – 1000	Difficult to assign
	C–Cl	800 – 700	Difficult to interpret
Bending Vibrations	R–N–H	1650 – 1500	Take care not to confuse N-H bend with the C=O stretch in amides
	R–C–H	1480 – 1350	Saturated alkanes and alkyl groups
	R–C–H	1000 – 680	Unsaturated alkenes and aromatics

4.4 Instrumentation

In simple terms, IR spectra are obtained by detecting changes in transmittance (or absorption) intensity as a function of frequency. This instrument uses a source of infrared radiation such as a nichrome wire or cooled rod of silicon carbide to produce a range of frequencies which are then separated into individual frequencies using a monochromator diffraction grating. The beam produced is then split into two; and one passes through the sample whilst the other is used as a reference beam. The two beams then converge on the detector which measures the difference in intensity and then sends a proportional signal to the recorder. The resulting plot is a measure of transmission against frequency which is usually plotted as wavenumber (cm^{-1}).

Most commercial instruments separate and measure IR radiation using dispersive spectrometers or Fourier transform spectrometers. This method has some obvious advantages. Firstly, it is much quicker, taking seconds instead of minutes to record a complete spectrum. A further advantage is that it is possible to get a spectrum from very small or very dilute samples by performing multiple scans and adding the data to improve the signal-to-noise ratio. Slow scans using diffraction gratings are inefficient. Almost all modern IR spectrometers use a different approach, the Fourier transform method, to scan the full spectral range at the same time.

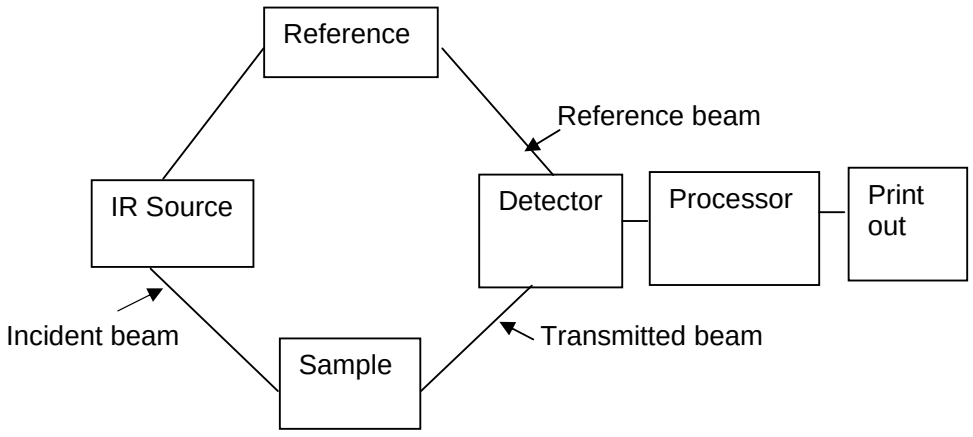

Figure 4.4.1 Schematic Diagram of a double beam Infrared Spectrometer

4.5 Differential Thermal Analysis

The term thermal analysis is frequently used to describe analytical experimental techniques, which is used to investigate the behavior of a sample as a function of temperature [2-4].

The DTA is a process of accurately measuring the difference in the temperature between a thermocouple embedded to a sample and a thermocouple in a standard inert material such as aluminum oxide while both are being heated at a uniform rate. The technique of DTA is an important tool to study the structural and phase changes occurring both in solid and in liquid materials during heat treatment. These changes may be due to dehydration, transition from one crystalline form to another, destruction of crystalline structure, oxidation, decomposition etc.

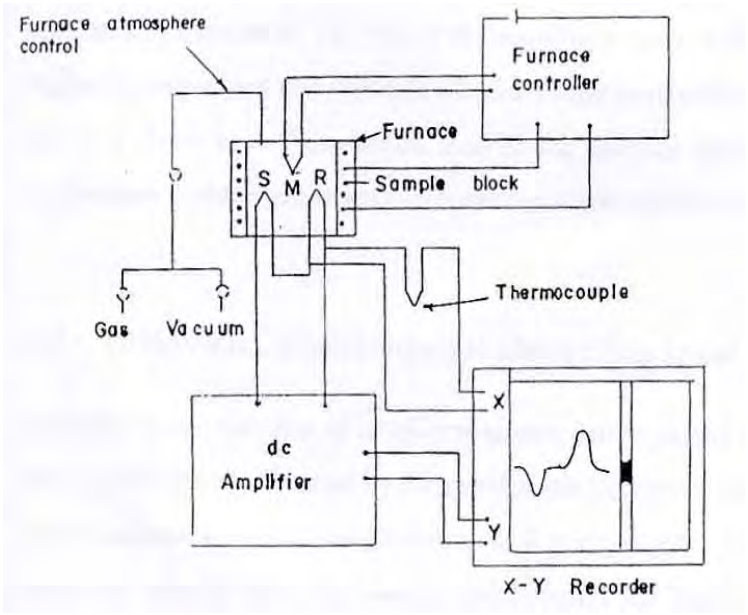

Figure 4.5.1 A schematic diagram showing different parts of a DTA apparatus.

The principle of DTA consists of measuring heat changes associated with the physical or chemical changes occurring when any substance is gradually heated. The thermocouple(platinum-platinum rhodium 13%) for DTA measurement is incorporated at the end of each of the balance beam ceramic tubes, and the temperature difference between the holder on the sample side and the holder on the reference side is detected. This signal is amplified and becomes the temperature difference signal used to measure the thermal change of the sample.

4.6 Thermogravimetric Analysis

The TGA is a branch of thermal analysis, which examines the mass change of a sample as a function of temperature in the scanning mode or as a function of time in the isothermal mode under a variety of conditions, and to examine the kinetics of the physico-chemical processes occurring in the sample. Sample weight changes are measured as described below in Figure 4.6.1.

Figure shows the sample balance beam and reference balance beam are independently supported by a driving coil/pivot. When a weight change occurs at the beam end, the movement is conveyed to the opposite end of the beam via the driving coil/pivot, when optical position sensors detect changes in the position of a slit. The signal from the optical position sensor is sent to the balance circuit.

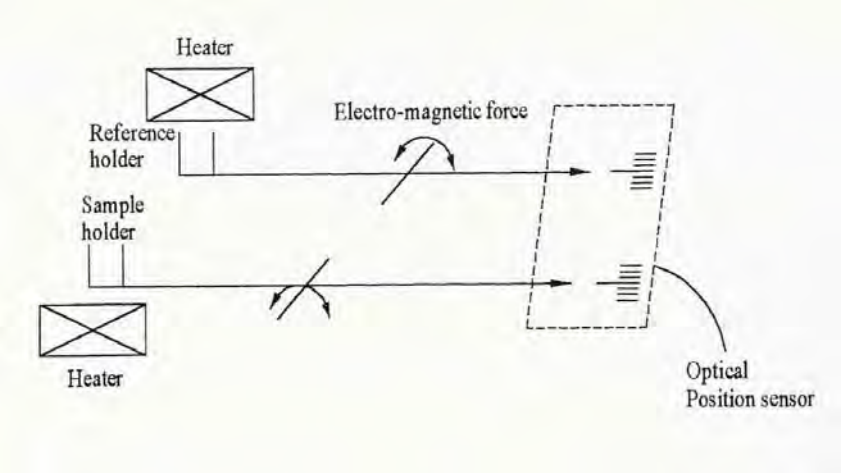

Figure 4.6.1 TGA measurement Principle.

The TGA is used to characterize the decomposition and thermal stability of materials. The balance circuit supplies sufficient feedback current to the driving coil so that the slit returns to the balance position. The current running to the driving coils on the sample side and the current running to the driving coil on the reference side is detected and converted into weight signals.

4.7. Results and Discussion

4.7.1 Fourier Transform Infrared Spectroscopic Analyses

4.7.1.1 PPPy and PPTMA Thin Films

Figure 4.7.1 represents the FTIR spectra of pyrrole monomer and PPPy, and in the Table 4.7.1 the peak assignments for the pyrrole monomer and peak assignments for the PPPy thin films are shown.

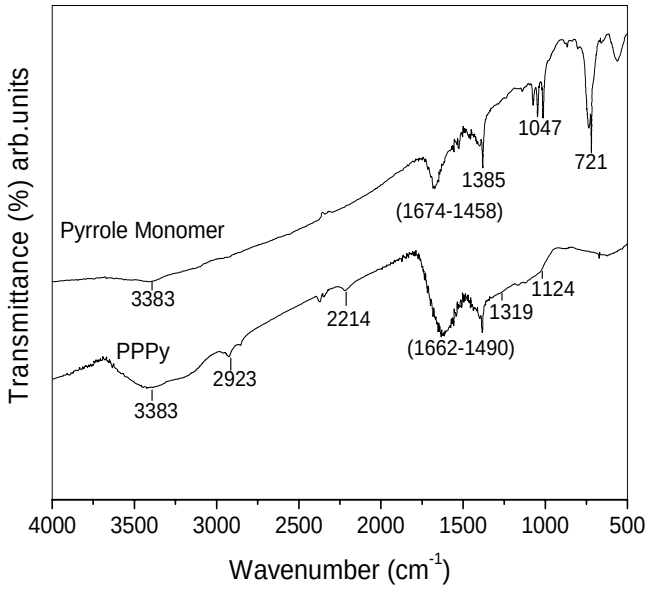

Figure 4.7.1 The FTIR spectra of Pyrrole monomer and PPPy.

In the FTIR spectrum of the pyrrole monomer and PPPy (Figure 4.7.1) the absorption bands are found to be very close to those reported previously [5, 6, 7]. It is seen that the FTIR spectrum of the PPPy is relatively complicated than that of the pyrrole monomer. Both spectra show a strong peak at about 3383 cm^{-1}, which is due to the N-H bond stretching vibration of primary and secondary amines and imines [6]. The absorption around 1650 cm^{-1} corresponds to the amines in the pyrrole structure. At about 2923 cm^{-1}, there is a sharp peak in PPPy spectrum but not in monomer spectrum. The peak is due to asymmetric and symmetric C-H stretching vibrations of saturated hydrocarbon. Pyrrole has highly strained ring so that the ring is easy to open under plasma polymerization. Therefore the FTIR spectrum of PPPy is very different to that of the monomer. In the molecular structure of the pyrrole monomer, all the carbon atoms are unsaturated. Thus, the peaks around 2900 cm^{-1} arise due to the plasma polymerization. There is another special peak around 720 cm^{-1} appearing in the spectrum of pyrrole monomer, but not in the spectrum of PPPy. This peak usually belongs to $–CH_2–$ unites. All of these differences indicated that the monomer undergone the re-organization during the plasma polymerization.

Table 4.7.1 Assignments of FTIR absorption peaks for Pyrrole monomer and PPPy

Vibrations	Wavenumber (cm^{-1})	
	Pyrrole	PPPy
N-H stretching vibration of primary and secondary amines	3383	3383
Asymmetric and symmetric **C-H** stretching vibration of saturated hydrocarbon	-	2923
—N=C=O	-	2214
C=C conjugated and **C=N** conjugated stretch and **N-H** deformation vibration	1674-1458	1652-1490
Alkane **C-H** deformation	1384	-
C-N stretching vibration	1047	1124
Tetra substituted Benzene	-	-
C-H out of plane bending	721	-

Figure 4.7.2 shows the FTIR spectra of TMA and PPTMA and in Table 4.7.2 the peak assignments for TMA and PPTMA are presented.

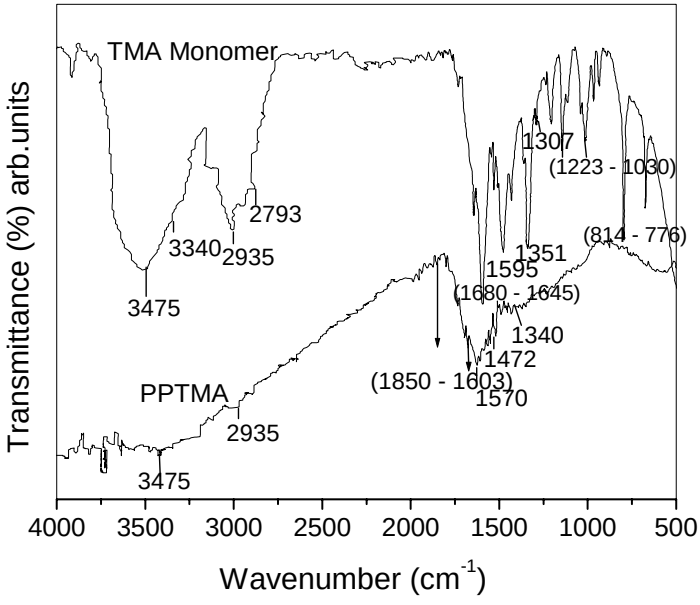

Figure 4.7.2 The FTIR spectra of TMA monomer and PPTMA [8].

Table 4.7.2 Assignments of FTIR absorption peaks for TMA monomer and PPTMA [8]

Vibrations	Wavenumber (cm^{-1})	
	TMA	PPTMA
N-H stretching vibration of primary and secondary amines	3475	3435
Symmetric **N-H** stretching vibration	3340	-
Asymmetric and symmetric **C-H** stretching vibration of saturated hydrocarbon	2935, 2793	2935
C=O	-	1850-1603
C=C stretching vibration	1680-1645	
C=C stretching vib. in benzenoid and quinoid	1595, 1484	1570, 1472
C-N stretching vibration	1351, 1307, 1223 -1030	1340
Tetra substituted Benzene	814 - 776	-

4.7.1.2 Plasma Polymerized Pyrroly-N,N,3,5 Tetramethylaniline Composite Bilayer Thin Films

Figure 4.7.3 represents the FTIR spectra of the PPPy-PPTMA bilayer thin films and in Table 4.7.3 the peak assignments for the Figure 4.7.3 is also given. For comparative study, the FTIR spectra of PPPy and PPTMA thin films are also presented in this figure.

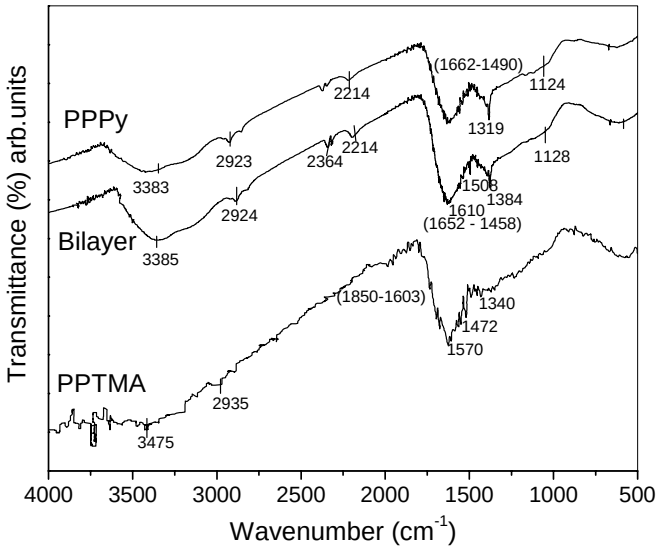

Figure 4.7.3 The FTIR spectra of PPPy, PPTMA and PPPy-PPTMA bilayer films.

Table 4.7.3 Assignments of FTIR peaks for PPPy, PPTMA and PPPy-PPTMA bilayer films

Vibrations	Wavenumber (cm^{-1})		
	PPPy	PPTMA	PPPy-PPTMA
N-H stretching vibration of primary and secondary amines	3383	3435	3385
Asymmetric and symmetric **C-H** stretching vibration of saturated hydrocarbon	2923	2935	2924
—N=C=O	2214	-	2214
C=O	-	1850-1603	-
C=C conjugated and **C=N** conjugated stretch and **N-H** deformation vibration	1652-1490	-	1652-1458
C=C stretching vib. in benzenoid and quinoid	-	1570, 1472	1610, 1508
Alkane **C-H** deformation	-	-	1384
C-N stretching vibration	1124	1340	1128

Comparing the FTIR spectra of PPPy and PPPy-PPTMA sample, it is seen that both the spectra exhibit a broad band between 3300 cm^{-1} and 3400 cm^{-1}, which is due to the N-H stretching vibration of primary and secondary amines and imines [6]. In the bilayer film the relative intensity of this peak is higher than that in the PPPy film. The bilayer film has a relatively more intense peak at 2924 cm^{-1} compared to 2923 cm^{-1} of PPPy film and 2935 cm^{-1} of PPTMA films, which is due to the symmetric and asymmetric C-H stretching vibration of saturated hydrocarbons. Since the peak around 2930 cm^{-1} can be attributed to the asymmetric CH_2 vibration, it can be suggested that the bilayer film contains more methylene groups than the other films. In addition to this, the bilayer spectrum exhibits peak at 1384 cm^{-1} which is due to the C-H deformation of a CH_3 group. This again shows that the bilayer film contains more methylene groups than the PPPy or PPTMA films. The absorption peak at 2214 cm^{-1} in both PPPy and PPPy-PPTMA films suggests the introduction of —N=C=O group [9, 10] which is very typical in plasma polymerization [11]. The absorption at 1508 cm^{-1} and 1610 cm^{-1} of bilayer films can be assigned to the benzoid and quinoid structures of the benzene rings in TMA. As expected, they are found due to the presence of TMA, because pyrrole does not contain any benzene rings. This study, however, shows that the bilayer films contain the characteristics of both the monomers.

Table 4.7.4 Assignments of FTIR absorption peaks for Pyrrole, PPPy, TMA, PPTMA and PPPy-PPTMA sample

Vibrations	Wavenumber (cm^{-1})				
	Pyrrole	PPPy	TMA	PPTMA	PPPy-PPTMA
N-H stretching vibration of primary and secondary amines	3383	3383	3475	3435	3385
Symmetric **N-H** stretching vibration	-	-	3340	-	-
Asymmetric and symmetric **C-H** stretching vibration of saturated hydrocarbon	-	2923	2935, 2793	2935	2924
—N=C=O	-	2214	-	-	2214
C=O	-	-	-	1850-1603	-
C=C conjugated and **C=N** conjugated stretch and **N-H** deformation vibration	1674-1458	1652-1490	-	-	1652-1458
C=C stretching vibration	-	-	1680-1645		-
C=C stretching vib. in benzenoid and quinoid	-	-	1595, 1484	1570, 1472	1610, 1508
Alkane **C-H** deformation	1384	-	-	-	1384
C-N stretching vibration	1047	1124	1351, 1307, 1223 -1030	1340	1128
Tetra substituted Benzene	-	-	814 - 776	-	-
C-H out of plane bending	721	-	-	-	-

Table 4.7.4 shows the peak assignments of FTIR spectra for pyrrole monomer and PPPy, TMA monomer and PPTMA and PPPy-PPTMA together for an overall comparison. As discussed above, a comparative study from the Table 4.7.4 between the pyrrole monomer and PPPy clearly shows characteristics differences, especially at 2923, 2214 and 721 cm^{-1}, which indicate that the monomer has undergone the re-organization during the plasma polymerization. In a similar comparative study between TMA monomer and PPTMA, the differences might be observed especially at 3340, 2793, 1850-1603, 1680-1645, and 814-776 cm^{-1}. From these differences it is indicated that the PPTMA film deposited by the plasma polymerization technique does not exactly resemble to that of the TMA structure. Finally, comparison between PPPy, PPTMA and PPPy-PPTMA shows that the bilayer films contain the characteristics of both the monomer.

4.7.2 Differential Thermal Analysis and Thermogravimetric Analysis

4.7.2.1 PPPy and PPTMA Thin Films

The DTA and TGA traces taken at 20 C / min for PPPy and PPTMA are shown in Figure 4.7.4 and Figure 4.7.5 respectively. The DTA thermogram shows an exotherm, which reaches a maximum at around 295^{o}C. The corresponding TGA trace of PPPy has been taken from 50 ^{o}C to 750^{o}C and showed different stages of thermal decomposition, which divided in three regions (A, B, and C). Every region may be associated with a different rate of weight loss. The weight losses in A, B, and C regions are about 1 %, 9%, and 23% at about 47 ^{o}C, 315 ^{o}C and 550^{o}C respectively.

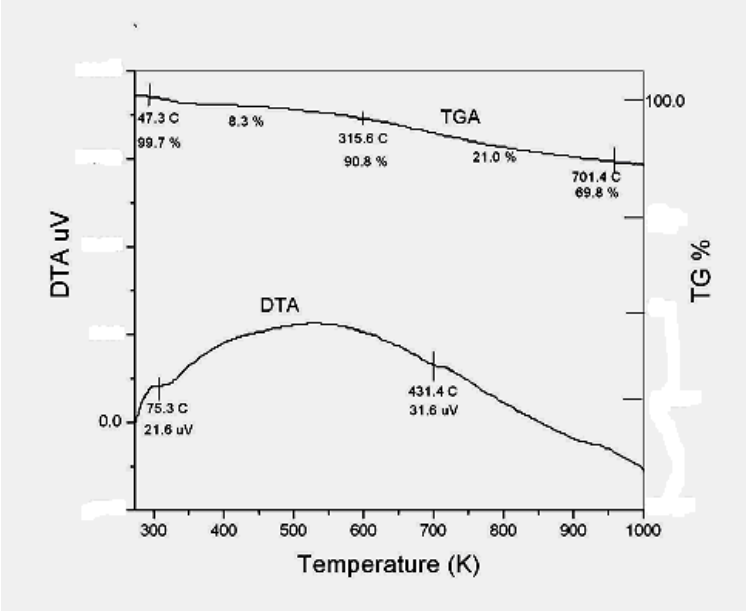

Figure 4.7.4 The DTA/TGA traces of PPPy thin films.

In the first region A, the weight loss may be due to the removal of water content, which is not necessarily associated with any change in the structure. Therefore, it could be ascertain that PPPy did not lose an important mass percentage during the first 100 °C because they had a humidity content lower than 1% mass. This low humidity content did not significantly influence the conductivity, resulting in an approximately linear behavior with temperature. In the region B the PPPy had a humidity reaching almost 9% mass. The capacity to store water in the structure of the polymers can be related to the crosslinking promoted by longer reaction times. Greater reaction times produced more crosslinked material, reducing the affinity of the polymers to the water molecules. Smaller reaction times produced more linear chains and conformations that tended to incorporate greater quantities of water molecules. However, the 9% of weight loss in the region B may also be attributed to the loss of non-constitutional or adsorbed water and unreacted monomer settled on PPPy films surface and/or due to evolution of hydrogen and low molecular mass hydrocarbons gases. The maximum change in the PPPy structure has been occurred in the region C. The weight loss of 23% in this region is important because the DTA curve exhibits a wide peak. In region C the weight loss may be caused by the thermal breakdown of the PPPy structure and

expulsion of higher molecular mass hydrocarbons, oxygen containing compounds, etc. Thus, it may be attributed that PPPy films are thermally stable up to about 400°C.

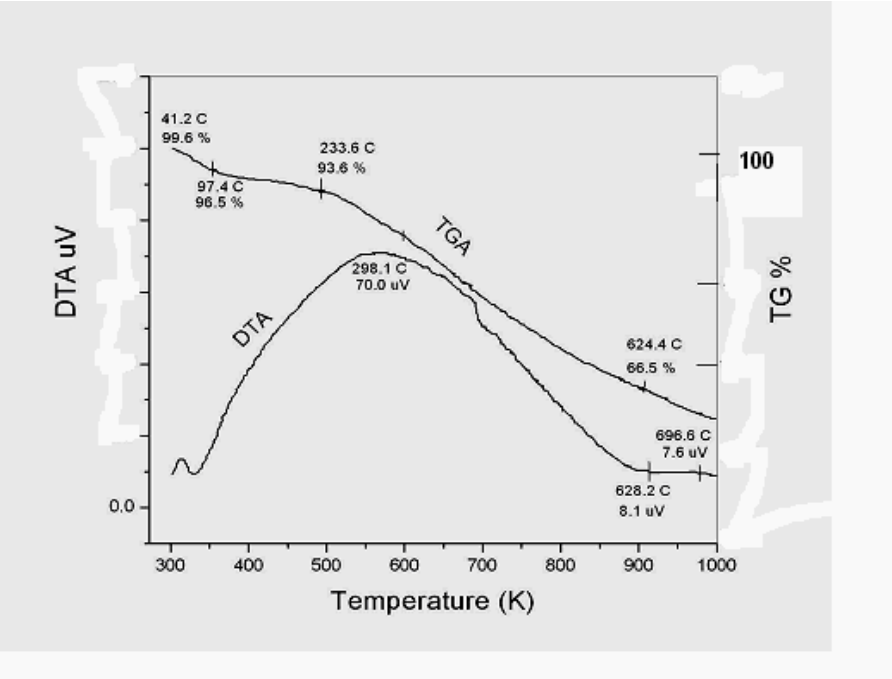

Figure 4.7.5 The DTA/TGA traces of PPTMA thin films.

4.7.2.2 Plasma Polymerized Pyrroly-N,N,3,5 Tetramethylaniline Bilayer Thin Films

The DTA and TGA traces taken at 20°C /min for PPPy-PPTMA are shown in Figure 4.7.6. The DTA thermogram shows an exotherm, which reaches a maximum at around 380°C. The corresponding TGA trace of PPPy-PPTMA bilayer thin films has been taken from 50 to 800°C and showed different stages of thermal decomposition, which divided in three regions (A, B, and C). Every region may be associated with a different rate of weight loss. Though no significant weight loss is observed in region A (at about 97°C), but the weight losses at B and C regions are about 8%, and 47% at about 220^{o}C and 450^{o}C respectively. In the region B the PPPy-PPTMA bilayer thin films had a humidity reaching almost 9 mass %. The capacity to store water in the structure of the polymers can be related to the crosslinking promoted by longer reaction times. Greater reaction times produced more crosslinked material, reducing the affinity of the polymers to the water molecules. Smaller reaction times produced more linear chains and conformations that tended to incorporate greater quantities of water molecules. However, the 8% of weight loss in the region B may also be attributed to the loss of non-constitutional or adsorbed water and unreacted monomer settled on PPPy-PPTMA bilayer thin films surface and/or due to evolution of hydrogen and low molecular mass hydrocarbons gases. The maximum change in the PPPy-PPTMA bilayer structure has been occurred in the region C. The weight loss of 47% in this region is important because the DTA curve exhibits a wide peak. In region C the weight loss may be caused by the thermal breakdown of the PPPy-PPTMA bilayer structure and expulsion of higher molecular

mass hydrocarbons, oxygen containing compounds, etc. Thus, it may be attributed that PPTMA films are thermally stable up to about 400 ^{o}C.

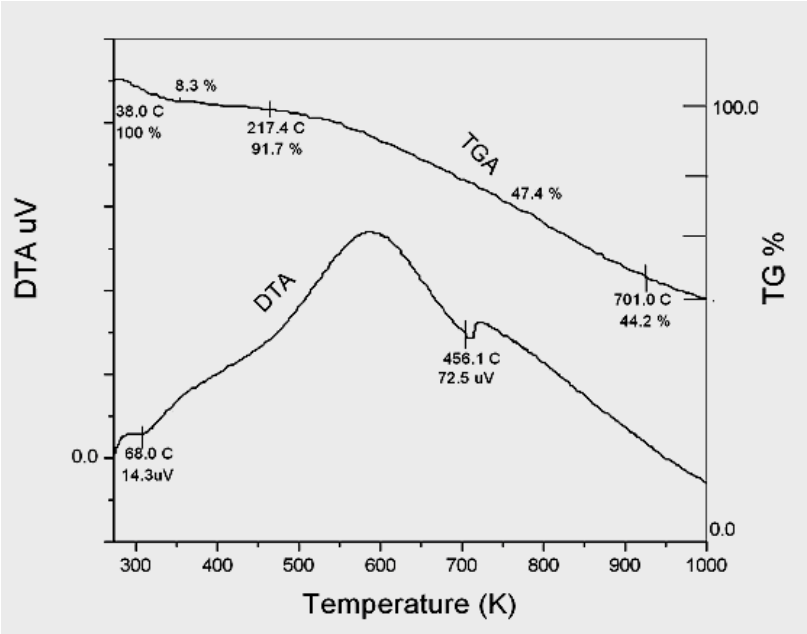

Figure 4.7.6 The DTA/TGA traces of PPPy-PPTMA bilayer thin films.

However, beginning around 400 °C, the polymers have a moderate mass loss that continues up to approximately 800 °C. After this point, only small fragments of the chains remain in the samples. At 800°C, the samples have less than 60% of their initial mass.

4.8 Conclusions

A comparative study of the FTIR spectra of pyrrole monomer and PPPy clearly shows characteristics differences, especially at 2923, 2214 and 721 cm^{-1}, which indicates that the monomer has undergone the re-organization during the plasma polymerization. It is reported that the PPTMA deposited by the plasma polymerization technique does not exactly resemble to that of the TMA structure. Finally, comparison between PPPy, PPTMA and PPPy-PPTMA shows that the bilayer films contain the characteristics of both the monomer.

It is observed by DTA and TGA that PPPy, PPTMA and PPPy-PPTMA bilayer composite thin films lose approximately 23%, 28% and 40% of their initial mass at 550, 650 and 450 C. The weight loss in PPPy-PPTMA bilayer samples is much higher than that of its components even at relatively lower temperature. This behavior suggests that less breakdown thermal energy is needed for PPPy-PPTMA samples than those of its components. The weight loss in PPPy and PPTMA are lower relatively at higher temperature, therefore they are more stable, and greater thermal energy is needed to breakdown. The significant loss in the mass in PPPy-PPTMA bilayer samples suggests that in the bilayer structure the bonds require less thermal energy to dissociate in comparison to the bonds formed in the PPPy and PPTMA chains, which need greater thermal energy to dissociate the bonds.

References

[1] Silverstein, R. M., Bassler, G. C., and Morrill, T.C., *Spectrometric identification of organic compounds*, John Willey & Sons, New York, 1981.

[2] Wu, L., Zhu, C., and Liu, M., *Study on plasma polymerization of 1.1.1-trifluoroethene: deposition and structure of plasma polymer films*, Desalination, 192, 234-240, 2006.

[3] Jafari, R., Tatoulian, M., Morscheidt, W., Arefi-Khonsari, F., *Stable plasma polymerized acrylic acid coating deposited on polyethylene (PE) films in a low frequency discharge*, Reactive and Functional Polymers, 66, 1757-1765, 2006.

[4] Zhao Xiong-Yan, Wang Ming-Zhu, and Xiao Jun; *Deposition of plasma conjugated polynitrile thin films and their optical properties*, Euro. Polym. J. 42, 2161-2167, 2006.

[5] John Rajan, K., and Sakthi Kumar, D., *Structural, electrical, and optical studies of plasma-polymerized and iodine-doped poly pyrrole*, J. Appl. Polym. Sci., 83, 1856 -1859, 2002.

[6] Eufinger, S., Van Ooij, W. J, Ridgway, H., *DC plasma-polymerization of pyrrole: comparison of films formed on anode and cathode*, J. Appl. Polym. Sci., 61, 1503 -1514, 1996.

[7] Sakthi Kumar, D., Kenji Nakamura, Satoko Nishiyama, Shigeru Ishii, Hiromichi Noguchi, Kunihiro Kashiwagi, and Yasuhiko Yoshida; *Optical and electrical characterization of plasma polymerized pyrrole films* J. Appl. Phys., 93, 2705-2711, 2003.

[8] Akther, H. and Bhuiyan, A. H., *Infrared and ultra violet-visible spectroscopic investigation of plasma polymerized N,N,3,5 -tetramethylaniline thin films*, Thin Solid Films 474, 14-18, 2005.

[9] Zhang, J., Wu, M. Z., Pu, T. S., Zhang, Z. Y., Jin, R. P., Tong, Z. S., Zhu, D. Z., Cao, D. X., Zhu, F. Y., and Cao, J. Q., Thin Solid Films 307, 14, 1997.

[10] Fally, F., Doneux, C., Riga, J., and Verbist, J. J., *Quantification of the functional groups present at the surface of plasma polymers deposited from propylamine, allylamine, and propargylamine* , J. Appl. Polym. Sci 56, 597-614, 1995.

[11] Yasuda, H., Bumgarner, M. O., Marsh, H. C., Morosoff, N., *Plasma polymerization of some organic compounds and properties of the polymers*, J. Polym. Sci. Polym. Chem., 14, 195-224, 1976.

Chapter 5

The Optical Characterization

The existing theories for optical characterization of plasma polymerized thin films are described in this chapter and the corresponding experimental results e.g. optical absorption, absorption coefficient, extinction coefficient, direct and indirect energy band etc, are also discussed.

5.1 Introduction

The investigations about the interactions between the matter and the light in different frequency range of the electromagnetic radiation to provide precise information about atomic and molecular structure is the main feature for optical characterization. Optical measurement constitutes the most important means of determining the band structures of materials. Photo induced transitions can occur between different bands, which lead to the determination of the energy band gap, or within a single band such as the free carrier absorption. Optical measurements can also be used to study lattice vibrations.

When light is incident on a material, the optical phenomena of absorption, reflection, and transmission are observed. From these optical effects, much of the information are obtained, e.g. from absorption spectrum, the absorption coefficients, the extinction coefficients, optical band gaps etc as a function of photon energy, could be evaluated.

At high energies, photons are absorbed by the transitions of electrons from filled valence band states to empty conduction band states. For energies just below the lowest forbidden energy gap, radiation is absorbed due to the formation of excitants, and electron transitions between band and impurity states. The transitions of free carriers within energy bands produce an absorption continuum which increases with decreasing photon energy. Also, the crystalline lattice itself can absorb radiation, with the energy being given off in optical phonons. Finally, at low energies, or long wavelengths, electronic transitions can be observed between impurities and there associated bands.

The Ultraviolet-Visible (UV-Vis) spectroscopy is being widely used to study the optical properties of plasma polymerized thin films. Using UV-visible spectroscopy, the precise information about atomic and molecular structure obtained by investigating the interactions between ultraviolet or visible electromagnetic radiation and matter, some functional groups in molecules can be identified. The other important application of UV-vis spectroscopy is to determine the presence, nature and extent of conjugation present in the material. Increasing conjugation length generally moves the absorption spectrum to longer wavelengths and finally into the visible region. Moreover, the impurity states, optical absorption coefficients, refractive index, extinction coefficients, optical energy gaps, the allowed direct and indirect forbidden transitions of optically active substances can also be evaluated by using this spectroscopic method. These properties refers to the potential applications such as light guide materials, optical fibers, photo diodes, optical coating to inhibit corrosion, etc [1-4].

Spectral lines observed in the UV-visible region correspond to the energy difference between two well-defined electronic energy levels of the absorbing atom or molecule. As the direct relationship between energy and frequency shows that light of lower frequency will carry fewer energetic photons than light of a higher frequency. Therefore, when an atom or molecule absorbs energy in that region, its electrons are promoted from a state of lowest energy, i.e. the ground state, to states, or orbitals, of higher energy. Because energy is quantized, it seems safe to assume that absorption peaks in a UV-vis spectrum will be sharp

peaks. This is because there are also vibrational and rotational energy levels available to absorbing materials. These vibrations and rotations also have discrete energy levels, which can be considered as being packed on top of each electronic level. UV-visible spectroscopy thus provides direct evidence about electron energy jumps between distinct energy levels. For example, the spectrum of hydrogen consists of a series of sharp spectral lines, each of which results from an electron jumping from one energy level to another while emitting a photon of energy equal to the energy difference between the two levels. Associated with the electronic transitions observed in the UV-visible region, changes of vibrational and rotational energy also influence the shape of the spectral bands. If the material is a gas, the molecular electronic spectrum is sharp and well-resolved, consisting of distinct lines, such as the hydrogen spectrum. If the material is in the liquid state, the spectral bands are blurred and significantly broadened because the vibrational motions can not occur as freely as they could in the gas phase. Not all molecules exhibit pure vibrational-rotational spectra, but all of them can produce electronic spectra because there will always be excited states to which the electrons of molecules can be raised by the absorption of UV-visible radiation.

5.2 Theory of Light

5.2.1 The Electromagnetic Spectrum and Quantum theory

The full electromagnetic radiation spectrum is continuous and each region merges slowly into the next. For convenience of reference, definitions of the various spectral regions have been set by the Joint Committee on Nomenclature in Applied Spectroscopy.

The electromagnetic spectrum does not stop with the visible lights. The wavelengths shorter than violet light or longer than red light are also possible. The human eye is only sensitive to a tiny proportion of the total electromagnetic spectrum between approximately 380 and 780 nm and within this area we perceive the colors of the rainbow from violet through to red. Figure 5.2.1 shows the visible region on a linear scale.

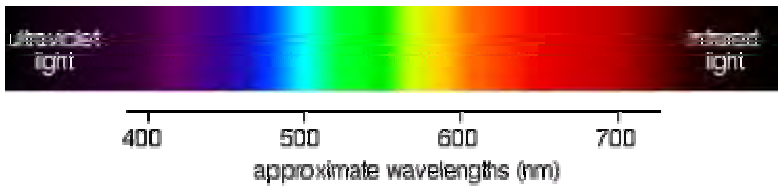

Figure 5.2.1 The visible region of light in an electromagnetic spectrum.

When white falls upon a sample, the light may be totally reflected, in which case the substance appears white or the light may be totally absorbed, in which case the substance will appear black. If, however, only a portion of the light is absorbed and the balance is reflected, the color of the sample is determined by the reflected light. A close relationship exists between the color of a substance and its electronic structure. A molecule or ion will exhibit absorption in the visible or ultraviolet region when radiation causes an electronic

transition within its structure. Thus, the absorption of light by a sample in the ultraviolet or visible region is accompanied by a change in the electronic state of the molecules in the sample. The energy supplied by the light will promote electrons from their ground state of lower energy to excited state of higher energy

To gain an understanding of the origins of practical absorption spectrometry, a short diversion into quantum theory is necessary. For this purpose, it is best to think of radiation as a stream of particles known as photons instead of the waves. Atoms and molecules exist in a number of defined energy states or levels and a change of level requires the absorption or emission of an integral number of a unit of energy called quantum, or in our context, a photon. The energy of a photon absorbed or emitted during a transition from one molecular energy level to another is given by the equation

$$E = h\nu \tag{5.1}$$

where h is known as Planck's constant E and ν are the energy and frequency of the photon respectively. This equation means that the absorbance of a higher frequency light requires high energy jump.

Each wavelength of light has a particular energy associated with it. If that particular amount of energy is just right for making an energy jump, then that wavelength will be absorbed and its energy will have been used in promoting an electron. Since the relationship between wavelength and frequency is given by the following equation

$$\lambda = \frac{c}{\nu} \tag{5.2}$$

Therefore, it is obvious that higher the frequency, the lower the wavelength is, i.e., the shorter the wavelength, the greater the energy of the light absorbed and vice versa.

A molecule of any substance has an internal energy which can be considered as the sum of

- the energy of its electrons
- the energy of vibration between its constituent atoms, and
- the energy associated with rotation of the molecule.

The electronic energy levels of simple molecules are widely separated and usually only the absorption of a high energy photon, that is one of very short wavelength, can excite a molecule from one level to another. In complex molecules the energy levels are more closely spaced and photons of near ultraviolet and visible light can effect the transition. These substances, therefore, will absorb light in some areas of the near ultraviolet and visible regions.

The vibrational energy states of the various parts of a molecule are much closer together than the electronic energy levels and thus photons of lower energy (longer wavelength) are

sufficient to bring about vibrational changes. Light absorption due to only to vibrational changes occurs in the infrared region.

The rotational energy states of molecules are so closely spaced that light in the far infrared and microwave regions of the electromagnetic spectrum has enough energy to cause these small changes.

For ultraviolet and visible wavelengths, one should expect that the absorption spectrum of a molecule (i.e., a plot of its degree of absorption against the wavelength of the incident radiation) should show a few very sharp lines. Each line should occur at a wavelength where the energy of an incident photon exactly matches the energy required to excite an electronic transition. But, in practice it is found that the ultraviolet and visible spectrum of most molecules consists of a few humps rather than sharp lines. These humps show that the molecule is absorbing radiation over a band of wavelengths. One reason for this band, rather than line absorption is that an electronic level transition is usually accompanied by a simultaneous change between the more numerous vibrational levels. Thus, a photon with a little too much or too little energy to be accepted by the molecule for a 'pure' electronic transition can be utilized for a transition between one of the vibrational levels associated with the lower electronic state to one of the vibrational levels of a higher electronic state. If the difference in electronic energy is 'E' and the difference in vibrational energy is 'e', then photons with energies of E, E+e, E+2e, E-e, E-2e, etc. will be absorbed.

Furthermore, each of the many vibrational levels associated with the electronic states also has a large number of rotational levels associated with it. Thus a transition can consist of a large electronic component, a smaller vibrational element and an even smaller rotational change. The rotational contribution to the transition has the effect of filling in the gaps in the vibrational fine structure.

In addition, when molecules are closely packed together as they normally are in solution, they exert influences on each other which slightly disturb the already numerous, and almost infinite energy levels and blur the sharp spectral lines into bands. In the vapor, the transitions between the vibration levels are visible as bands superimposed on the main electronic transition bands. In solution they merge together and at high temperature or pressure even the electronic bands can blur to produce single wide band.

5.2.2 Electronic Transitions

When the energy supplied by the light to a material and an atom or molecule absorbs this energy, then the electrons are promoted from their ground state (lowest energy state) to an excited state of higher energy. Since each wavelength of light has a particular energy associated with it, so, if that particular amount of energy is just right for making energy jumps, then that wavelength will be absorbed.

There are mainly three types of electronic transition:

- Transitions involving π, σ, and *n* electrons
- Transitions involving charge-transfer electrons
- Transitions involving *d* and *f* electrons

Since the energy supplied by the light promotes the electrons from their ground state orbitals to excited state orbitals or antibonding orbitals, it is important to know about the nature of these orbitals. Potentially, three types of ground state orbitals may be involved:

- σ (bonding) molecular as in

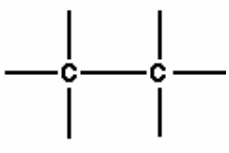

- π (bonding) molecular orbital as in

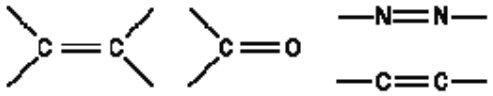

- n (non-bonding) atomic orbital as in

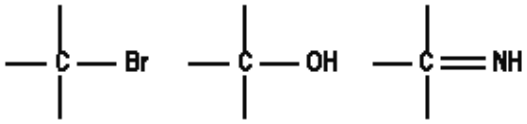

In addition, two types of antibonding orbitals may be involved in the transition:

- σ* (sigma star) orbital
- π* (pi star) orbital

Note that, a bond is actually an interaction between two or more atoms or groups of atoms which holds the atoms together. This interaction results from the sharing of electrons in (normally) incomplete shells of adjacent atoms. The predicted paths (orbitals) of the bonding electrons about the nucleus give each atom a particular shape which affects the way it bonds with the adjacent atoms. A molecule can have a combination of different types of bond orientations. Bonding occurs where there is a single electron in an orbital intended for two electrons. Antibonding occurs where both electrons are present in an orbital and this inhibits bonding.

The important jumps are:

- from π bonding orbitals to π* anti-bonding orbitals
- from n non-bonding orbitals to π* anti-bonding orbitals
- from n non-bonding orbitals to σ* anti-bonding orbitals
- from σ bonding orbitals to σ* anti-bonding orbitals etc.

A transition in which a bonding s electron is excited to an antibonding σ orbital is referred to as σ to σ* transition. In the same way π to π* represents the transition of one electron of a lone pair (non-bonding electron pair) to an antibonding π orbital. However, means that in order to absorb light in the region from 200 - 800 nm the molecule must contain either π bonds or atoms with non-bonding orbitals. It is to be noted that a non-bonding orbital is a lone pair on, say, oxygen, nitrogen or a halogen.

$\sigma \rightarrow \sigma^*$ Transitions

An electron in a bonding σ orbital is excited to the corresponding antibonding orbital. The energy required is large. For example, methane (which has only C-H bonds, and can only undergo $\sigma \rightarrow \sigma^*$ transitions) shows an absorbance maximum at 125 nm. Absorption maxima due to $\sigma \rightarrow \sigma^*$ transitions are not seen in typical UV-vis spectra (200 - 800 nm).

$n \rightarrow \sigma^*$ Transitions

Saturated compounds containing atoms with lone pairs (non-bonding electrons) are capable of $n \rightarrow \sigma^*$ transitions. These transitions usually need less energy than $\sigma \rightarrow \sigma^*$ transitions. They can be initiated by light whose wavelength is in the range 150 - 250 nm. The number of organic functional groups with $n \rightarrow \sigma^*$ peaks in the UV region is small.

$n \rightarrow \pi^*$ and $\pi \rightarrow \pi^*$ Transitions

Most absorption spectroscopy of organic compounds is based on transitions of n or π electrons to the π^* excited state. This is because the absorption peaks for these transitions fall in an experimentally convenient region of the spectrum (200 - 800 nm). These transitions need an unsaturated group in the molecule to provide the π electrons.

Absorption of ultraviolet and visible radiation in organic molecules is restricted to certain functional groups (*chromophores*) that contain valence electrons of low excitation energy. The spectrum of a molecule containing these chromophores is complex. This is because the superposition of rotational and vibrational transitions on the electronic transitions gives a combination of overlapping lines. This appears as a continuous absorption band.

A chromophore (literally color-bearing) group is a functional group, not conjugated with another group, which exhibits a characteristic absorption spectrum in the ultraviolet or visible region. If any of the simple chromophores is conjugated with another (of the same type or different type) a multiple chromophore is formed having a new absorption band which is more intense and at a longer wavelength than the strong bands of the simple chromophore. This displacement of an absorption maximum towards a longer wavelength (i.e. from blue to red) is termed a bathochromic shift. The displacement of an absorption maximum from the red to ultraviolet is termed a hypsochromic shift.

Some examples of chromophore and their excitation are shown in Table 5.2.1.

Table 5.2.1 Some simple chromophores and their light absorption characteristics

Chromophore	Example	Excitation	λ_{max}, nm
C=C	Ethene	$\pi \rightarrow \pi^*$	171
C≡C	1-Hexyne	$\pi \rightarrow \pi^*$	180
C=O	Ethanal	$n \rightarrow \pi^*$ $\pi \rightarrow \pi^*$	290 180
N=O	Nitromethane	$n \rightarrow \pi^*$ $\pi \rightarrow \pi^*$	275 200
C-X ; X=Br X=I	Methyl bromide Methyl Iodide	$n \rightarrow \sigma^*$ $n \rightarrow \sigma^*$	200 360

From the table 5.2.1 it is clear that the only molecular moieties likely to absorb light in the 200 to 800 nm region are pi-electron functions and hetero atoms having non-bonding valence-shell electron pairs. Such light absorbing groups are referred to as chromophores. The presence of chromophores in a molecule is best documented by UV-Visible spectroscopy, but the failure of most instruments to provide absorption data for wavelengths below 200 nm makes the detection of isolated chromophores problematic. Fortunately, conjugation generally moves the absorption maxima to longer wavelengths, and therefore conjugation becomes the major structural feature identified by this technique.

The solvent in which the absorbing species is dissolved also has an effect on the spectrum of the species. Peaks resulting from $n \rightarrow \pi^*$ transitions are shifted to shorter wavelengths (*blue shift*) with increasing solvent polarity. This arises from increased solvation of the lone pair, which lowers the energy of the *n* orbital. Often (but *not* always), the reverse (i.e. *red shift*) is seen for $\pi \rightarrow \pi^*$ transitions. This is caused by attractive polarization forces between the solvent and the absorber, which lower the energy levels of both the excited and unexcited states. This effect is greater for the excited state, and so the energy difference between the excited and unexcited states is slightly reduced - resulting in a small red shift. This effect also influences $n \rightarrow \pi^*$ transitions but is overshadowed by the blue shift resulting from solvation of lone pairs.

The possible electronic transitions which can occur by the absorption of ultraviolet and visible light are shown in Figure 5.2.2. This figure illustrates the general pattern of energy levels and the fact that the transitions are brought about by the absorption of different amounts of energy. In each possible case, an electron is excited from a full orbital into an empty anti-bonding orbital. Each jump takes energy from the light, and a big jump obviously needs more energy than a small one. Both s to σ* and n to σ* transitions require a great deal of energy and therefore occur in the far ultraviolet region or weakly in the region 180-240nm. Consequently, saturated groups do not exhibit strong absorption in the ordinary ultraviolet region. Transitions of the n to π* and π to π* type occur in molecules with unsaturated

centers; they require less energy and occur at longer wavelengths than transitions to σ* antibonding orbitals. Table 5.2.2 illustrates the type of transition and the resulting maximum wavelength.

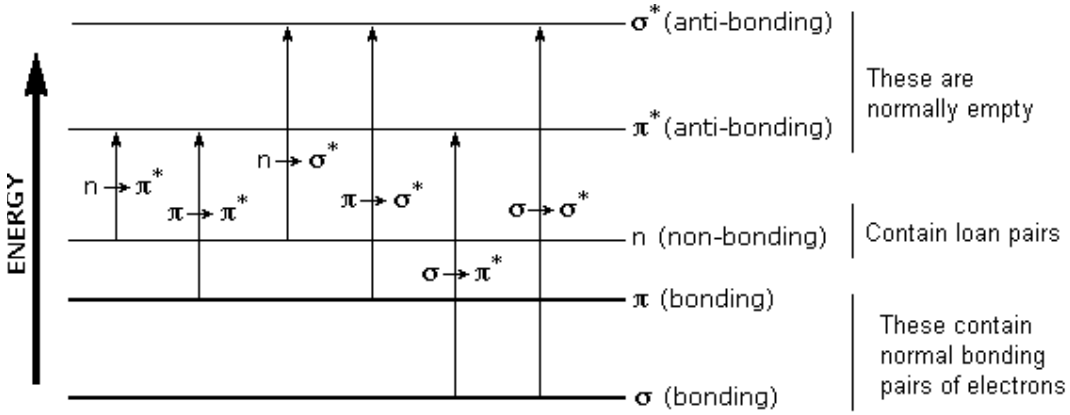

Figure 5.2.2 possible electronic transitions in the UV-visible region.

Table 5.2.2 Examples of transitions and resulting λ_{max}

Molecules		λmax (nm)
Ethane	σ → σ*	135
Methanol	σ → σ*	150
	η → σ*	163
Ethylene	π → π*	175
Benzene	π → π*	254
Acetone	η → π*	290

5.2.3 The Importance of Conjugation and Delocalization

Consider these three molecules:

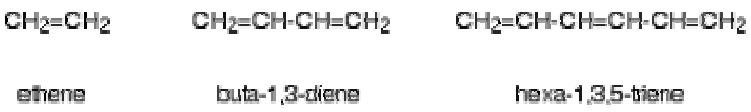

Ethane contains a simple isolated carbon-carbon double bond, but the other two have conjugated double bonds. In these cases, there is delocalization of the pi bonding orbitals over the whole molecule. The wavelengths of the light which each of these molecules absorbs is shown below :

molecule	wavelength of maximum absorption (nm)
ethene	171
buta-1,3-diene	217
hexa-1,3,5-triene	258

All of the molecules give similar UV-visible absorption spectra - the only difference being that the absorptions move to longer wavelengths as the amount of delocalization in the molecule increases. So,

- The maximum absorption is moving to longer wavelengths as the amount of delocalization increases.
- Therefore maximum absorption is moving to shorter frequencies as the amount of delocalization increases.
- Therefore absorption needs less energy as the amount of delocalization increases.

Therefore there must be less energy gap between the bonding and anti-bonding orbitals as the amount of delocalization increases.

Compare ethane with buta-1,3-diene. In ethane, there is one pi bonding orbital and one π anti-bonding orbital. In buta-1,3-diene, there are two π bonding orbitals and two π* anti-bonding orbitals. The highest occupied molecular orbital is often referred to as the HOMO - in these cases, it is a π bonding orbital. The lowest unoccupied molecular orbital (the LUMO) is a π* anti-bonding orbital.

Notice that the gap between these has fallen. It takes less energy to excite an electron in the buta-1,3-diene case than with ethene, in the hexa-1,3,5-triene case, it is less still.

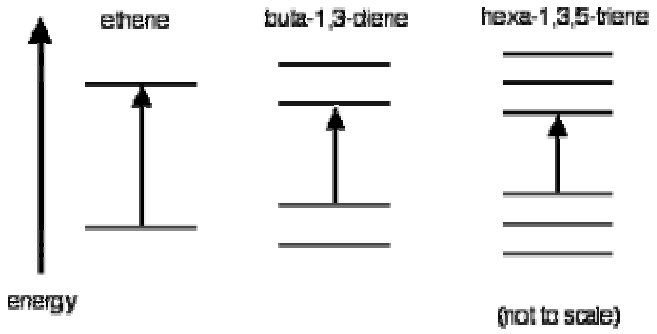

Ethane contains a simple double bond between two carbon atoms, but the two parts of this bond are different. Part of it is a simple σ bond formed from end-to-end overlap between orbitals on each carbon atom, and part is caused by sideways overlap between a p-orbital on each carbon.

The important diagram is the one leading up to the formation of the pi bond - where the two p-orbitals are overlapping sideways:

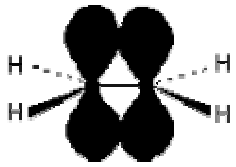

giving the familiar pi bond.

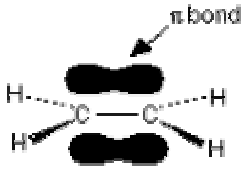

Consider the conjugated double bonds in buta-1,3-diene also. Buta-1,3-diene :

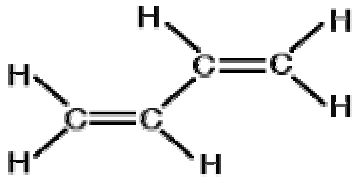

In this case, the sigma bonds have been formed by the end-to-end overlap of various orbitals on the carbons and hydrogens, leaving with a p-orbital on each carbon atom.

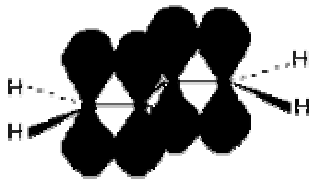

Those p-orbitals will overlap sideways - all of them! A system of delocalized pi bonds is formed, similar to the benzene case that you are probably familiar with. The diagram shows one of those molecular orbitals.

The diagram shows only one of the delocalized molecular orbitals. The interaction of the two double bonds with each other to produce a delocalized system of pi electrons over several atoms is known as conjugation. Conjugation in this context literally means "joining together".

In reality, we have started by overlapping four atomic orbitals, and ended up with four molecular orbitals. The four electrons will go into the two lowest energy of these - two in each. That means we get two π bonding orbitals.

The presence of conjugated double bonds in a molecule containing more than one double bond could also be recognized because of the presence of alternating double and single bonds.

The double bonds do not have to be always between carbon atoms. All of the following molecules contain conjugated double bonds, although in the last case, the conjugation does not extend over the whole molecule:

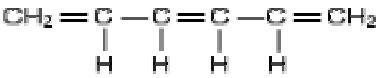

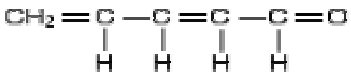

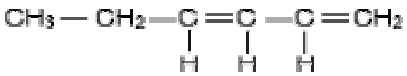

However, although the next molecule contains two double bonds, they are not conjugated. They are separated by two single bonds.

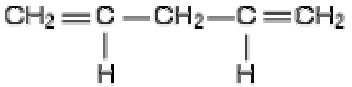

The reason why it is important to have the double and single bonds alternating is that this is the only way we can get all the p-orbitals overlapping sideways. In the last case, sideways overlapping at each end of the molecule is seen to produce two individual π bonds. But the extra single bond in the middle stops them from interacting with each other.

The importance of conjugation is that in the conjugated molecules, the absorption maxima are shifted to longer wavelengths.

The appearance of several absorption peaks or shoulders for a given chromophore is common for highly conjugated systems, and is often solvent dependent. This fine structure reflects not only the different conformations such systems may assume, but also electronic transitions between the different vibrational energy levels possible for each electronic state. Vibrational fine structure of this kind is most pronounced in vapor phase spectra, and is increasingly broadened and obscured in solution as the solvent is changed from hexane to methanol.

However, there are different types of absorption shifts which are readily observed, e.g.

- Bathochromic Shift : to longer wavelength
- Hypsochromic Shift : to shorter wavelength
- Hyperchromic Shift : to greater absorbance
- Hypochromic Shift : to lower absorbance

To understand why conjugation should cause bathochromic shifts in the absorption maxima of chromophores, we need to look at the relative energy levels of the pi-orbitals. When two double bonds are conjugated, the four p-atomic orbitals combine to generate four pi-molecular orbitals (two are bonding and two are antibonding). In a similar manner, the three double bonds of a conjugated triene create six pi-molecular orbitals, half bonding and half antibonding. The energetically most favorable $\pi \rightarrow \pi^*$ excitation occurs from the highest energy bonding pi-orbital (HOMO) to the lowest energy antibonding pi-orbital (LUMO).

In general, the greater the length of a conjugated system in a molecule, the nearer the λ_{max} comes to the visible region.

Thus, the characteristic energy of a transition and hence the wavelength of absorption is a property of a group of atoms rather than the electrons themselves. When such absorption occurs, two types of groups can influence the resulting absorption spectrum of the molecule.

5.3 A Simple UV-visible Double Beam Spectrometer

Ultraviolet and visible spectrometers have been in general use for the last couple of years and over this period have become the most important analytical instrument in the modern day laboratory. In many applications other techniques could be employed but none rival UV-Visible spectrometry for its simplicity, versatility, speed, accuracy and cost-effectiveness.

An absorption spectrometer measures the way that the light absorbed by a compound varies across the UV and visible spectrum and gives a measurement of the amount of optical absorption in a material, as a function of wavelength. The basic setup of a UV-visible spectrometer for measuring the absorption or transmission of light through a sample is shown in Figure 5.3.1.

There main components of a spectrometer are described below:

The light source

A light source gives the entire visible spectrum plus the near ultra-violet so that the range from about 200 nm to about 800 nm could be covered. Since this range of wavelengths can not be obtained from a single lamp, therefore a combination of two is used - a deuterium lamp for the UV part of the spectrum, and a tungsten / halogen lamp for the visible part. The combined output of these two bulbs is focused on to a diffraction grating.

The diffraction grating and the slit

A diffraction grating splits light into its component colors efficiently. The arrows in the figure show the way the various wavelengths of the light are sent off in different directions. The slit only allows light of a very narrow range of wavelengths through into the rest of the spectrometer. By gradually rotating the diffraction grating, light from the whole spectrum can be passed (a tiny part of the range at a time) through into the rest of the instrument.

The rotating discs

Each disc is made up of a number of different segments, e.g. transparent section, mirrored section, black section etc. The light coming from the diffraction grating and slit will hit the rotating disc and one of three things can happen.

- If it hits the transparent section, it would go straight through and pass through the cell containing the sample. It is then bounced by a mirror onto a second rotating disc. This disc is rotating such that when the light arrives from the first disc, it meets the mirrored section of the second disc. That bounces it onto the detector.
- If the original beam of light from the slit hits the mirrored section of the first rotating disc, it is bounced down along the mirror, and then it passes through a reference cell (more about that later). Finally the light gets to the second disc which is rotating in such a way that it meets the transparent section. It goes straight through to the detector.
- If the light meets the first disc at the black section, it is blocked - and for a very short while no light passes through the spectrometer. This just allows the computer to make allowance for any current generated by the detector in the absence of any light.

The sample and reference cells

These are small rectangular glass or quartz containers. They are often designed so that the light beam travels a distance of 1 cm through the contents. The sample cell contains the thin films and the reference cell just contains the transparent glass, since we have used the glass as the substrate to deposit the thin films.

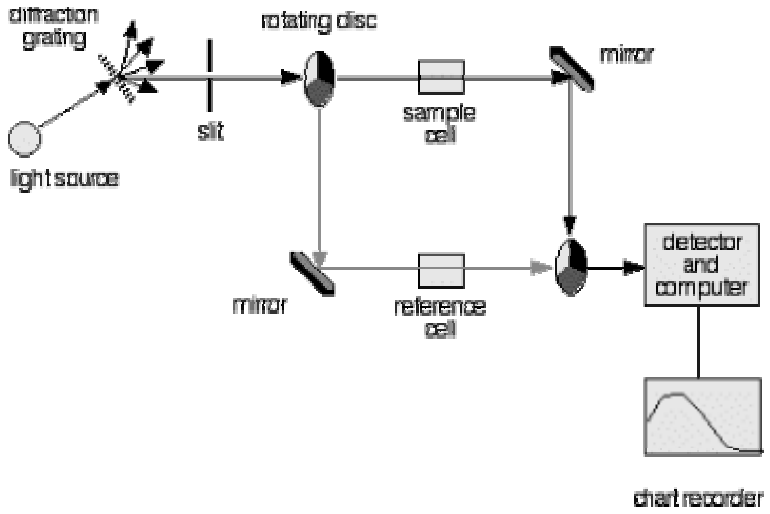

Figure 5.3.1 Schematic of a UV-visible spectrometer.

The detector and computer

The detector converts the incoming light into a current. The higher the current, the greater the intensity of the light. For each wavelength of light passing through the spectrometer, the intensity of the light passing through the reference cell is measured. This is usually referred to as I_o - that's I for Intensity. The intensity of the light passing through the sample cell is also measured for that wavelength - given the symbol, I. If I is less than I_o, then obviously the sample has absorbed some of the light. A simple bit of mathematics is then done in the computer to convert this into something called the absorbance of the sample - given the symbol, A.

There are two basic types of spectrometers, single-beam and double-beam. In a single-beam spectrometer the reference intensity I_0 and the intensity of the light, I, after passing through the sample are obtained sequentially. The double-beam design greatly simplifies this process by simultaneously measuring I and I_0 of the sample and reference cells, respectively. The advantage of the double-beam instrument is that any time-dependent variations in the intensity of the light emitted by the source can be compensated thus improving sensitivity and reducing uncertainty.

In addition to transmission, another useful way to report the optical absorption is in units of optical absorbance or optical density. Absorbance is a dimensionless quantity defined as the negative of the base-10 logarithm of the transmission:

$$A = \log_{10}(\frac{1}{T}) \quad (5.3)$$

An absorbance of 1 corresponds to a transmission of 0.1; an absorbance of 2 corresponds to a transmission of 0.01, and so on. Most spectrometers, after measuring T, use internal circuitry or, common nowadays, operating software to obtain the absorbance.

Absorbance units are useful when working with Beer's Law, which states that the absorbance of a solution is proportional to the concentration, C, of the absorber in that solution:

$$A = KC \quad (5.4)$$

Most simple molecules obey Beer's Law, particularly at low concentration. Others, such as organic dyes, often exhibit a significant departure from Beer's Law at high concentration. This occurs because at higher concentrations, the molecules begin to interact with each other, and can no longer be treated as independent absorbers.

Another important quantity that can be measured from the absorption spectra is the absorption coefficient. The absorption coefficient is a useful quantity when comparing samples of varying thickness. The absorption coefficient is typically the only value reported when discussing the absorption characteristics of absorbing media. To determine the absorption coefficient we first start with Beer's Law which relates I to I_0 via the equation (5.5) given as [5],

$$I = I_0 e^{-\alpha d} \quad (5.5)$$

In this expression "d" is the thickness of the sample in units of centimeters (cm) and, consequently, the absorption coefficient α is to be reported in units of cm^{-1}.

5.4 The Beer-Lambert law

For most spectra the solution obeys Beer's Law, which states that the light absorbed is proportional to the number of absorbing molecules. This is only true for dilute solutions.

A second law - Lambert's law - tells us that the fraction of radiation absorbed is independent of the intensity of the radiation. Combing these two laws gives the Beer-Lambert law:

$$I = I_0 e^{-\alpha d} \quad (5.5)$$

and

$$\log_e\left(\frac{I_o}{I}\right) = \alpha d \qquad (5.6)$$

where is I_o the intensity of the incident radiation, I is the intensity of the transmitted radiation, *d* is the path length of the absorbing species and α is the absorption co-efficient. The absorption spectrum can be analyzed by Beer-Lambert law which governs the absorption of light by the molecules and states that, "When a beam of monochromatic radiation passes through a homogeneous absorbing medium the rate of decrease in intensity of electromagnetic radiation in UV-vis region with thickness of the absorbing medium is proportional to the intensity of incident radiation".

The intensity of transmittance is expressed as the inverse of intensity of absorbance. The absorption coefficient α, can be calculated from the absorption data using the equation (5.6) as [6],

$$\alpha = \frac{2.303A}{d} \qquad (5.7)$$

where $A = \log_{10}\left(\frac{I_o}{I}\right)$ is the Absorbance and d is the thickness of the material.

$\alpha(\lambda)$ is used in to describe the reduction in intensity of light in a medium as a function of distance.

Another important quantity, the extinction co-efficient *k,* is related with α as

$$\alpha = \frac{4\pi k}{\lambda} \qquad (5.8)$$

The extinction coefficient describes the attenuation of light in a medium. The variation of *k* with the photon energy, hν, has an important meaning. The increase of *k* with the increase of hν indicates the probability of raising the electron transfers across the mobility gap with the photon energy.

5.5 Optical Properties of Amorphous and Crystal Materials

5.5.1 A General Introduction to Direct and Indirect Band Gaps

In semiconductor physics, the band gap of a semiconductor is always one of two types, a direct band gap or an indirect band gap. The minimal-energy state in the conduction band, and the maximal-energy state in the valence band, are each characterized by a certain k-vector (momentum vector) in the Brillouin zone. If the k-vectors are the same, it is called a "direct gap". If they are different, it is called an "indirect gap".

The semiconductor in which bottom of the conduction band does not occur at k = 0 at which top of the valence band occur is called indirect band gap semiconductor; energy released

during electron recombination with a hole is converted primarily into phonon; e.g. Si, Ge, GaP. (Phonon: A quasiparticle which is a quantized sound wave). In other type of semiconductor the bottom of the conduction band and the top of the valence band occur at the momentum k = 0, is called indirect band gap semiconductor; energy released during band-to-band electron recombination with a hole is converted primarily into radiation (radiant recombination) wavelength of which is determined by the energy gap; e.g. GaAs, InP. Direct band gap semiconductors are sometimes referred to as "optically active" and indirect as "optically inactive".

Energy vs. momentum for a semiconductor with an indirect band gap, showing that an electron cannot shift from the lowest-energy state in the conduction band to the highest-energy state in the valence band without a change in momentum. Here, almost all of the energy comes from a photon, while almost all of the momentum comes from a phonon. On the other hand, Energy vs. momentum for a semiconductor with a direct band gap, showing that an electron can shift from the lowest-energy state in the conduction band to the highest-energy state in the valence band without a change in momentum.

The band gap represents the minimum energy difference between the top of the valence band and the bottom of the conduction band. However, the top of the valence band and the bottom of the conduction band are not generally at the same value of the electron momentum. In a direct band gap, the top of the valence band and the bottom of the conduction band occur at the same value of momentum, as in the schematic below.

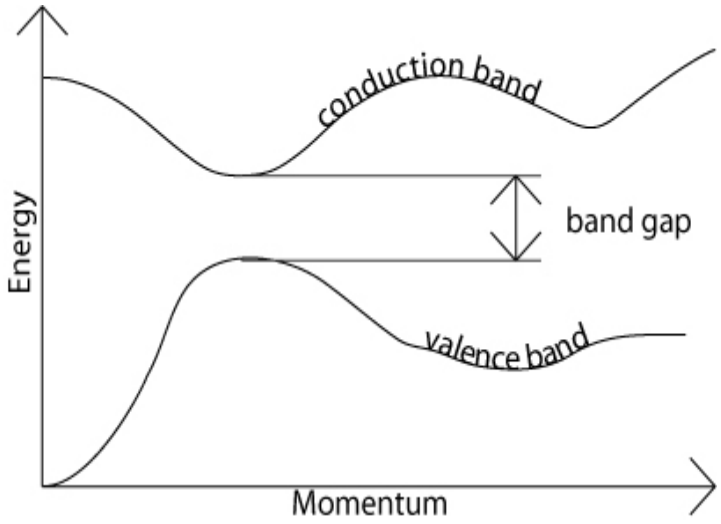

Figure 5.5.1 schematic representation of direct energy band gap

In an indirect band gap semiconductor, the maximum energy of the valence band occurs at a different value of momentum to the minimum in the conduction band energy, which is shown in Figure 5.5.2.

The difference between the two is most important in optical devices. Since a photon can provide the energy to produce an electron-hole pair and each photon of energy *E* has momentum $p = \frac{E}{c}$, where *c* is the velocity of light. An optical photon has an energy of the order of 10^{-19} J, and, since $c = 3 \times 10^8$ ms^{-1}, a typical photon has a very small amount of momentum.

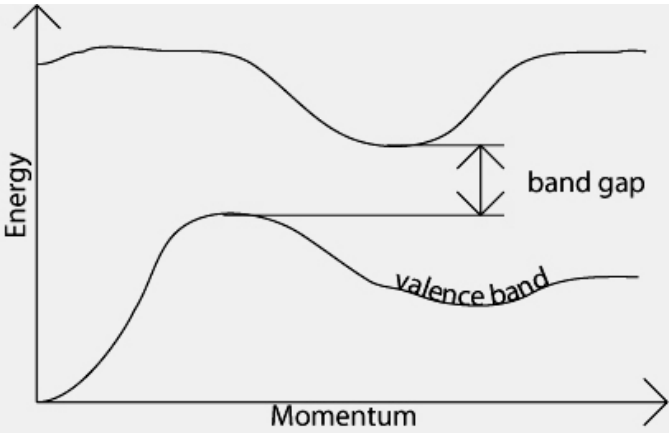

Figure 5.5.2 schematic representation of indirect energy band gap

A photon of energy E_g, where E_g is the band gap energy, can produce an electron-hole pair in a direct band gap semiconductor quite easily, because the electron does not need to be given very much momentum. However, an electron must also undergo a significant change in its momentum for a photon of energy E_g to produce an electron-hole pair in an indirect band gap semiconductor. This is possible, but it requires such an electron to interact not only with the photon to gain energy, but also with a lattice vibration called a phonon in order to either gain or lose momentum.

The indirect process proceeds at a much slower rate, as it requires three entities to intersect in order to proceed: an electron, a photon and a phonon. This is analogous to chemical reactions, where, in a particular reaction step, a reaction between two molecules will proceed at a much greater rate than a process which involves three molecules.

The same principle applies to recombination of electrons and holes to produce photons. The recombination process is much more efficient for a direct band gap semiconductor than for an indirect band gap semiconductor, where the process must be mediated by a phonon.

For a direct gap material, if it absorbs light and the light source is then removed, the optically generated electrons and holes recombine. Since the minimum in the conduction band has the same k value as the maximum in the valance band. The electron can drop back easily into the hole in the valance band and the energy lost in the process is emitted as radiation of wavelength $\lambda_c = hc/E_g$, where E_g is the band gap. i.e. the total energy and the momentum of the electron-photon system must be conserved.

5.5.2 The General Theory on the Optical Properties of Amorphous Materials

The general theory and many of the experimental results on amorphous materials have been summarized by Mott and Davis [7]. They show that one feature of such materials is some sort of energy band structure, but show also that the normally sharp cutoff in the density of states curves at the band edges is replaced by a tailing into the normally forbidden energy gap .Thus a difference in the absorption spectra, particularly at the fundamental absorption edge, between samples of the same basic material but for which one is, say, crystalline and the other amorphous is expected and obvious phenomenon.

From the stand point of electron motion a mobility or pseudo gap is defined and is larger for amorphous materials than for crystals having the same chemical compositions. The equivalent gaps from the optical stand point will depend on the form of excitation process taking place in the material when photons are absorbed. Thus a variety of possibilities will arise, depending on whether the transitions involved are direct or indirect.

The theory of such transitions has been presented by Davis and Mott [7] and they take account of the localized electronic states in the mobility gap. In amorphous materials the momentum vector k conservation rule breaks down and thus k is not a good quantum number. If we assume that the matrix element for optical transitions has the same value whether or not the initial and final states are localized, and also that the densities of states at the band edges are linear functions of the energy, then the absorption coefficient α may be deduced. The equation for optical absorption coefficient α at a given angular frequency ω then reduces to the form:

$$\alpha(\omega) = A\frac{\left(\hbar\omega - E_{opt}\right)^2}{\hbar\omega} \qquad (5.9)$$

where

$$A = \frac{(4\pi/c)\sigma_0}{n_0 \Delta E} \qquad (5.9a)$$

and σ_0 is the electrical conductivity at absolute zero, ΔE the width of the tail of the localized states in the normally forbidden energy gap, n_0 the refractive index and E_{opt} the optical energy gap. Thus the optical energy gap can be calculated from the extrapolation to $(\alpha\hbar\omega)^{1/2} = 0$ of a plot of $(\alpha\hbar\omega)^{1/2}$ vs. $\hbar\omega$, or $(\alpha\hbar\omega)^2 = 0$ of a plot of $(\alpha\hbar\omega)^2$ vs. $\hbar\omega$. Such theory describes optical absorptions associated with forbidden indirect and direct transitions respectively.

There are two kinds of optical transition at the fundamental edge of crystalline and non-crystalline semiconductors, direct transitions and indirect transition, both of which involve the interaction of an electromagnetic wave with an electron in the valance band, which is then raised across the fundamental gap to the conduction band. For the direct optical transition from the valence band to the conduction band, it is essential that the wave vector for the

electron be unchanged. In the case of indirect transition the interactions with lattice vibrations (phonons) take place; thus the wave vector of the electron can change in the optical transition and the momentum change will be taken or given up by phonons. In other words, if the minimum of the conduction band lies in a different part of k-space from the maximum of the valence band, a direct optical transition from the top of the valence band to the bottom of the conduction band is forbidden.

The energy gap in a semiconductor is responsible for the fundamental optical absorption edge. The fundamental absorption process is one in which a photon is absorbed and an electron is excited from an occupied valence band state to an unoccupied conduction band state. If the photon energy is less than the gap energy, such processes are impossible and photon will not be absorbed. Such band absorption processes are possible only if the photon energy is higher than the gap energy.

The condition is readily satisfied if the maximum of the VB and minimum of the CB occurs in the same k-value (often at k = 0). If the band structure has this feature the gap is said to be direct. A graphical representation of direct band gap for amorphous material is shown in Figure 5.5.3.

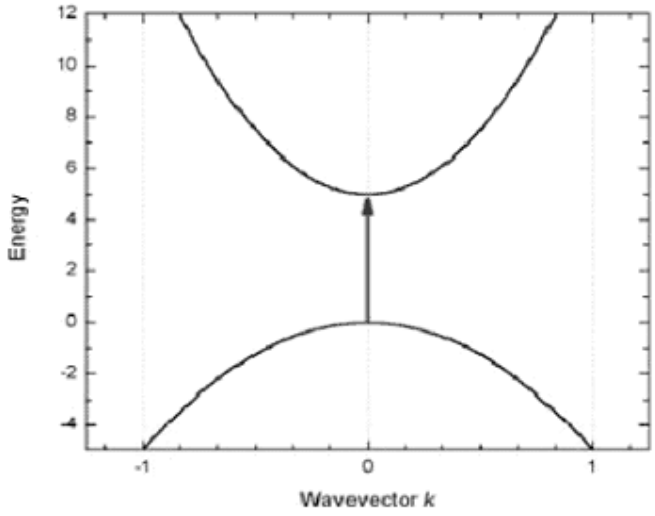

Figure 5.5.3 A graphical representation of direct band gap

What if the VB maximum and CB maximum do not occur at the same k-value? In this case the gap is said to be an indirect gap. Absorption over the band gap cannot conserve energy and momentum without the participation of another particle, usually a phonon. The process then corresponds to photon→ conduction electron plus phonon. A graphical representation of indirect band gap for amorphous material is shown in Figure 5.5.4.

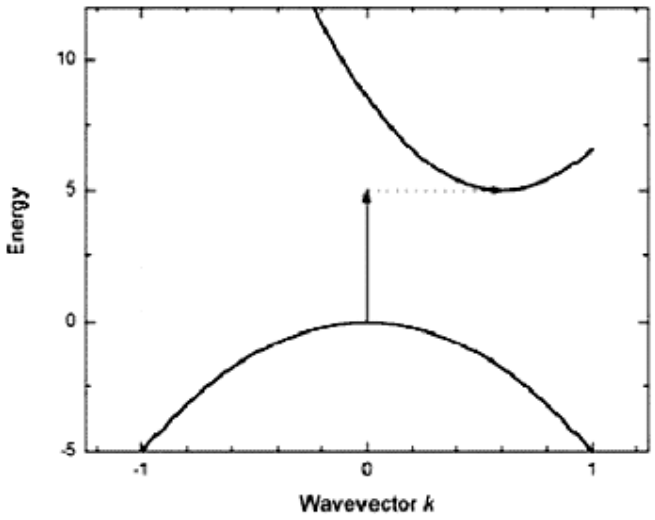

Figure 5.5.4 A graphical representation of indirect band gap

For the indirect gap material the momentum has to be adjusted by a cooperative process involving a phonon (quantized lattice vibration). Such a process does not emit radiation at the band gap wavelength and the energy lost during a recombination process is effectively dissipated as heat i.e. indirect transition involves the absorption or emission of a phonon to converse momentum. Thus in this case the top of the valence band and the bottom of the conduction band take place at different wave vectors in the Brillouin zone. In this respect it is unfortunate therefore that k is not effectively a good quantum number in amorphous non-crystalline materials and such materials are usually regarded as indirect gap materials.

To estimate the nature of absorption a random phase model is used where the k momentum selection rate is completely relaxed. The integrated density of states *N(E)* has been used and defined by

$$N(E) = \int_{-\infty}^{+\infty} g(E)dE \qquad (5.10)$$

The density of states per unit energy interval may be represented by

$$g(E) = \frac{1}{V}\sum \delta(E - E_n) \qquad (5.11)$$

where *V* is the volume, *E* is the energy at which *g(E)* is to be evaluated and E_n is the energy of the nth state.

If $g_v \propto E^p$ and $g_c(E) \propto (E - E_{opt})^q$, where energies are measured from the valance band mobility edge in the conduction band (mobility gap), and substituting these vales into an expression for the random phase approximation, the relationship obtained $\nu^2 I_2(\nu) \propto (h\nu - E_o)^{p+q+1}$, where $I_2(\nu)$ is the imaginary part of the complex permittivity. If the density of states of both band edges is

parabolic, then the photon energy dependence of the absorption becomes $\alpha\nu\infty\nu^2 I_2(\nu)\infty(h\nu - E_{opt})^2$. So for higher photon energies the simplified general equation which is known as Tauc relation [9] is,

$$\alpha h\nu = B(h\nu - E_{opt})^n \qquad (5.12)$$

where hν is the energy of absorbed light, n is the parameter connected with distribution of the density of states and B is the proportionality factor, called Tauc parameter. The index n equals ½ for allowed direct transition and 2 for allowed indirect transition energy gaps respectively [8].

Physical processes that control the behavior of gap states in non-crystalline materials are structural disorder responsible for the tail states and structural defects in deep states [9]. The Tauc parameter, B is a measure of the steepness of band tail (Urbach region) density of states. Higher value of B in thin film is due to less structural disorder.

Thus, from the straight-line plots of $(\alpha h\nu)^2$ versus hν and $(\alpha h\nu)^{1/2}$ versus hν the direct and indirect energy gaps respecting of insulators and /or dielectrics can be determined.
However, a comparison between the direct and indirect absorption is depicted in the Figure 5.5.5, whereas Figure 5.5.6 shows all possibile electronic transitions resulting from the optical absorption viz allowed direct and indirect transitions, forbidden direct and indirect transitions etc.

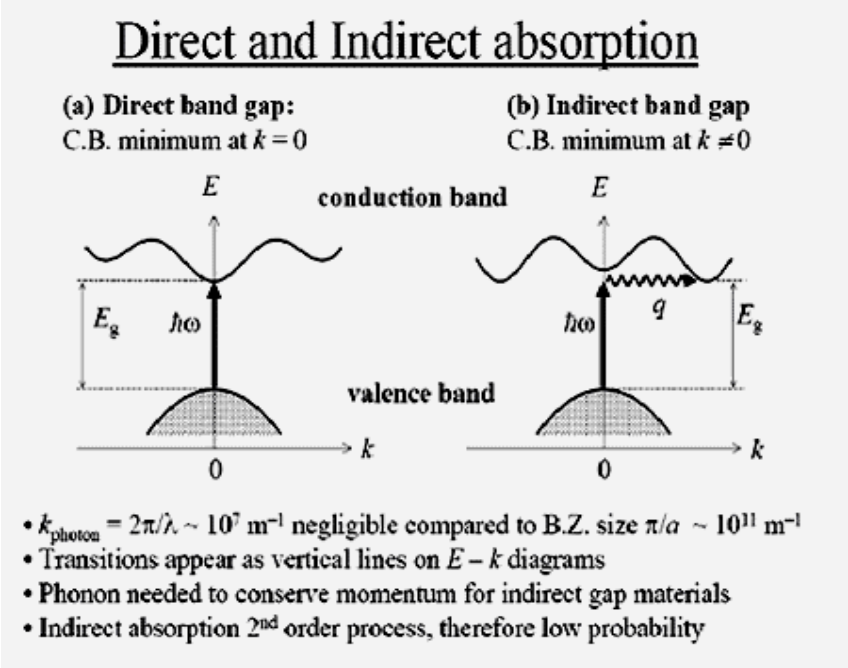

Figure 5.5.5 Comparison between direct and indirect transitions.

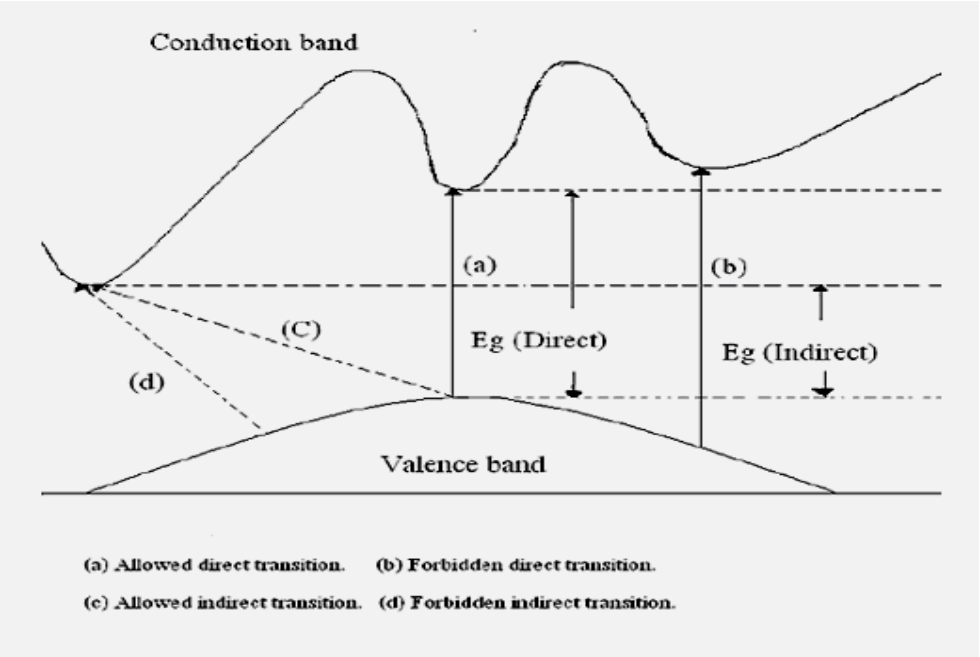

Figure 5.5.6 Electronic transitions resulting from the optical absorption.

5.6 The Behavior of Light in Thin Films

Light can be considered as an electromagnetic wave travelling in a medium, the speed of light c assumes that the medium is a vacuum. A description of how light propagates in a medium is required to understand the behavior of light in the thin film configuration and this usually described by the complex refractive index. The complex refractive index is comprised of a real and imaginary term and is given by the equation (5.13).

$$n^* = n + ik \qquad (5.13)$$

where n is the real refractive index which is a constant of proportionality between the phase velocity of light in a vacuum and the phase velocity of light, v, in the medium under examination. This relationship is given in equation (5.14) and k is the extinction coefficient that describes the attenuation of light in a medium, it is related to the absorption coefficient by equation (5.15).

$$v = c / n \qquad (5.14)$$

$$\alpha(\lambda) = \frac{4\pi k(\lambda)}{\lambda} \qquad (5.15)$$

$\alpha(\lambda)$ is used in Beer's law (equation 5.5) to describe the reduction in intensity of light in a medium as a function of distance.

Beer's law would allow direct determination of $\alpha(\lambda)$ from a transmission spectrum of a thin film if it were not for the presence of interference fringes. When interference fringes are present, only the maxima are valid points where and therefore k can be directly determined.

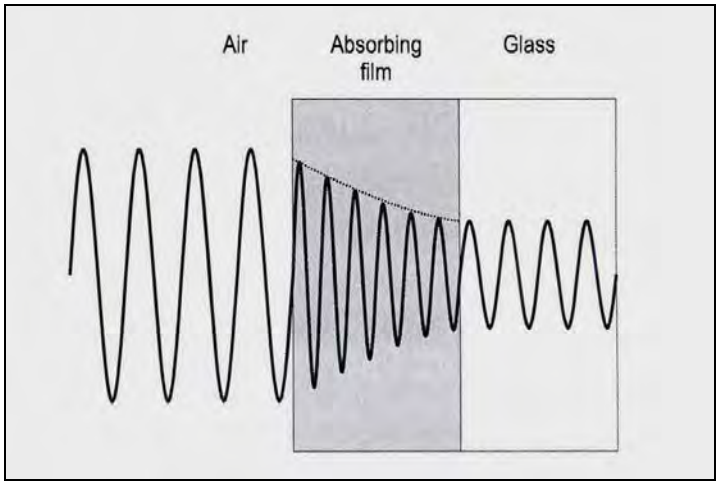

Figure 5.6.1 The effect of the complex refractive index on the amplitude and phase velocity of a light wave travelling in air that encounters an absorbing thin film and then a glass.

The propagation of light through an absorbing medium is illustrated in Figure 5.6.1. A light waves travels through air (n = 1, k = 0) and encounters an absorbing film (n = 3.5, k>0). The absorbing film has a positive value of k and as such the amplitude of the light waves is attenuated exponentially as a function of the distance it travels in the thin films according to equation (5.5). Note that the exponential absorption in the thin film due to the non zero value of k and change in phase velocity due to variation in n. The phase velocity of the wave also decreases due to the increase of the real part of the complex refractive index. Upon leaving the film, the light wave encounters a transparent glass substrate (n = 1.5, k = 0) and reverts to a phase velocity closed to its original, whilst the amplitude remains constant again.

The behavior of light at an interface is more complicated than depicted in Figure 5.6.1. When light encounters an interface between two medium of different refractive index n_1 and n_2, some of the light will be reflected at the same angle of incidence (θ_i) and some will be refracted into the new medium at a changed angle (θ_r). The angles are measured relative to a vector normal to the medium interface. This behavior is Snell's law and is given by the equation (5.16),

$$n_1 \sin\theta_i = n_2 \sin\theta_r \qquad (5.16)$$

With knowledge of how light behaves at medium interfaces and the rate of its absorption in a medium with k>0, it is possible to build a picture of its behavior when encountering single or multiple thin films. Light entering a thin film reflects and refracts at every boundary causing a coherent wavefront to exit the thin film in both directions, each successive bounce of the light reduces the electric field amplitude. Light entering the substrate does not return to it coherently because the substrate is infinitely thick in comparison to the thin films, it is assumed to be lost.

5.7 Results and Discussion

5.7.1 Plasma Polymerized Pyrrole Thin Films

The variation of absorption (ABS) with wavelength, λ, for as grown plasma polymerized pyrrole (PPPy) thin films of different thicknesses of about 400, 450, 500, 550 and 600 nm from the UV-Visible absorption spectra have been recorded at room temperature and are presented in Figure 5.7.1.

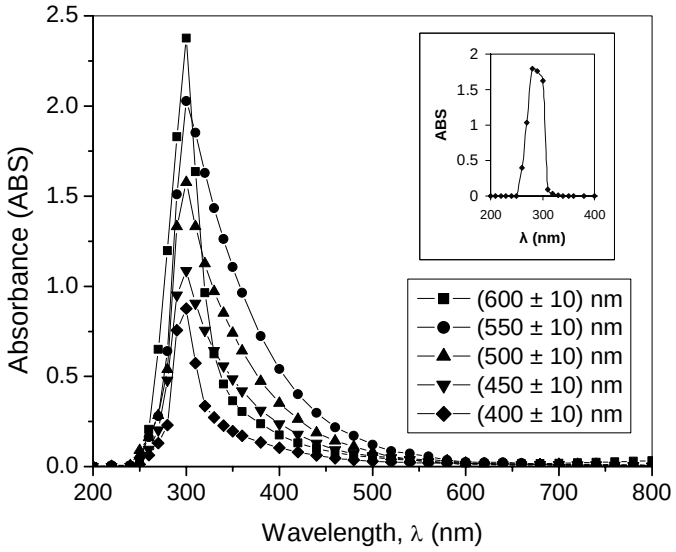

Figure 5.7.1 Variation of absorption (ABS) with wavelength, λ, for as grown PPPy thin films of different thicknesses (inset : absorption for monomer pyrrole).

From the figure a bathochromic shift (a shift towards longer wavelength) of PPPy of about 20 nm is observed with respect to the pyrrole monomer, i.e., the peak values of PPPy (about 300 nm) have been shifted to higher wavelength compared to the peak wavelength (λ_{max}) value, 280 nm of the liquid monomer (inset of Figure 5.7.1). It is well known that increasing conjugation generally moves the absorption to longer wavelength [10], which is discussed in section 5.2.3 of this chapter in detail. Therefore this bathochromic shift (or red shift) in PPPy indicates the presence of an increased degree of conjugation in the resulting films.

To get a more clear presentation of the absorption nature, the Figure 5.7.1 is reproduced for only three samples of thicknesses about 400, 450 and 500 nm and shown in Figure 5.7.2. It is seen from the figure that absorption peak intensity increases and broadens with increasing thickness of the films and a sharp rise of the absorption in the low wavelength side is observed. Then the absorption decreases rapidly up to about 400 nm with a peak at around 300 nm; above 400 nm absorption the decrease is slow.

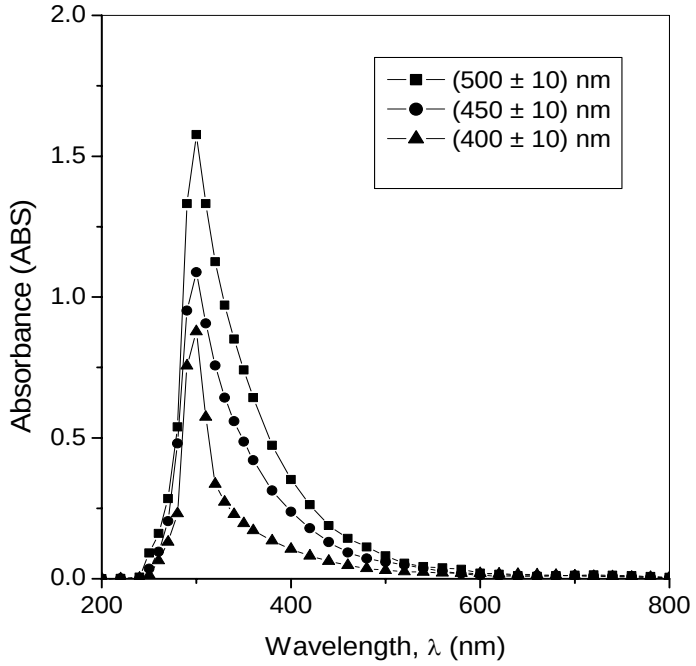

Figure 5.7.2 Variation of absorption (ABS) with wavelength, λ, for as grown PPPy thin films of thicknesses about 400, 450 and 500 nm.

The absorption co-efficient α was calculated from the absorbance data of Figure 5.7.2 using the equation (5.7), namely, [6]

$$\alpha = 2.303\left(\frac{A}{d}\right) \qquad (5.8)$$

where A is the absorbance and d is the thickness of the thin film.

The spectral dependence of α as a function of energy $h\nu$ for PPPy thin films of thicknesses 400, 450 and 500 nm is shown in Figure 5.7.3. It is observed that in the low energy region the edges follow linear fall for values of α below about 5,000 cm^{-1} for all types of samples. These falling edges may either be due to lack of long-range order or due to the presence of defects in the thin films [7].

However, since α is used to describe the reduction in intensity of light in a medium as a function of distance, therefore higher values of α is an indication of more reduction in intensity. From figure 5.7.3, it is observed that the thin films of lower thickness have higher values of the absorption coefficients α. This result indicates that in the films of lower thickness the intensity of light is reduced more.

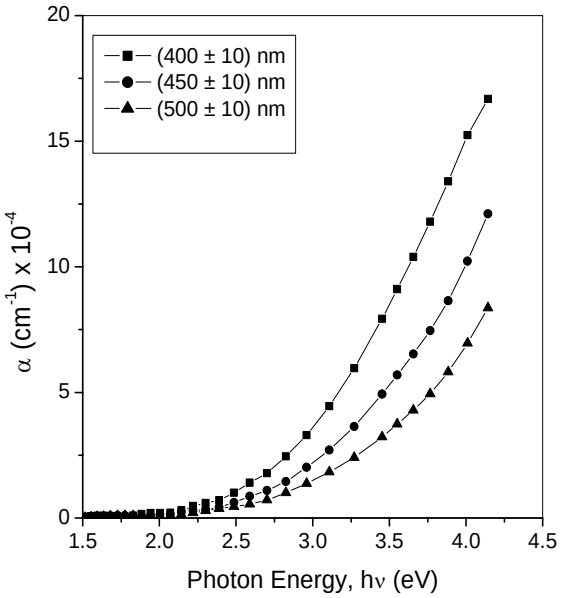

Figure 5.7.3 Plots of absorption co-efficient, α, as a function of photon energy, $h\nu$, for as grown PPPy thin films of thicknesses about 400, 450 and 500 nm.

The extinction co-efficient, k, can be computed from the absorption co-efficient α, by using the equation (5.8), namely,

$$\alpha = \frac{4\pi k}{\lambda} \qquad (5.9)$$

where λ is the wavelength.

Figure 5.7.4 shows the plots of extinction co-efficient, k, as a function of $h\nu$ for as grown PPPy thin films of thicknesses about 400, 450 and 500 nm.

Since the extinction coefficient describes the attenuation of light in a medium and the increase of k with the increase of $h\nu$ indicates the probability of raising the electron transfers across the mobility gap with the photon energy, therefore higher values of k are the representation of greater attenuation of light in a thin film and also the higher probability of raising the electron transfer across the mobility gap with the photon energy. In figure 5.7.4 it is seen that the film of lower thickness has higher value of k, which indicates that the light is more attenuated in the films of lower thicknesses than that of the films of higher thicknesses and the probability of raising the electron transfers across the mobility gap with the photon energy is higher in the films of lower thicknesses.

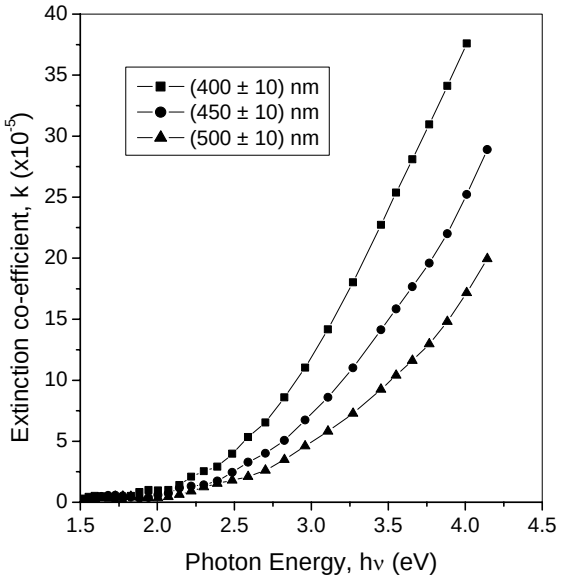

Figure 5.7.4 Plot of extinction co-efficient, k, as a function of hν for as grown PPPy thin films of thicknesses about 400, 450 and 500 nm.

One of the most significant optical parameters, which is related to the electronic structure, is the optical band gap. The optical band gap, E_{opt}, can be calculated by Tauc relation [8] which is given by equation (5.12), namely,

$$\alpha h\nu = B\left(E_{opt} - h\nu\right)^n \qquad (5.12)$$

where B is the Tauc parameter, n is the parameter connected with distribution of the density of states and E_{opt} is the optical band gap obtained from the extrapolation of the linear part of the curve.

To indicate the presence of direct and indirect transitions in the PPPy thin films, the curves in Figure 5.7.3 could be characterized by two different slopes. The allowed direct transition energy gap, E_{qd}, can be evaluated from the plots of $(\alpha h\nu)^2$ as a function of hν which is shown in Figure 5.7.5. The allowed indirect transition energy gap, E_{qi}, can be evaluated from $(\alpha h\nu)^{1/2}$ versus hν plots shown in Figure 5.7.6. Both the energy gaps are determined from the intercept of the extrapolation of the curves to zero α in the photon energy axis. The values E_{qd} and E_{qi} obtained from the plots of Figure 5.7.5 and Figure 5.7.6 are documented in Table 5.7.1.

It is seen from Table 5.7.1, that both the E_{qd} and E_{qi} are decreased with the decrease of the thicknesses of the films, which is an indication of decreasing the resistivity of the film of lower thickness. This result would in turn cause an increase in electrical conductivity in the low-thickness thin film.

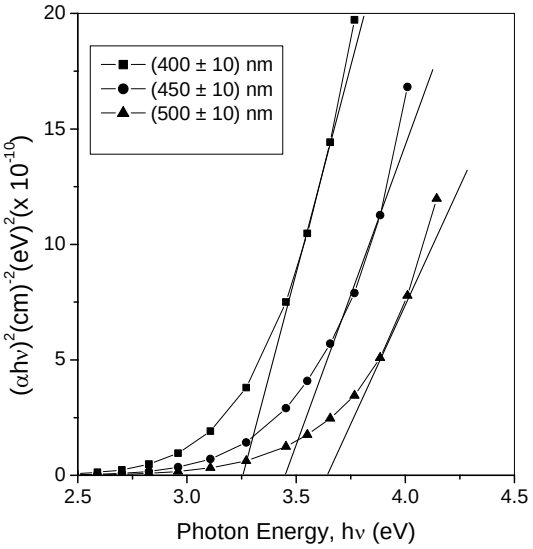

Figure 5.7.5 $(\alpha h\nu)^2$ versus $h\nu$ curves for as grown PPPy thin films of thicknesses about 400, 450 and 500 nm.

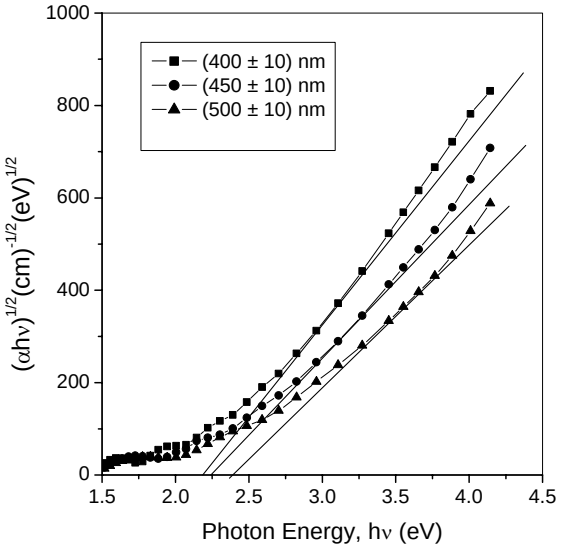

Figure 5.7.6 $(\alpha h\nu)^{1/2}$ versus $h\nu$ curves for as grown PPPy thin films of thicknesses about 400, 450 and 500 nm.

Table 5.7.1 The direct transition energy gap, E_{qd} and indirect transition energy gap, E_{qi} of PPPy thin films of thicknesses about 400, 450 and 500 nm.

Thickness of the PPPy thin films (nm)	Direct transition energy gap(eV) (E_{qd})	Indirect transition energy gap (eV) (E_{qi})
500	3.58	2.35
450	3.47	2.25
400	3.25	2.22

5.7.2 Plasma Polymerized Pyrrole - N,N,3,5 Tetramethylaniline Composite Bilayer Thin Films

The variation of absorption (ABS) with wavelength, λ, for as grown PPPy-PPTMA bilayer composite thin films of different thicknesses for all composition from the UV-Visible absorption spectra have been recorded at room temperature and are presented in Figure 5.7.7. It is, however to be noted that, to prepare the PPPy-PPTMA bilayer films, pyrrole-monomer has been used as the mother-material and TMA monomer has been deposited in different time ratio after the pyrrole films were formed. The deposition time-ratios of PPPy : PPTMA were (50 min : 10 min), (45 min : 15 min), (40 min : 20 min), (35 min : 25 min) and (30 min : 30 min) and corresponding thicknesses were 550, 525, 500, 450 and 400nm respectively.

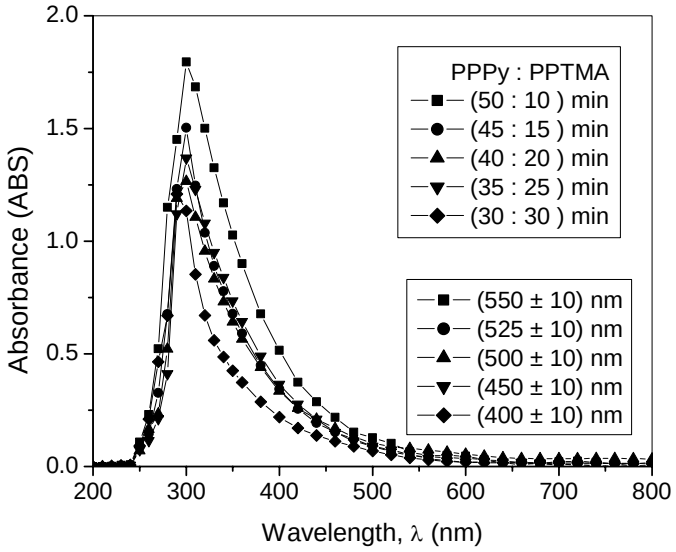

Figure 5.7.7 Variation of absorption (ABS) with wavelength, λ, for as grown PPPy-PPTMA bilayer thin films with different deposition time-ratio of PPPy and PPTMA.

To get a more precise presentation of the absorption nature of PPPy-PPTMA, the Figure 5.7.7 is reproduced for only three samples of thicknesses about 400, 500 and 550 nm and shown in Figure 5.7.8. The absorption peak intensity of bilayer films is also found to increases as like its component thin films and broadens with increasing thickness of the films. It is, however, also seen from the figure that absorption peak intensity decreases with increasing PPTMA in the bilayer structure. From the study of deposition nature, it is observed that as the deposition time of TMA is increased in the bilayer thin film formation process, the thicknesses of the films are decreased. This is because, the deposition rate of TMA is lower than that of the pyrrole, i.e., if the deposition parameters are remain same, then PPTMA thin films are found to be thinner than PPPy thin films. Therefore, as the thicknesses of the bilayer films are found to be dependent upon the deposition ratio of PPPy

and PPTMA, the absorption is also found to be dependent on the same factor. As the proportion of PPTMA is increased, the intensity of absorption peaks is reduced. This result could be checked from the comparative study on the variation of with wavelength for as deposited PPPy, PPTMA [11] and PPPy-PPTMA bilayer films of nearly equal thickness (500 nm) which is presented in Figure 5.7.9. It is seen from the figure that, the peak wavelength value, λ_{max}, for PPPy, PPTMA and bilayer thin films are 300 nm, 380 nm and 300 nm respectively, i.e., the peak of PPPy and bilayer thin films are formed at the same λ_{max} value. But the intensity of the absorption (peak) of the bilayer film is reduced with respect to that of PPPy but has reached to very close to the peak intensity of the absorption of PPTMA.

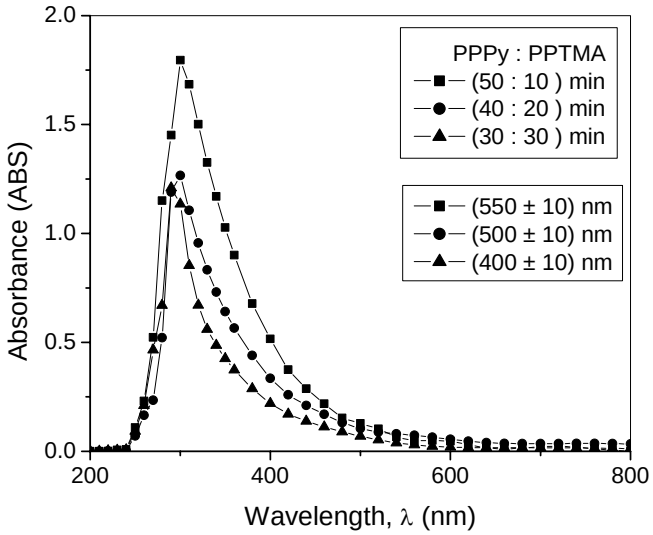

Figure 5.7.8 Variation of absorption (ABS) with wavelength, λ, for as grown PPPy-PPTMA bilayer thin films of thicknesses 400, 500 and 550 nm.

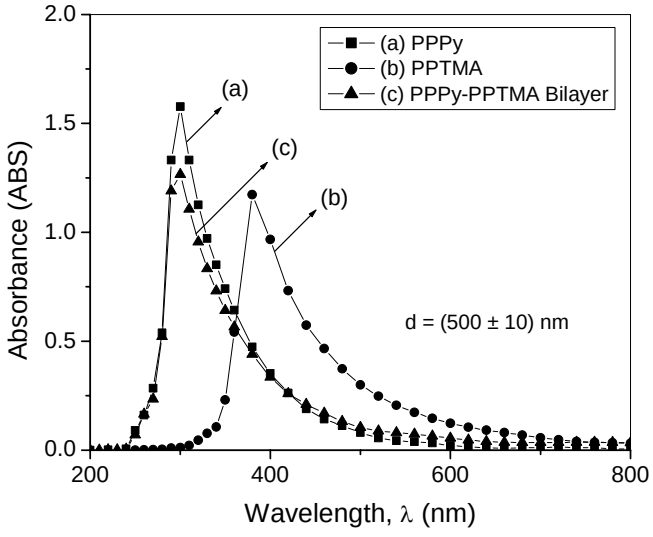

Figure 5.7.9 Variation of absorption (ABS) with wavelength, λ, for as grown (a) PPPy (b) PPTMA and (c) PPPy-PPTMA bilayer films.

The absorption co-efficient α have been calculated from the absorbance data of Figure 5.7.8 and Figure 5.7.9 using the equation (5.7), and the spectral dependence of α as a function of energy $h\nu$ is shown for PPPy-PPTMA bilayer composite films in Figure 5.7.10. A comparative study of the same for PPPy, PPTMA [11] and PPPy-PPTMA bilayer thin films is presented in Figure 5.7.11. It is observed that in the low energy region the edges follow linear fall for values of α below about 3000 cm^{-1} for all types of samples, which is very similar to those of PPPy and PPTMA. These falling edges may either be due to lack of long-range order or due to the presence of defects in the thin films.

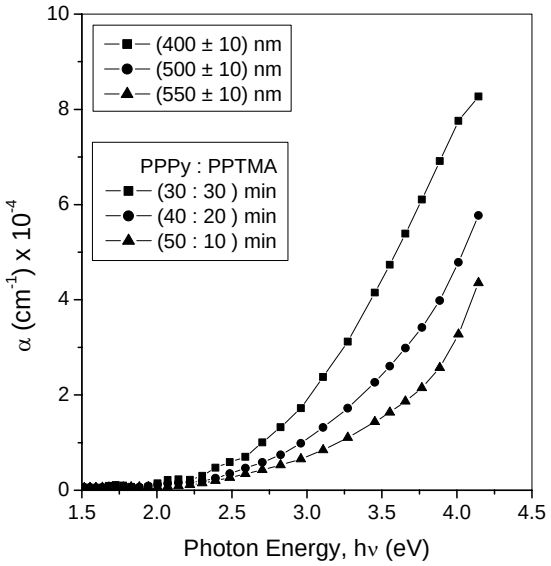

Figure 5.7.10 Plots of absorption co-efficient, α, as a function of photon energy, $h\nu$, for as grown PPPy-PPTMA bilayer thin films of thicknesses 400, 500 and 550 nm.

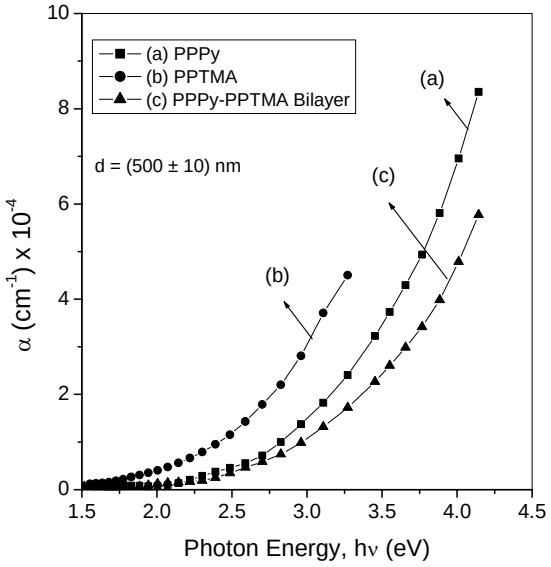

Figure 5.7.11 Plots of absorption co-efficient, α, as a function of photon energy, $h\nu$, for as grown (a) PPPy (b) PPTMA and (c) PPPy-PPTMA bilayer thin films.

It is however, known that α is used in to describe the reduction in intensity of light in a medium as a function of distance and higher values of α indicates more reduction in intensity in a particular thin film. From figure 5.7.10, it is observed that the thin films of lower thickness have higher values of the absorption coefficients α, which indicates that in the films of lower thickness the intensity of light is reduced more. But since low-thickness bilayer film is formed with the higher proportion of PPTMA in the bilayer structure, therefore it could be concluded that as the proportion of PPTMA is increased the absorption coefficients of bilayer thin films is also increased which causes more reduction of the intensity in the film. This result is consistent which is observed in the absorption curves of Figure 5.7.7 and 5.7.8.

From the Figure 5.7.11, it is seen that PPTMA thin film has higher value of α than that of PPPy for any particular photon energy. Therefore increase of α with the increase of PPTMA in the bilayer structure is not unexpected. Moreover, higher values of α of PPTMA thin film than those of the PPPy and PPPy-PPTMA bilayer thin films of same thickness indicates that intensity of light is reduced more in PPTMA films than that of other films. This result is also consistent with the observation for the absorption curves of Figure 5.7.9

It could be noted that, the absorption co-efficient α has been calculated from the experimental absorption data of the PPPy-PPTMA bilayer thin film and found to be reduced than those of the component thin films i.e., PPPy and PPTMA. The α, however, could also be calculated for an ideal bilayer thin films from the absorption data of the component films, by using the following equation [12] ,

$$\alpha' = \frac{\alpha_1 d_1 + \alpha_2 d_2}{d_1 + d_2} \qquad (5.19)$$

where α_i and d_i are the absorption coefficient and thickness of the components respectively, and α' is the absorption co-efficient of the PPPy-PPTMA ideal bilayer thin films which has been calculated from the absorption data of the individual components by using the equation (5.19). It should be noted that the relationship between components thickness has been evaluated from Figure 5.7.11 with an approximation of PPPy : PPTMA = 0.6 : 0.4, with d =1 as the bilayer thickness, since the bilayer film of Figure 5.7.16 was prepared by depositing the PPPy and PPTMA thin films with a time ratio (40 min : 20 min). The theoretically calculated values of α' for the ideal bilayer thin films from the absorption data of the individual components has been plotted in Figure 5.7.12 as a function of photon energy, $h\nu$, to compare with the α calculated from experimental absorption data of real PPPy-PPTMA bilayer thin films. The α's for component thin films (PPPy and PPTMA) are also shown in the same figure for comparison.

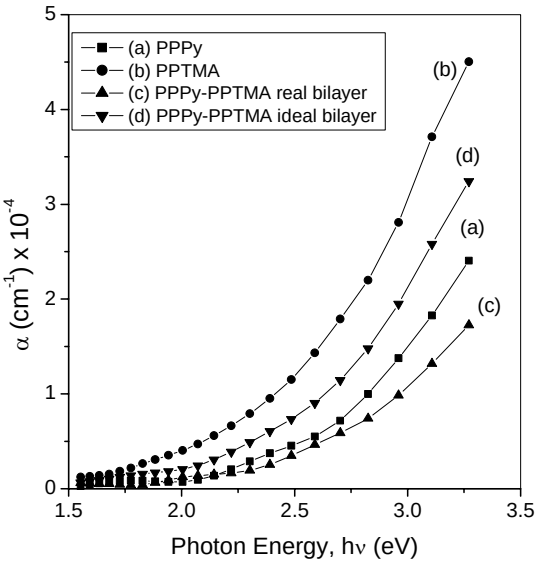

Figure 5.7.12 Plots of absorption co-efficient, α, as a function of photon energy, $h\nu$, for as grown (a) PPPy (b) PPTMA (c) PPPy-PPTMA real bilayer thin films (d) PPPy-PPTMA ideal bilayer thin films

It is seen from the 5.7.12 that the theoretically calculated values of the absorption coefficient α' lie in between the values of α of the two individual components; whereas the experimental values of α indicate an apparent reduction in absorption coefficient of the bilayer films with respect to that of its components. The difference in Urbach tails of the real and ideal bilayer thin films indicates different activation energy in the real bilayer film (curve c) than what would be expected from the ideal situation (curve d). Like any other ideal bilayer of two materials without interface effect, where the physical properties of the bilayer usually lie in between of those of the original materials, in the present case the ideal PPPy-PPTMA bilayer films show similar behavior. Since both PPPy and PPTMA layers in the bilayer thin film have the same structure as in the component films, therefore the result, that the theoretical values of absorption coefficient α' of the PPPy-PPTMA ideal bilayer films lies in between those of the components, is not unexpected. But when the absorption coefficient is calculated from the absorption data of the components, the interaction in the interface of the two component thin films could not be considered. In this study, since thin films of the components were deposited one over the other to prepare the PPPy-PPTMA bilayer thin films by using plasma polymerization technique, therefore the interaction in the interface has occurred which may give rise to a system with polymer-polymer complex interface between the PPPy and PPTMA thin films. This complex interface may not be homogeneous and therefore, there are some possibilities of presence of irregularities in the interface which may cause more amorphous structure of the bilayer thin film. It should be noted that in most inhomogeneous/amorphous polymeric systems, the electronic conductivity is affected by this interface. The crosslinking between the interfaces should also be taken into consideration in this system, which may cause less absorption coefficient and consequently higher optical band gaps.

The extinction co-efficient, *k*, has been computed from the absorption coefficient α, by using the equation (5.8), and Figure 5.7.13 shows the plots of extinction co-efficient, k, as a function of hν for as grown PPPy-PPTMA bilayer thin films of thicknesses about 400, 500 and 550 nm. Figure 5.7.14 is the plots of k as a function of hν for as grown PPPy, PPTMA [11] and PPPy-PPTMA bilayer thin films of nearly equal thickness 500 nm.

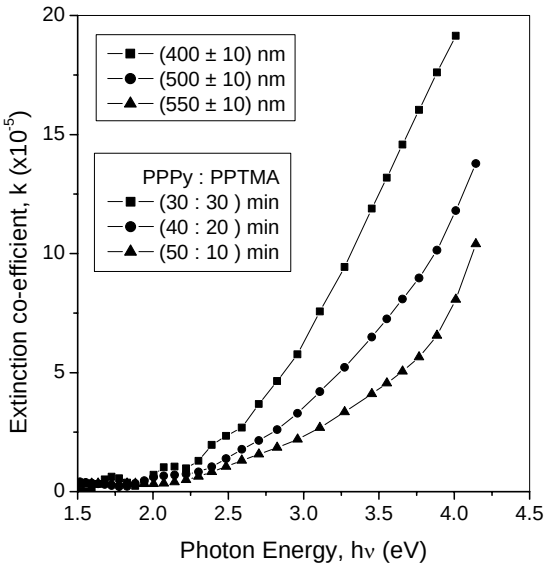

Figure 5.7.13 Plot of extinction co-efficient, *k,* as a function of hν for as grown PPPy-PPTMA bilayer composite thin films of thicknesses about 400, 450 and 500 nm.

In figure 5.7.13 it is seen that the extinction co-efficient, *k* increases with decreasing thickness of the films. It is known that the extinction coefficient describes the attenuation of light in a medium and the increase of *k* with the increase of hν indicates the probability of raising the electron transfers across the mobility gap with the photon energy. Therefore from the nature of the figure 5.7.13, it could be concluded that a greater attenuation of light would be occurred in a low-thickness thin film and also the probability of raising the electron transfers across the mobility gap with the photon energy is higher in low-thickness films. This observation might be an indication of higher conductivity for the films which have lower thicknesses. But, as discussed earlier, higher proportion of PPTMA in the bilayer structure causes of lowering the thickness, therefore it could also be concluded that as the proportion of PPTMA is increased the extinction co-efficient of bilayer thin films is also increased and vice-versa.

From the Figure 5.7.14, it could be observed that PPTMA thin film has higher value of k than that of PPPy for any particular photon energy. Therefore increase of *k* with the increase of PPTMA in the bilayer structure is not unusual. Moreover, higher values of *k* of PPTMA thin film than that of the PPPy and PPPy-PPTMA bilayer thin films of same thickness indicates that probability of raising the electron transfers across the mobility gap with the photon energy is higher in PPTMA thin films than that of other films, which might cause a higher conductivity PPTMA thin films than that of both PPPy and PPPy-PPTMA bilayer composite thin films.

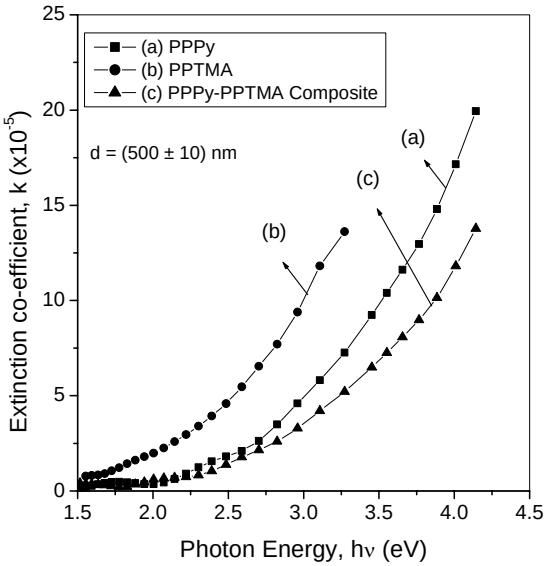

Figure 5.7.14 Plot of extinction co-efficient, k, as a function of hν for as grown (a) PPPy (b) PPTMA and (c) PPPy-PPTMA bilayer thin films

One of the most significant optical parameters, the optical band gap, E_{opt}, can be calculated by Tauc relation [7] which is given by equation (5.12), namely,

$$\alpha h\nu = B\left(E_{opt} - h\nu\right)^n \qquad (5.12)$$

where B is the Tauc parameter, n is the parameter connected with distribution of the density of states and E_{opt} is the optical band gap obtained from the extrapolation of the linear part of the curve.

To indicate the presence of direct and indirect transitions in the PPPy-PPTMA bilayer composite thin films, the curves in Figure 5.7.10 could be characterized by two different slopes. The allowed direct transition energy gap, E_{qd}, can be evaluated from the plots of $(\alpha h\nu)^2$ as a function of hν which is shown in Figure 5.7.15. The allowed indirect transition energy gap, E_{qi}, can be evaluated from $(\alpha h\nu)^{1/2}$ versus hν plots shown in Figure 5.7.16. Both the energy gaps are determined from the intercept of the extrapolation of the curves to zero α in the photon energy axis. The values E_{qd} and E_{qi} obtained from the plots of Figure 5.7.15 and Figure 5.7.16 are documented in Table 5.7.2.

It is seen from Table 5.7.2, that both the E_{qd} and E_{qi} are decreased with the decrease of the thicknesses of the films. This result can also be stated in terms of the deposition rate of PPPy and PPTMA in the film. As the proportion of PPTMA is increased in the bilayer structure, the band gaps are decreased. Therefore, it seems that increase of PPTMA in the PPPy-PPTMA bilayer films causes a decrease in the resistivity of the film.

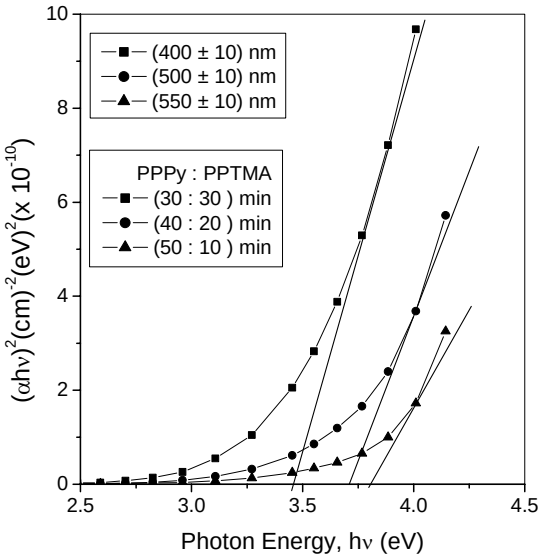

Figure 5.7.15 $(\alpha h\nu)^2$ versus $h\nu$ curves of PPPy-PPTMA bilayer thin films

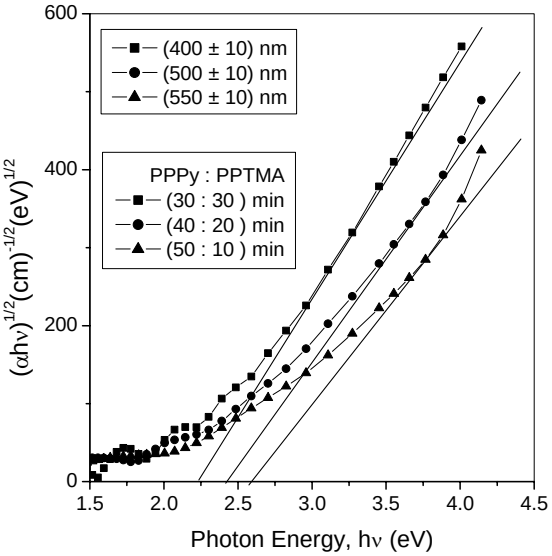

Figure 5.7.16 $(\alpha h\nu)^{1/2}$ versus $h\nu$ curves of PPPy-PPTMA bilayer thin films

Table 5.7.2 The direct transition energy gap, E_{qd} and indirect transition energy gap, E_{qi} of PPPy-PPTMA bilayer thin films with different deposition time-ratio of pyrrole and TMA.

PPPy : PPTMA (minute)	Thickness of the films (nm)	Direct transition energy gap(eV) (E_{qd})	Indirect transition energy gap (eV) (E_{qi})
50 min : 10 min	550	3.88	2.57
40 min : 20 min	500	3.69	2.45
30 min : 30 min	400	3.48	2.24

For a comparative study of direct and indirect transitions in the PPPy, PPTMA [11] and PPPy-PPTMA bilayer thin films, the curves in Figure 5.7.11 has been characterized by two different slopes. The allowed direct transition energy gap has been evaluated from the plots of $(\alpha h\nu)^2$ as a function of $h\nu$ and the allowed indirect transition energy gap has been evaluated from $(\alpha h\nu)^{1/2}$ versus $h\nu$ plots, shown in Figure 5.7.17 and Figure 5.7.18. The values of E_{qd} and E_{qi} obtained from the plots of Figure 5.7.17 and Figure 5.7.18 are documented in Table 5.7.3.

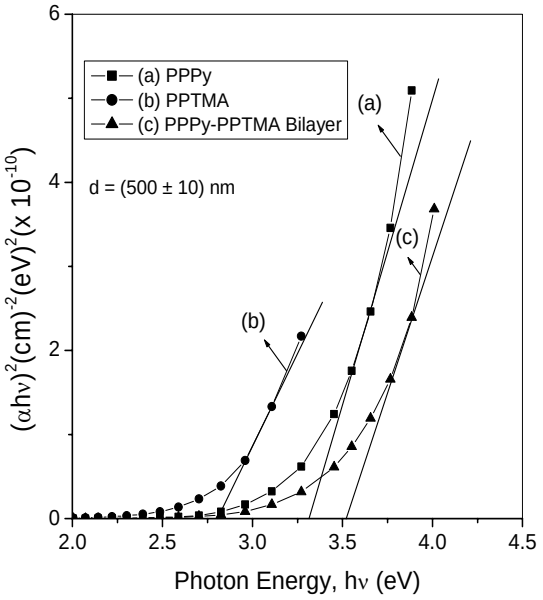

Figure 5.7.17 $(\alpha h\nu)^2$ vs. $h\nu$ curves of (a) PPPy (b) PPTMA (c) PPPy-PPTMA bilayer thin films

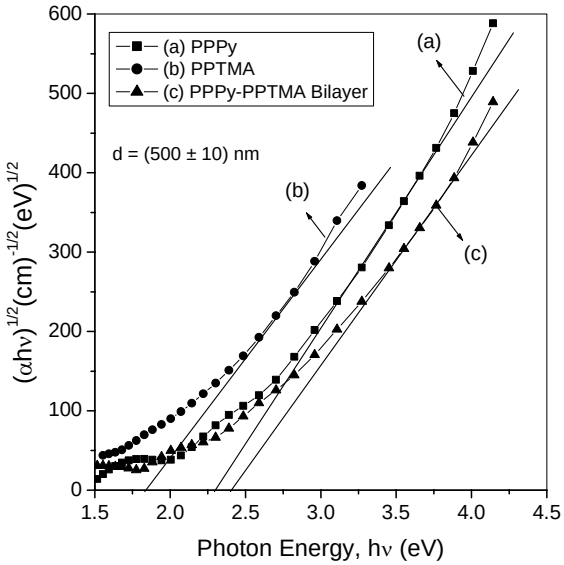

Figure 5.7.18 $(\alpha h\nu)^{1/2}$ vs. $h\nu$ curves of (a) PPPy (b) PPTMA (c) PPPy-PPTMA bilayer thin films.

It is observed from Table 5.7.3 that the energy gaps of the PPPy-PPTMA bilayer films are higher compared to those of the PPPy and PPTMA films for nearly same thickness which indicates a higher resistivity of the bilayer thin films that those of its component films, i.e., PPPy and PPTMA thin films. It is also seen that the PPTMA thin films has the lower values of E_{qd} and E_{qi} than those of PPPy and PPTMA thin films which indicates that PPTMA is more conducting films than that of the PPPy and PPPy-PPTMA bilayer thin films.

Table 5.7.3 Allowed direct and indirect energy gaps for PPPy, PPTMA and PPPy-PPTMA bilayer thin films.

Samples	Direct transition energy gap(eV) (E_{qd})	Indirect transition energy gap (eV) (E_{qi})
PPTMA	2.85	1.80
PPPy	3.30	2.27
PPPy-PPTMA Bilayer	3.52	2.38

From the study of the optical behavior of PPPy, PPTMA and PPPy-PPTMA bilayer thin films a general trend is observed that both the optical band gaps are increased with increasing thickness of the films. Moreover the PPPy-PPTMA bilayer thin films have higher band gaps than that of its component thin films even if the thickness remains same. An increase of optical band gaps is an indication of increasing resistivity in the films. Though the resistivity is an inherent physical property of most materials, and is expected to remains constant, in our study a change in the resistivity is observed which suggests a probable change in physical properties during the formation of the plasma polymerized thin films. It is known that, the resistivity in a material arises due to the deviation from the periodicity of the potential in which the electron moves. This deviation, however, may arise from the presence of defects in the films' structure or due to displacement of atoms by lattice vibrations, or lattice defects such as vacancies, interstitials and dislocations or foreign impurity atoms, or/and grain boundaries etc. Any of these effects could be happened during the deposition of the films by plasma polymerization. For example, the incorporation of oxygen is a typical phenomenon in plasma polymer as a contamination may be due to the reaction of trapped free radicals with oxygen from the plasma reactor even though the monomers do not contain oxygen [13]. The FTIR analyses of PPPy, PPTMA and PPPy-PPTMA films in this study (which have been discussed in Chapter 4) have also indicated the presence of oxygen by the appearance of the absorption band at 2214, 1850-1603, and 2214 cm^{-1} respectively, Therefore, during the subsequent formation of the films by plasma polymerization, there may

be adsorbed and/or trapped oxygen of the interface in between the PPPy and PPTMA thin film layers. The oxidation of the interface of the bilayer might affect the physical properties of the bilayer thin films. The increase of optical band gap may be due to this reason. Furthermore, it is observed that the electrical conductivity of the PPPy-PPTMA bilayer thin films is lower than those of the individual thin films, which would be discussed in Chapter 6. It could be noted that in the present system, thin films of the components were deposited one over the other to prepare the PPPy-PPTMA bilayer thin films, which may give rise to a system with polymer–polymer complex interface, i.e., the interface between the PPPy and PPTMA thin films may not be homogeneous and therefore there are some possibilities of presence of irregularities in the interface. It should also be noted that in most inhomogeneous polymeric systems, the electronic conductivity is affected by this interface. The electrical conductivity depends upon the movement of adventitious ions generated either by impurities centers or induced impurities [14]. The crosslinking between the interfaces should be also taken into consideration in this system, which may cause less electrical conduction or high resistivity in the films.

5.8 Conclusions

From the absorption spectra of PPPy, PPTMA and PPPy-PPTMA bilayer composite thin films, it is observed that the absorption peak intensity increases and broadens with increasing thickness of all types of thin films, which is very expected result, since thicker materials usually absorb more radiation than that of the thinner materials. A bathochromic shift (or a red shift) of PPPy of about 20 nm is observed with respect to the pyrrole monomer, and a red shift of about 79 of PPTMA is reported to be observed with respect to the TMA monomer, which indicate the presence of an increased degree of conjugation in the resulting films. Since the red shift is higher in PPTMA thin films than that of PPPy films, therefore the PPTMA thin films have more conjugation than that of PPPy thin films.

The results of dependence of α on $h\nu$ indicate that in the films of lower thickness the intensity of light is reduced more. A similar trend is observed in the plots of extinction co-efficient, *k,* as a function of $h\nu$. It is seen that the film of lower thickness has higher value of *k*, which indicates that the light is more attenuated in the films of lower thicknesses than that of the films of higher thicknesses and the probability of raising the electron transfers across the mobility gap with the photon energy is higher in the films of lower thicknesses. From the comparative study of PPPy, PPTMA and PPPy-PPTMA bilayer composite thin films of same thickness, it is however observed that the PPTMA thin film have higher values of both α and *k* than those of the PPPy and PPPy-PPTMA bilayer thin films. This result indicates that intensity of light is more reduced and more attenuated in PPTMA films than those of other

films, even if the thickness of the different types of films is remained same. Moreover, the probability of raising the electron transfers across the mobility gap with the photon energy is higher in PPTMA thin films than that of other films, which might cause higher conductivity PPTMA thin films than that of both PPPy and PPPy-PPTMA bilayer thin films.

From the optical characterization of PPPy, PPTMA and PPPy-PPTMA bilayer composite thin films, it is observed that both the E_{qd} and E_{qi} are decreased with the decrease of the thicknesses for all types of films, which is an indication of decreasing the resistivity of the film of lower thickness. This result would in turn cause an increase in electrical conductivity in the low-thickness thin film. From the comparative study of the optical band gaps of PPPy, PPTMA and PPPy-PPTMA bilayer thin films of nearly equal thickness, it is observed from that the energy gaps of the PPPy-PPTMA bilayer films are higher compared to those of the PPPy and PPTMA films which indicates a higher resistivity of the bilayer thin films that those of its component films. The change in the resistivity suggests a probable change in physical properties during the formation of the plasma polymerized thin films. In this system, thin films of the components were deposited one over the other to prepare the PPPy-PPTMA bilayer composite thin films, which may give rise to a system with polymer–polymer complex interface, i.e., the interface between the PPPy and PPTMA thin films may not be homogeneous and therefore there are some possibilities of presence of irregularities in the interface. This inhomogeneity of the interface may give rise to a higher resistivity in bilayer thin films. Moreover, during the subsequent formation of the films by plasma polymerization, there may be adsorbed and/or trapped oxygen of the interface in between the PPPy and PPTMA thin film layers, which has been already indicated in the FTIR spectra of the films. The oxidation of the interface of the bilayer might affect the physical properties of the bilayer thin films. The increase of optical band gap may be due to this reason.

References

[1] Morosoff, N., *An introduction to plasma polymerization*, in "Plasma deposition, treatment, and etching of polymers", d'Agostino, R., Ed, Academic Press, San Diego, CA, 1990.

[2] Xiao, H., Xiongyan Zhao, Uddin, A-., and Lee, C.B., *Preparation, characterization and electronic and optical properties of plasma-polymerized nitrites*, Thin Solid Films 477, 51-57, 2005.

[3] Morosoff, N., *Surface modification by plasma polymerization*, in "Innovations in materials processing", Plenum, New York, 1985.

[4] Tauc, J., in *Optical Properties of Solids*, Abeles, F., Ed., North-Holland, Amsterdam, 1972.

[5] Yasuda, H., *Plasma Polymerization*, Academic Press; New York, 1985.

[6] Al-Ani, S. K. J., and Higazy, A. A., J. Mater. Sci., 26, 3670, 1991.

[7] Mott, N. F., and Davis, E. A., *Electronic Processes in non-crystalline materials*, Clarendon, Oxford, 1971.

[8] Tauc, J., *Amorphous and Liquid Semiconductors*, Plenum, London, (1974).

[9] Lambert, J. H., David A. Lightner, Herbert F. Shurvell, and Graham Cooks, R., *Introduction to organic spectroscopy*, Macmillan Publishing Co., New York, 1987.

[10] Xiaoyi Gong, Liming Dai, Albert W.H. Mau, and Hans J. Griesser, *Plasma-polymerized polyaniline films: Synthesis and Characterization*, J. Polym. Sci.: PartA: Polym. Chem., 36, 633-643, 1998.

[11] Akther, H. and Bhuiyan, A. H., *Infrared and ultra violet-visible spectroscopic investigation of plasma polymerized N,N,3,5-tetramethylaniline thin films*, Thin Solid Films 474, 14-18, 2005.

[12] Kamal, M. M., and Bhuiyan, A. H., *Optical Characterization of Plasma Polymerized Pyrrole-N,N,3,5 Tetramethylaniline Bilayer Thin Films*, J. Appl. Polym. Sci. (DOI # 33176), In Press, 2010..

[13] Yasuda, H., Bumgarner, M. O., Marsh, H. C., Morosoff, N., *Plasma polymerization of some organic compounds and properties of the polymers*, J. Polym. Sci. Polym. Chem., 14, 195-224, 1976.

[14] Seanor, D. A., *Electrical Properties of Polymers*, Academic Press, Inc, New York, 1982.

Chapter 6

Direct Current Electrical Properties

This chapter describes the existing theories of direct current electrical conduction in plasma polymerized thin films, and discusses the experimental results; J-V characteristics, conduction mechanism, temperature dependent conductivity, etc.

6.1 Introduction

The direct current (dc) field behavior of a material provides information about the nature of charge carriers, their mobility, conduction mechanism etc, whereas a study in alternating current (ac) field provides information about the electrical nature of the molecular or atomic species, which constitutes the dielectric materials.

Electrical and electronic insulating materials, also known as dielectrics, are essential for the proper operation and reliability of all electrical and electronic equipment. These materials have the property of storing and dissipating electrical energy when subjected to electromagnetic field. The energy-storing property leads to the fabrication of most important constituents of electrical circuit known as capacitor. The dielectric phenomena arise from the interaction of electric field with different charged particle such as electrons, ions, protons and electrons shells. The type and size of dielectrics determine the size and the operational limitations of the electrical equipment. The prime objective of insulating materials is to prevent the flow of electric current where it is not wanted and to support high electric fields. The main requirement of the material is to have the lowest electrical conductance coupled with the maximum resistance to electrical breakdown, long life, low cost, mechanical strength, high corrosion resistance, ease of forming and manufacturing, chemical inertness, and the ability to withstand elevated temperatures [1]. There is a need and desire to reduce the size, enhance reliability, reduce degradation, and increase the life of electrical power equipment.

Electronic conduction in amorphous organic insulating solids has received considerable attention in recent years because of their importance in electronic devices. Charge transport measurements in disordered semiconductors and insulators can provide information about the electronic structure of these materials. The disorder in the atomic configuration is thought to cause localized electronic states or groups of states within the material. In the case of organic solids, the conductivity due to electrons excited from valence band to conduction band is negligible and a complex behavior of the dc electronic conduction is observed for these types of materials.

Traditional involvement of polymer thin films in micro electronics was as element with excellent insulating properties. Naturally, investigations were directed more towards conditions under which they act as passive electrical elements. Synthetic organic polymers are generally insulators with electrical resistivity ranges from 10^7 ohm-m to 10^{17} ohm-m [2]. Extensive studies on the electrical conductivity of insulating polymer thin films deal mainly with the dependence on parameters like temperature, pressure, voltage and thickness [3]. Valuable insight into the different transport mechanisms can be obtained from such studies, and since polymers are, generally, composed of both polycrystalline and amorphous phases [4], therefore, it is not surprising that several theories such as electron, ion and proton

conduction mechanisms are postulated to explain experimental observations in polymer films.

6.2 Theory of Conductivity : Basic concepts

The most important property characterizing the electrical properties of a solid is the electrical conductivity, *σ*. The conductivity is an inherent property of most materials, and ranges from extremely conductive materials like metals to very much non-conductive materials like plastics or glass or any polymeric materials. The electrical conductivity of a material is closely related to another inherent property of the material, called resistivity, *ρ*, which is, however related to the resistance, *R*, of the material as,

$$R = \rho \frac{d}{A} \tag{6.1}$$

where *d* and *A* are the length and the area of cross section of the conductor and *ρ* is the proportionality constant called electrical resistivity, with the unit Ω-m. Then *(1/ ρ)* is the electrical conductivity, *σ*. The basic unit of conductivity is Siemens (S) or $(\Omega\text{-m})^{-1}$.

The actual cause of the resistivity arises due to the deviation from the periodicity of the potential in which the electron moves. It is on this concept that the modern theory of conductivity is based. One of the effects of quantum mechanical wave behavior of electrons is that electrons do not scatter from a perfect lattice, they scatter by defects. The deviation from the periodicity of the potential which causes the resistivity may be also due to

- displacement of atoms by lattice vibrations
- lattice defects such as vacancies, interstitials and dislocations
- foreign impurity atoms
- dislocations, grain boundaries etc.

In metals, electrons act as moving charge carriers. The electrical conductivity of a metal is defined as,

$$J = \sigma E \tag{6.2}$$

where $J = I/A$ is the current density resulting from an applied electric field E, and $E = V/d$. Therefore

$$J = \sigma \frac{V}{d} \tag{6.3}$$

where V is the applied voltage.

The famous Ohm's law can then be derived as,

$$J = \frac{I}{A} = \sigma \frac{V}{d} = \frac{d}{RA}\frac{V}{d} \Rightarrow V = IR \qquad (6.4)$$

The charge carriers can be either ions or electrons/hole and the conductivity are then said to be either ionic or electronic respectively. However, the nature of the chemical bonding also plays a vital role in determining the type of the conductivity.

In metals and in broadband semiconductors, electrons and holes carry the electric current. In ionic crystals the electrical conductivity is due to the diffusion of ions through the lattice. The dielectric materials, however, have very few electrons to take part in normal electric conductivity but have interesting electrical properties to polarize the material and to create electric dipole when an electric field is applied.

When atoms come close together to form a solid, their valence electrons interact due to Coulomb forces, and they also feel the electric field produced by their own nucleus and that of the other atoms. In addition, two specific quantum mechanical effects happen. First, by Heisenberg's uncertainty principle, constraining the electrons to a small volume raises their energy, which is called promotion. The second effect, the Pauli Exclusion Principle limits the number of electrons that can have the same property (which includes the energy). As a result of all these effects, the valence electrons of atoms form wide valence bands when they form a solid. The bands are separated by gaps, where electrons cannot exist. The precise location of the bands and band gaps depends on the type of atom (e.g., Silicon vs. Aluminum), the distance between atoms in the solid, and the atomic arrangement (e.g., carbon vs. diamond). The energy gap between the valence and conduction bands in insulators is large, so energy is needed to promote an electron to the conduction band. This energy may come from heat, or from energetic radiation, like light of sufficiently small wavelength.

Electrons are accelerated in an electric field *E*, in the opposite direction to the field because of their negative charge. The force acting on the electron is *-eE*, where *e* is the electric charge. This force produces a constant acceleration, so that, in the absence of obstacles (in vacuum, like inside a TV tube) the electron speeds up continuously in an electric field. In a solid, the situation is different. The electrons scatter by collisions with atoms and vacancies that change drastically their direction of motion. Thus electrons move randomly but with a net drift in the direction opposite to the electric field. The drift velocity is constant, equal to the electric field times a constant called the mobility μ,

$$v_d = -\mu E \qquad (6.5)$$

The mobility, μ, of the carriers can be defined from equation (6.5) as the average drift velocity of the carriers per unit electric field.

The electrical conductivity σ can be expressed in terms of the mobility μ. The magnitude of σ is determined by the density of charge carrier, the charge of each carrier, and the mobility of the carriers, and is expressed as,

$$\sigma = nq\mu \tag{6.6}$$

where q is the elementary electric charge, n is the free charge carriers density and μ is the effective charge carrier mobility. Equation (6.3) is then rewritten as,

$$J = Nq\mu\frac{V}{d} = \sigma\frac{V}{d} \tag{6.7}$$

This is a determining equation of evaluating σ, p and μ which is obtained from the measurements of current density J resulting due to the applied voltage V.

6.3 Electrical Conduction in Polymer Thin Films

6.3.1 Introduction

Electrical properties of polymer thin films are very important from the theoretical and applicative point of view. Polymers are insulators and they are not supposed to conduct electrical current, but the electrical properties are changed when subjected to high electric fields and temperatures for long time, and consequently polymers starts to conduct current. The classical conduction and transport mechanism found in conductors and semiconductors, but are not found in polymers, and therefore different conduction mechanisms are observed in these materials. This is due to the difference of morphology and chemistry of the polymer. Charge injection from electrodes into polymer, traps and volumetric conduction, tunneling and hopping conduction are found to play important roles in conduction and charge transport in polymers. For most polymers the current - voltage relation is ohmic and linear at low applied fields, but at high fields, non-linear characteristics are often observed. A number of experimental observations can be interpreted in terms of carrier injection from metal electrodes and charge transport phenomena in polymer films.

The electrical property of polymers is a subject which is inherently interdisciplinary in nature, being closely allied with the mechanical properties of polymers on the one hand, and with the semiconductive properties of inorganic substances on the other. The electrical behavior

of polymers covers an extremely diverse range of molecular phenomena. In metals the electrical field response is overwhelmingly one of electronic conduction, but polymers may respond in a more varied manner, and a whole set of delicate electrical effects may be observed. No known polymer is completely free of conduction processes. However, small amount of charge carriers it may possess and low level conduction in insulating polymers can take a variety of forms. Conduction may very often be contributed by impurities that provide a small concentration of charge carriers in the form of electrons or ions. At high fields, the electrodes may inject new carriers (holes and electrons) into polymers. At very high fields, these and other processes will lead to complete breakdown of polymers as insulating materials. The imposition of an electrical field upon a polymer will cause a redistribution of any charges in the polymer, provided they are mobile enough to respond in the time scale in the applied field. If some of the mobile charges are able to diffuse throughout the specimen and charge migration through the electrode sample interface is possible, then the charges will support a dc conductance. It should be mentioned that the vacuum-deposited thin film insulators can contain a large density of both impurity and trapping centers. A well judged study of electrical conduction in vacuum deposited thin films cannot be accomplished without consideration of these possibilities [5].

In the study of the dc electrical conduction in the polymer thin films, the current conduction is considered through the film, rather than along the plane of the film and the carriers may either be electronic or ionic in nature. The low field properties are usually Ohmic in nature, but the high field electrical properties cannot be described by a single conduction process. A power law in the form $J \infty V^n$, can express the variation of current density with voltage in a material, where *n* is a power factor. When *n* is unity, the conduction is Ohmic, and if the value of n is less or more than unity, then the conduction process is other than Ohmic.

There are various dc electronic conduction mechanisms by which electrons are transported under the influence of an applied electric field [6]. Generally, one mechanism will dominate the observed current but more than one conduction mechanisms may possibly operate at one particular voltage. However the conduction mechanism is explained usually in terms of electron emission from cathode by the field assisted thermal excitation, where the electrons are transported from the cathode into the conduction band of the contact barrier (Schottky-Richardson mechanism); or by electron liberation from the traps in the bulk of the material, and/or electron transportatin by field-assisted thermal excitation over the lower coulombic potential barrier i.e. Poole–Frenkel mechanism. The possibilities of tunneling (Fowler–Nordheim mechanism), space charge limited conduction etc have also been investigated in the literature. All these conduction mechanism would be discussed in detail in the following sections.

6.3.2 Factors Influencing the Electrical Properties

The following factors influence the electrical properties [7]:

- **Size effect :** which covers surface scattering and quantum mechanical tunneling of charge carriers.
- **Method of film preparation :** The electrical properties of the metal or insulating films depends on the method of deposition and the deposition parameter. Depending on the deposition conditions employed, structural and electronic defect concentrations, dislocation densities, porosity content, chemical composition, electron trap densities, contact etc would affect the electrical properties.
- **Electrode effect :** The electrodes used for measuring electrical properties also influences the electrical properties. In case of insulating films, electrodes are required to deposit the contact on their surface. The electrical properties of structure containing insulator (I) or oxide (O) films between metals (MIM), semiconductors (SOS), and mixed electrodes (MIS, MOS) strongly depends on the specific electrode materials used.
- **Degree of film continuity :** Conduction mechanisms in discontinuous, island structure films differ from those in continuous structure films.
- **Existence of high electric field conduction phenomena :** Small voltage applied across very small dimension produces high field effects in films.
- **High chemical reactivity :** Corrosion, absorption of water vapor, atmospheric oxidation, and sulfidation and low-temperature solid-state reaction bring changes in electrical properties.

6.4 Conduction Mechanisms

6.4.1 Introduction

The various types of conduction mechanism in insulating film have been extensively studied. In general an insulator possesses very few free charge carriers at normal temperatures and large energy band gap. In most cases, insulating films are amorphous in nature and the usual model of sharply defined energy bands can not be readily applied, but fuzzy tails arise both at the top of the valence band and the bottom of the conduction band [7]. A relatively high density of charge carriers may be present due to structural imperfection and they tend to be localized or trapped at these centers which cause the insulating property having very low mobilities. In general, amorphous solid has very complicated conduction mechanism, in

which electrons, holes and ions influence on the current transport. Different electrical phenomena may arise by insulating films when sandwiched between combinations of metal and semiconductor electrodes. The various conduction processes may take place in case of wide gap semiconductor and insulators, depending on the trap density, the depth of the trap energy levels below the conduction band and the size of the Schottky barrier at the contacts. Under the influence of an applied electric field, the probable migrating electrons, holes and ions might give rise to the conduction current.

6.4.2 Charge Transport Process

The charge transport process from one electrode to another under the influence of external field in thin polymer films can be divided into two different stages: charge injection and charge transport.

6.4.2.1 Charge Injection

Charge injection at the interface between a metallic electrode and insulator plays a crucial role in the performance of electronic and optoelectronic devices. Other than injection, however, generation of charge carriers in polymer films can be either intrinsic by thermal, photolytic and other means, or extrinsic. In the extrinsic case the creation of charge carrier is effected by introducing electron donors and acceptors into the host matrix. The charge injection process is described as thermally assisted tunneling from the delocalized states of the metal into the localized states of the insulator, whose energy includes contributions from the mean barrier height, the image potential, the energetic disorder, and the applied electric field. There is no satisfactory analytical theory for the field and temperature dependence of the injection current which, for well-characterized interfaces, exhibit behavior relating to both the thermoionic emission and the field-induced tunneling [8].

The electrode-insulator interface, however, is very complicated [9, 10]. Electrical, chemical and physical defects are likely to exist at the interface. Such defects include protrusions, imperfect contact, dangling bonds, and local polarization, contaminates, and traps. The main two theories that describe the interface phenomenon are Schottky and Fowler-Nordheim [11]. Electrons are injected from electrodes into the bulk of material and are required to overcome a potential barrier to move from electrode to insulator. Crossing the barrier depends on applied electric field and the interface defects [12].

Two main categories of carrier injection mechanisms are summarized :

a) Barrier-Limited

In this method, charge carriers are injected through potential barriers from contacts. The potential barrier at the interface between the metal electrode and the insulator (or a semiconductor) prevents the easy injection of electron from the metal into the insulator [13]. When a depletion layer is formed on the insulator side near the interface, the conduction becomes electrode limited because the free carrier concentration in this case is higher in the bulk than what the contact can provide. This means the current-voltage characteristics are controlled by the charge carrier injection from the injecting contacts. Charge carriers injection from an electrode to an insulator/semiconductor may happen either by Schottky emission or quantum mechanical tunneling.

b) Bulk-Limited

In this case the electrical contact must be Ohmic. For electrical conduction involving mainly one type of charge carriers, say electron, the cathode region can be considered a carrier reservoir that supplies charge carriers to the anode region by the applied voltage. Examples include space charge-limited, intrinsic and Poole-Frenkel conduction mechanism. The main features of current transport in insulating films are current-voltage or field characteristics are non-ohmic, and, with the exception of tunneling, the conduction mechanism is thermally activated.

6.4.2.2 Charge Transport

The explanation of charge transport mechanism in polymer thin films, according to their electrical behavior, is a controversial topic and no unified theory is available to explain the experimental results under different conditions to an acceptable degree of accuracy. Various models have been developed to explain the charge transport mechanism in these materials. Among them, two models have been used most frequently to explain the experimental results [14] : (a) Trapping model and (b) Field dependent mobility model.

The trapping model assumes that there is a certain distribution of traps in the energy space between highest occupied molecular orbitals (HOMO) and lowest unoccupied molecular orbitals (LUMO) called localized states, where the free charge can be trapped. These trapped carriers may be released after some specific period because of either temperature, photo absorption or any other excitation methods and eventually they take part in the

electrical response of a polymer thin film. Most frequently, many researchers assume an exponential distribution of traps in the energy band.

The field dependent mobility model assumes exponentially dependence of mobility, μ, on square root of electric field, F, over a wide range of electric field as defined by the Pool-Frenkel law and can be expressed as [15],

$$\mu = \mu_0 \exp\left(\sqrt{\frac{F}{F_0}}\right) \tag{6.8}$$

where μ_0 is the mobility at F_0 and is referred as pre factor and their values are sample dependent.

Mark and Helfrich [16] were first, who proposed the exponential trap distribution model with constant mobility. They assumed that the free carrier concentration, N_0, is much less than the trap carrier concentration, N_t, and the trap distribution, h as a function of energy, E is given by,

$$h(E) = \frac{N_t}{E_c} \exp\left(\frac{E_n}{E_c}\right) \tag{6.9}$$

where N_t is the density of traps and E_c is the characteristic energy constant of the distribution which often is related to the characteristics temperature T_c as $E_c = kT_c$ (k is the Boltzmann's constant).

Since traps plays a vital role in thin film's conduction mechanism, therefore the current density is expressed in terms of exponentially distributed trap theory for an organic thin films of thickness d, relative permittivity ε', and the density of states N in the valence band as [17],

$$J = N_V \mu q^{1-n} \left(\frac{\varepsilon' \varepsilon_0 n}{N(n+1)}\right)^n \left(\frac{2n+1}{n+1}\right)^{n+1} \frac{V^{n+1}}{d^{2n+1}} \tag{6.10}$$

where N_V is defined as the effective density of states in the valence band, q the electronic charge, and $n = (T_C / T) > 1$. This equation shows that the J-V characteristic may be predicted by power law of the form J-V^m where $m = n+1$. Thus experimental J-V characteristics may be used to determine the electrical parameters of an organic material by using the equation (6.10) to its different region of operation [18].

6.4.2.3 Traps : Origin, Effects, Distribution and Detection

Traps are locations that arise from disorders, dangling bonds, impurity etc. Very often, the traps capture free charge carriers and thus play a very significant role in the conduction process. Traps are actually localized energy states, which exist between HOMO and LUMO level of an organic material. When charges are excited in HOMO level due to any reason e.g. the electrical or optical excitation, they jump to the LUMO band and create an electron-hole pair. However, generally in amorphous and polycrystalline organic material, electrical charge transport is always accompanied by more or less frequent capture of charge carriers in these localized states. Such trapped carriers may be released after specific retention period or may recombine with opposite charge carriers. Traps may be classified into two types : electron traps and hole traps. The localized states below and close to the LUMO level, which are able to capture electrons, are electron traps and localized states above and close to the HOMO level, which are able to capture holes, are called hole traps [18].

There are several sources for trap states such as the presence of impurities, structural defects, and self trapping phenomena etc [19]. Process parameters such as deposition rate and substrate temperature etc are also reported to create traps [20].

Traps strongly affect the electrical charge transport phenomena in three different ways :

- As traps capture the mobile charges, therefore the trapped charge carriers no longer actively take part in the charge transport.
- Captured charges behave as static charges and create their own localized electric fields. As distributions of traps are not uniform, the localized static electric field is also not uniform. Their localized field will influence the electric field distribution in a device and hence the transport.
- Charge transport is always accompanied by more or less frequent capture and release of involved charge in traps. If the release rate for trapped carriers is sufficiently low, there will be significant time necessary to reach equilibrium condition. This causes delay and hysteresis effect in operated devices.

The nature of traps in organic materials is widely debated, and there is a variation in their treatment in both analytical calculations and numerical models. It is, however, frequently assumed that the trap density decays exponentially from the band edge into the band gap as shown in Figure 6.4.1. Therefore, the exponential traps distribution model is used with the assumption that traps are in thermal equilibrium with the conduction band.

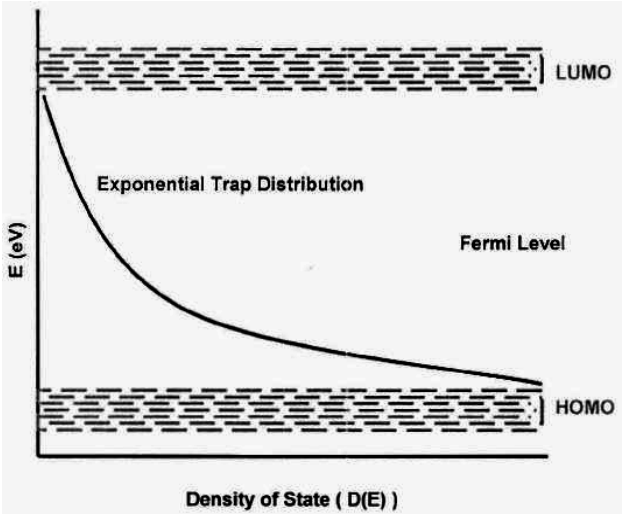

Figure 6.4.1 Exponential trap distribution for amorphous organic materials

There is no unanimously accepted experimental method or technique available, which directly access the information on the energy distribution of trap sates. There are several experimental methods for the detection of trap states, but most of them allowing only for an indirect conclusion on the energy distribution. Some of the most common methods are optically stimulated current (OSC), thermally stimulated current (TSC), thermally stimulated luminescence (TSL) and *I-V* characteristics. Among them *I-V* characteristics method is widely used. In this method, space charge limited current with traps model is applied on experimentally observed electrical properties of the sample. By applying analytical method to this model, both information on the charge carrier mobility and the trap energy distribution are determined. Therefore *I-V* Characteristics method is used to determine the trap depth as well as trap distribution. It gives very precise information related to the trap energy distribution and depth as compared with other experimental trap detection techniques.

6.4.3 Mechanisms Affecting the Current Transport

The different mechanism affecting the current transport through a thin Metal-Insulator-Metal structure is illustrated schematically in the energy band diagram as shown in Figure 6.4.2 and Figure 6.4.3 in the presence of applied electric field [7]. From the diagram, the different electrical transport mechanisms that observed are summarized below:

Mechanism 1 (Schottky Emission): From the Figure 6.4.2(a) it is observed that electron can be injected into the conduction band of the insulator by means of thermal activation over the potential barrier at the electrode-insulator interface. The electrons overcome the potential barrier, leave the metal electrode and move to the adjacent insulation material. The barrier is

assumed to be abrupt between the metal and the insulator, and is modified by the electrostatic attraction between the positively charged electrode and the electron. This electrostatic attraction leads to a change in the barrier due to the electron potential energy. This process is referred to as Schottky emission. Schottky emission is considered as electrode limited conduction mechanism [10, 11, 12, 14].

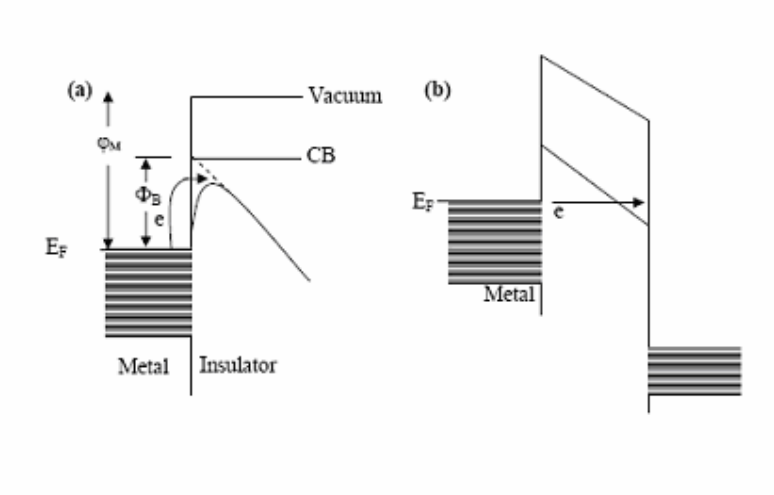

Figure 6.4.2 : Barrier limited conduction mechanism (a) Schottky emission and (b) Tunneling

Mechanism 2 (Tunneling): Electrons may also tunnel directly (Figure 6.4.2-b) into the conduction band of the insulator from either the cathode. If an insulating film is extremely thin or contains a large number of imperfections, or both, electrons can tunnel directly between the metal electrodes and produces a current without the movement of carriers in the conduction band or in the valence band. At high fields and short distances the potential barrier become very thin and non-classical mechanism comes to play. Particles exhibit the wave-particle duality and the principle of uncertainty plays a role in the conduction [10, 11], and leads the electrons tunneling through a potential energy despite not having enough energy to overcome them normally. Also electrons will have a finite probability of existing at two different localized states. This process is also known as Fowler-Nordheim injection [10, 11].

Mechanism 3 (Space-charge-limited conduction): This bulk-limited mechanism occurs because the rate of carrier injection from the contacts exceeds the rate at which charge can be transported through the film. If the cathode emits more electrons per second than the space can accept, the remainder will form a negative space charge, which creates a field to reduce the rate of electron emission from the cathode. Hence the current is controlled not by the electron injecting electrode but by the bulk of the insulator i.e. by the carrier mobility in the space inside the material. This type of conduction is known as space charge limited conduction (SCLC).

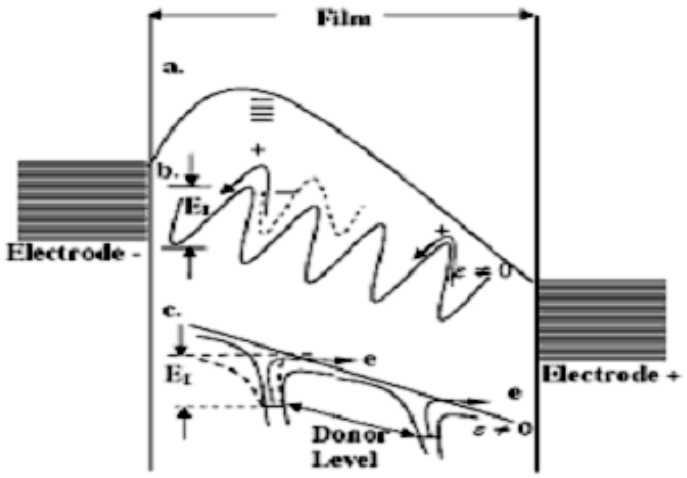

Figure 6.4.3 Bulk-limited conduction mechanisms (a) Space-charge-limited (b) Ionic conduction of cations (c) Poole-Frenkel [7]

Mechanism 4 (Ionic conduction): High temperature conduction in thick film and bulk insulators frequently occurs by ionic rather than electronic motions. Ionic conduction occurs if the actual impurities or defects in the film migrate. The most distinguishing feature of ionic conduction is the extremely low mobility of the carriers and high activation energy.

Mechanism 6 (Poole-Frenkel emission): Electrons may also be thermally excited into the conduction band of the insulator from trapping levels in its forbidden bands. The mechanism of this effect is associated with field enhanced thermal excitation (or detrapping) of trapped electrons or holes, which is very similar to the Schottky effect in the thermionic emission.

Mechanism 5 (Intrinsic Conduction): This mechanism involves direct electronic excitation from the valence to the conduction band. E_g is large in insulator, intrinsic conduction is negligible.

Furthermore, the transport mechanism through the insulator may occur through the presence of impurities, for example foreign atoms or defects, such as Schottky defects or Frenkel defects, causing either impurity or ionic conduction.

A number of above mechanism may operate simultaneously at a particular applied potential difference across the device, but generally one mechanism will dominate the observed current. Some of the above mentioned conduction process will now be considered in greater details.

6.4.4 Schottky Mechanism

The Schottky mechanism is the emission of electrons into the conduction band of an insulator from the metal contact electrode by thermal activation over the electric field which lowers the metal-insulator interfacial barrier. The phenomena, that the lowering of the potential barrier height by the interaction of the applied electric field and the image force is called Schottky effect.

The emission mechanism is shown in Figure 6.4.4. This figure shows that the potential barrier height is $(\phi_m - \chi)$ provided the image force is ignored and there is no applied electric field. Considering the applied and the image force, the total lowering of the potential barrier height is given by,

$$\Delta\phi_B = (\phi_m - \chi) - \phi_B = \left(\frac{q^3 F}{4\pi\varepsilon'\varepsilon_0}\right)^{1/2} = \beta_S F^{1/2} \quad (6.11)$$

where $\beta_S = \left(\frac{q^3}{4\pi\varepsilon'\varepsilon_0}\right)^{1/2}$ (6.12)

is called the Schottky constant, and *F* is the static electric field and is equal to *V/d*, *V* is applied voltage, *d* is film thickness, *T* is temperature in Kelvin, *k* is Boltzmann's constant, *q* is the elementary charge of the electron and ε' is the high frequency dielectric constant of the material.

The potential step changes smoothly at the metal insulator interface as a result of the image force. This happens when the metal surface become polarized (positively charged) by escaping an electron, which in turn exerts an attractive force on the electron given by,

$$F = -\frac{q^2}{16\pi\varepsilon' x^2} \quad (6.13)$$

The potential of the electron due to the image force is thus

$$\phi_m = -\frac{q}{16\pi\varepsilon' x} \quad (6.14)$$

where *x* is the distance of electron from the electrode surface.

So the effective potential barrier height can be written as

$$\phi_B = (\phi_m - \chi) - \left(\frac{q^3}{4\pi\varepsilon'\varepsilon_0}\right)^{1/2} \quad (6.15)$$

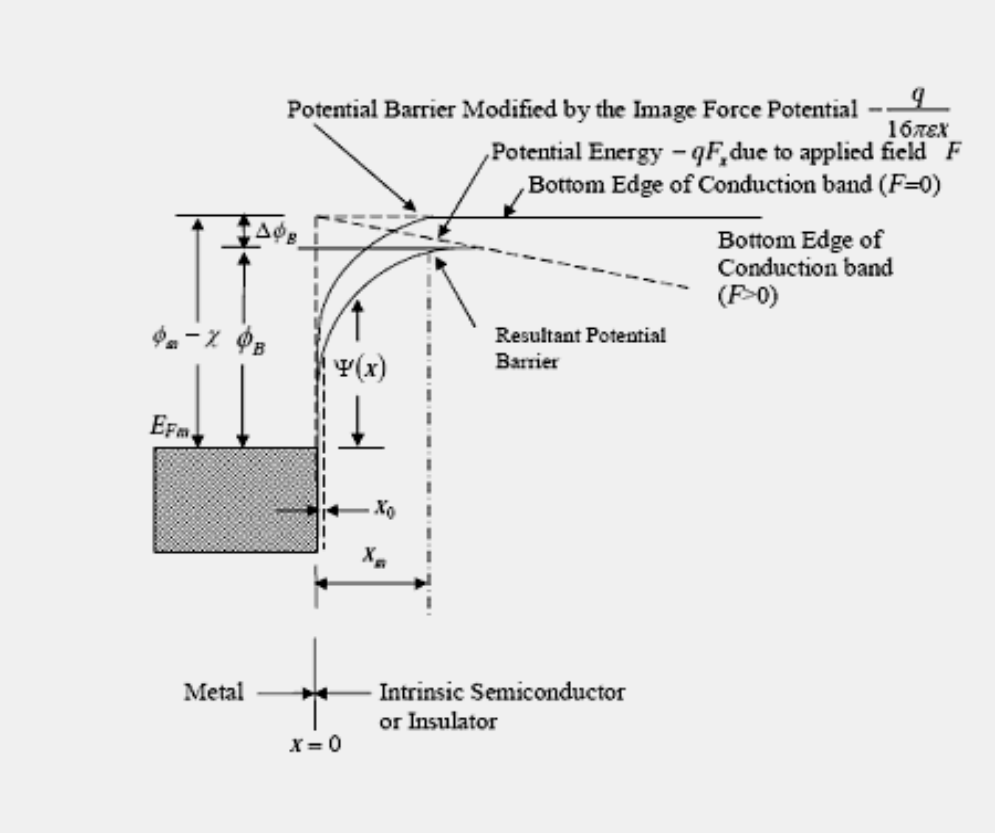

Figure 6.4.4 Energy level diagram showing the lowering of the potential barrier due to the combination of image force and the applied uniform field (Schottky effect) [14]

This type of electron emission from the electrode at a negative potential is analogous to thermionic emission except that the applied electric field lowers the barrier height ϕ_B is given by Richardson equation,

$$J = AT^2 \exp-\left[\frac{\phi_B - \Delta\phi_B}{kT}\right] \times \exp\left[\frac{qV}{kT} - 1\right] = J_0 \exp\left[\frac{qV}{kT} - 1\right] \quad (6.16)$$

where J_0 is the saturation current density, which may be written in the form

$$J_0 = AT^2 \exp-\left[\frac{\phi_B - \Delta\phi_B}{kT}\right] \quad (6.17)$$

where $A = \frac{4\pi mqk^2}{h^3}$ (6.18)

is known as the Richardson constant. For most metals, A is about 60-120 $Acm^{-2}K^{-2}$. In expression, h is Planck's constant, and m is the electronic mass.

Because of the image-force lowering of the potential barrier, the electrode limited current does not saturate according to the Richardson equation, but, rather, obeys the Richardson-Schottky law. If we let the current density under this condition be identified by *J* then,

$$J = J_0 \exp\left(\frac{\beta_s F^{1/2}}{kT}\right) \qquad (6.19)$$

In deriving the equation (6.18), however, Schottky neglected the electron-electron interaction term in calculating the carrier density using the Fermi-Dirac statistics. This assumption is practically not true because the emission current has a significant magnitude and hence there is always the possibility of electron-electron interaction. He also assumed a constant value of work function. In practice, however, the work function will increase if an electronic space charge exists in the vicinity of the contact. It also decreases with increasing field strength. In addition, the emitting area is much less than the actual surface area because of filamentary injection [21, 22]. The value of the dielectric constant ε is less than the dc or static value of ε in the vicinity of the contact [23, 24]. The presence of this discrepancy suggests that a rigorous fit of theoretical and experimental results can not be expected.

The electrode limited Richardson-Schottky effect in insulators appears to have been first observed by Emptage and Tantraporn, who reported a *log I* vs. $F^{1/2}$ relationship in their samples. It was suggested that the plot should have to be linear in nature for Schottky type conduction mechanism [25].

6.4.5 Poole-Frenkel Mechanism

The original theory of the Poole-Frenkel (PF) effect was put forward by Frenkel [26]. The Poole-Frenkel effect is sometimes called the internal Schottky effect, since the mechanism of this effect is associated with the field enhanced thermal excitation (detrapping) of trapped electrons or holes, which is very similar to the Schottky effect in the thermionic emission. It is a bulk-limited conduction process. In this process emission of electrons occurs from trapping centers in semiconductors and insulators by the joint effect of temperature and electric field. It is also called the field-assisted thermal ionization. Figure 6.4.5 depicts the PF emission mechanism. In this diagram, the solid lines represent the normal potential energy of the electron as a function of distance *x* from the positive ion.

The PF effect also lowers the Coulombic potential barrier when it interacts with an electric field, as shown in Figure 6.4.5. As the potential energy of an electron in a Coulombic field $-e^2/4\pi\varepsilon x$ is four times that due to the image force effects, the PF attenuation of a Coulombic

barrier $\Delta\varphi_{PF}$, uniform electric field is twice that due to the Schottky effect at a neutral barrier:

$$\Delta\varphi_{PF} = 2\Delta\varphi_s = 2\left(\frac{q^3F}{4\pi\varepsilon}\right)^{1/2} = \beta_{PF}F^{1/2} \qquad (6.20)$$

With the applied field, the Coulombic barrier height between electrode and the film is lowered, and the carrier can escape more easily giving rise to field assisted conductivity:

$$\sigma = \sigma_o \exp\left[\frac{\beta_{PF}F^{1/2}}{2kT}\right] \qquad (6.21)$$

From equation (6.21) it can be written that

$$\log\sigma = \log\sigma_0 + \frac{\beta_{PF}}{2kT}F^{1/2} \qquad (6.22)$$

where F = V/d, is the dc applied field, k is Boltzmann constant, T is the absolute temperature, σ_o is the low field conductivity, β_{PF} is the Poole-Frenkel co-efficient and is given by

$$\beta_{PF} = 2\left[\frac{e^3}{4\pi\varepsilon_o\varepsilon}\right]^{1/2} = 2\beta_s \qquad (6.23)$$

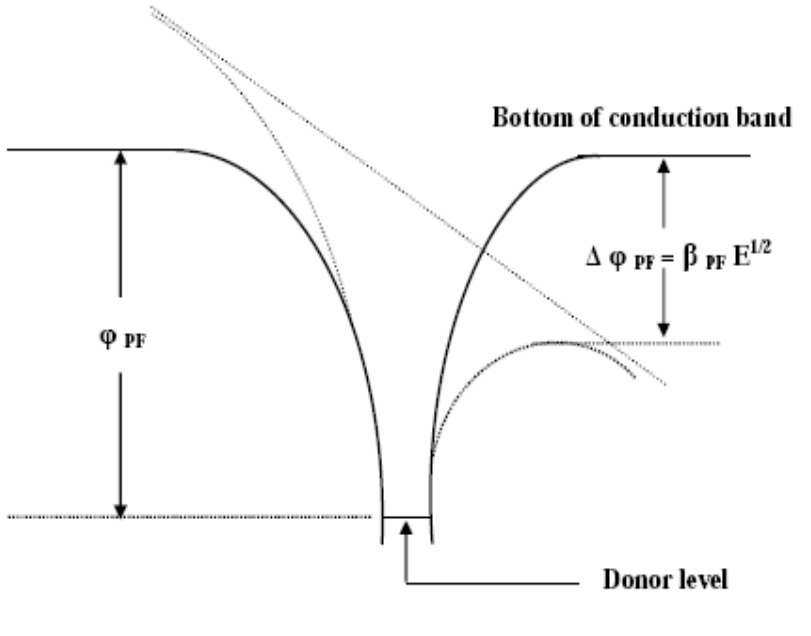

Figure 6.4.5 Poole-Frenkel effect at a donor center.

The general expression for J that is equally valid for both the PF and Schottky mechanisms is of the form,

$$J = J_o \exp\left[\frac{\beta F^{1/2} - \varphi}{kT}\right] \quad (6.24)$$

where J_o is the low field current density; β is the coefficient: F is the static electric field and φ is the ionization energy of the localized centers in Poole-Frenkel conduction and Coulomic barrier height of the electrode-polymer interface in Schottky conduction. It could be noted that φ results from the injection of electrons or holes from the electrodes into the conduction band of the dielectric, and it involves the emission of trapped electrons/holes from localized centers or potential wells within the dielectric.

By taking natural logarithms of equation (6.23) we can write

$$\beta_{\exp} = skTd^{1/2} \quad (6.25)$$

where, β_{exp} denotes the value of β obtained experimentally and

$$s = \left[\frac{\Delta \ln J}{\Delta V^{1/2}}\right] \quad (6.26)$$

is the slope of graph plotted between *lnJ* and $V^{1/2}$.

6.4.6 Space Charge Limited Conduction Mechanism

Space charge literally means charges in space, i.e. in a region where there is a concentration of charges in the form of electrons, holes or ions. These charges may be mobile or localized, but constitute non-uniform localized field. Transport of the charges under the influence of non-uniform electric field is called Space Charge Limited Conduction (SCLC), which is observed in many polymer semiconducting and insulating materials [27].

Space charges in materials may arise from several sources: electrode injection of electrons and/or holes, ionized dopants in interfacial depletion regions and accumulation of mobile ions at electrode interfaces are just three examples. Traps may be present in the bulk material or at interfaces where they will act to reduce carrier mobility. When present at interfaces they may also influence charge injection into the material.

If the cathode supplies large number of free carriers in the dielectric near the injecting electrode, a space-charge will build up within the insulator. A field will be created to reduce the rate of electron from the cathode. Current flows through the insulator will then saturate. For low values of potential difference, if the injected carrier density is lower than the

thermally generated free carrier density *N*, Ohm's law will be obeyed, and the current density *J* is given by equation (6.7),

$$J = Nq\mu\frac{V}{d} = \sigma\frac{V}{d} \qquad (6.7)$$

However, it should be noted that when the injected carrier density is greater than the free carrier density the current becomes space-charge-limited.

Two requirements need to be fulfilled in order to observe SCL current flow of significant magnitude. These are: (i) at least one of the two electrodes must make an ohmic contact with the insulator, and (ii) the insulator must be relatively free from trapping defects.

The mechanism of SCLC in solids was first proposed by Mott and Gurney [28] in 1941, and then a simplified theory of one-carrier SCLC was presented by Lampert in 1956 [29]. In a trap-free material and neglecting diffusion effects, it is readily shown that when the concentration of carriers injected from the ohmic contact exceeds the thermally generated carrier concentration, the current density, *J*, flowing through the semiconductor for an applied voltage, *V*, is given by

$$J = \frac{9}{8}\varepsilon'\varepsilon_0\mu\frac{V^2}{d^3} \qquad (6.27)$$

where μ is the carrier mobility in the transport band, *d* the semiconductor thickness, ε' is the insulator's relative permittivity and ε_0 is the permittivity of free space.

The equation (6.27) is the well known Mott-Gurney equation and is sometimes referred to as the square law for trap-free SCL currents. The interesting features of relation are that, it predicts that *J* is directly proportional to V^2 and inversely proportional to d^3.

However, equation (6.27) predicts much higher current than that is observed in practice, and also that SCLC is temperature insensitive. They obtained this expression for the current density *J* for the simple case of single carrier trap-free SCLC in an insulator. The deviations from the trap free theory are readily observed in case of more realistic insulators, which contains trap. The theory of SCLC in defect insulators was put forward by Rose [30]. In the presence of traps, a large fraction of the injected space charge will condense therein, which means that the free-carrier density will be much lower than in a perfect insulator. Since the occupancy of traps is a function of temperature, the SCL current will be temperature-dependent.

When the insulator is characterized by a set of shallow traps with spatially uniform distribution, the mobility in equation (6.27) is replaced by an effective mobility, $\mu_{eff,}$ and is written as,

$$J = \frac{9}{8}\varepsilon'\varepsilon_0\mu_{eff}\frac{V^2}{d^3} \quad (6.28)$$

where

$$\mu_{eff} = \mu\left(\frac{\theta}{1+\theta}\right) \quad (6.29)$$

and

$$\theta = \frac{N}{N+N_t} \quad (6.30)$$

where θ is the ratio of free to trapped carriers and N_t is the density of trapped holes [31].

From equation (6.26) and (6.27) the free charge carriers' density *N* can be calculated at the transition voltage from the Ohmic to the SCLC regime as follows:

$$N = \frac{9}{8}\varepsilon\frac{V_\Omega}{qd^2} \quad (6.31)$$

where $\varepsilon = \varepsilon'\varepsilon_0$ is the polymer permittivity and V_Ω is the transition or threshold voltage from the Ohmic regime to the SCLC regime.

It could be noted that, If the insulator contains N_t shallow traps, all assumed to be at the same energy level E_t below the bottom of the conduction band, then the free component of the space charge is given by,

$$N_f = eN\exp\left(\frac{-E_F}{kT}\right) \quad (6.32)$$

and trapped component of the space charge is given by,

$$N_t = eN_t\exp\left[-\frac{(E_F - E_t)}{kT}\right] \quad (6.33)$$

then the trapping factor, θ, which is defined as the ratio of the free charge to the total carriers (free and trapped) charge is given by,

$$\theta = \frac{N_f}{N_t} = \frac{N}{N_t}\exp\left(-\frac{E_t}{kT}\right) \quad (6.34)$$

The current density, including the effect of shallow traps is given by,

$$J = \frac{9}{8}\varepsilon'\varepsilon_0\mu\theta\frac{V^2}{d^3} \quad (6.35)$$

Since θ is independent of *V*, *J* is directly proportional to V^2, as in the trap free case. As θ is very small temperature-dependent quantity, the inclusion of shallow traps in the insulator satisfies the theory with the experimental observation.

According to equation (6.35) *J* varies as d^{-1} in the ohmic region and as d^{-3} in the SCLC region except for the trap-filled SCLC part, and therefore for a fixed V, the dependence of *ln J* on *ln d* should be linear with slope l ≥ -3 to obtain SCL conduction.

For a shallow trap SCLC and trap-free SCLC, θ =1. At low injection rates, when θ << 1, transport is dominated by trapping. At sufficiently high injection rates, it may become possible to fill all the traps so that the free carrier concentration greatly exceeds the trapped concentration in which case θ >> 1 and equation (6.28) reverts to Child's law [equation (6.27)]. The transition from trap-mediated to trap-free SCLC is accompanied by a sharp rise in current at the so-called
trap-filled limit voltage, V_{TFL}, which is related to the trap density, N_t, by the expression,

$$V_{TFL} = \frac{qd^2}{2\varepsilon'\varepsilon_0}N_t \quad (6.36)$$

and from this equation, trap density, N_t, can be calculated as,

$$N_t = \frac{2\varepsilon'\varepsilon_0}{qd^2}V_{TFL} \quad (6.37)$$

Where traps are distributed in energy, the situation becomes more complex but still tractable. For example, Mark and Helfrich [16] analyzed the situation for a distribution of traps of density, $N_t(E)$, decreasing in energy away from the transport band i.e.,

$$N_t(E) = \frac{N_t}{kT_c}\exp\left(-\frac{E}{kT_c}\right) \quad (6.38)$$

where N_t, is the total trap density, *k* is Boltzmann's constant and T_C is a characteristic temperature of the distribution which is assumed greater than the sample temperature *T.* For their case of hole injection into organic crystals, the current density is given by equation (6.10).

Now, throughout the trap-controlled region, the steady-state current is proportional to V^{n+1} until it merges with the trap-free case [equation (6.7)]. Such behavior is a consequence of an

increasing injection rate filling the deeper traps first so that the current becomes controlled by traps of ever decreasing energy, equivalent to increasing the effective carrier mobility. Although adding significantly to the experimental burden, an effective test for SCLC is to establish the sensitivity to the sample thickness [32]. Both the single-trap and distributed-trap cases may be further developed to include a PF reduction of the trap depth [16].

A typical current-voltage (I-V) characteristics curve for a polymer thin film is shown in Figure 6.4.6. It is clear from the Figure (6) that the I-V characteristics can be divided into three well-defined charge transport phenomena.

Region I

Region I is called an ohmic charge region. At initial stage when applied voltage is increased very slowly, the charges injected from electrodes are used to fill the traps. However, some charges succeed in reaching the opposite electrodes and hence very small current is observed. The current in this region changes linearly with the voltage and follow the equation (6.7), namely

$$J = qN\mu\frac{V}{d} = \sigma\frac{V}{d} \qquad (6.7)$$

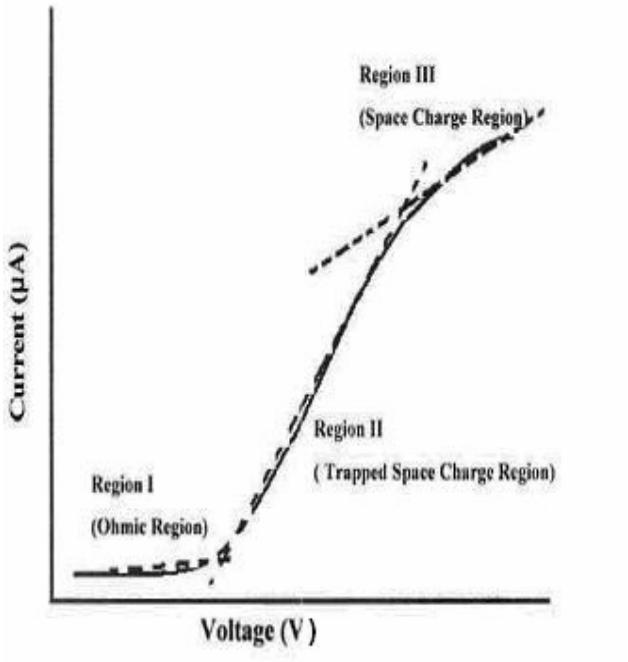

Figure 6.4.6 A typical I-V characteristics curve for a polymer thin film

Region II

When applied voltage is further increased then a departure from the ohmic linear region I is observed to region II which has a higher slope than the previous region. This region is called the trapped space charge region. At higher voltages there is an increase in the probability of excess charge carrier transport from thin film are influenced by the density of traps leading to a departure from Ohm's law. Then the charge transport phenomena is explained by the equation (6.35) namely,

$$J = \frac{9}{8}\varepsilon'\varepsilon_0\mu\theta\frac{V^2}{d^3} \qquad (6.35)$$

where θ is called trap factor, which differentiates region II from Region III and reflects the extent to which the traps reduce the effective mobility.

Region III

When voltage is further increased, a stage is reached where all the traps are filled up by the charge and the device behaves just like as trap free thin film, then space charge limited current is expressed by the equation (6.27) namely,

$$J = \frac{9}{8}\varepsilon'\varepsilon_0\mu\frac{V^2}{d^3} \qquad (6.27)$$

This equation, as stated above is known as the Mott-Gurney equation and is the solid-state analogy of Child's law of SCLC in a vacuum.

6.4.7 Thermally Activated Conduction Processes

Polymer conductivity is very low, usually less than 10^{-13} $(\text{Ohm-m})^{-1}$ [33]. Consequently charge will find it very difficult to travel in the polymer by normal conduction mechanisms. In amorphous solids the band structure is not well-defined and explanation of conduction mechanisms in these materials is very complicated. However, as the polymer chain is made up, degenerate monomer molecular orbitals form a series of extended electronic states, band theory is therefore applicable along chains. But since polymer chains are joined by secondary weak (Van der Waals) attractions, therefore there is no valance band between chains. The band theory assumes that the electrons are delocalized and can extend over the lattice. When electronic conduction is considered in polymers, band theory is not totally suitable because the atoms are covalently bonded to one another, forming polymeric chains

that experience weak intermolecular interactions. But macroscopic conduction will require electron movement, not only along the chain but also from one chain to another. This changes the classic band theory and limits the movement of charge. However the band gap is very large in polymer material and it is very difficult to create mobile charge [34, 35].

An important feature of the band system is that electrons are delocalized and spread over the lattice. Some devocalizations are naturally expected when an atomic orbital of any atom overlaps appreciably with those of more than one of its neighbors, but delocalization reaches an extreme form in the case of a regular 3-D lattice.

The carrier mobility in organic molecules is usually very low. This is due to the fact that electrons, while jumping from one molecule to another, lose some energy. But the mobilities of electrons are found to increase with molecular size in such type of compounds. In polymer system, the conductivity is influenced by the factors such as dopant level, morphology of polymer, concentration of conducting species, temperature, etc. It is difficult to generalize the temperature dependence of dc conduction whether it is ionic or electronic, since so many processes are possible. As the temperature is increased the charge carrier concentration increases strongly with temperature. This dominates the temperature dependence of the conductivity, giving it an Arrhenius-like character, and Ohmic (low field) conduction whether ionic or electronic, gives exponential temperature dependence, given by,

$$J = J_0 \exp \frac{-\Delta E}{kT} \qquad (6.39)$$

where J_0 is a constant and ΔE is the activation energy for carrier generation. . Whatever the Ohmic mechanism, a *log J* vs. *1/T* plot (Arhennius plot) will usually exhibit increasing linear slopes (activation energies) as T is raised [25].

With extrinsic electronic conduction, the electrons may move by hopping, but in extrinsic ionic conduction the mobility μ is activated and ΔE being the energy for the ion to hop. However, for variable range hopping the electrical conductivity is given by,

$$\sigma = \sigma_o \exp -\left(\frac{T_o}{T}\right)^{\frac{1}{d+1}} \qquad (6.40)$$

where “d” is the dimensionality of transport, σ is the conductivity, σ_o is the initial value of conductivity, T is the absolute temperature and T_o is the activation energy in terms of temperature.

In bulk material ionic conduction occurs due to the drift of defect under the influence of an applied electric field. The degrees of ionic impurities that may be totally ignored in the context of other properties may have a significant effect on conductivity. A theoretical expression may be derived for the current density,

$$J = Sinh\left(\frac{qaE}{2kT}\right) \qquad (6.41)$$

where *E* is the electric field, *a* is the distance between neighboring potential well, and *q* is the electronic charge.

6.4.8 Traps and Volumetric Conduction

Charge conduction is limited even further by the existence of what are called traps, which are actually region-localized states of low potential energy. For charge carriers to leave traps, they must have enough energy to overcome a large potential barrier. Charges can reside in traps from seconds to antiquity or can move from one trap to another in a nearby localized state by hopping and tunneling. The probability of hopping and tunneling is highly dependent on the inter-site distance. The existence of traps alters the band gap model as shown in Figure 6.4.7. Charge in the traps makes large increases in net space charge. This may have a significant effect on electrical ageing.

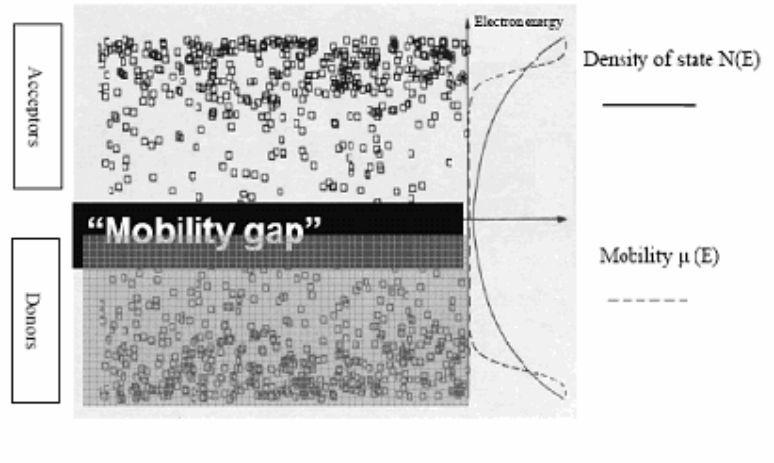

Figure 6.4.7 Localized states in an amorphous material [33]

Figure 6.4.7 shows localized states in an amorphous material (indicated by squares) as a function of electron energy together with the density of states *N (E)*, and the mobility *μ (E)*. It is seen from the Figure that the band gap is not well defined and the effective mobility

decreases sharply near the centre of the gap where the concentration of state is very low. Overlapping squares show the states between which charge transport is likely to be found.

6.4.9 Tunneling and Hopping Conduction

Trapped charge can lead to the polarization and distortion of the lattice structure and could result in local energy band deformation making it very hard for trapped charge to be free. However, charge carriers in polymers may move from one site to another by hopping over a potential barrier, or tunneling through it, or a combination of both [11, 12, 35]. Hopping is the transfer of a thermally activated charge carriers between localized states. Carriers acquire enough energy from the lattice by means of thermal fluctuations to overcome the potential barrier. Tunneling is a quantum mechanical process and the particles exhibit the wave-particle duality. The principle of uncertainty plays a role in the conduction [10, 11] and leads the electrons tunneling through a potential energy despite not having enough energy to overcome them normally. Also electrons will have a finite probability of existing at two different localized states, because in accordance with the uncertainty principle, the position of an electron is not fully determinate. If the energy barrier is thin enough, then the spatially distributed uncertainty of location of the electron may actually pass through the energy barrier and have non-zero probability on the "other" side of the boundary. Electrons, in this manner, can "tunnel" out of traps that they do not have enough energy to simply overcome and hop into another trap.
This process is also known as Fowler-Nordheim conduction [10, 11].

The Fowler–Nordheim relation [36] for current density *J* can be expressed as,

$$\log\frac{J}{V^2} = \log A - \frac{\varphi}{V} \qquad (6.42)$$

and the log *J*/ V^2 vs. 1/ *V* plot is expected to be a linear relation with a negative slope.

6.5 Results and Discussion

6.5.1 Plasma Polymerized Pyrrole Thin Films

6.5.1.1 *J* – *V* characteristics

The current density-voltage (*J-V*) characteristics for PPPy thin films of thicknesses about 400, 450, 500, 550 and 600 nm, were recorded at room temperature in the voltage region of 0.1 V to 30 V, and are presented in Figure 6.5.1. From the figure, it is observed that the current density is higher in the thin films of lower thickness at the same voltage. In many investigations [37, 38] it is reported that the conduction in the plasma polymerized films is thickness dependent and current density is found to increase for lower thicknesses in the same applied voltage range, and the present results show the similar behavior. It is also seen that the curves in Figure 6.5.1 follow a power law of the form $J \propto V^n$, where n is a power index, with two different slopes in the lower and higher voltage regions. At low voltages the J-V characteristics of thin polymer films may follow Ohm's law, provided the transport is not limited by the polymer/electrode interface, and the current density *J* is given by the equation (6.7).

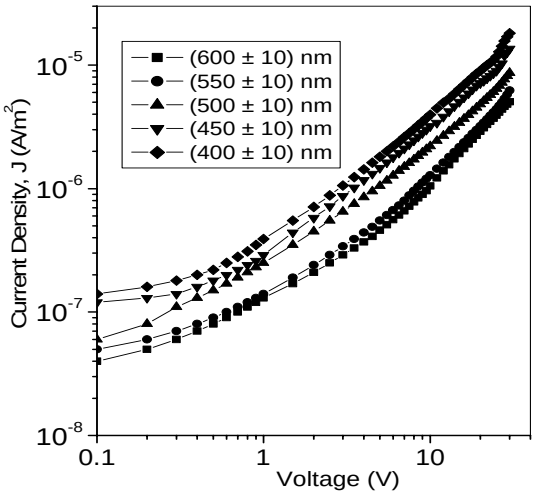

Figure 6.5.1 The J-V characteristics for PPPy thin films of different thicknesses at room temperature.

In Figure 6.5.1, however, the value of slopes at lower voltage region (1~7 V) is found to be 0.80<n<1.15 indicating a probable Ohmic conduction, while at higher voltages (15~27 V) the slopes 1.65<n<2.65 represent the non-Ohmic conduction.

Figure 6.5.2 to Figure 6.5.6 represents the *J-V* characteristics of all the samples of thicknesses about 400, 450, 500, 550 and 600 nm respectively at different temperatures of 300, 323, 348 and 373 K. It is observed that the current density of all the samples for both the voltage regions is increased slightly with increasing temperature. This increase may be due to the increased molecular motion at higher temperatures, and indicates probable temperature dependence of the conductivity.

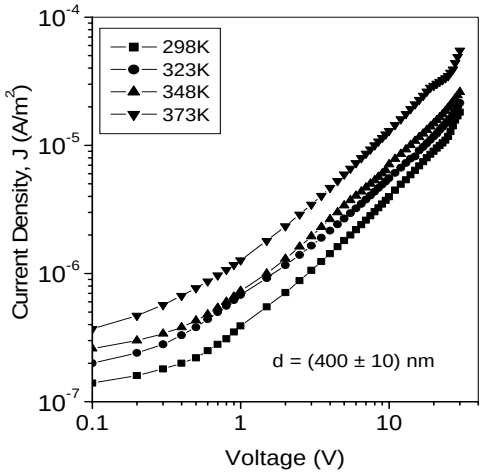

Figure 6.5.2 The J-V characteristics for PPPy thin film at different temperatures.

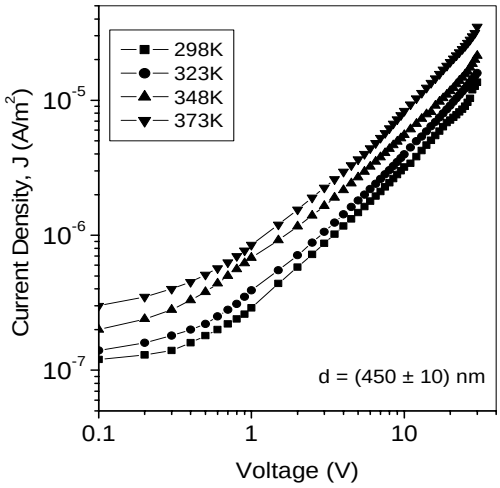

Figure 6.5.3 The J-V characteristics for PPPy thin film at different temperatures.

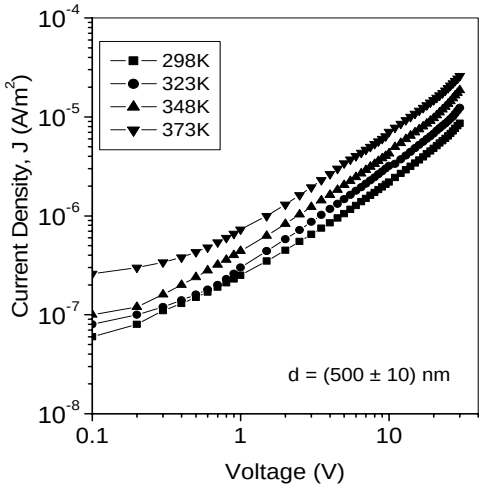

Figure 6.5.4 The J-V characteristics for PPPy thin film at different temperatures.

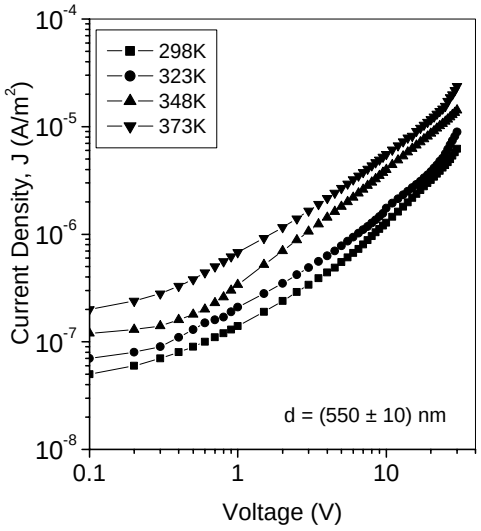

Figure 6.5.5 The J-V characteristics for PPPy thin film at different temperatures.

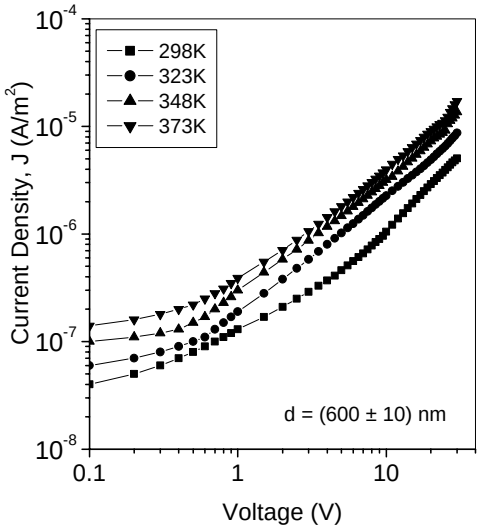

Figure 6.5.6 The J-V characteristics for PPPy thin film at different temperatures.

The dc electrical conductivity of PPPy thin films for different thicknesses 400, 450, 500, 550 and 600 nm have been calculated at different applied voltage from Figure 6.5.1 using equation (6.7). Figure 6.5.7 shows the plots of σ vs. V. Though the conductivity σ, and consequently the resistivity ρ, is an inherent physical property of most materials, and it is expected that, σ or ρ should remains constant in any circumstances, it is seen from Figure 6.5.7 that, the conductivity is changed with the change in the thickness of the PPPy thin films. This change in the conductivity for different thicknesses suggests a probable change in physical properties during the formation of the plasma polymerized thin films. It is important to note from the figure that, for the lower thicknesses of the PPPy thin films (e.g. 400 and 450 nm), the conductivities remain almost constant throughout the whole voltage range, but for higher thickness (e.g. 550 and 600 nm) a slight variation of the conductivity is observed.

It is also to be noted that the conductivity is found to be increased with the decrease in thickness of the PPPy thin films and vice versa. The most probable reason of this behavior may be due to better morphological characteristics of the films of lower thickness. It has been reported by Valaski et al. [38] that the film morphology is highly thickness dependent, and better morphology (lower roughness) has been observed for lower thickness, which causes increased charge mobility. It is also important to note that the electrical behavior of polymer films is strongly influenced by the morphology of the films. Yuan et al. [39] investigated the morphology of electrochemically deposited polypyrrole (PPy) films and demonstrated that the PPy films can form well-ordered neural networks by controlling the thickness and the improvement in structural disorder affords an increase in the charge carrier mobility. The grain formation in PPy films was also observed by them. However, the lower roughness in the films of smaller thickness suggests smaller grain size. Thinner films should present more structural order due to more homogeneous surfaces, decreased grain size and improve interchain conduction, and as a result, an increased conductivity could be observed. On the other hand, as the average grain size is smaller for lower thicknesses and the grains are closer to each other, the energy barrier between them decreases, which improves intergrain conduction also, and conductivity could also be increased. However, since the films with smaller thicknesses have more structural order due to more homogeneous surfaces and smaller grain size which increases the conductivity of the film, therefore the films with higher thickness might have opposite characteristics, and consequently reduces the conductivity of the films.

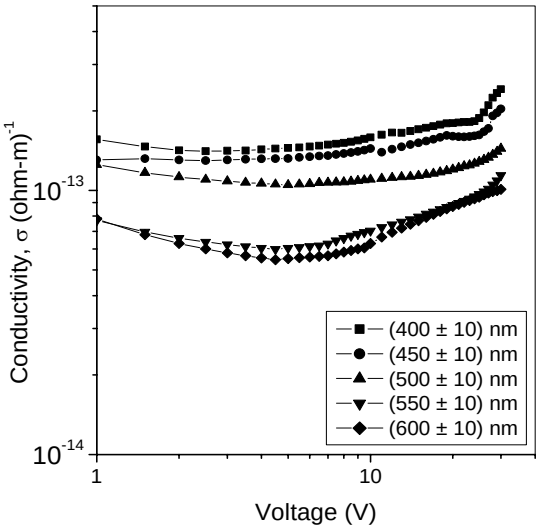

Figure 6.5.7 Plots of dc conductivity vs. voltage for PPPy thin films of different thicknesses.

This decrease in the conductivity of plasma polymerized PPPy thin films with the increase of the thickness of the films may be due to some other reasons. It is known that the resistivity in a material arises due to the deviation from the periodicity of the potential in which the electron moves, and it is on this concept that the modern theory of conductivity is based. One of the effects of quantum mechanical wave behavior of electrons is that, electrons do not scatter from a perfect lattice, they scatter by defects. Therefore, the deviation from the periodicity of the potential which causes the resistivity may be also due to displacement of atoms by lattice vibrations, or lattice defects such as vacancies, interstitials and dislocations

or foreign impurity atoms, or dislocations, or/and grain boundaries etc. Any of these effects could be happened during the deposition of the films by plasma polymerization. For example, the incorporation of oxygen is reported by Yasuda et al. [40] as a typical phenomenon in the plasma polymerization, and in this study, the FTIR analyses of PPPy have also indicated the presence of oxygen by the appearance of the absorption band at 2214 cm^{-1} [41]. This oxidation of the films might affect the physical properties of the thin films, which might increase the resistivity of the films of higher thickness.

6.5.1.2 Conduction Mechanism in PPPy Thin Films

The J-V characteristics (Figure 6.5.1) of PPPy thin films are characterized by two different slopes in the lower and higher voltage regions. The slopes at lower voltage region (1~7 V) is found to be $0.81<n<1.15$ indicating a probable ohmic conduction, while at higher voltages (15~27 V) the slopes $1.65<n<2.66$ represent the non-Ohmic conduction. The Ohmic conduction could be described by equation (6.7), but to analyze the non-ohmic conduction different conduction mechanism has to be considered.

The complex conduction behavior in organic solids could be explained usually in terms of electron emission from cathode, i.e. Schottky–Richardson mechanism [42] or by electron liberation from the traps in the bulk of the material, i.e., PF mechanism [31]. The possibilities of tunneling or Fowler–Nordheim mechanism [36], SCLC [30] etc have also been investigated. However, the thickness and voltage dependence of current density of PPPy thin films at the higher voltage region suggests that the current may be due to Fowler–Nordheim, PF, Schottky or SCLC mechanisms in PPPy thin films.

The Fowler–Nordheim mechanism or tunneling effect is usually observed in very thin films. The Schottky emission is defined only when the carriers are injected from the electrode by means of thermal or field assisted emission. The other process in which carriers are produced by the dissociation of donor-acceptor centers in the bulk of the material, is called PF generation. If the generation process is slower than transport by the carriers through the material, the conduction is controlled by generation, specifically by either the Schottky, or PF mechanisms. Conversely, when the transport is slower than generation, it constitutes the rate-determining step, and the conduction is described by the theory of SCLC.

However, the direct current conduction mechanisms for the PPPy thin films are discussed in the light of the following mechanisms.

(a) Tunneling or Fowler–Nordheim Mechanism

If the applied voltage is not too high and the film is extremely thin or contains a large number of imperfections, or both, electrons can tunnel directly between the metal electrodes and produces a current without the movement of carriers in the conduction band or in the valence band. This process is known as tunneling or Fowler-Nordheim mechanism [10, 11].
In this process, the electron may flow by tunneling from the negative electrode into unoccupied levels of the positive electrode; but if the voltage is higher or the film is thicker

the tunnel transfer or conveys the electrons into the conduction band of the dielectric rather than directly to the second metal. If the dielectric contains a large number of traps, the tunneling can take place through some of the traps.

The Fowler–Nordheim relation [36] for *J* can be expressed as,

$$\log \frac{J}{V^2} = \log A - \frac{\varphi}{V} \qquad (6.42)$$

and to be operative of this mechanism, the log *J/ V*^{2} vs. 1*/ V* plot is expected to be a linear relation with a negative slope.

In the Figure 6.5.8, the Fowler–Nordheim plots, i.e., log *J/ V*^{2} vs. 1*/ V* plots for PPPy thin films of thicknesses 400, 450, 500, 550 and 600 nm are shown. It is seen from the figure, that the curves are not at all linear and all of them have positive slopes, indicating the absence of tunneling effect in PPPy thin films.

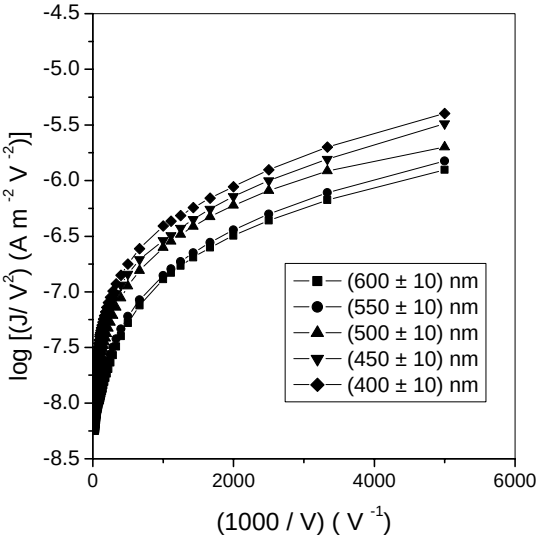

Figure 6.5.8 Fowler–Nordheim plots for PPPy thin films of different thicknesses.

(b) Schottky Mechanism

The Schottky–Richardson current voltage relationship is expressed as,

$$\log J = \log AT^2 - \frac{\varphi}{kT} + \beta_s F^{1/2} \qquad (6.43)$$

where F is the electric filed, and therefore *log J* vs. *F*$^{1/2}$ (or *log J* vs. *V*$^{1/2}$) plot is referred to as Schottky plots, and should be a straight line with a positive slope to become Schottky mechanism operative.

The Schottky plots i.e., log J vs. $V^{1/2}$ plots for PPPy thin films of thicknesses 400, 450, 500, 550 and 600 nm have been shown in Figure 6.5.9. It is seen from the figure, that the curves in this case is not also linear though all of them have positive slopes, indicating the absence of Schottky mechanism in PPPy thin films.

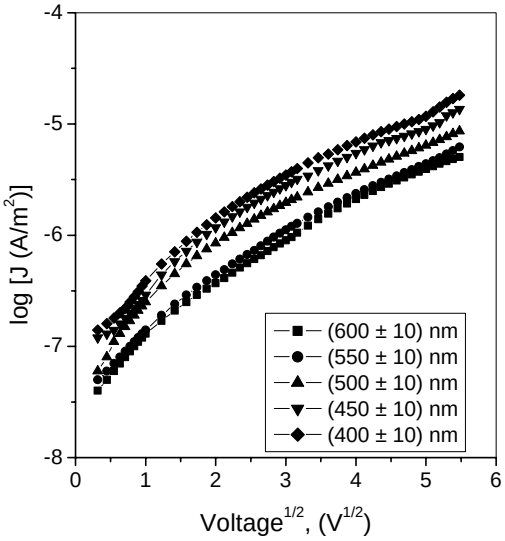

Figure 6.5.9 Schottky plots for PPPy thin films of different thicknesses

(c) Poole–Frenkel Mechanism

The PF effect is sometimes called the internal Schottky effect, since the mechanism of this effect is associated with the field enhanced thermal excitation (detrapping) of trapped electrons or holes, which is very similar to the Schottky effect in the thermionic emission. It is a bulk-limited conduction process, in which the emission of electrons occurs from trapping centers in thin films by the joint effect of temperature and electric field. It is also called the field-assisted thermal ionization.

The PF field-dependent conductivity can be expressed as

$$\sigma = \sigma_o \exp\left[\frac{\beta_{PF} F^{1/2}}{2kT}\right] \qquad (6.21)$$

where β_{PF} is the Poole-Frenkel co-efficient and F is the static electric field.

or $\log\sigma = \log\sigma_0 + \frac{\beta_{PF}}{2kT} F^{1/2}$ (6.22)

so that the PF mechanism is characterized by the linearity of *log σ* vs. $F^{1/2}$ plots (or *log σ* vs. $V^{1/2}$ plots) with a positive slope.

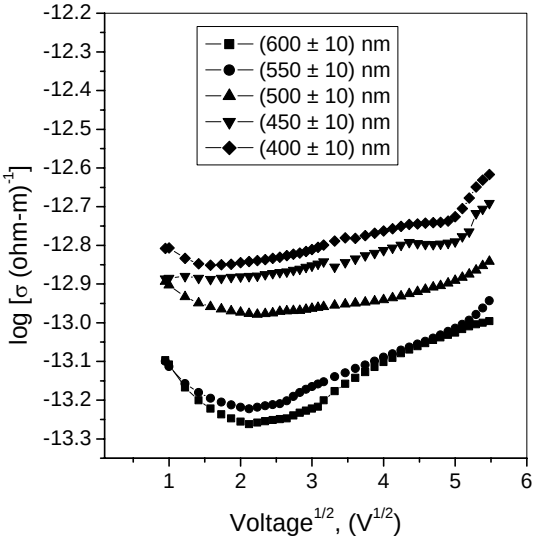

Figure 6.5.10 Poole–Frenkel plots for PPPy thin films of different thicknesses

Figure 6.5.10 shows the PF plots i.e., $log\ \sigma$ vs. $V^{1/2}$ plots for PPPy thin films of thicknesses 400, 450, 500, 550 and 600 nm. It is observed that none of the curves shows linearity and no particular types of slope-character (positive or negative) could be mentioned from the curves, which ruled out the possibility of PF conduction mechanism in PPPy thin films.

(d) Space Charge Limited Conduction

This bulk-limited mechanism occurs because the rate of carrier injection from the contacts exceeds the rate at which charge can be transported through the film. If the cathode emits more electrons per second than the space can accept, the remainder would form a negative space charge, which creates a field to reduce the rate of electron emission from the cathode. Hence the current is controlled not by the electron injecting electrode but by the bulk of the insulator i.e. by the carrier mobility in the space inside the material. This type of conduction is known as SCLC.

However, when the applied voltage is increased over a certain value, the injected charge carrier density largely exceeds the free charge density under thermal equilibrium, then the system transits to SCLC, Schottky or PF conditions. For SCLC, the current density can be described by the equation (6.27), namely,

$$J = \frac{9}{8}\varepsilon'\varepsilon_0\mu\frac{V^2}{d^3} \qquad (6.27)$$

This relation indicates that J is inversely proportional to d^3. The thickness dependence of current follows the relation $J\ \alpha\ d^{-l}$ where l is a parameter depending upon the trap distribution. A slope $l<3$ suggests the possibility of Schottky or PF conduction mechanism and $l \geq 3$ reveals the possibility of SCLC.

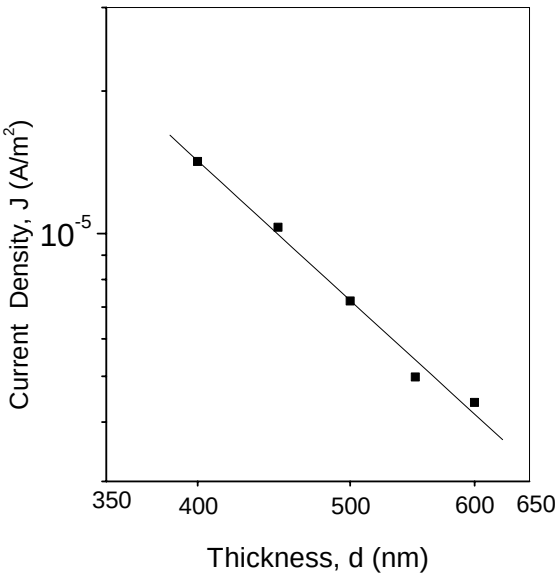

Figure 6.5.11 Plots of *J-d* for PPPy thin films in the non-Ohmic region (at voltage 27 V).

To study the actual conduction mechanism, J is plotted against d, of different thin films at a higher voltage of 27 V, which is presented in Figure 6.5.11. The linear slope derived from Figure 6.5.11 gives a negative value of 3.54, which is much higher than corresponding to Schottky or PF conduction mechanism. Therefore, the conduction mechanism in PPPy thin films is suggested to be SCLC.

6.5.1.3 Free Charge Carriers' Density, Trap Density and Mobility of the Carriers

The free charge carriers' density *N* can be calculated at the transition voltage from the Ohmic to the SCLC regime by using the equation (6.31) as,

$$N = \frac{9}{8}\varepsilon'\varepsilon_0 \frac{V_\Omega}{qd^2} \qquad (6.31)$$

where ε' is the dielectric constant of the thin films, ε_0 is the permittivity of the free space, and V_Ω is the transition or threshold voltage from the Ohmic regime to the SCLC regime. The transition or threshold voltage from the Ohmic regime to the space charge limited regime has been found to be about 12 V from the Figure 6.5.1. To calculate the dielectric constant ε', the capacitance of the PPPy thin films of thicknesses 400, 450, 500, 550 and 600 nm are measured in the frequency range 50 - 100 kHz, which is listed in Table 6.5.1.

The transition from trap-mediated to trap-free SCLC is accompanied by a sharp rise in current at the so-called trap-filled limit voltage, V_{TFL}, which is related to the trap density, N_t, by the equation (6.36),

$$V_{TFL} = \frac{qd^2}{2\varepsilon'\varepsilon_0} N_t \qquad (6.36)$$

and from this equation, trap density, N_t, can be calculated as,

$$N_t = \frac{2\varepsilon'\varepsilon_0}{qd^2} V_{TFL} \qquad (6.37)$$

From the Figure 6.5.1, the trap-filled limit voltage, V_{TFL}, is found to be 25 V.

The mobility of charge carrier in PPPy thin films can be calculated by fitting the non-Ohmic region (V = 5 V) of Figure 6.5.1 to equation (6.27), and from the relation,

$$\mu = \frac{8}{9} \frac{J}{\varepsilon'\varepsilon_0} \frac{d^3}{V^2} \qquad (6.27\text{-a})$$

Since dielectric constant ε' is related to the permittivity constant ε as $\varepsilon = \varepsilon'\varepsilon_o$, therefore, the permittivity of the PPPy thin polymer films can also be calculated.

By using V_Ω = 12 V ; V_{TFL}= 25 V, and the voltage at non-Ohmic region V = 5 V, the free charge carriers' density *N*, the trap density, N_t and the mobility of the charge carriers μ, for the PPPy thin films have been calculated and are listed in Table 6.5.1.

Table 6.5.1 The dielectric constant, free charge carriers' density, trap density and mobility of the charge carriers for the PPPy thin films of different thicknesses.

Thickness of the samples (nm)	Dielectric Constant (ε')	Free charge carriers' density (*N*) (m^{-3}) ($\times 10^{22}$)	Trap density (N_t) (m^{-3}) ($\times 10^{23}$)	Mobility of the charge carriers (μ) ($m^2 V^{-1}s^{-1}$) ($\times 10^{-19}$)
400±10	9	4.17	1.56	5.18
450±10	11	4.03	1.49	4.91
500±10	12	3.56	1.33	4.38
550±10	14	3.43	1.28	3.22
600±10	16	3.29	1.23	3.08

From the Table 6.5.1, it is seen that, all the calculated quantities, i.e., the free charge carriers' density *N*, the trap density, N_t and the mobility of the charge carrier μ, have higher values for lower thickness and gradually decrease with the increase of the thickness. The higher values of N and μ for lower thickness confirm our observation that the conductivity of the thin films of lower thickness is higher than that of the films of higher thickness.

6.5.1.4 Temperature Dependence of Current

The carrier mobility in polymer system is usually very low and the conductivity is influenced by the factors such as dopant level, morphology of polymer, concentration of conducting species, temperature, etc. It is difficult to generalize the temperature dependence of dc conduction whether it is ionic or electronic, since so many processes are possible. As the temperature is increased the charge carrier concentration increases strongly which dominates the temperature dependence of the conductivity, and low field conduction gives exponential temperature dependence, given by equation (6.39).

Figures 6.5.12 – 6.5.16 represent the plots of *J* with inverse absolute temperature 1/T for all the PPPy thin films of thicknesses about 400, 450, 500, 550 and 600 nm respectively. Every figure having two curves in two different voltage regions, one in the ohmic region with an applied voltage, 5V, and other in the SCLC region with an applied voltage, 20V. Moreover, each of the curves has two different slopes in the low and high temperature regions. The activation energies calculated from the slopes of the curves from Figures 6.5.12– 6.5.16 and are listed in Table 6.5.2.

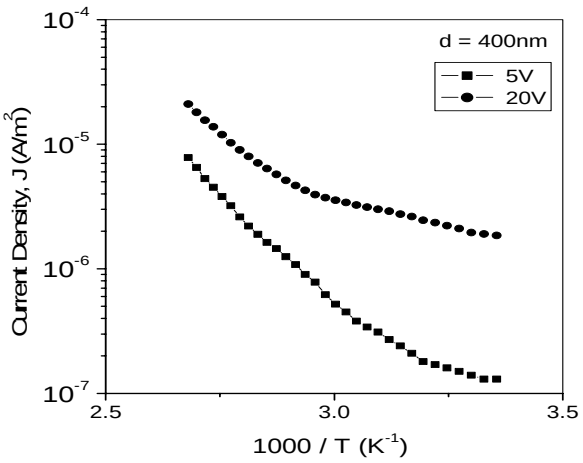

Figure 6.5.12 : Plots of J vs. 1/T for PPPy thin films in ohmic and non-ohmic regions.

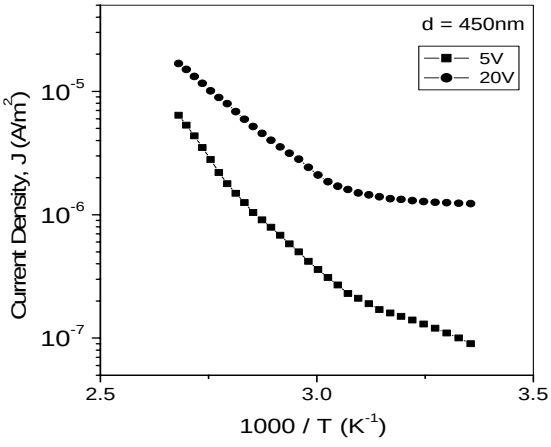

Figure 6.5.13 Plots of J vs. 1/T for PPPy thin films in ohmic and non-ohmic regions.

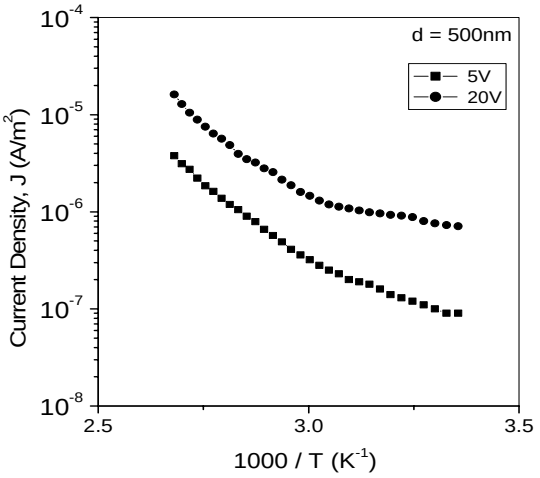

Figure 6.5.14: Plots of J vs. 1/T for PPPy thin films in ohmic and non-ohmic regions.

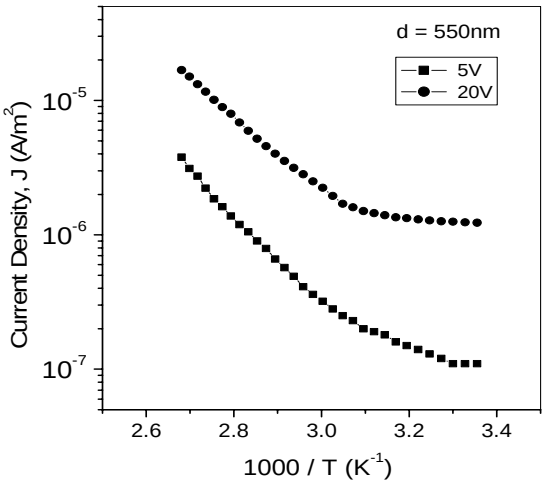

Figure 6.5.15 Plots of J vs. 1/T for PPPy thin films in ohmic and non-ohmic regions.

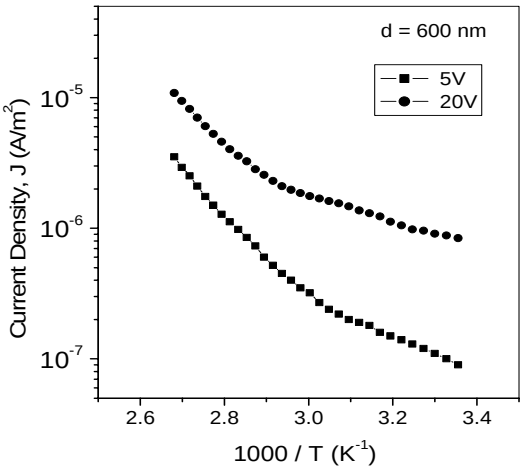

Figure 6.5.16 Plots of J vs. 1/T for PPPy thin films in ohmic and non-ohmic regions.

Table 6.5.2 Values of activation energy, ΔE, for PPPy thin films of different thicknesses.

Thickness d (nm)	Activation energy ΔE (eV)			
	5 V		20 V	
	Temperature (K)		Temperature (K)	
	low (298-323)	high (348-323)	low (298-323)	high (348-398)
400±10	0.062±0.002	0.145±0.002	0.035±0.002	0.123±0.002
450±10	0.051±0.002	0.125±0.002	0.015±0.002	0.125±0.002
500±10	0.075±0.002	0.175±0.002	0.025±0.002	0.115±0.002
550±10	0.043±0.002	0.125±0.002	0.015±0.002	0.113±0.002
600±10	0.041±0.002	0.116±0.002	0.051±0.002	0.135±0.002

It is known that, the trapped charges can lead to the polarization and distortion of the lattice structure and could result in local energy band deformation, which makes it very hard for trapped charge to be free. However, charge carriers in polymer thin films may move from one site to another by hopping over a potential barrier [11, 12]. Hopping is the transfer of a thermally activated charge carriers between localized states. Carriers acquire enough energy from the lattice by means of thermal fluctuations to overcome the potential barrier. Here the ΔE values at lower and higher temperature regions suggest that there may not be any transition of the conduction process from the hopping regime to a regime dominated by distinct energy levels. Therefore the carrier may take part in the conduction process throughout the bulk of the material. From the low temperature activation energy, which are very low, suggests to draw a correlation with the hopping behavior. Moreover the decrease in activation energy with decreasing temperature also indicates a gradual transition to the hopping regime [43].

The theory of SCLC in defect insulators, which contains traps, was developed by Rose [30]. In the presence of traps, a large fraction of the injected space charge will condense therein, which means that the free-carrier density will be much lower than in a perfect insulator. The conduction mechanisms in PPPy thin films, it is observed that at higher voltage a trap-mediated SCLC mechanism is shown by the thin films, and since the occupancy of traps is a function of temperature, the SCL current will be temperature-dependent. The change in activation energies at higher temperatures in comparison to those at lower temperatures also suggests a considerable temperature-dependence of SCLC mechanism.

6.5.2 Plasma Polymerized Pyrrole-*N, N, 3, 5* tetramethylaniline Bilayer Composite Thin Films

6.5.2.1 *J*–*V* characteristics

The *J*-*V* characteristics for PPPy-PPTMA bilayer composite thin films of various thicknesses deposited in different deposition time ratios of PPPy and PPTMA were recorded at room temperature in the voltage region of 0.1 V to 30 V, and are presented in Figure 6.5.17. It is to be noted that, to prepare the PPPy-PPTMA bilayer films, pyrrole-monomer were used as the mother-material and thin films of TMA were deposited onto the thin films of pyrrole in different time ratio. The deposition time-ratios of PPPy and PPTMA were (50 min :10 min), (45 min :15 min), (40 min :20 min), (35 min :25 min) and (30 min :30 min) corresponding to the thicknesses of 550, 525, 500, 450 and 400 nm. Though the total deposition time was kept 60 min for all the samples, variation in the thickness has been observed at different deposition-time ratios. From the study of deposition nature, however, it is seen that the thicknesses are found to decrease with the increase of the proportion of PPTMA in the bilayer structure. This is because, the deposition rate of TMA is lower than that of the pyrrole, i.e., if the deposition parameters remain same then PPTMA thin films are found to be thinner than PPPy thin films. However, from the Figure 6.5.17, a change in the current density with the change in the deposition time-ratio is observed in the same voltage range. It is also to be observed that the current flow in bilayer thin films is increased as the proportion of PPTMA is increased in the bilayer structures.

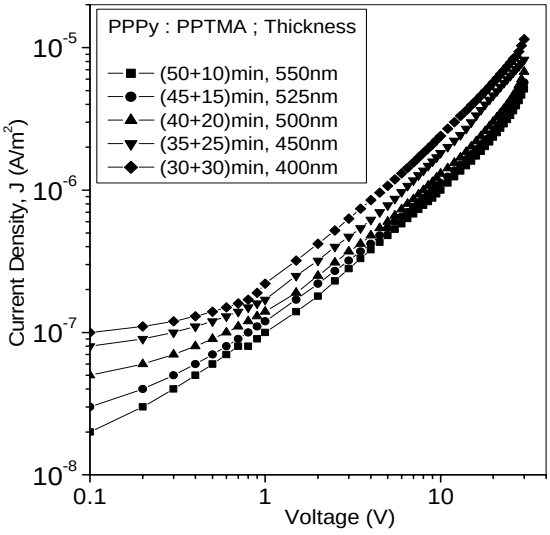

Figure 6.5.17 J-V characteristics for PPPy-PPTMA bilayer thin films of different deposition time ratio and different thicknesses at room temperature.

This result is also consistent with the reports on thickness-dependent conductions [37, 38]. Since the increased proportion of PPTMA in the bilayer structure causes a decrease in the thickness, therefore increase in the current conduction in bilayer thin films with the increase of PPTMA is not unexpected. Moreover it would be also seen that the conductivity of PPTMA

is higher than that of PPPy, and therefore the increase of the conductivity of bilayer thin films with the increase of PPTMA is also not ambiguous.

The conductivity calculation is also found to be consistent with this observation. The conductivity of different bilayer thin films of different deposition time-ratio were calculated from Figure 6.5.17 at the lower voltage region by using the equation (6.7) and presented in Table 6.5.3. It is clearly seen from Table 6.5.3 that as the deposition time-ratio of PPTMA is increased, the conductivity of the PPPy-PPTMA bilayer thin films is also increased.

Table 6.5.3 DC electrical conductivity of PPPy-PPTMA bilayer thin films for different deposition-time ratios.

PPPy-PPTMA deposition time ratio (minute)	Film Thickness (nm)	Conductivity, σ $(ohm\text{-}m)^{-1}$ $(x\ 10^{-14})$
50 : 10	550±10	5.32
45 : 15	525±10	5.81
40 : 20	500±10	6.12
35 : 25	450±10	7.15
30 : 30	400±10	8.53

The *J-V* curves in Figure 6.5.17, however, follow a power law of the form $J \infty V^n$, where n is a power index, with two different slopes in the lower and higher voltage regions. At the low voltage region (1~7 V) the curves of the J-V characteristics have slopes $0.87<n<1.12$, indicating a probable Ohmic conduction and the current density *J* is given by equation (6.26). On the other hand, at the higher voltages (15~27 V) the slopes $1.68<n<2.52$ represent the non-Ohmic conduction, which is to be explained by considering different conduction mechanisms, since the transport in this region is dominated by the polymer/electrode interface.

Figures 6.5.18 – 6.5.22 represent the *J-V* curves of PPPy-PPTMA bilayer thin films of different deposition time ratios, corresponding to different thicknesses 550, 525, 500, 450 and 400 nm, at different temperatures 300, 323, 348 and 373 K. It is observed that the current densities of both the voltage regions are increased slightly with increasing temperature, which may be an indication of temperature dependent conductivity of bilayer thin films. This increase may be due to the increased molecular motion at higher temperatures.

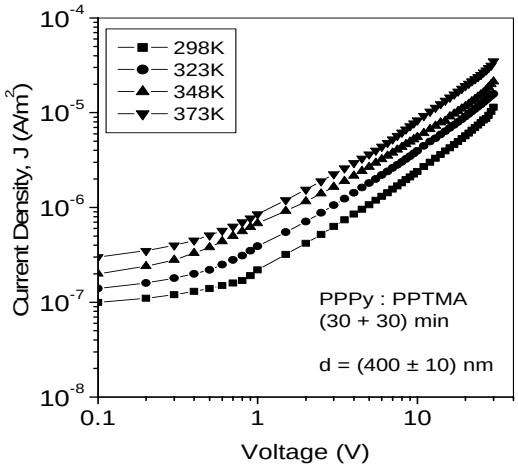

Figure 6.5.18 The J-V characteristics for PPPy-PPTMA bilayer thin films for the composition PPPy: PPTMA = (30 : 30) min at different temperatures.

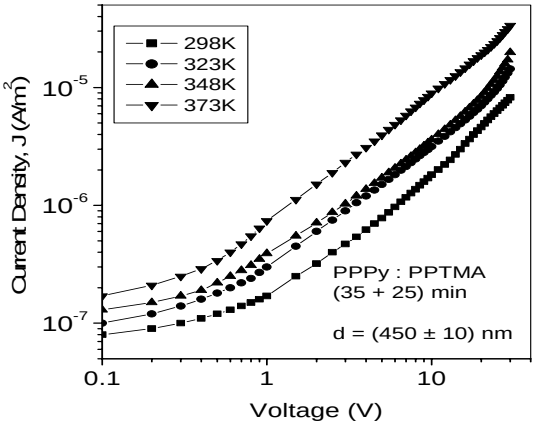

Figure 6.5.19 The J-V characteristics for PPPy-PPTMA bilayer thin films for the composition PPPy : PPTMA = (35 :25) min at different temperatures.

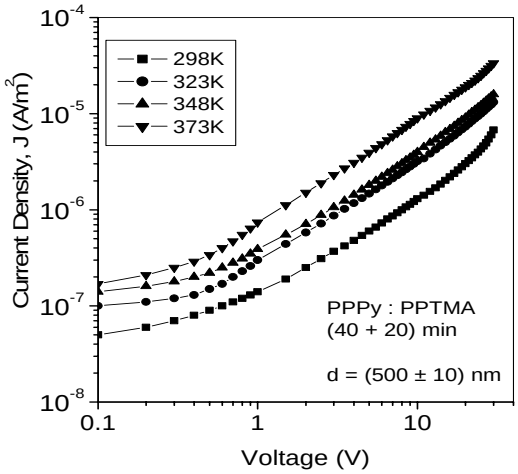

Figure 6.5.20 The J-V characteristics for PPPy-PPTMA bilayer thin films for the composition PPPy: PPTMA = (40 : 20) min at different temperatures.

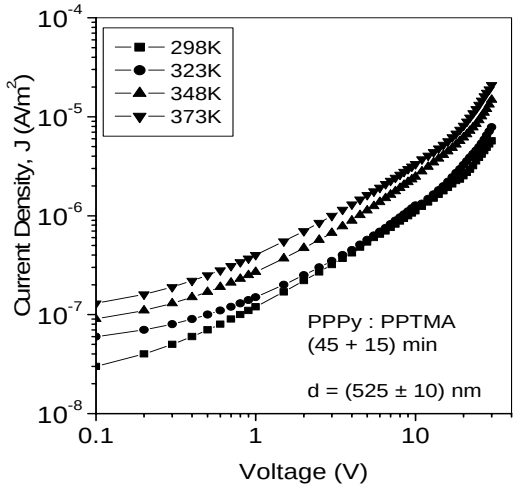

Figure 6.5.21 The J-V characteristics for PPPy-PPTMA bilayer thin films for the composition PPPy: PPTMA = (45 :15) min at different temperatures.

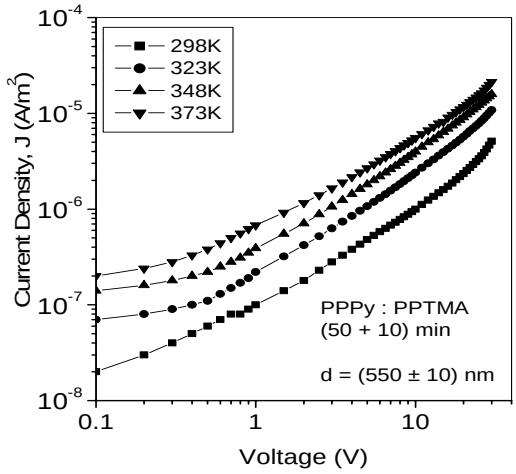

Figure 6.5.22 The J-V characteristics for PPPy-PPTMA bilayer thin films for the composition PPPy: PPTMA = (50 :10) min at different temperatures.

The DC electrical conductivity of PPPy-PPTMA bilayer thin films for different deposition time-ratios (50 min :10 min), (45 min :15 min), (40 min :20 min), (35 min :25 min) and (30 min :30 min) corresponding to the thicknesses of 550, 525, 500, 450 and 400 nm have been calculated at different voltage region from Figure 6.5.17 by using equation (6.7) and are plotted in Figure 6.5.23.

It is seen from Figure 6.5.23 that the conductivity is changed as the deposition time-proportion is changed, though, as expected, for any particular time proportion the conductivity of the bilayer thin film remain same. Since the conductivity is a physical property of a material which should remain constant for any circumstances, therefore the change in the conductivity for different deposition time-proportion suggests a probable change in physical properties during the formation of the bilayer thin films. Moreover, it is obvious that

in the bilayer thin film formation process, the physical properties of a film with (25%TMA + 75%Pyrrole) must not be exactly same to another film with (50% TMA+ 50% Pyrrole). It is also to be noted that, since the conductivity is increased with the increase of PPTMA and since PPTMA is more conducting than that of the PPPy thin films, therefore, it could be concluded that the electrical conductivity of bilayer thin films is dominated by the properties of the component monomer.

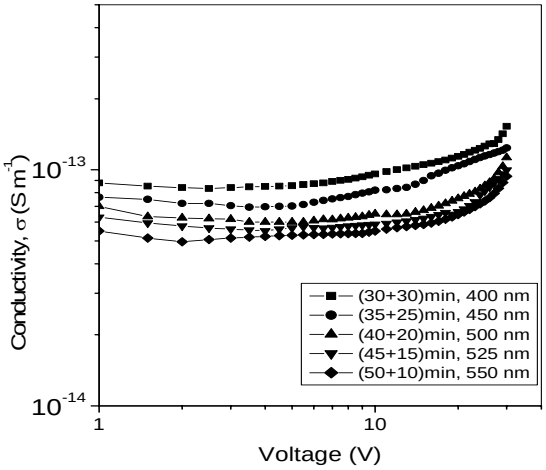

Figure 6.5.23 Plots of dc electrical conductivity vs. voltage for different deposition time-ratio and different thicknesses for PPPy-PPTMA bilayer thin films.

For a comparative study of the conductivity of PPPy-PPTMA bilayer thin films with that of the PPPy and PPTMA [37] thin films, the *J-V* characteristics of these three types of films of nearly same thickness (about 400 and 500 nm) were recorded at room temperature and are presented in Figure 6.5.24 and Figure 6.5.25 respectively. It is observed that the current conduction and conductivity of the PPTMA are higher than that of the PPPy films and the conductivity of the PPPy-PPTMA bilayer thin films are lower than those of its component thin films. The conductivities of different films were calculated at the lower voltage region by using the equation (6.7) and are presented in Table 6.5.4.

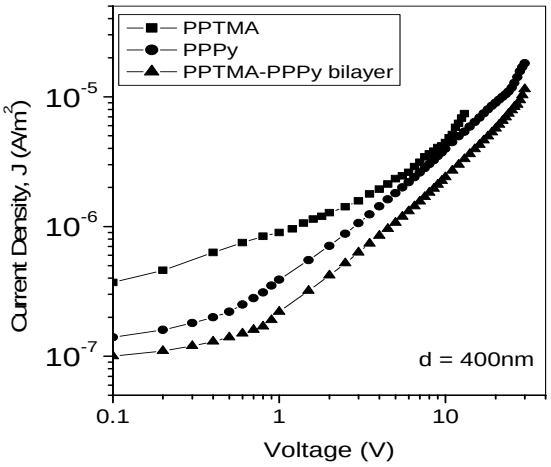

Figure 6.5.24 J-V characteristics for PPPy, PPTMA and PPPy-PPTMA bilayer thin films at room temperatures (d = 400 nm).

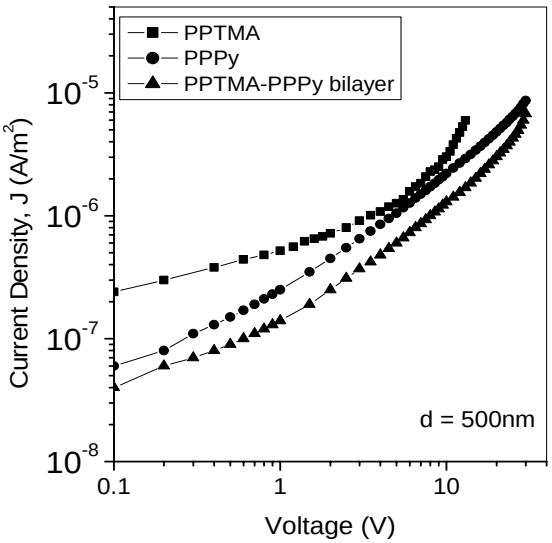

Figure 6.5.25 J-V characteristics for PPPy, PPTMA and PPPy-PPTMA bilayer thin films at room temperatures (d = 500 nm).

From Table 6.5.4, it could be noted that the conductivity of the bilayer thin films is less compared to those of the components, which can be confirmed by estimating the optical band gap of each of the films. It is observed that both the direct and indirect energy band gaps are higher for PPPy-PPTMA bilayer films than those for PPPy and PPTMA, which has been discussed in Chapter 5.

Table 6.5.4 Comparison of dc electrical conductivity for PPPy, PPTMA and PPPy-PPTMA bilayer composite films of nearly same thickness (about 400 and 500nm)

Samples	Thickness (nm)	Conductivity, σ (ohm-m)$^{-1}$ (x 10^{-13})
PPTMA	400±10	1.94
PPPy	400±10	1.42
PPPy-PPTMA bilayer thin film [PPPY : PPTMA = (30 :30) min]	400±10	0.85
PPTMA	500±10	1.36
PPPy	500±10	1.05
PPPy-PPTMA bilayer thin film [PPPY : PPTMA = (40 :20) min]	500±10	0.61

The fact that the physical properties of the PPPy-PPTMA bilayer thin films have been changed due to the formation of the bilayer thin films could be confirmed by considering an ideal situation. In any ideal bilayer of two materials without interface effect, the physical

properties of the bilayer usually lie in between those of the constituents, but in the present case, the PPPy-PPTMA bilayer thin films show a different behavior. The current density, *J′*, for an ideal PPPy-PPTMA bilayer thin films can be calculated from the current densities of PPPy and PPTMA thin films at a fixed applied voltage by using the following equation,

$$J' = \frac{J_1 J_2}{m_1 J_2 + m_2 J_1} \qquad (6.44)$$

where J_i and m_i are the current densities and the fraction of the thicknesses of the components respectively. It should be noted that the relationship between the thickness of the component has been evaluated from Figure 6.5.25 with an approximation of m_1: m_2 = PPPy : PPTMA = 0.6 : 0.4, with m = 1 as the bilayer thin film thickness, since the bilayer thin film of Figure 6.5.25 was prepared by depositing the PPPy and PPTMA thin films with a deposition time ratio (40 min : 20 min). The theoretically calculated values of *J′* for the ideal bilayer thin film has been plotted in *J-V* characteristic curves of Figure 6.5.26 to compare with those of the real PPPy-PPTMA bilayer thin films and also with those of the component films.

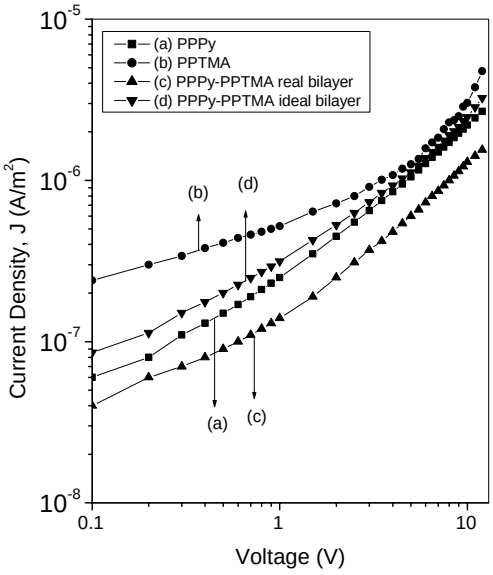

Figure 6.5.26 J-V characteristics for (a) PPPy (b) PPTMA (c) PPPy-PPTMA real bilayer, and (d) PPPy-PPTMA ideal bilayer thin films.

It is observed in Figure 6.5.26 that the theoretically calculated values of *J′* lie in between the values of *J* of two individual components, but the experimental values of *J* is found to be reduced than those of its components. This experimental result thus shows a clear departure from the ideal nature as seen from the calculated values of *J′* using equation (6.44). Since both PPPy and PPTMA layers in the bilayer thin film have the same chemical nature as those of the component thin films, therefore the result that the theoretical values of the *J′* of

the PPPy-PPTMA ideal bilayer film lie in between those of the components, is not unusual. But when the current density is calculated from the data of the components, the interaction in the interface of the two component thin films is not considered, though this interface might affect the physical properties of the bilayer structure. This type of anomalous effect could give misleading results if they are not recognized or avoided [44]. Therefore, to analyze the electrical behavior of plasma polymerized bilayer thin films, the effect of the interface should be taken into consideration.

It is known that the incorporation of oxygen in the polymers, even though the monomers do not contain oxygen, is a typical trend of plasma polymer. This incorporation of oxygen in plasma polymer as a contamination may be due to the reaction of trapped free radicals with oxygen from the plasma reactor as well as from the overall environment of the film-formation process. The FTIR analyses of PPPy, PPTMA and PPPy-PPTMA films in this study have also indicated the presence of oxygen by the appearance of the absorption band at 1850-1603 and 2214 cm^{-1}. Therefore, during the subsequent formation of the films by plasma polymerization, there may be adsorbed and/or trapped oxygen in the interface in between the PPPy and PPTMA thin film layers. The oxidation of the interface of the bilayer might affect the physical properties of the bilayer thin films. The increase of optical band gap and the increase of the resistivity of the bilayer thin films may be due to this reason. Furthermore, in the present system, the individual thin films were deposited one over the other to prepare the PPPy-PPTMA bilayer thin films, which may give rise to a system with polymer-polymer complex interface, i.e., the interface between the PPPy and PPTMA thin films may not be homogeneous and therefore there are some possibilities of presence of irregularities in the interface. It should be noted that in most inhomogeneous polymeric systems, the electronic conductivity is affected by this interface. The conductivity depends upon the movement of adventitious ions generated either by impurities centers or induced impurities [45]. The crosslinking between the interfaces should be also taken into consideration in this system, which may cause less electrical conduction.

6.5.2.2 Conduction Mechanism in PPPy-PPTMA Bilayer Composite Thin Films

From J-V characteristics (Figure 5.17) of PPPy-PPTMA bilayer composite thin films, it is observed that the curves follow a power law of the form $J \propto V^{n}$, with two different slopes in the lower and higher voltage regions, indicating a probable Ohmic conduction at lower voltage, and non-Ohmic conduction higher voltages region. The Ohmic conduction can be described by the equation (6.7), but non-Ohmic conduction shows a complex conduction behavior, which is explained usually by using different conduction mechanism, e.g. Schottky–Richardson mechanism, Poole–Frenkel mechanism, tunneling or Fowler–Nordheim mechanism, space charge limited conduction mechanism etc. However, the direct

current conduction mechanisms for the PPPy-PPTMA bilayer composite thin films are discussed in the light of the following mechanisms.

(a) Tunneling or Fowler–Nordheim mechanism

The Fowler–Nordheim relation for current density *J* can be expressed by the equation (6.42), and to be operative of this mechanism, the Fowler–Nordheim plots, i.e., the log J/V^2 vs. $1/V$ plots are expected to be a linear relation with a negative slope.

In the Figure 6.5.27, *log J/ V² vs. 1/ V plots* for PPPy-PPTMA bilayer thin films of thicknesses 550, 525, 500, 450 and 400 nm have been presented. It is seen from the figure, that all the curves have positive slopes and none of them shows linear nature, which indicates the absence of tunneling effect in PPPy-PPTMA bilayer composite thin films.

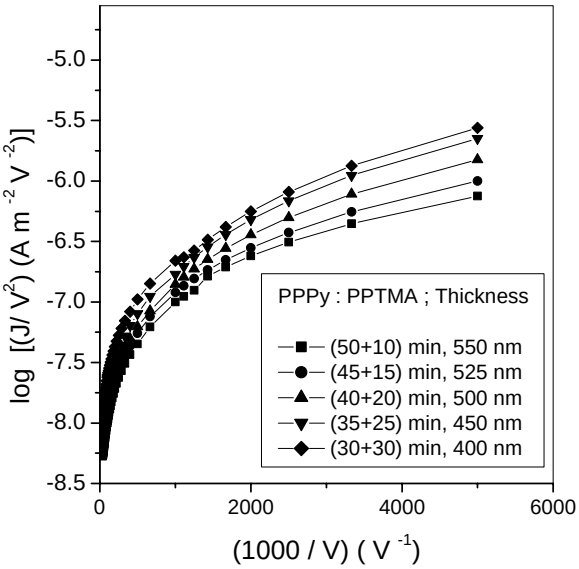

Figure 6.5.27 Fowler–Nordheim plots for PPPy-PPTMA bilayer thin films of different thicknesses.

(b) Schottky Mechanism

The Schottky–Richardson current voltage relationship is expressed by the equation (6.43), and Schottky plots, i.e., log *J* vs. $E^{1/2}$ (or *J* vs. $V^{1/2}$) plots and should be a straight line with a positive slope to become this mechanism operative.

The Schottky plots for PPPy-PPTMA bilayer thin films of different thicknesses have been shown in Figure 6.5.28. The curves in this figure are not also linear though all of them have positive slopes, indicating the absence of Schottky mechanism in PPPy-PPTMA bilayer composite thin films.

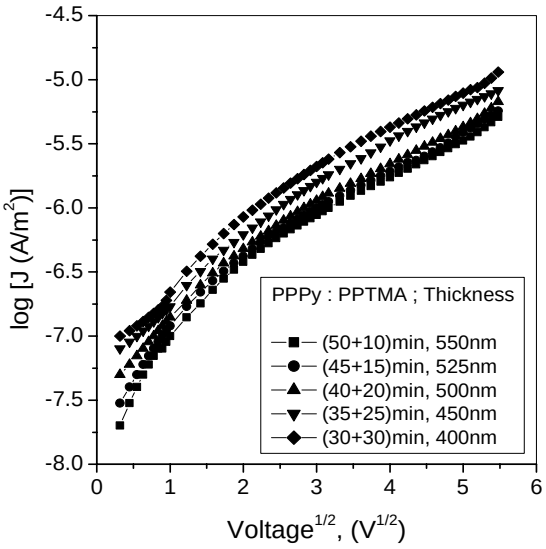

Figure 6.5.28 Schottky plots for PPPy-PPTMA bilayer thin films of different thicknesses

(c) Poole–Frenkel mechanism

The Poole–Frenkel relation for field-dependent conductivity given by equation (6.21), and according to the equation (6.22) the Poole–Frenkel mechanism is characterized by the linear curves in $log\ \sigma$ vs. $V^{1/2}$ plots with a positive slope.

The Poole–Frenkel plots i.e., $log\ \sigma$ vs. $V^{1/2}$ plots for PPPy-PPTMA bilayer thin films of thicknesses 550, 525, 500, 450 and 400 nm is presented in Figure 6.5.29. Since no linear curve is observed no particular slope-character (positive or negative) is seen, therefore the possibility of PF conduction mechanism in PPPy-PPTMA bilayer composite thin films could be also ruled out.

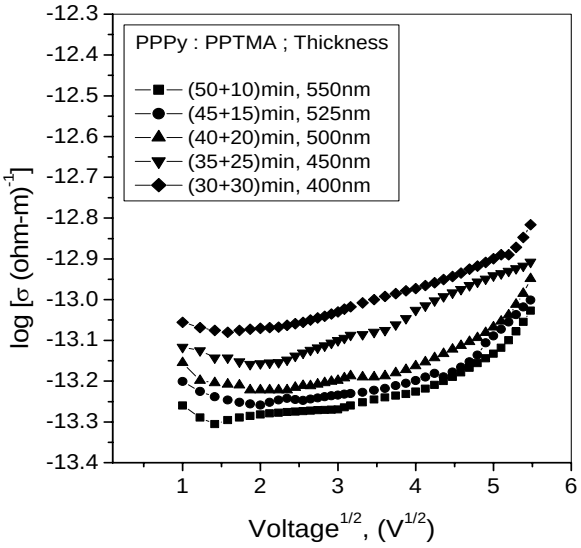

Figure 6.5.29 Poole–Frenkel plots for PPPy-PPTMA bilayer thin films of different thicknesses

(d) Space Charge Limited Conduction

The current conduction in plasma polymerized thin films transits from Ohmic to non-Ohmic i.e., SCLC, Schottky or PF conditions, when the applied voltage is increased over a certain value and the injected charge carrier density largely exceeds the free charge density under thermal equilibrium. The current density for SCLC is then described by the equation (27), which indicates that *J* is inversely proportional to d^3. The thickness dependence of current follows the relation $J \alpha d^{-l}$ where *l* is a parameter depending upon the trap distribution. A slope $l<3$ suggests the possibility of Schottky or PF conduction mechanism and $l \geq 3$ reveals the possibility of SCLC.

To study the actual conduction mechanism, *J* is plotted against d, of different thin films at a higher voltage of 27 V, which is presented in Figure 6.5.30. The linear slope derived from Figure 6.5.30 gives a negative value of 3.32, which is much higher than corresponding to Schottky or PF conduction mechanism. Therefore, the conduction mechanism in PPPy-PPTMA bilayer composite thin films is suggested to be SCLC.

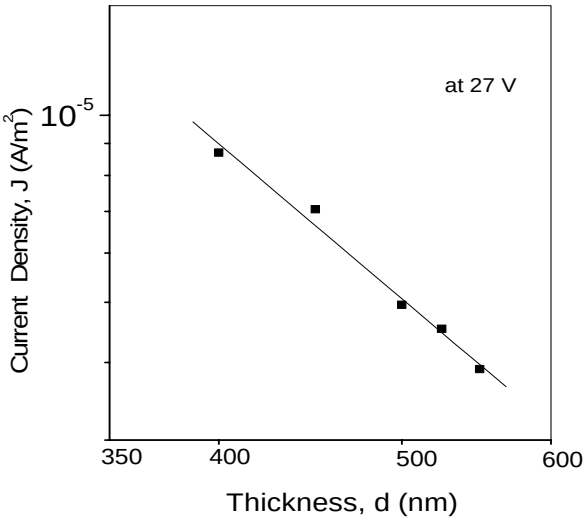

Figure 6.5.30 Plots of J-d for PPPy-PPTMA bilayer thin films in the non-Ohmic region (at 27 V).

6.5.2.3 Free Charge Carriers' Density, Trap Density and Mobility of the Carriers

The free charge carriers' density *N* at the transition voltage from the Ohmic to the SCLC regime can be calculated by using the equation (6.31) as,

$$N = \frac{9}{8}\varepsilon'\varepsilon_0 \frac{V_\Omega}{qd^2} \qquad (6.31)$$

where symbols carry their usual meaning.

The transition or threshold voltage from the Ohmic regime to the space charge limited regime has been found to be about 15 V from the Figure 6.5.17. To calculate the dielectric

constant ε', the capacitance of the PPPy-PPTMA bilayer composite thin of thicknesses 550, 525, 500, 450 and 400 nm are measured in the frequency range 50 kHz - 100 kHz, which is listed in Table 6.5.6.

The transition from trap-mediated to trap-free SCLC is accompanied by a sharp rise in current at the so-called trap-filled limit voltage, V_{TFL}, is given by the equation (6.36). The V_{TFL} is related to the trap density, N_t, and can be calculated from equation (6.36) as,

$$N_t = \frac{2\varepsilon'\varepsilon_0}{qd^2} V_{TFL} \qquad (6.37)$$

From the Figure 6.5.17, the trap-filled limit voltage, V_{TFL}, is found to be 25V.

The mobility of charge carrier in PPPy-PPTMA bilayer composite thin films can be calculated by fitting the non-Ohmic region (V = 5 V) of Figure 6.5.17 to equation (6.27), as

$$\mu = \frac{8}{9} \frac{J}{\varepsilon'\varepsilon_0} \frac{d^3}{V^2} \qquad (6.27\text{-a})$$

Since dielectric constant ε is related to the permittivity constant ε' as $\varepsilon' = \varepsilon\varepsilon_o$, therefore, the permittivity of the PPPy-PPTMA bilayer composite thin films can also be calculated.

The trapping factor, θ, which is defined as the ratio of the free charge to the to trapped carriers, is given by

$$\theta = \frac{N}{N + N_t} \qquad (6.30)$$

where θ is the ratio of free to trapped carriers and N_t is the density of trapped holes [31].

By using V_Ω = 15 V ; V_{TFL}= 25V, and the voltage at Ohmic region V = 5 V, the free charge carriers' density *N*, the trap density, N_t and the mobility of the charge carriers μ, for the PPPy-PPTMA bilayer thin films have been calculated and are listed in Table 6.5.5.

Table 6.5.5 The dielectric constant, free charge carriers' density, trap density and mobility of the charge carriers for the PPPy-PPTMA bilayer composite thin films

Thickness of the samples (nm)	Dielectric Constant (ε')	Free charge carriers' density (*N*) (m^{-3}) ($\times 10^{22}$)	Trap density (N_t) (m^{-3}) ($\times 10^{23}$)	Mobility of the charge carriers (μ) ($m^2 V^{-1}s^{-1}$) ($\times 10^{-19}$)
400±10	11	5.75	1.72	2.79
450±10	12	5.62	1.67	2.34
500±10	14	5.19	1.55	2.12
525±10	15	4.97	1.24	2.09
550±10	16	4.77	1.43	2.05

From the Table 6.5.5 it is seen that, all the calculated quantities, i.e., the free charge carriers' density *N*, the trap density, N_t and the mobility of the charge carriers μ, have higher values for lower thickness and gradually decrease with the increase of the thicknesses. The higher values of N and μ for lower thicknesses confirm our observation that the conductivity of the films with lower thickness is higher than that of the films of higher thickness.

The trapping factor, θ, for PPPy-PPTMA bilayer composite thin films of different thicknesses have been calculated by using the equation (6.30) and found to be around 0.25 for all the samples. It is already discussed in the theory of SCLC mechanism that, the current density, including the effect of shallow traps is given by,

$$J = \frac{9}{8}\varepsilon\varepsilon_0\mu\theta\frac{V^2}{d^3} \qquad (6.35)$$

For a shallow trap SCLC and trap-free SCLC, θ = 1, and equation (6.35) reverts to the equation (6.27). Also, for trap-mediated SCLC, and at sufficiently high injection rates, it may become possible to fill all the traps so that the free carrier concentration greatly exceeds the trapped concentration in which case θ >> 1 and equation (6.28) reverts to Child's law [equation (6.27)]. On the other hand, at low injection rates, when θ << 1, transport is dominated by trapping. In this study, it is found that θ << 1 for PPPy-PPTMA bilayer thin films, and therefore it could be concluded that the current conduction mechanism in PPPy-PPTMA bilayer composite thin films is trap-dominated SCLC mechanism.

6.5.2.4 Temperature Dependence of Current

The current conduction in PPPy-PPTMA bilayer composite thin films is found to be temperature-dependent, which could be observed in J-V characteristics curves of Figure 5.30 - 5.34. With the increase of the temperature the charge carrier concentration increases strongly which dominates the temperature dependence of the conductivity, and low field conduction gives exponential temperature dependence, given by equation (6.39). The Arhennius plots i.e., the plots of *log J* vs. *1/T* usually exhibits increasing linear slopes as T is raised. The Arrhenius model, however, postulates that the electrical conductivity depends on the charge carrier production and the internal energy of molecules [43, 44]. This means that if other factors are neglected, the electrical conductivity would solely depend on the charge carrier production and the thermal energy supplied to the system. The Arrhenius model also provides direct information about the activation energy of the charge carriers. The activation energy, however, for the conduction in the polymer films can not be easily identified. The conductivity overlapped the contributions due to the intrinsic activation energy of the charge carriers in the polymer, and the contributions due to the conductivity originated from the interaction in the complex interface and also due to the polymeric chains.

The charge-transfer mechanisms in polymer thin films, although widely studied, are not well understood. One topic that has not been thoroughly studied yet is the transition from insulating behavior to conductive behavior in polymers. This characteristic can be induced in

polymers through doping processes. Another area waiting to be studied more extensively is the nature of the charge transportation via energetic electron jumps in the insulating regime. For this reason, the effect of temperature on conductivity is important for investigating the nature of charge transportation in conjugated polymers.

The plots of *J* with inverse absolute temperature 1/T for all the PPPy-PPTMA bilayer composite thin films of thicknesses about 400, 450, 500, 525 and 550 nm are presented in Figure 6.5.31 – Figure 6.5.35 respectively . All the figures having two curves in two different voltage region, one in the ohmic region with an applied voltage, 5 V, and other in the SCLC region with an applied voltage, 20V. Each of the curves is characterized by two different slopes in the low and high temperature regions. The activation energies calculated from the slopes of the curves from Figure 6.5.31 to Figure 6.5.35 and listed in Table 6.5.6.

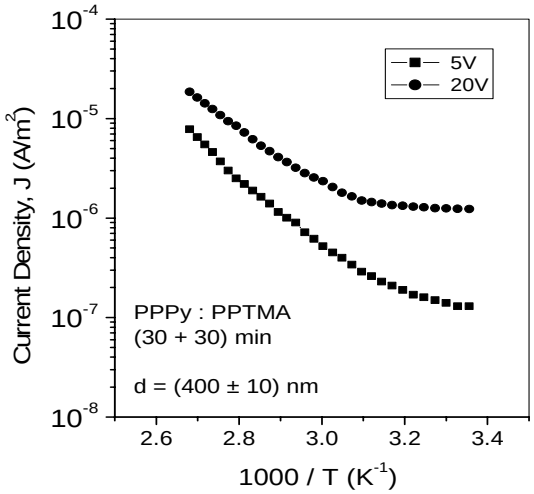

Figure 6.5.31 Plots of J vs. 1/T for PPPy-PPTMA bilayer composite thin films in ohmic and non-ohmic regions.

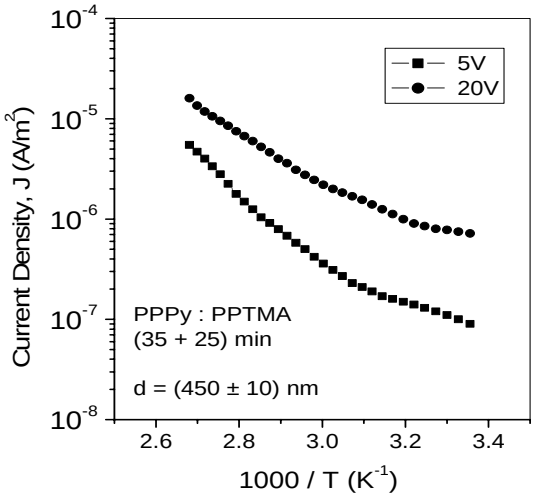

Figure 6.5.32 Plots of J vs. 1/T for PPPy-PPTMA bilayer composite thin films in ohmic and non-ohmic regions.

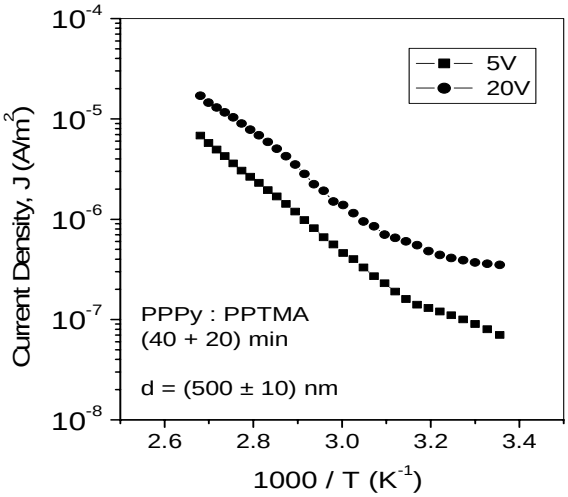

Figure 6.5.33 Plots of J vs. 1/T for PPPy-PPTMA bilayer composite thin films.

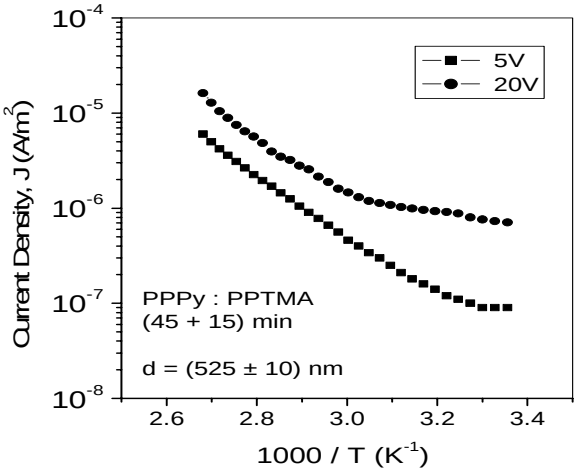

Figure 6.5.34 Plots of J vs. 1/T for PPPy-PPTMA bilayer composite thin films.

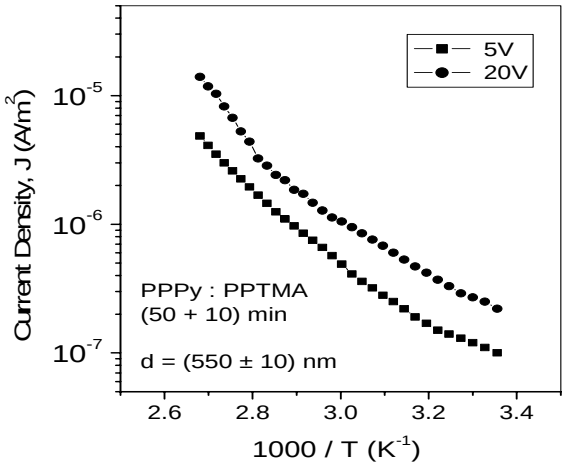

Figure 6.5.35 Plots of J vs. 1/T for PPPy-PPTMA bilayer composite thin film.

It is seen from the Table 6.5.6 that, the activation energies are increased with the increase of temperature in both ohmic and non-ohmic voltages, which is an indication of increasing conductivity in higher temperature. From the Figure 6.5.18 - Figure 6.5.22, it could be observed that the conductivity is higher at higher temperature than that at lower temperature. This increase in the activation energy at higher temperature indicates that the structure of the thin films has been changed with the increase of temperature. The effect might have been due to the formation of more ordered regions which would lead to better electronic conduction. This explanation arises because the thin films have different slopes in the Figures 6.5.31 – 6.5.35 and, consequently, different activation energies. It is reported [46] that when a thermal treatment is applied to polyaniline thin films from ambient temperature up to 150°C, some structural and conformational changes are induced in the polymer in the form of packaging of the polymeric network, which affects the interaction between the polymer chains and the charge carriers, and conductivity is observed to be increased. This effect could contribute to the evolution of the activation energy and suggests that the PPPy-PPTMA thin films modify its structure because of the thermal energy supplied in the form of increasing temperature. This would explain the evolution of the activation energy at higher temperature. However, Table 6.5.6 shows that the activation energies varies from 0.058 to 0.178 eV from lower to higher temperature at ohomic region (at 5 V), and from 0.023 to 0.172 eV respectively at non-ohmic voltage region (at 20 V). Different activation energies that depended on the temperature possibly because of structural and conformational changes in the polymeric network.

Table 6.5.6 Values of activation energy, ΔE, for PPPy-PPTMA bilayer composite thin films of different thicknesses.

Thickness d (nm)	Activation energy ΔE (eV)			
	5 V		20 V	
	Temperature		Temperature	
	low (298-323)K	high (348-373)K	low (298-323)K	high (348-373)K
400±10	0.059±0.002	0.178±0.002	0.023±0.002	0.118±0.002
450±10	0.067±0.002	0.155±0.002	0.055±0.002	0.105±0.002
500±10	0.058±0.002	0.141±0.002	0.043±0.002	0.101±0.002
525±10	0.085±0.002	0.135±0.002	0.026±0.002	0.143±0.002
550±10	0.071±0.002	0.123±0.002	0.078±0.002	0.176±0.002

It is known that, the charge carriers in polymer thin films may move from one site to another by transferring thermally activated charge carriers between localized states over a potential

barrier [12, 13], which is known as hopping. The charge carriers acquire enough energy from the lattice by means of thermal fluctuations to overcome the potential barrier. In our observation, the ΔE value at lower and higher temperature regions, i.e., the decrease in activation energy with decreasing temperature indicates a gradual transition to the hopping regime [43].

In this study of the conduction mechanisms for PPPy-PPTMA bilayer composite thin films, a trap-mediated SCLC mechanism is observed and since the occupancy of traps is a function of temperature, the SCL current will be temperature-dependent. The change in activation energy at higher temperature in comparison to that at lower temperature also suggests a considerable temperature-dependence of SCLC mechanism.

6.6 Conclusions

From *J-V* characteristics of PPPy, PPTMA and PPPy-PPTMA bilayer thin films, a general trend is observed that the current conduction is higher in the films of lower thickness than that of the highger-thickness films at the same voltage. This difference in the conductivity for different thicknesses suggests a probable change in physical properties during the formation of the plasma polymerized thin films. The most probable reason of this behavior may be due to better morphological characteristics of the films of lower thickness. The film morphology is highly thickness dependent, and better morphology (lower roughness) is usually observed for smaller thickness, which causes increased charge mobility. Thinner films present more structural order due to more homogeneous surfaces, decreased grain size and improve interchain conduction, and as a result, an increased conductivity could be observed.

The J-V characteristics of PPPy, PPTMA and PPPy-PPTMA bilayer thin films are characterized by two different slopes in the lower and higher voltage regions. The slopes at lower voltage region indicate a probable ohmic conduction, while at higher voltages a non-ohmic conduction is observed. This complex conduction behavior has been explained in terms Schottky–Richardson mechanism, Poole–Frenkel mechanism, tunneling or Fowler–Nordheim mechanism and space charge limited conduction mechanism, and it is found that the current conduction in PPPy, PPTMA and PPPy-PPTMA bilayer thin films follow a SCL conduction mechanism.

The free charge carriers' density N, the trap density, N_t and the mobility of the charge carriers μ, have been calculated from the conduction data and it is observed that all the calculated quantities have higher values for lower thickness and gradually decrease with the increase of the thicknesses. The higher values of N and μ for lower thicknesses confirm our observation that the conductivity of the films with lower thickness is higher than that of the films of higher thickness.

The dc electrical properties of PPPy-PPTMA bilayer thin films have been investigated in a slightly different way and results have been compared to those obtained from its component thin films, i.e., PPPy and PPTMA. From the J-V characteristics of PPPy-PPTMA bilayer thin films, it is observed that the current conduction is increased with an increased proportion of PPTMA in the bilayer structure. To confirm this observation, the conductivity of PPPy-PPTMA bilayer thin films of different thicknesses and different deposition time ratios were calculated and were found to be increased with the increase of PPTMA in the films. The conductivity of PPPy, PPTMA and PPPy-PPTMA bilayer thin films of nearly same thickness have also been calculated to compare the conduction nature of these films and is observed that the conductivity of PPTMA films are higher than that of the PPPy thin films, but the conductivity in PPPy-PPTMA films was found to be lower than the component thin films. This suggests an increase in the resistivity of the PPPy-PPTMA films during the formation, which might be an effect of inhomogeneous complex interface between the PPPy and PPTMA film in the bilayer structure.

The temperature dependence of current has also been studied for PPPy, PPTMA and PPPy-PPTMA bilayer thin films and a trend of decreasing activation energy with decreasing temperature has been observed, which also indicates a gradual transition to the hopping regime. Moreover, from the low temperature activation energy, which is very low, suggests to draw a correlation with the hopping behavior. However, the change in activation energy at higher temperature in comparison to that at lower temperature could be attributed to a considerable temperature-dependence of SCLC mechanism.

References

[1] Ieda, M., Nagao M., and Hikita, M., *High-field conduction and Breakdown in Insulating Polymers: Present Situation and Future Prospects*, IEEE Tran. DEI, 1 (5) 934-945, 1994.

[2] Vou Roggen, A., Phys. Rev. Letters, 9, 368, 1962.

[3] Saito, S., Sasabe, H., Nakajima T., and Yada, K., J. Polym. Sci. 6A2,1297, 1965.

[4] Bunn, C. W., *Fibers from synthetic polymers*, Elsevier, Amsterdam, 1959.

[5] Chen C. Ku and Raimond Liepins, *Electrical properties of polymers*, Hanser Publishers, Munich – Vienna – New York, 1987.

[6] Bashar, S. A., Sheng, H., and Rezazadeh, A. A., Proc. IEEE Int. workshop on high performance electron devices for microwave and optoelectronic applications, EDMO, London, U.K, pp. 1−6, 1994.

[7] Ohring, M., *The Material Science of Thin Film*, Academic Press, USA, 1992.

[8] Scott, J. C., *Metal-organic intrface and charge injection in organic electronic devices*, J. Vac. Sci. & Tech. A : Vacuum, Surfaces, and Films, 21, 521-531, 2003.

[9] Dissado L. A., and Fothergill, J. C., *Electrical degradation and breakdown in polymers*, P. Peregrinus for IEE, London 1992.

[10] Lewis, T. J., *Electrical Effect at Interfaces and Surfaces*, IEEE Transactions on Electrical Insulation, EI-21(3), 289-295, 1986.

[11] Taylor, D. M., and Lewis, T. J., *Electrical conduction in polyethylene terephthalate and polyethylene films*, J.Phys D: Appl.Phys, 4, 1346-1357, 1971.

[12] Lewis, T. J., *The micro-physics of charge in solid dielectrics*, Published in 'Space Charge in Solid Dielectrics' by the Dielectric Society, Edited by J.C. Fothergill and L.A. Dissado, 1998.

[13] Kao, K. C., *Dielectric Phenomena in Solids*, Elsevier Academic Press, USA, 2004.

[14] Kapoor, A. K., Jain, S. C., Poortmans, J., Kumar, V., and Mertens, R., *Temperature Dependence of carrier transport in conducting polymer : similarity to amorphous inorganic semiconductor*, J. Appl. Phys. 92, 3835-3838, 2002.

[15] Rakhmonova, S. V. and Conwell, E. M., *Electric field dependence of mobility in conjugated polymer films*, Appl. Phys. Letter, 76, 3822-3824, 2000.

[16] Mark, P., and Helfrich, W., *Space-Charge-Limited Currents in Organic crystals*, J. Appl. Phys., 33, 205-215, 1962.

[17] Lampert, M. A., *Current injection in solids*, Academic Presss, New York, 1970.

[18] Schmechel, R., and Seggern, H. V., *Electronic traps in organic transport layers*, Physica Status Solidi (a), 201, 1215- 1235, 2004.

[19] Brutting, W., (Ed.), *Physics of Organic Semiconductors*, Wiley-VCH, Verlag GmbH & Co. KGaA Weinheim, 2005.

[20] Hepp, A., von Malm, N., Schmechel, R., and Von Seggern, H., *Effect of process parameters on trap distributions in organic semiconductor*, Syntetic Metals, 138, 201-207, 2003.

[21] Kao, K. C., IEEE Trans. Electr. Insul., EI-11, 121, 1976,.

[22] Hwang, W., and Kao, K. C., J. Chem Phys., 60, 3845, 1974.

[23] Sze, S. M., Crowell, C. R., and Kahng, D., J. Appl. Phys., 35, 2534, 1964.

[24] Thornber, K. K., McGill, T. C., and Mead, C. A., J. Appl. Phys., 38**,** 2384, 1967.

[25] Maisel Leon, I., and Glang, R., *Hand Book of Thin Film Technology*, McGraw Hill Book Company, New York, 1970.

[26] Frenkel, J., Phys. Rev., 54, 647, 1938.

[27] Gutman, F., and Lyons, L. E., *Organic Semiconductors- Part A*, Robert E. Krieger Publishing Company, Malabar, Florida, 1981.

[28] Mott, N. F., and Gurney, R. W., *Electronic Process in Ionic Crystals*, Dover, New York, 1940.

[29] Lampert, M. A., *Simplified theory of space-charge-limited currents in an insulator with traps*, Phys. Rev., 03, 1648-1656, 1956.

[30] Rose, A, Phys. Rev., 97, 1538, 1955.

[31] Kao, K. C., and Hwang, W., *Electrical Transport in Solids*, Pergamon, Oxford, 1981.

[32] Taylor, D. M., *Space Charges and Traps in Polymer Electronics*, IEEE Transactions on Dielectrics and Electrical Insulation, 13 (5), 1063-1073, 2006.

[33] Dissado, L. A., and Fothergill, J. C., *Electrical degradation and breakdown in polymers*, P. Peregrinus for IEE, London 1992.

[34] Das-Gupta, D. K., Doughty, K., *Dielectric and Conduction processes in Polyetherether Ketone*, Trans E.I., EI-22, 1-7, 1987.

[35] Ieda, M., *Electrical Conduction and Carrier Traps in Polymeric Materials*, IEEE Trans .EI., l. EI-19, (1984) 162-178.

[36] Fowler, R. H., and Nordheim. L., Proc. R. Soc. London 119, 173, 1928.

[37] Akther, H. and Bhuiyan, A. H., *Space charge limited conduction in plasma polymerized N,N,3,5 tetramethylaniline thin films,* Thin Solid Films 488, 93-97, 2005.

[38] Valaski, R., Ayoub, S., Micaroni, L., Hümmelgen, I. A., *Influence of thin thickness on charge transport of electrodeposited polypyrrole thin films*, Thin Solid Films, 415, 206-210, 2002.

[39] Yuan, C., Li, P., Shan, J., and Zhang, H., Supramol. Sci. 5 (1998) 751.

[40] Yasuda, H., Bumgarner, M. O., Marsh, H. C., Morosoff, N., *Plasma polymerization of some organic compounds and properties of the polymers*, J. Polym. Sci. Polym. Chem., 14, 195-224, 1976.

[41] Kamal, M. M., and Bhuiyan, A. H., *Optical Characterization of Plasma Polymerized Pyrrole-N,N,3,5 Tetramethylaniline Bilayer Thin Films*, J. Appl. Polym. Sci. (DOI # 33176), In Press, 2010.

[42] Schottky, W. Z., Phys. 15, 872, 1914.

[43] Mott, N. F., and Davis, E. A., *Electronic Processes in Non-crystalline Materials*, Clarendon, Oxford, 1979, 2Nd Edition.

[44] Blythe, A. R., *Electrical Properties of Polymers*, Cambridge University, Press, Cambridge, London, 1979.

[45] Seanor, D. A., *Electrical Properties of Polymers*, Academic Press, Inc, New York, 1982.

[46] Boyle, A., Penneau, J.-F., Genies, E., Riekel, C. J., Polym Sci Part B: Polym Phys 30, 265–274, 1992.

Chapter 7

Alternating Current Electrical Properties

This chapter describes the existing theories of alternating current electrical conduction in plasma polymerized thin films, and discusses the experimental results e.g. frequency and temperature dependence of ac conductivity and dielectric constants, dielectric relaxation, dielectric loss etc.

7.1 Introduction

The alternating current (ac) field behavior of a material provides information about the electrical nature of the molecular or atomic species, which constitutes the dielectric materials. Dielectric spectroscopic analysis measures the electrical properties of a material as a function of frequency and temperature. This analysis measures two fundamental electrical characteristics of materials: *(a)* the capacitive (insulating) nature, which represents its ability to store electric charge; *(b)* the conductive nature, which represents its ability to transfer electronic charge. Therefore the ac measurements are important means for studying the dynamic properties e.g. the conductivity, dielectric constant, permittivity, loss factor etc of a dielectric.

The advantage of ac measurements is that, it investigates the time-dependent properties such as a carrier hopping and also of other conduction processes taking place in the dielectric even though the conduction process may be electrode-limited. Moreover the ac voltage bias need never exceed a few hundred millivolts. Thus the maximum field within the insulator film is kept to a minimum and there is a little danger of more than one conduction process being active. This measurement also helps to distinguish between localized and free band conduction. In the case of localized conduction the conductivity (σ_{ac}) increases with frequency ω, while in the free band conduction the conductivity decreases with frequency. It has been pointed out by Elliott [1] that a variety of conduction mechanisms can yield the ω^s behavior for the ac conductivity, but in general, it is difficult to establish which of the above effects determines a given observed conduction process.

The analysis of dielectric data over a wide temperature and frequency range provides deep insight into the nature of dominant polarization mechanism in polymer films, and therefore a dielectric study throws light on the molecular structure and relaxation behaviors of the polymers.

7.2 Dielectric Fundamentals

7.2.1 Introduction

Electrical and electronic insulating materials, also known as dielectrics, have the property of storing and dissipating electrical energy when subjected to electromagnetic field. The energy-storing property leads to the fabrication of most important constitutes of electrical circuit known as capacitor. The dielectric phenomena arise from the interaction of electric field with different charged particle such as electrons, ions, protons and electrons shells. Dielectrics materials have interesting electric properties because of the ability of an electric filed to polarize the material to create dipoles. When exposed to an electric field, the electric charges in a dielectric material, including permanent and induced electric dipoles, can be

moved, thus polarizing the material. Although the equilibrium polarization of a material remains constant for a given electrical field, it is the dielectric constant, ε', that is used to characterize the dielectric properties of the dielectric.

Organic polymers are considered as suitable dielectric for capacitor since they offer highly desirable electrical and mechanical properties. Because of good dielectric properties, however, plasma polymerized thin films found to be useful as dielectrics in integrated microelectronics and insulating layers for semiconductors. Thin films produced through plasma-polymerization are known to have free radicals or polar groups independent of the nature of monomers. Owing to this reason, these polymers are good candidates for the investigation of dielectric properties.

Depending on the dielectric behavior the polymers are broadly divided into two groups *(a)* Non-polar polymer and *(b)* Polar polymer. Non-polar polymer are with very low dielectric constant, no dielectric loss and very little frequency dependence on either of these properties because the lack of permanent dipole moment in them. But majority of polymers belong to polar group. They have permanent dipole moment and hence exhibit dielectric dispersion. The polar polymer show very high dielectric constant and the dielectric loss. The frequency dependence of these quantities also are higher. Highly polar polymer dielectrics have excellent charge storage capabilities. Hence they are better employed as polymer electrets rather than as capacitor dielectric.

7.2.2 Dielectric Constant and Dielectric Loss

The dielectric constant, ε' is the ratio of the permittivity of a substance, ε, which is a measure of the ability of a material to be polarized by an electric field, to the permittivity of free space, ε_0. It is also defined as the ratio of the field without the dielectric (E_o) to the net field (E) with the dielectric, or as the ratio of the amount of stored electrical energy when a voltage is applied, relative to the permittivity of a vacuum.

$$\varepsilon' = \frac{\varepsilon}{\varepsilon_0} = \frac{E_0}{E} \qquad (7.1)$$

E is always less than or equal to E_o, so the dielectric constant is greater than or equal to unity. The larger the dielectric constant, the more charge can be stored in a material. Materials with high dielectric constants are useful in the manufacture of high-value capacitors. The dielectric constant is an essential piece of information when designing capacitors, and in other circumstances where a material might be expected to introduce capacitance into a circuit. If a material with a high dielectric constant is placed in an electric field, the magnitude of that field will be measurably reduced within the volume of the

dielectric. This fact is commonly used to increase the capacitance of a particular capacitor design.

A low-ε' dielectric is a dielectric that has a low permittivity, or low ability to polarize and hold charge. Low-ε' dielectrics are very good insulators for isolating signal-carrying conductors from each other. Thus, low-ε' dielectrics are a necessity in very dense multi-layered integrated circuits, wherein coupling between very close metal lines need to be suppressed to prevent a degradation in device performance. A high-ε' dielectric, on the other hand, has a high permittivity. Because high-ε' dielectrics are good at holding charge, they are the preferred dielectric for capacitors. High-ε' dielectrics are also used in memory cells that store digital data in the form of charge.

Dielectric constant, ε′, however is a critical electrical parameter for a microelectronic polymer dielectric. The magnitude of ε′ depends on the amount of mobile (polarizable) electrical charges and the degree of mobility of these charges in the material. Because the charge mobility depends on temperature, ε′ is temperature dependent, and since polarization of the material requires a finite amount of time, the frequency of the electric field also influences the measured dielectric constant. The lower the dielectric constant, the faster the signal propagation velocity, as given by:

$$v_p = \frac{c}{\sqrt{\varepsilon'}} \qquad (7.2)$$

where v_p is the velocity of propagation and *c* is the speed of light. A lower dielectric constant allows for wider signal traces and a decrease in the dielectric thickness. It also allows a designer to maintain the same characteristic impedance while lowering the line resistance and crosstalk. Characteristics of a good dielectric should include invariance of the dielectric constant with respect to frequency and temperature.

In an alternating (ac) field, the dielectric constant is a complex quantity, ε*, and is the combination of a real component, called the relative permittivity or dielectric constant, ε′, and an imaginary component, called the dielectric loss or dissipation factor, ε″. This form, also called the complex dielectric permittivity, is defined as,

$$\varepsilon^* = \varepsilon' - j\varepsilon'' \qquad (7.3)$$

A key issue is the variation of both ε′ and ε″ with respect to frequency and temperature for the ac measurements in plasma polymerized thin films, which would be presented in this chapter.

Dissipation factor or loss factor (ε″) and loss tangent (tan δ) are also important electrical parameters, especially at high frequencies. As the frequency increases, the inertia of the charged particles tends to prevent the particle displacements from keeping in phase with the field changes. This leads to a frictional damping mechanism that causes power loss, because work must be performed to overcome these damping forces. Additionally, ohmic losses due to free charge carriers are also included in the complex permittivity. It is customary to include the effects of both the damping and the ohmic losses in the imaginary part of the complex permittivity, ε*:

$$\sigma = \omega\varepsilon'' \qquad (7.4)$$

where σ is the conductivity and ω is the angular frequency.

Using equation (7.4) we can rewrite equation (7.3l) as follows:

$$\varepsilon^* = \varepsilon' - j\frac{\sigma}{\omega} \qquad (7.5)$$

On the basis of equation (7.5) a medium is said to be a good conductor if σ >> ωε' and a good insulator if ωε' >> σ. Thus, a material may be a good conductor at low frequencies, but may have the properties of a lossy dielectric at very high frequencies. In contrast, most dielectrics, including ceramics and polymers, exhibit low loss at low frequencies, but become lossy at high frequencies. In low-loss media, damping losses are very small, and the real part of ε* in equation (7.5) is usually written as ε without a prime.

In response to a varying electric field, the finite time involved to displace charges in dielectric material results a time lag between field and polarization. This implies an irreversible degradation of free energy to heat and is referred to as the dielectric loss. Dielectric loss is a bulk property and should not depend on film thickness. However this is an ideal concept and deviation from this are often observed. When the defect structure of the films takes part in the dielectric relaxation process, the loss can be thickness dependent. Due to the deviations from stochiometry, dielectric loss may show strong dependence on the films preparation conditions. The presence of impurities can also affect the permittivity and loss values in thin films dielectric. In certain plasma polymerized films, it is observed that both of these parameters are highly influenced by the presence of polar groups formed by exposure to Oxygen or humid atmosphere [2]. The dependence of permittivity and loss on a wide range of temperature and frequency can be utilized to investigate the behavior of a larger number of thin films dielectrics.

However, If δ is the phase lag between field and polarization, the dielectric loss is generally expressed as tan δ and is given by

$$\tan\delta = \frac{\varepsilon''}{\varepsilon'} \qquad (7.6)$$

Low values of dielectric loss are indicative of minimal conversions of electrical energy to heat and little overall power loss. Thus, multilayer power circuits require thin film materials that exhibit low values for dissipation factor.

7.2.3 Polarization Mechanisms

If a material contains polar molecules, they will generally be in random orientations when no electric field is applied. An applied electric field will polarize the material by orienting the dipole moments of polar molecules. This would decrease the effective electric field between the plates and would increase the capacitance of the parallel plate structure.

Different types of polarization can be caused by an electric field in a dielectric material:

- *Electronic polarization*: the electrons in atoms are displaced relative to the nucleus.
- *Ionic polarization*: cations and anions in an ionic crystal are displaced with respect to each other.
- *Dipolar or Orientation polarization*: permanent dipoles (like H_2O) are aligned.
- *Interfacial polarization* : It is the consequence of space charge accumulation at the structural interfaces of an inhomogeneous dielectric material.

All possible types of polarization in a dielectric material can be explained by their intrinsic physical mechanisms.

- **Electronic polarization:** The distortion of the electronic distribution about the atomic nucleus under the action of external electric field constitutes electronic polarization. This is observed in all dielectric irrespective of whether other types of polarization are present in the dielectric or not. It is predominant at optical (high) frequencies. At these frequencies dielectric possessing electronic polarization satisfies the relation $\varepsilon = n^2$ where n is the high frequency refractive index of the material and ε is the relative permittivity of material. Electronic polarization sets in during very brief interval of time (of the order of 10^{-15} sec).

- **Ionic polarization:** In ionic materials the displacements of charged ions with respect to other ions in response to an applied electric field causes ionic polarization. This usually appears at and beyond the infrared frequencies. A short time of the order 10^{-12} sec, but no longer than that of the ionic polarization is required for ionic polarization set in. In the presence of ionic polarization $\varepsilon > n^2$. In highly deformable ionic compounds such as oxides, deformation ionic polarization is usually observed.

- **Dipolar polarization:** When molecule having permanent dipole moments charge orientation in response to an applied electric field, orientational or true dipolar polarization results. Such molecules tend to response to the external field by realignment in order to reduce their potential energy. The possibility of rotational polarization also exists for pendants polar groups hung flexibly on molecules. This plays a significant role in the low, medium and high frequency polarization of macromolecular solids. Debye has made significant contribution to develop the theory of dipolar polarization [3].

- **Interfacial polarization:** Interfacial polarization is the consequence of space charge accumulation at the structural interfaces of an inhomogeneous dielectric material. Charge carriers migrating under the influence of an applied electric field, though the several phases of the dielectric produce varying charge accumulation at the interface. These charges may be impeded in their motion by trapping at impurity centers or at interfaces, or because they can not be freely discharged or replaced at an interface. The resulting space charges produce distortions of the microscopic field which appears as a polarization to the external observer. Interfacial polarization which occurs rather more often than is generally appreciated is a frequent reminder of the way in which real matter behaves in real fields. The phenomenon was first recognized by Maxwell and explored thoroughly by Wagner and a mathematical treatment was given in terms of a two-layer dielectric. But the Maxwell-Wagner theory is a very crude description of interfacial polarization. A more realistic theory has been given by Sultan [4] by considering the build up of charges and the resultant field distortion as a function of frequency and thickness.

All the above mentioned polarization mechanisms are possible in thin films, both amorphous and polycrystalline. In bulk dielectric materials, the interface effects may be neglected. However, in metal-dielectric-metal thin films sandwich structure, interfacial polarization is observed owing to the space charge accumulation at metal-dielectric interfaces. The possible polarization mechanism in thin films can be treated in two different perspectives, those which are characteristics of bulk properties of the material and those which are due to interfacial effects. Electronic and ionic polarization belongs to the first category. True dipolar and dipole-like polarization resulting from permanent dipoles and effective dipoles from imperfection respectively. Interfacial polarization is not a characteristics property of the

dielectric material. Highly insulating thin films materials though have a few numbers of mobile carriers, can develop appreciable space charge build up at the metal-insulator interface under the influence of an applied electric field. This often leads to interfacial polarization effects. In certain thin film dielectrics the permittivity value is seen to be increased towards the low frequency side [5]. With rise in temperature the permittivity also increases. This observation can be attributed to the effect of interfacial polarization.

7.3 Theory of Dielectric

7.3.1 Dielectric spectroscopy

The dielectric spectroscopy is used to study the dielectric properties of materials, especially to explore the molecular dynamics in polymer samples as a function of frequency and temperature. This spectroscopic method is sensitive in dipolar species as well as localized charges and determines their strength, their kinetics and interaction; and therefore it is a powerful tool for the electrical characterization of nonconducting and semiconducting materials. The measured dielectric spectra can be used to provide quantified insights to the molecular level dynamics of polymeric materials, and a broad variety of dynamics in this wide frequency range can be studied by this method. Dielectric spectroscopy, however, measure the frequency dependent complex dielectric constant ε* of materials. The ε* reflects the molecular relaxation and transport processes of the material, which depend on nearly any other physical quantity like temperature, time, superimposed electromagnetic fields, pressure etc; and therefore the applications in science and technology seem to be almost unlimited. Some examples for scientific application are studies

- on the molecular dynamics liquids, liquid crystals and polymer
- charge transport in insulators, semiconductor, organic crystals etc
- monitoring of chemical reactions or polymerization processes
- structural material properties like phase compositions, phase transition and crystallization processes.
- non linear electrical and optical effects etc.

Dielectric spectroscopy can be described in the frequency domain [i.e. described by ε'(ω), ε″ (ω) or tanδ (ω); where ω represents the angular frequency] or described in the temperature domain [i.e. described by ε' (T), ε″ (T), or tanδ (T), where *T* represents temperature]. The relaxation processes (α-relaxation and secondary relaxations) can be characterized by the presence of resonance peaks in ε″ (ω) or ε″ (T). The shape parameters of the resonance peaks in ε″ (ω) or ε″ (T) provide useful information about the molecular dynamics in polymer samples. For example, the widening of the α-relaxation peaks in ε″ (ω) obtained from a

polymer sample may suggest the widening of the distribution of the molecular relaxation times. However, although many efforts have been put into the study of the shape parameters of the relaxation peaks in ε″ (ω), only a few reports [6] are related to the study of the shape parameters of the relaxation peaks in ε″ (T). As to the dielectric spectroscopy of ε″ (T) obtained from polymer samples, the α-relaxation peaks of many polymers are close to symmetric [7]. In contrast it is widely accepted that in the ε″ (ω) obtained from some of these samples the α- relaxation peaks are not symmetric (the high frequency ends of these peaks are usually wider). The symmetry is more striking when the large discrepancy among the constituents of those polymers is taken into consideration.

7.3.2 AC Conductivity

The capacitance of a parallel plate capacitor having a dielectric medium is expressed as

$$C = \varepsilon' \varepsilon_0 \frac{A}{d} \tag{7.7}$$

where ε_o is the permittivity of free space, ε' is the dielectric constant of the medium, A is the surface area of each of the plates/electrodes and d is the thickness of the dielectric. A real capacitor can be represented with a capacitor and a resistor. The parameters such as angular frequency (ω) of the applied field, the parallel resistance R_p, parallel capacitance C_p are related to the dielectric constant ε', dielectric dissipation factor ε'' and loss tangent as :

$$C_p = \varepsilon' C_0 \tag{7.8}$$

$$\varepsilon'' = \frac{1}{R_p C_0 \omega} \tag{7.9}$$

and

$$\tan\delta = \frac{\varepsilon''}{\varepsilon'} = \frac{1}{R_p C_p \omega} = \frac{G_p}{2\pi f C_p} \tag{7.10}$$

The ac conductivity, σ_{ac}, can be calculated using the relation,

$$\sigma_{ac} = G_p \frac{d}{A} \tag{7.11}$$

where G_p is the conductance of the material.
The dependance of σ_{ac} on frequency may be described by the power law [8]:

$$\sigma_{ac}(\omega) = A\omega^n \tag{7.12}$$

where A is a proportonality constant and ω (=2 πf, f is the linear frequency) is the angular frequency and n is the exponent, which generally takes the value less than unity for Debye type mechanism and is used to understand the conduction/relaxation mechanism in amorphous materials.

7.3.3 The Debye Theory

The Debye model of dielectric spectroscopy assumes that the dipolar molecules concentration is very small and that the electrostatic interaction between dipoles can be ignored. The dipolar molecules experience Brownian motion in the solvent, and the rotation of dipole orientation is hindered by friction force. When samples are not in external electric field, the distribution of the orientation of the dipoles is random and the total dipole moment equals to zero. When an external electric field is applied to the medium, more dipoles will point to the direction of the external electric field. This model, however, did not consider the interaction between dipoles. In many cases the interaction can not be ignored. But variety of approaches has been brought up with to address different types of the interactions between the dipoles. However, the interactions between the atoms/molecules and the exerted external electric field are usually very complex, and it is quite difficult to build an extensive model for dielectric dynamics.

The polarization of a medium as the response to an external electric field is usually composed of two components. One follows the changing of the external electric field intimately and the other one lags behind. As illustrated in Figure 7.3.1, when a step external electric field is applied to a medium, the polarization of the media jumps immediately to another level, and then the polarization slowly evolves to a saturated level.

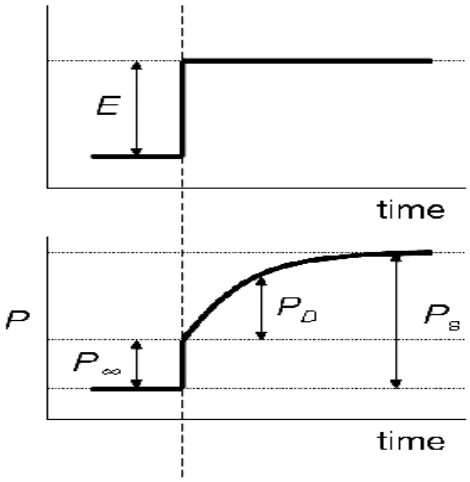

Figure 7.3.1 A step electric field is exerted on a medium, and the polarization of the medium is composed of two components: P_∞ and P_D. P_∞ follows the electric field intimately and P_D slowly evolves to a saturated level, which is represented by P_s.

The quick polarization is thought to be related to relaxation processes with very short relaxation times, such as the polarization of the atoms. The slow polarization is related to relaxation processes with long relaxation times, such as the cooperative relaxation of polymer molecules. Hereby the quick component is represented by P_∞, the slow component

is represented by P_D and the saturated value of polarization by P_s. Since P_∞ and P_s both are proportional to the change of the electric field, so we can define two parameters ε_s and ε_∞ as:

$$\varepsilon_\infty = \frac{4\pi P_\infty}{E} - 1 \tag{7.13}$$

and

$$\varepsilon_s = \frac{4\pi P_s}{E} - 1 \tag{7.14}$$

Oscillating electrical field is much more useful in dielectric spectroscopy. For a periodic field that is applied on the medium,

$$E(t) = E_0 e^{i\omega t} \tag{7.15}$$

And then, the dielectric behavior of a material is usually described by Debye dispersion equation [9]:

$$\varepsilon^*(\omega, T) = \varepsilon' - j\varepsilon'' = \varepsilon_\infty + \frac{(\varepsilon_s - \varepsilon_\infty)}{(1 + j\omega\tau)} \tag{7.16}$$

where ε^* is the complex dielectric permittivity, ε' (energy dissipated per cycle) is the real part of cmplex dielectric permittivity and ε'' (energy stored per cycle) is the imaginary part of the complex dielectric permittivity. where ε_s is the static dielectric constant, ε_∞ is the high frequency dielectric constant and the quantity τ is a characteristic time constant, usually called the dielectric relaxation time, it refers to a gradual change in the polarization following an abrupt change in applied field.

Now equating real and imaginary part of equation (7.16) leads to

$$\varepsilon' = \varepsilon_\infty + \frac{(\varepsilon_s - \varepsilon_\infty)}{(1 + \omega^2\tau^2)} \tag{7.17}$$

and

$$\varepsilon'' = \varepsilon_\infty + \frac{(\varepsilon_s - \varepsilon_\infty)\omega\tau}{(1 + \omega^2\tau^2)} \tag{7.18}$$

The dielectric loss tangent is then expressed as

$$\tan\delta = \frac{\varepsilon''}{\varepsilon'} = \frac{(\varepsilon_s - \varepsilon_\infty)\omega\tau}{(\varepsilon_s + \varepsilon_\infty\omega^2\tau^2)} \tag{7.19}$$

The equations (7.17), (7.18) and (7.19) are known as the Debye equation.

As $\omega \to 0$, $\varepsilon'(\omega) \to \varepsilon_s$, the static dielectric constant and when $\omega \to \infty$, $\varepsilon'(\omega) \to \varepsilon_\infty$, dielectric constant at optical frequency i.e., real part of dielectric constant has two limits, one at lower frequency (static field) and the other at optical frequency as denoted by ε_s and ε_∞.

At $\omega = 0$ and $\omega = \infty$, ε'' becomes 0 and ε' becomes ε_s and ε_∞ respectively. Further, when $\omega\tau = 1$, ε'' attains maximum loss value. It is seen that ε' continously falls with the increase of ω, particularly very rapidly at a critical frequency $\omega_{max} = 1/\tau$, and location of this peak provides the easiest way of obtaining the relaxation time from the experimental results. The variation of ε'' with ω shows a broad peak, which is due to relaxation. This arises from the rotational behaviour of the dipole in solid or liquid where polarized dipole can not rotate freely as in gaseous state. The behavior of ε' and ε'' is generally in accordance with the Debye's equation. This phenomenon can be more effectively shown in a graphical form by Cole-Cole diagram [10].

The Figure 7.3.2 however shows the Debye dielectric dispersion curves.

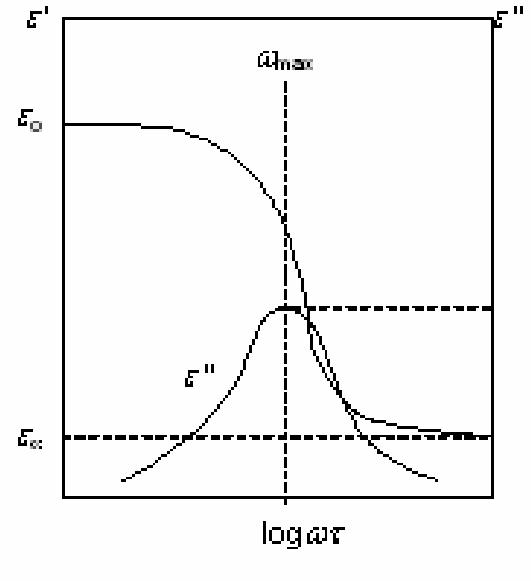

Figure 7.3.2 Debye dielectric dispersion curves.

In the derivation of Debye's equation it has been assumed that the dielectric has average single relaxation time, which implies that the charged particle or an ion has two equilibrium position separated by a distance d. In many cases dipoles have more than two equilibrium positions, and in such cases it is not possible to assign an average relaxation time unlike the Debye relaxation cases. [11].

The Debye equation, however, fits well to many dielectric spectra, especially to those measured from dilute solutions of large polar molecules in non-polar solvents. It also gives basic understanding of the origin and properties of dielectric spectra. In practice there could be several relaxation processes exist in a sample. An example is in polymer samples where several relaxation processes often exist. The most pronounced one is the segmental cooperative relaxation, and this relaxation process is called α-relaxation. The weaker relaxation processes are usually related to some chemistry processes which follows the Arrhenius law, and these weaker relaxation processes are called β, γ... relaxations. The

dielectric spectrum of a polymer like this can be theoretically treated as the overlap of several Debye relaxation spectrums. There are also some cases where the dielectric spectrum cannot be described by Debye equation (or overlap of several Debye equations). For example, the peaks of ε'' as a function of log ω are often observed to be wider than expected, or to have asymmetric shapes, or even to behave further away from Debye relaxation. There exist several treatments to this issue. One of them is to describe the relaxation with an empirical function, which is usually an altered Debye relaxation function. In polymer physics one of the most important empirical functions is the Havriliak-Negami (H-N) function [12]. It describes the widening and asymmetry of the relaxation peaks of ε'' vs. log ω by two extra exponential parameters. The Havriliak-Negami function is:

$$\varepsilon^* = \varepsilon_\infty + \frac{\Delta\omega}{\left[1+(j\omega\tau)^\alpha\right]^\beta} \qquad (7.20)$$

ε' and ε'' vs. frequency or temperature is used as the results of dielectric spectroscopy measurements. A typical plot of ε', ε'' and $\tan\delta$ against log (ωτ) are shown in Figure 7.3.3, where the parameters ε_s and ε_∞ are taken as 8 and 2 respectively. The relaxation frequency is at the peak point in the ε'' vs. frequency plot, or at the maximum slope in the ε' vs. frequency plot.

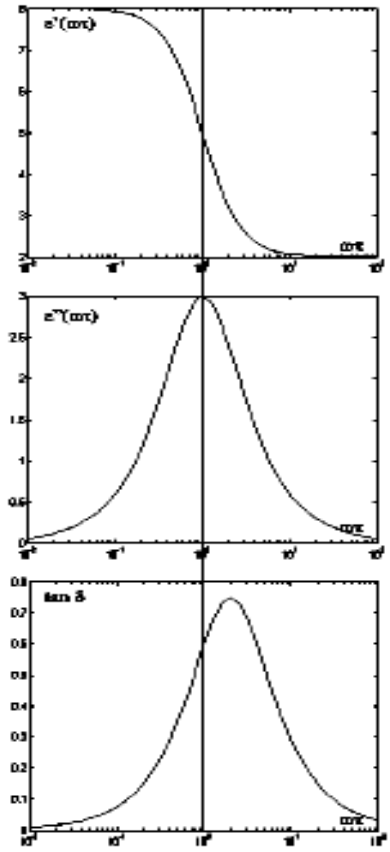

Figure 7.3.3 ε', ε'' and $\tan\delta$ as a function of log (ωτ). The peak point of $\tan\delta$ is not at the same place as that of the ε''.

However, the relaxation process of P_D can be described by the following equation,

$$\tau\frac{dP_D}{dt}+P_d(t)=(\varepsilon_s-\varepsilon_\infty)\frac{E(t)}{4\pi} \tag{7.21}$$

The general solution of this equation is,

$$P_D(t)=Ke^{-\frac{t}{\tau}}+\frac{1}{4\pi}\frac{(\varepsilon_s-\varepsilon_\infty)}{(1+\omega\tau)}E_0e^{i\omega t}\approx\frac{1}{4\pi}\frac{(\varepsilon_s-\varepsilon_\infty)}{(1+\omega\tau)}E_0e^{i\omega t} \tag{7.22}$$

where *K* characterizes the initial polarization. The first term decays with time and that is why it is neglected.

The solution of *P* as a function of time provides a proof to an important assumption that with electric field disturbance dielectric response complies with linearity and causality. Linearity means that the response at a certain time point is the sum of all responses to stimuli, and the causality means that only previous stimuli will affect current response. While it is easy to accept that the response of a dielectric medium follows the causality. The linearity of

dielectric system was not realized until Boltzmann [13] proposed it in 1874 and J. Hopkinson [14] verified it in 1876. Later experiments showed that under small electric field dielectric systems hold linearity pretty well.

The activation energy (ΔE) of the relaxation process, however, is related to the relaxation time by the Arrhenius equation:

$$\tau = \frac{1}{2\pi f_{\max}} = \tau_0 \exp\left[\frac{\Delta E}{k_B T}\right] \qquad (7.23)$$

Where f_{max}, is the frequency of maximum loss for a given temperature, τ_0 is a constant and T is the absolute temperature and k_B is the Boltzman constant. ΔE was evaluated in the present work from the slope of the plot log $f_{max,}$ versus 1/T.

7.3.4 Dielectric Relaxation

A relaxation process can be treated as a delayed response to a changing stimulus in systems where the response and stimulus are proportional to each other in equilibrium. The dielectric relaxation is concerned with the delayed response manifested as a polarization to a time dependent dielectric field.

The microscopic behavior of a dielectric material under a varying electric field can be attributed to the polarization phenomena of the charged particles, which constitutes the dielectrics. This may be an extra nuclear electron, and positively charged nuclei, anion, and cataions etc. The oppositely charged species with a reasonable bond between them will form a dipole which will behave as one unit. These dipoles under an electric field may undergo special translational or rotational displacement, which will be reflected in macroscopic behavior of dielectric. The polarization effect will also be dependent on the nature of the dipole and frequency of the applied ac field, but the polarization of the dielectric may not follow the field variation. This displacement due to polarization may persist even when the field is stopped. This gives rise to a decay time to attain the equilibrium and the phenomenon is called the Debye relaxation. The decay time is called relaxation time.

However, since the relaxation times are found to be temperature dependent, a complete study of the dielectric properties might be represented by contour maps of ε' and ε'' against frequency *f* and temperature *T*. The frequency f_{max}, at which ε'' is maximum, is determined and is treated as analogous to rate constant. Thus, a convenient summary of the effect of temperature on the relaxation process is a plot of log f_{max}, versus *I/T* or relaxation map. If the characteristic of a specimen is the principal goal, the loss versus temperature plot is required. For this, a number of relaxation curves log f_{max} versus *I/T* are to be presented, and then the activation energy can be calculated.

The various dielectric relaxations may be observed in the scan of dielectric loss at constant frequency as presented in Figure 7.3.5. With the increase in temperature, the molecular

motilities of various kinds of a material become successively energized and available for dipolar orientation. By convention, the dielectric relaxation processes are labeled as α, β, γ and so on, beginning at the high temperature end. The same relaxation processes were generally responsible for dispersions in mechanical properties too, although a particular molecular rearrangement process may produce stronger dielectric than mechanical effect or vice versa. In case of amorphous solid polymer, there is always a high temperature α-relaxation associated with the micro-Brownian motion of the whole chains and in addition, at least, one low temperature ($\beta, \gamma,$ etc.) auxiliary relaxation may occur.

The relative strength of α and β relaxations depends on how much orientation of the tail groups can occur through the limited mobility allowed by the β process before the more difficult but more extensive mobility of the a process comes into play; there is a partitioning of the total dipolar alignment among the molecular rearrangement processes.

The high frequency β, γ auxiliary peaks in amorphous polymers are characteristically very broad with half height width of several decades, although, a good linear Arrhenius plot is usually obtained suggesting a non-cooperative mechanism. The mechanism of a β relaxation may be one of several different types depending on the nature of the dipole group concerned and its position on the polymer chain.

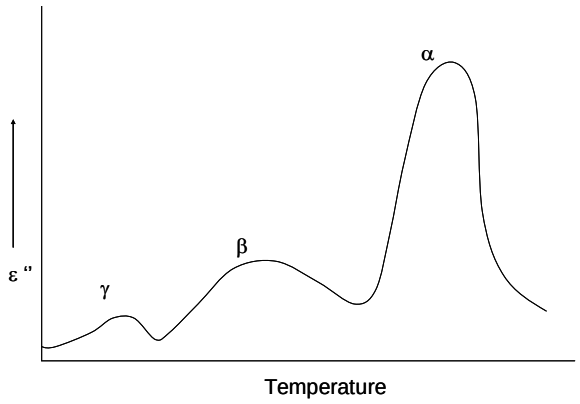

Figure 7.3.5 The various dielectric relaxations in the scan of dielectric loss with temperature at constant frequency.

If, however, the dielectric relaxation is related to the thermally activated process the relaxation time should have the form

$$\tau_0 = \tau_\infty \exp\left[\frac{E_0}{kT}\right] \qquad (7.24)$$

7.4. Results and Discussion

7.4.1 Plasma Polymerized Pyrrole Thin Films

7.4.1.1 Variation of Dielectric Constant with Frequency and Temperature

Figure 7.4.1 represents the dielectric constant ε', as a function of frequency for the plasma polymerized pyrrole (PPPy) thin films of different thicknesses 400, 450, 500, 550 and 600 nm at room temperature.

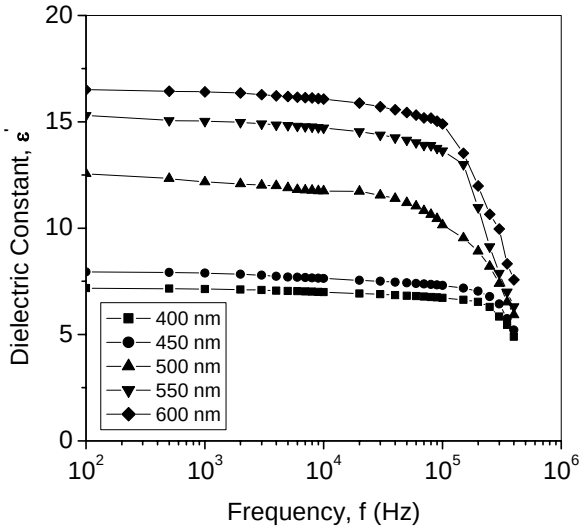

Figure 7.4.1 Dielectric constant ε', as a function of frequency of the PPPy films of different thicknesses at room temperatures.

From the figure, it is observed that at the low frequencies, the dielectric constant for all the samples are almost independent of frequency, but at high frequencies the decrease in ε' is very prominent. It could also be noticed from the figure that for the films of lower thickness (e.g. d = 400 nm), the dielectric constant is frequency-independent up to 100 kHz, and after that decreases a little. But for higher thicknesses (e.g. 550 or 600 nm) of the films the ε' start decreasing at frequencies below 100 kHz and then decreases drastically. The extent of the decrease of dielectric constant is more remarkable in the high frequency range than in the low-frequency ranges.

The behavior that dielectric constant of polymer thin films varies with film thickness has been reported by several authors [15, 16], and two factors were mentioned to be responsible for much different electrical properties of polymer thin films than those of bulk materials, namely *(a)* the orientation of polymer chains along the substrate and *(b)* the interaction of polymer chains with the substrate or the electrode. The fact that the decrease of dielectric constant with decreasing film thickness was explained as the restriction of polymer chains by the solid wall of the substrate; or electrode in the interfacial region between the polymer film and the substrate or electrode.

However, this type of dependence of the ε' on frequency could be explained with space charge accumulation at the structural interface of the PPPy thin films. The charges present in the PPPy thin films can migrate under the influence of an electric field. It is possible that they get blocked at the electrode dielectric interface, which leads to space charge polarization. Such distortion causes an increase in ε' of PPPy thin films at the low frequencies.

The dielectric behavior of a material is usually described by using Debye dispersion equation [9]

$$\varepsilon = \varepsilon' - i\varepsilon'' = \varepsilon_\infty + \frac{\varepsilon_s - \varepsilon_\infty}{1+(\omega\tau)^2} \qquad (7.16)$$

where ε_s is the static or relaxed dielectric constant at (ω=*0*), ε_∞ is the high frequency or unrelaxed dielectric constant and the quantity τ is a characteristic time constant, usually called the dielectric relaxation time; it refers to a gradual change in the polarization following an abrupt change in applied field. When frequency reaches the characteristic frequency (ω=1/τ), the ε' drops, which means the presence of a relaxation process. At very high frequency ($\omega \geq 1/\tau$) dipoles can no longer follow the field, and $\varepsilon' \approx \varepsilon_\infty$. Relaxation may be occurred above 1 MHz ($1/\tau \geq 1MHz$) which is an indication of a fast polarization mechanism and the polarization process will be labeled by the γ process. The γ process dominates the behavior of ε' from 100 Hz to 10^5 Hz.

Figure 7.4.2 - Figure 7.4.6 show the variation of the dielectric constant ε' with the frequency of all the samples of thicknesses about 400, 450, 500, 550 and 600 nm respectively at different temperatures 298, 323, 348, 373 and 398 K.

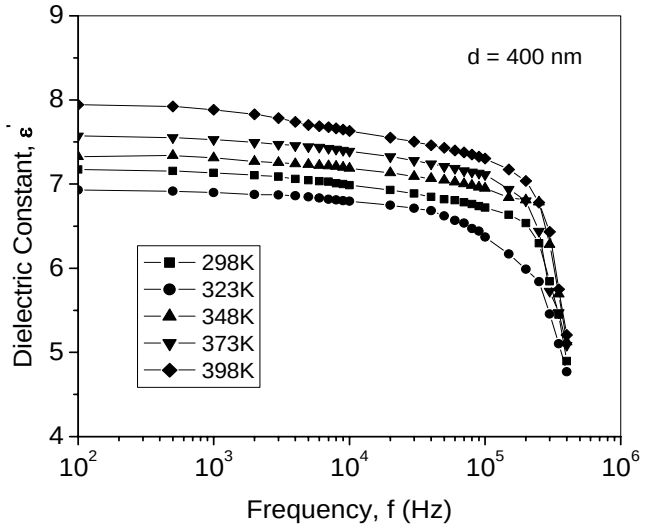

Figure 7.4.2 Dielectric constant, ε' as a function of frequency of the PPPy thin films of thickness 400 nm at different temperatures.

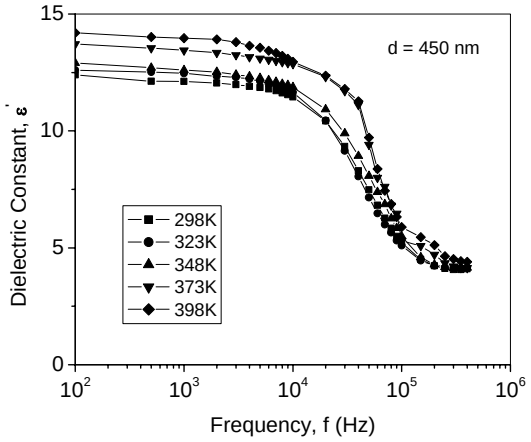

Figure 7.4.3 Dielectric constant, ε', as a function of frequency of the PPPy thin films of thickness 450 nm at different temperatures.

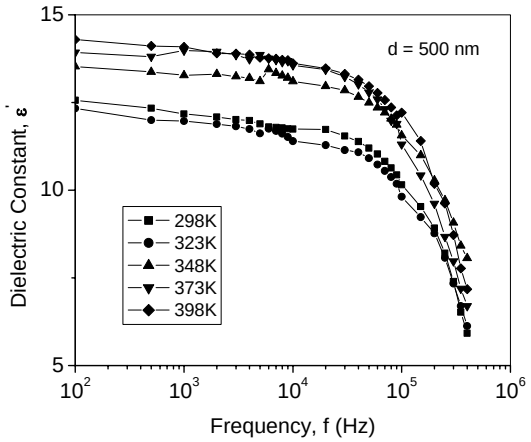

Figure 7.4.4 Dielectric constant, ε', as a function of frequency of the PPPy thin films of thickness 500 nm at different temperatures.

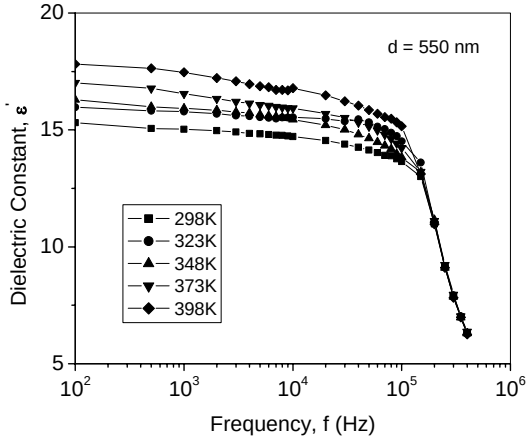

Figure 7.4.5 Dielectric constant, ε', as a function of frequency of the PPPy thin films of thickness 550 nm at different temperatures.

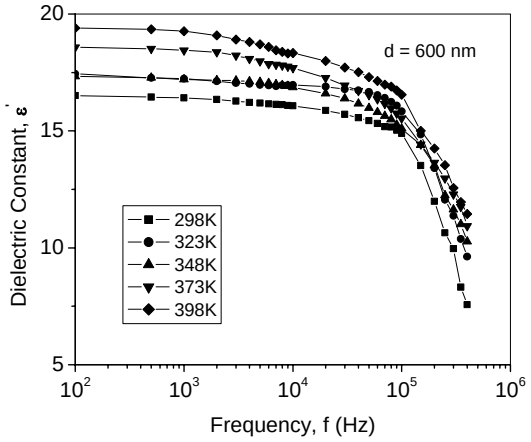

Figure 7.4.6 Dielectric constant, ε', as a function of frequency of the PPPy thin films of thickness 600 nm at different temperatures.

From all the figures (Figures 7.4.2 - 7.4.6), the general trends of the dielectric constants ε' are observed to be decreased with the increase of the frequency at a certain temperature. It is also to be noted from these figures that at the low frequencies, a very little dependence of ε' on the frequency is observed, whereas at high frequencies the decrease in ε' with the increase in frequency is very prominent at a certain temperature. The figures also show that, the dielectric constants have higher values at higher temperature for any certain frequency and thickness of the films.

The decrease of ε' with frequency can be attributed to the electrical relaxation processes and multi-component contribution of polarizability of the polar materials, such as, deformational (electronic and ionic) and relaxation (orientational and interfacial) polarization. The observed frequency dependence of ε' is due to the interfacial or space charge polarization, which is usually observed in sandwich type configurations. The interfacial or space charge polarization occurs due to the space charge accumulation at the structural interfaces of an inhomogeneous dielectric material. These charge carriers become mobile under the influence of an applied electric field. The space charge polarization typically occurs at frequency range from 1 to 10^3 Hz.

However since the interfacial polarization is very typical in sandwich type configurations, the other relaxation processes can be superimposed with this polarization. For example, the decrease of ε' with increasing frequency is the expected behavior in most dielectric materials, and could be attributed to the orientation polarization of molecular chains, which is also the cause of anomalous dispersion. Since the orientation polarization depends upon the molecular arrangement of dielectric and at higher frequencies the rotational motion of the polar molecules of dielectric is not sufficiently rapid for the attainment of equilibrium with the field. The orientational polarization is therefore decreased with increasing frequencies which in turns results in a decrease of dielectric constant with increasing frequency [17]. It is also

known that the effect of polarization is to reduce the field inside the medium. Therefore, the dielectric constant of a substance may be decreased substantially as the frequency is increased. The total polarization of the dielectric material can be given as the sum of these four types of polarization [18]. But since the electronic and ionic polarization occurs at very high frequencies (10^{10} ~10^{16} Hz) which are beyond of our range of measurement, therefore these two types polarization could not be attributed to the relaxation process of the present system.

The increase of ε' with temperature, however, can be attributed to the fact that the orientional polarization is connected with the thermal motion of molecules. The dipoles can not orient themselves at low temperatures. When the temperature is increased, the orientation of dipole is facilitated and this increases the value of orientational polarization, which leads to increase of the dielectric constant ε' with temperature.

The variation of the ε' with the temperature at different frequency for all the sample of thickness about 400 nm respectively is presented in Figure 7.4.7. It is observed from the figure that at high frequencies (50 kHz and above), ε' remains almost constant with increasing temperature, but at low frequencies (100 to below 50 kHz), it increases with increasing temperature. The rate of increase is different at different frequencies.

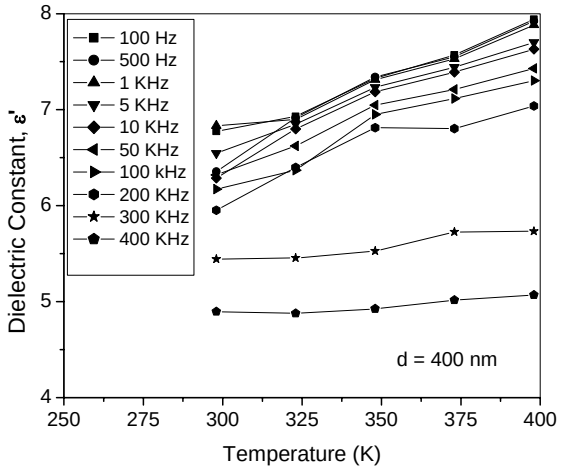

Figure 7.4.7 Variation of dielectric constant, ε', with temperature of the PPPy thin films at different frequencies.

From the above figure, it can be seen that, ε' exhibit strong temperature dependence at higher temperature and lower frequencies. This behavior can be accounted for by assuming that the contribution of dipole orientation would be insignificant [19]. The ε' is strongly temperature dependent in the high-temperature region. This may related to the fact that, at high temperatures the loss is dominated by thermally activated electron hopping where as in the low-temperature region such an activated process is frozen out, resulting in a decrease of ε' at low temperature [20].

The variation of ε' with temperature is different for nonpolar and polar polymers. In general, for nonpolar polymers, ε' is independent of temperature. However, in the case of polar polymers, the dielectric constant increases with increasing temperature [21]. This behavior is typical of polar dielectrics because dipole orientation is facilitated by increasing the temperature, thus increasing the permittivity. Therefore, the increase in ε' with temperature may be an indication of better movement of dipole molecular chain of polymer thin films at high temperature. Since the dipoles are usually fixed in the dielectric rigidly, therefore the condition of dipoles can not be changed even by the applied electric field at lower temperature. As the temperature increases, the dipoles comparatively become free and they respond to the applied electric field which causes an increase of polarization and consequently dielectric constant with the increase of temperature [22].

7.4.1.2 Variation of Dielectric Loss Factor with Frequency and Temperature

In an ac field, the dielectric constant is a complex quantity, ε^*, and is the combination of a real component, called the relative permittivity or dielectric constant, ε', and an imaginary component, called the dielectric loss or dissipation factor, ε''. This form, also called the complex dielectric constant, is defined by the equation (7.3).

The dielectric constant ε' is sometimes used to describe the stored energy in the materials; on the other hand, the imaginary part of dielectric constant (or loss factor) ε'' is used to describe the dissipation energy. Therefore, as well as the study on the dielectric constant ε', the variation of loss factor ε'' with the frequency and temperature is also an important area of study of the dielectric nature in ac fields.

Figure 7.4.8 represents the imaginary part of the dielectric constant or dielectric loss factor, ε'', as a function of frequency for the PPPy thin films of different thicknesses 400, 450, 500, 550 and 600 nm at room temperatures. From the figure it is seen that the loss factor increases with the decrease of thickness.

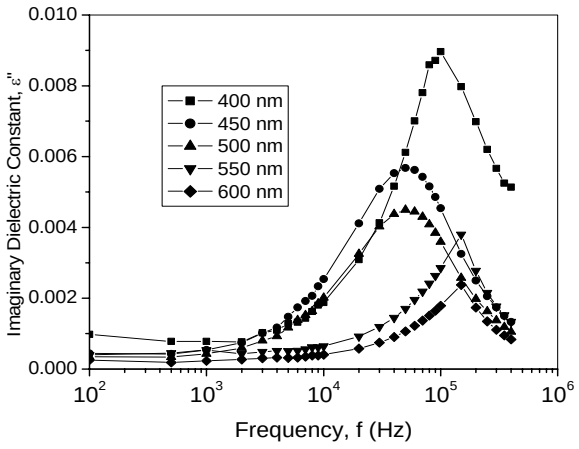

Figure 7.4.8 Variation of dielectric loss factor, ε'', as a function of frequency of the PPPy thin films of different thicknesses at room temperature.

Though the dielectric loss is a bulk property of a material and should not depend on the film thickness, this is, however, an ideal concept and deviation from this are often observed. When the defect structure of the films takes part in the dielectric relaxation process, the loss can be thickness dependent. Due to the deviations from stochiometry, dielectric loss may show strong dependence on the films preparation conditions also. From our study changes of loss factors have been observed with the thickness. This result may be an indication of the presence of dielectric relaxation process. However, deviation from stochiometry in the films of different thickness is also a strong possibility.

Figure 7.4.9 - Figure 7.4.13 show the variation of the dielectric loss factor, ε'', with the frequency of all the samples of thicknesses about 400, 450, 500, 550 and 600 nm respectively at different temperatures 298, 323, 348, 373 and 398 K.

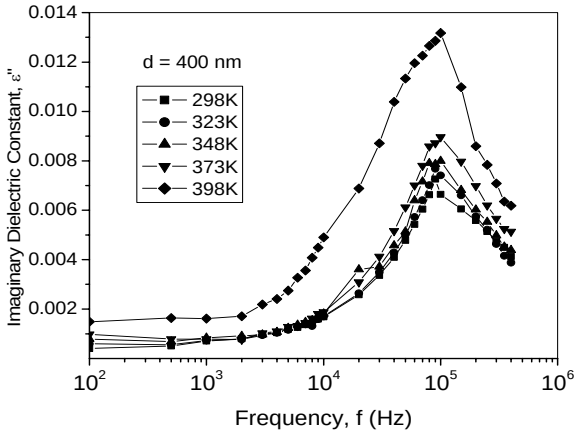

Figure 7.4.9 Variation of dielectric loss factor, ε'', as a function of frequency of the PPPy thin films of thickness 400 nm at different temperatures.

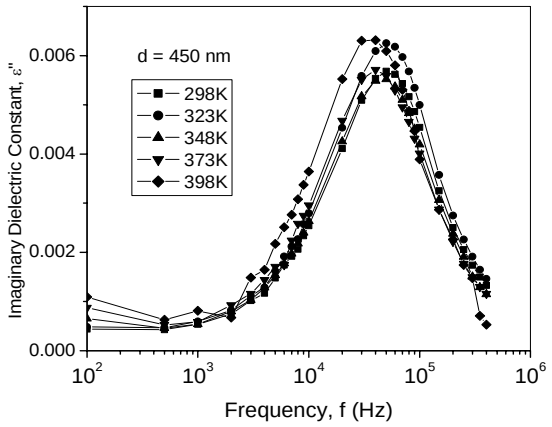

Figure 7.4.10 Variation of dielectric loss factor, ε'', as a function of frequency of the PPPy thin films of thickness 450 nm at different temperatures.

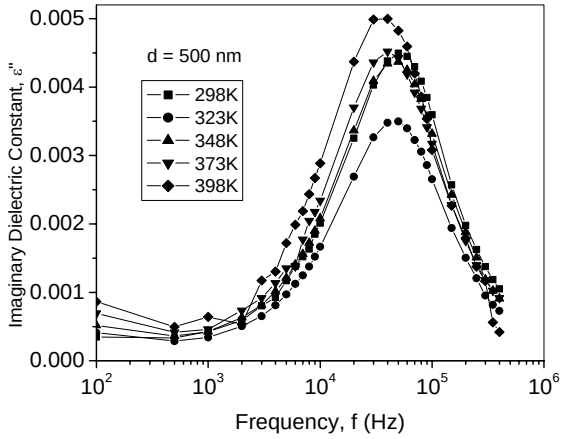

Figure 7.4.11 Variation of dielectric loss factor, ε'', as a function of frequency of the PPPy thin films of thickness 500 nm at different temperatures.

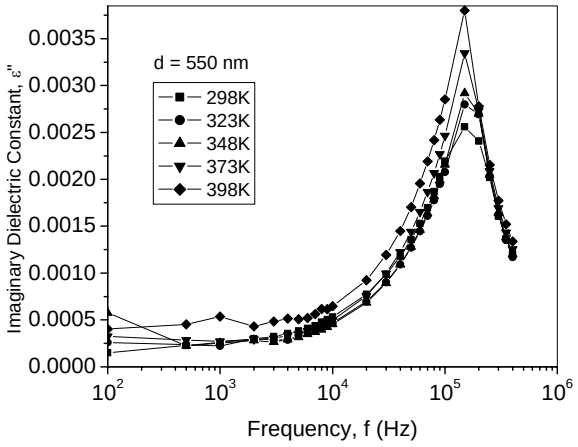

Figure 7.4.12 Variation of dielectric loss factor, ε'', as a function of frequency of the PPPy thin films of thickness 550 nm at different temperatures.

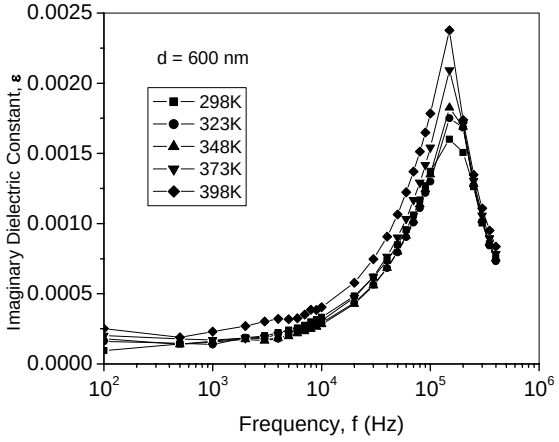

Figure 7.4.13 Variation of dielectric loss factor, ε'', as a function of frequency of the PPPy thin films of thickness 600 nm at different temperatures.

From all the figures (Figures 7.4.9 - 13) It is observed that the ε'' first decreases with rise in frequency in low frequency region followed by a peak in the loss spectra (at about 1kHz) and then increases with the frequency up to a characteristics frequency f_{max} with a sharp peak (at about 100 kHz) and after that decreases again. The increase of ε'' at high frequency, peaking near 100 kHz, is likely due to resonant loss of the dipoles. This is also evident in the decrease of ε'' as dipole rotation cannot keep up at high frequency (> 10^4 Hz). The loss spectra characterized by peak appearing at a characteristic frequency for all the samples suggest the presence of relaxing dipoles in all the samples. The strength and frequency of relaxation depend on characteristic property of dipolar relaxation. Dielectric relaxation is a result of the reorientation process of dipoles in the polymer chains, which show a peak in ε'' spectra. Therefore, the behavior can be attributed to structural rearrangement of the molecule, the α-relaxation process, connected with segment motion in polymers [23]. The dielectric dispersion exhibits dielectric resonance at about 100 kHz and conductive electronic or ionic loss below 100 Hz. The dielectric resonance is consistent with rotational α-type motion of the chains and shows pronounced dispersion, likely due to a distribution of relaxation times.

It is generally believed that dielectric data is characterized by superposition of two processes: a conductivity contribution that produces an increase of both real part ε' and the imaginary part ε'' of the dielectric function on decreasing frequency and a relaxation process exhibiting a maximum in ε'' that shifts higher frequency side with increase in temperature. In our results the contribution from the conductivity is less pronounced and therefore the measured dielectric loss ε'' spectrum could be mainly attributed to the dipolar orientation i.e., to the dielectric polarization processes. However, for polymeric materials the movement of charges from one site to another would perturb the electric potential of the surroundings. Motion of the other charges in this region will be affected by perturb potential. Such a cooperative motion of ions will lead to non-exponential decay, or a conduction processes with distribution of relaxation time [24].

The variation of the dielectric loss factor, ε'' with the temperature at different frequency for the sample of thicknesses about 400 nm is presented in Figure 7.4.14.

From the Figure 7.4.14 an increasing trend of the dielectric loss factor with temperature is observed, especially at low frequency region. At very high frequency, the loss factor is almost independent of temperature. At lower frequencies the increase of loss factor with temperature may be due to more effective chain motion of polymer, whereas at high frequencies, however, the dielectric loss factor is low and remains more or less constant with increasing temperature because the orientation polarization due to chain motion of polymer can not keep phase with the rapidly oscillating electric field.

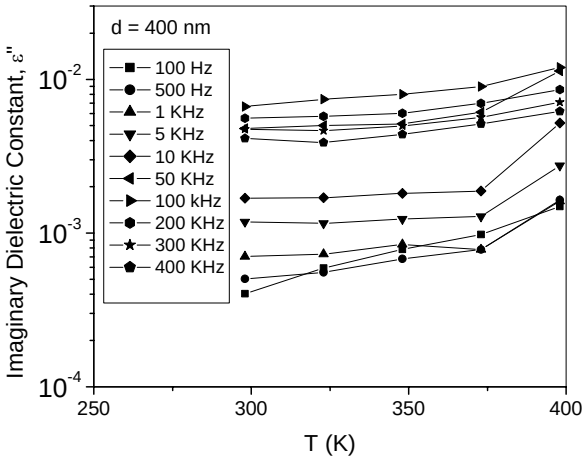

Figure 7.4.14 Variation of dielectric loss factor, ε'', with temperature of the PPPy thin films at different frequency.

An important characteristic of dielectric is the loss tangent, tan δ, is defined by the equation (7.6), namely,

$$\tan\delta = \frac{\varepsilon''}{\varepsilon'} \qquad (7.6)$$

Since ε' is a measurement of energy stored per cycle energy and ε'' is the energy dissipated per cycle, therefore the loss tangent is a measure of the ratio of the electric energy lost to the energy stored in a periodic field. The tan δ, however, is an important characteristic, which indicates the dissipation of energy due to the exponential decay of polarization with time in a dielectric material once the applied field is removed.

Figure 7.4.15 represents the variation of the loss tangent (tanδ) with frequencies for the PPPy thin films of different thicknesses 400, 450, 500, 550 and 600 nm at room temperatures. The dielectric loss peaks are observed at about 100 kHz for samples of low thickness (e.g. 450, 500 nm) and is shifted to higher frequency with increasing thickness (e.g. d = 550nm or 600nm). This may be due to the increased formation of complexity in polymer chains of the films of higher thickness.

According to the defining equation of tanδ, a maximum value of loss tangent at a certain frequency should be observed when ε' has a minimum value i.e. the stored energy at that frequency is minimum. But our results show a different behavior. From all the figures it is observed that at first tanδ decreases slightly with increasing frequency up to a frequency' say f_{min}, then increases with frequency until reaches a maximum value, and thereafter decreases.

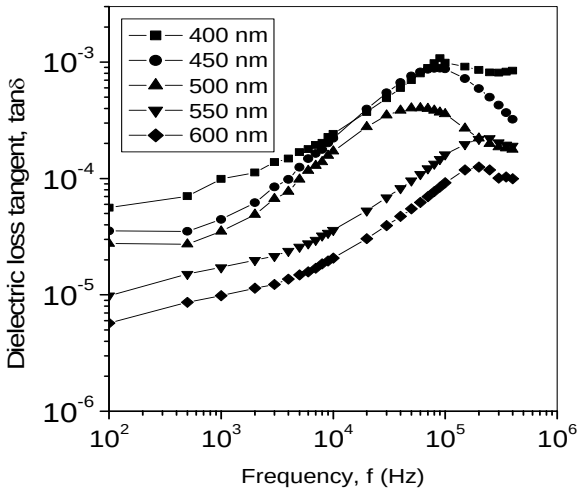

Figure 7.4.15 Variation of loss tangent, tanδ, with frequency of the PPPy thin films of different thicknesses at room temperature.

This type of behavior can be explained in terms of an equivalent circuit model proposed by Goswami and Goswami [11]. In this model the capacitor system is assumed to comprise a frequency independent capacitive element C' in parallel with a discrete temperature resistive element R, both in series with a constant low value resistance *r*. According to this model, loss tangent is given by,

$$\tan\delta = \frac{(1+r/R)}{\omega RC'} + \omega RC' \qquad (7.33)$$

The expression for tanδ according to equation (7.33) predicts a decrease in tanδ with increasing ω, where the term ω^{-1} is dominant for lower frequencies. It is then followed by a loss minimum at

$$\omega_{\min} \cong \frac{1}{C'(rR)^{1/2}} \qquad (7.34)$$

and finally increases with ω above ω_{min}, where the term ω is dominant.

As predicted by equation (7.33) tanδ decreases with increasing frequency until a loss minimum is observed and thereafter it increases with increase in frequency (above f_{min}) at a particular temperature, reaches a maximum value, and thereafter decreases. An increase in tanδ with increasing applied frequency is dominated by resistive losses since the mobile charges contained in the film cannot follow high-frequency electric fields. This loss of energy is associated with the degree of orientation of molecules in addition to the degree of internal friction of the films [25]. At higher frequencies, the very fast periodic reversal of the electric field occurs and no excess ion diffusion would become possible in the direction of the field. Above f_{max} the polar ionization decreases due to the charge accumulation results to a decrease in the value of the loss tangent. Further, the frequency corresponding to maximum loss was found to shift to higher frequencies with increasing temperature. The loss peaks and their shifts with temperature suggest a dielectric relaxation process. Phadke [26] worked

on PP-benzene polymers and reported that since PP-benzene films are strongly cross-linked, the polymer backbones have limited molecular mobility. The increase in tanδ with frequency was then attributed to the introduction of polar impurities in the PP-benzene polymers.

The condition for observing a maximum in tanδ of a dielectric material is given by the relaxation $\omega'\tau \sim 1$, where $\acute{\omega} = 2\pi f_{max}$ and f_{max} is proportional to the hopping probability. The relaxation time τ is a characteristic time constant of the thin films, and $\omega = 2\pi f$. From the figures the relaxation time is found to be approximately equal to constant value which is about 10^{-6}sec for all samples.

It can be seen that (tan δ) increases with increasing temperature and the variation is more pronounced at low frequencies, but it remains almost constant at higher frequency region. The increase in tan δ with temperature is consistent with equation (7.33) as the ω^{-1} term becomes dominant because of the decreasing value of R with temperature.

7.4.1.3 Variation of ac Conductivity with Frequency and Temperature

Figure 7.4.16 represents the plot of the ac conductivity σ_{ac} as a function of the frequency for all the samples of thicknesses about 400, 450, 500, 550 and 600 nm respectively at room temperature. From the figure it is observed that σ_{ac} increases with the decrease of thickness of the films in the same frequency range. This is a similar behavior of dc conductivity σ_{dc}. In the previous chapter, we calculated the dc conductivity over a range of applied voltage and found that σ_{dc} is increased in the films of lower thickness in the same voltage range.

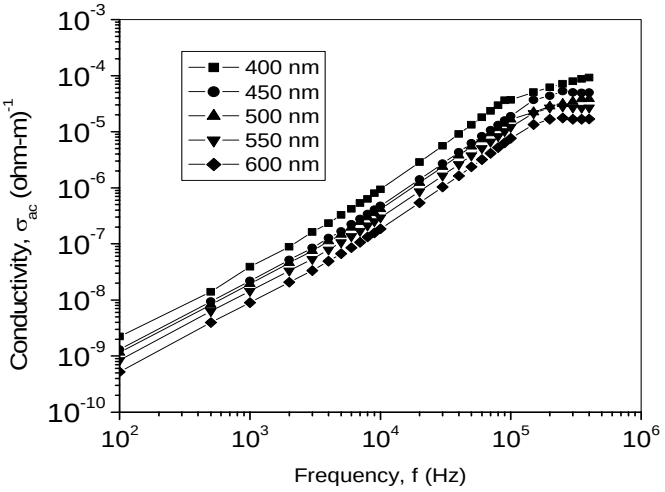

Figure 7.4.16 Plots of ac conductivity σ_{ac} as a function of the frequency for the PPPy films of different thicknesses at room temperatures.

Figure 7.4.17 - Figure 7.4.21 show the variation of the ac conductivity σ_{ac} with the frequency of all the samples of thicknesses about 400, 450, 500, 550 and 600 nm respectively at different temperatures 298, 323, 348, 373 and 398 K.

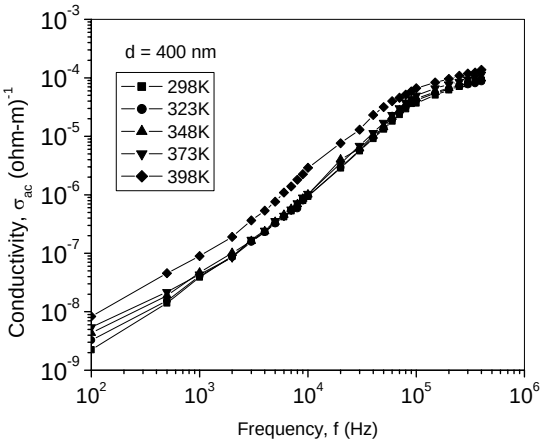

Figure 7.4.17 Plots of ac conductivity σ_{ac} as a function of the frequency for the PPPy films of thicknesses 400 nm at different temperatures.

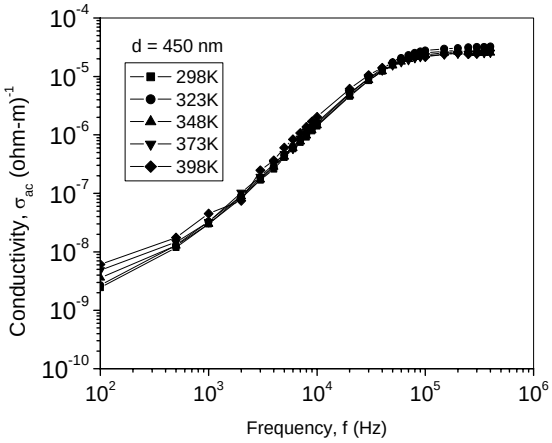

Figure 7.4.18 Plots of ac conductivity σ_{ac} as a function of the frequency for the PPPy films of thicknesses 450 nm at different temperatures.

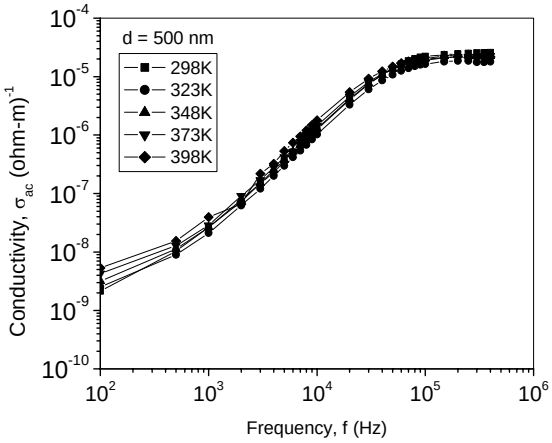

Figure 7.4.19 Plots of ac conductivity σ_{ac} as a function of the frequency for the PPPy films of thicknesses 500 nm at different temperatures.

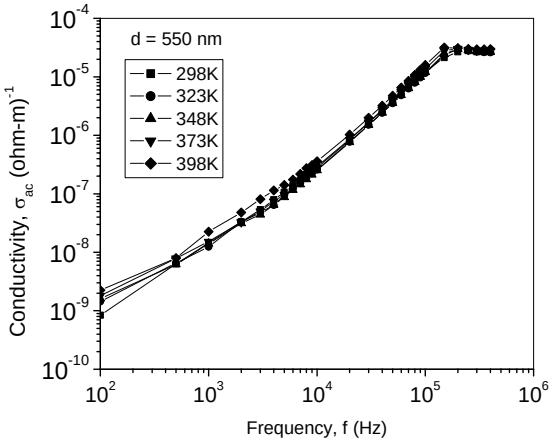

Figure 7.4.20 Plots of ac conductivity σ_{ac} as a function of the frequency for the PPPy films of thicknesses 550 nm at different temperatures.

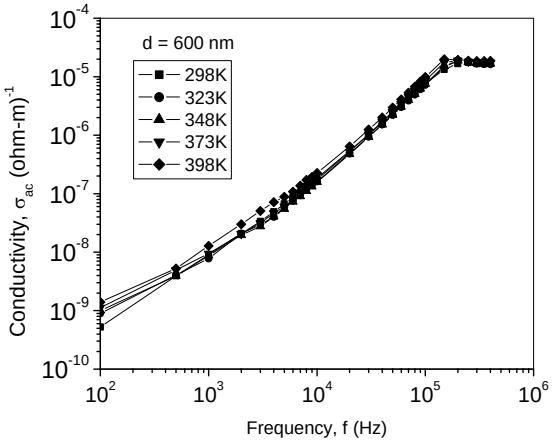

Figure 7.4.21 Plots of ac conductivity σ_{ac} as a function of the frequency for the PPPy films of thicknesses 600 nm at different temperatures.

All the figures (Figures 7.4.17 - 21) show a common pattern of linear behavior, i.e. the ac conductivity σ_{ac} is linear function of the frequency; and an increase of σ_{ac} is observed with increasing frequency. The dependence of ac conductivity, σ_{ac}, on frequency may be described by the power law [8]:

$$\sigma_{ac}(\omega) = A\omega^n \qquad (7.12)$$

where A is a proportonality constant and ω (=2 πf, f is the linear frequency) is the angular frequency and n is the exponent, which generally takes the value less than or equal to unity for Debye type mechanism and is used to understand the conduction/relaxation mechanism in amorphous materials.

For physical convenience, the values of s are usually between 0.4 and 0.8 [8]. The values of n, however, for all the samples for all temperature and frequency ranges have been found to lie in between 0.726 to 0.938, which is close to the values of physical convenience. The results could be attributed to relaxations caused by the motion of electrons or atoms. Such

motion can involve hopping or tunneling between equilibrium sites [27]. By analyzing the observed behavior of the σ_{ac}–f relationship it can therefore be concluded that, the ac conduction mechanism may be due to the hopping or tunneling between equilibrium sites.

However, from the σ_{ac} – frequency figures, it could be noticed that, σ_{ac} increases up to a certain frequency, say f_{max} (~100 kHz), and then becomes constant or sometimes decreases, i.e., for the applied frequency $f > f_{max}$ the conductivity seems to be not affected by the applied external field. This means that the applied frequency is higher than the f_{max} and thus it does not affected the hopping conduction mechanism i.e. for $f > f_{max}$ the applied field obstruct the hopping mechanism and consequently the conductivity remains unaffected or decreases with increasing frequency. It can be therefore concluded that for $f<f_{max}$ the applied field accelerates the charge carriers and the conductivity increases.

The variation of the ac conductivity σ_{ac} with the temperature at different frequency for all the sample of thicknesses about 400 nm is presented in Figure 7.4.22.

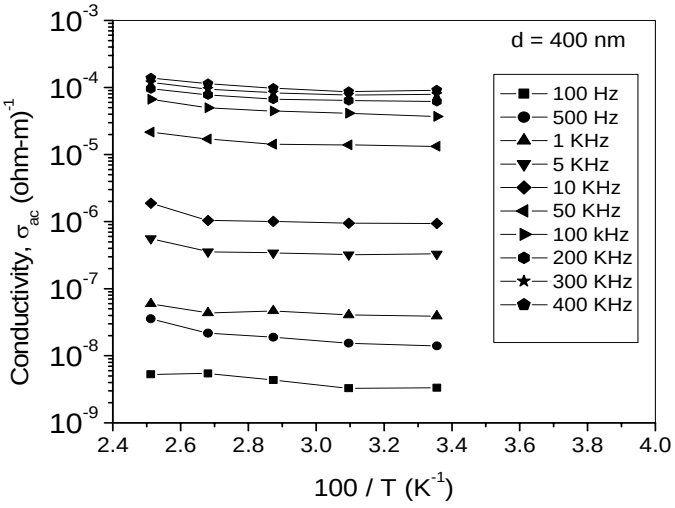

Figure 7.4.22 Variation of ac conductivity σ_{ac} with temperature of the PPPy thin films at different frequency.

In the Figure 7.4.22, the variation of σ_{ac} vs. 1000/T have been studied and a weak dependence of σ_{ac} on temperature is observed. More precisely, it is observed that at higher frequency the conductivity is almost temperature independent, and at low frequency σ_{ac} decreases slightly with the reciprocal of temperature.

The ac conductivity σ_{ac} can be explained in terms of the hopping of electrons between pairs of localized states at the Fermi level. The frequency-dependent σ_{ac} can usually be expressed as the sum of two different conduction mechanisms [28]:

$$\sigma_{ac} = \sigma_{ac}(f) + \sigma_{ac}(s) \qquad (7.35)$$

where $\sigma_{ac}(f)$ represents the relatively weak temperature dependence mechanism which has been interpreted as being due to hopping between localized states at the Fermi level, and $\sigma_{ac}(s)$ represents the stronger temperature dependence component of ac conductivity. Since, in our study, the σ_{ac} is found to be weakly dependent on temperature, therefore $\sigma_{ac}(s)$ can be neglected and only $\sigma_{ac}(f)$ is activated which allow us to interpret the ac conduction mechanism as the hopping between localized states at the Fermi level.

However the activation energy calculated from the curves are found to lie between 0.052 to 0.093 eV, which is very low. The strong dependence of conductivity on frequency and the low activation energies of the carriers are also an indication of a hopping conduction mechanism at low temperatures, and at high temperatures it may be due to the movements of thermally excited carriers from energy levels within the band gap [29].

7.4.2 Plasma Polymerized Pyrroly-N,N,3,5 tetramethylaniline Composite Bilayer Thin Films

7.4.2.1 Variation of Dielectric Constant with Frequency and Temperature

Figure 7.4.23 shows the variation of the ε' with frequency at room temperature for PPPy-PPTMA bilayer composite thin films for all compositions. It is to be noted that, to prepare the PPPy-PPTMA bilayer films, pyrrole-monomer has been used as the mother-material and TMA monomer has been deposited in different deposition time ratio after the pyrrole films were formed. The deposition time-ratios of (PPPy : PPTMA) were (50 min : 10 min), (45 min : 15 min), (40 min : 20 min), (35 min : 25 min) and (30 min :30 min) and corresponding thicknesses of the bilayer thin films were 550, 525, 500, 450 and 400 nm respectively. At room temperature, it is observed that the dielectric constant ε' of bilayer thin films decreases considerably in the same frequency range with the increase of PPTMA in the bilayer structure, which could be explained by the fact that PPTMA thin films has lower ε' than the PPPy thin films for the same thickness and in the same temperature range. This observation can also be stated in terms of PPPy component in the bilayer structure. Since PPPy thin films has higher ε' than that of the PPTMA thin films for the same thickness and in the same temperature range, therefore the increased proportion of PPPy component in the bilayer structure results in a increase of dielectric constant.

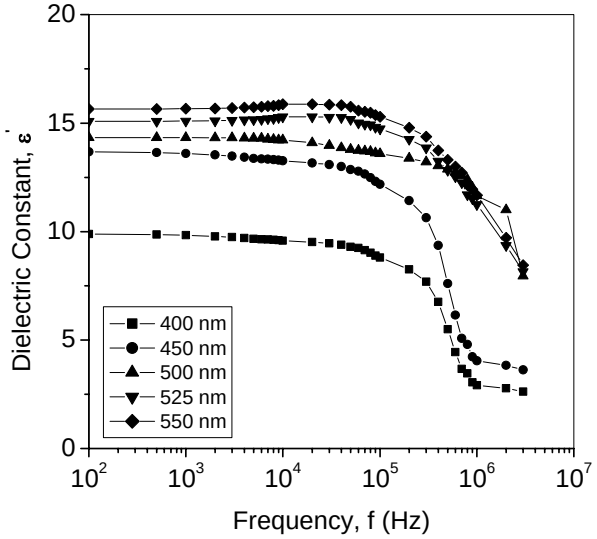

Figure 7.4.23 Dielectric constant, ε', as a function of frequency of the PPPy-PPTMA composite thin films of different thicknesses at room temperatures.

However, the decrease of ε' of bilayer thin films with the increase of PPTMA could also be explained by Maxwell-Wagner two-layered model [9]. A system may not be always homogeneous; there may be some region of non-uniformity and irregularities in the materials. Effects of dielectric properties attributable to material discontinuities are usually called Maxwell-Wagner effect. Complications also often arise at electrodes where contact with the specimen may be incomplete and where entities like discharged ions may form spurious boundary layers. This type of anomalous effect could give misleading results if they are not recognized or avoided.

According to this model the dielectric function depends on the conductivity and permittivity of the two layers. Examining the effect of a field applied across a specimen of two different materials with dielectric constants ε_1', ε_2' and conductivities σ_1, σ_2 respectively, it was found that charges will accumulate in time at the interfaces between layers whenever $\varepsilon_1'\sigma_2 = \varepsilon_2'\sigma_1$.

The dielectric constant arises due to static dielectric permittivity, ε_s, which can be given as

$$\varepsilon_s = C_{gb} / C_0 \qquad (7.36)$$

where ε_s is the static dielectric permittivity, C_{gb} is the grain boundary capacitance and C_0 is the capacitance in the free space. The above equation demonstrates that the dielectric constant mainly depends on the grain boundary capacitance. Probably, the grain size decreases with increasing PPTMA content in the bilayer structure resulting the reduction of grain boundary capacitance gives rise to a decrease in dielectric constant.

However all the phenomena of plasma polymerized bilayer thin films could not be explained by Maxwell-Wagner two-layered model. The strong possibilities of growing polymer-polymer inhomogeneous complex interface in between two polymer thin films might affect the physical properties of bilayer structure. This issue will be discussed in the following section.

Figure 7.4.24 - Figure 7.4.28 show the variation of the dielectric constant ε' with the frequency of all the samples of PPPy-PPTMA composite thin films of thicknesses about 400, 450, 500, 525 and 550 nm respectively at different temperatures 298, 323, 348, 373 and 398K.

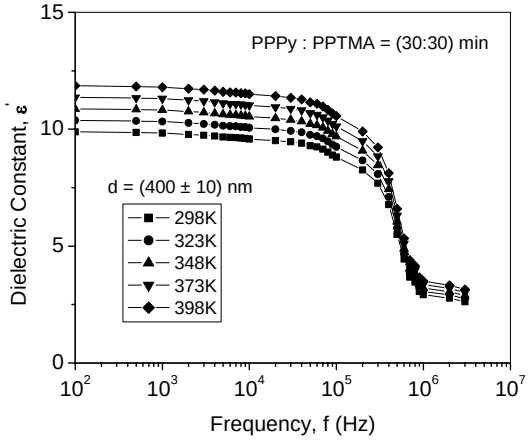

Figure 7.4.24 Dielectric constant, ε', as a function of frequency of the PPPy-PPTMA composite thin films of thickness 400 nm at different temperatures.

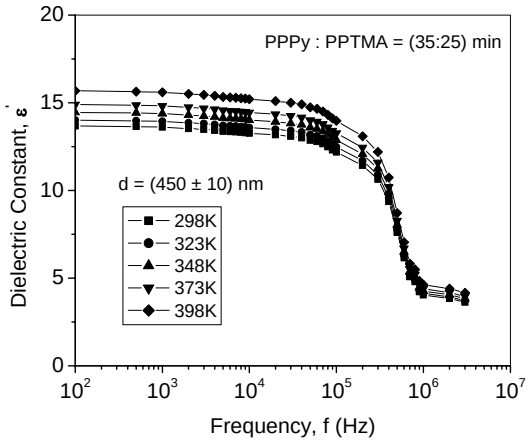

Figure 7.4.25 Dielectric constant, ε', as a function of frequency of the PPPy-PPTMA composite thin films of thickness 450 nm at different temperatures.

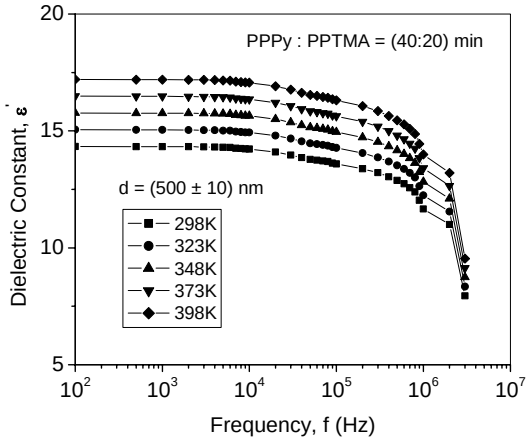

Figure 7.4.26 Dielectric constant, ε', as a function of frequency of the PPPy-PPTMA composite thin films of thickness 500 nm at different temperatures.

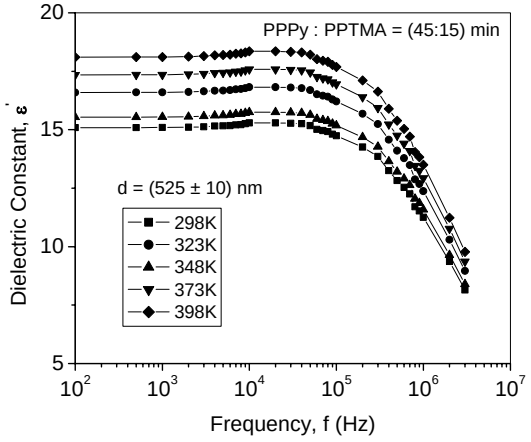

Figure 7.4.27 Dielectric constant, ε', as a function of frequency of the PPPy-PPTMA composite thin films of thickness 525 nm at different temperatures.

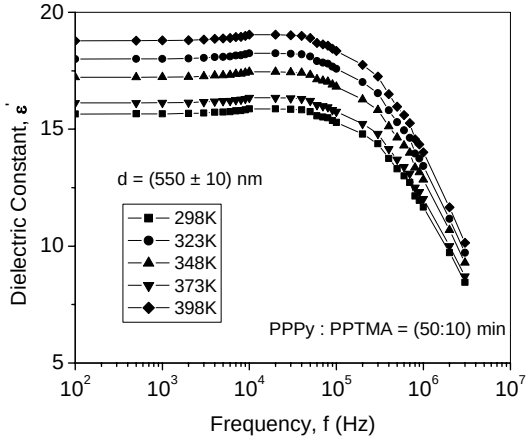

Figure 7.4.28 Dielectric constant, ε', as a function of frequency of the PPPy-PPTMA composite thin films of thickness 550 nm at different temperatures.

From the above figures, a general trend of decreasing ε' with increasing frequency is observed; and the decrease in ε' is very prominent at both high frequencies and high temperature. This is a similar behavior of ε'-f curves for PPPy thin films. The decrease of ε' with increasing frequency, however, is an expected behavior in most dielectric materials, and is usually attributed to the dielectric relaxation process. In a system of inhomogeneous structure, ε' may arise due to interfacial and space charge polarization at frequencies from 100 Hz to few MHz. At lower frequency the dipole can respond rapidly to follow the field and dipole polarization has its maximum value, and therefore higher values of dielectric constant and dielectric loss are usually observed in low frequency region. At higher frequencies dipole polarization has minimum values, since the field cannot induce the dipole moment, and values of ε' attain minimum values.

The variation of ε' with temperature at different frequencies for the PPPy-PPTMA bilayer thin films of thicknesses 400 nm is presented in Figure 7.4.29.

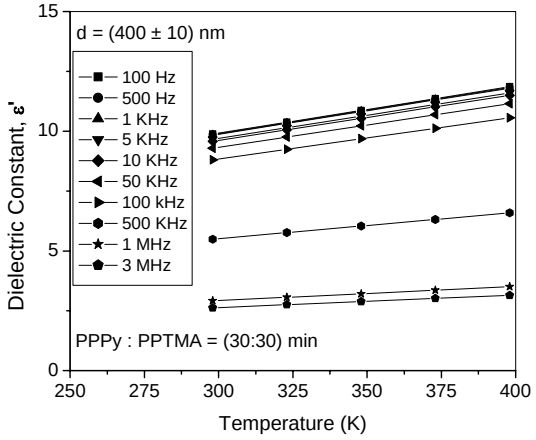

Figure 7.4.29 Variation of dielectric constant, ε', with temperature of the PPPy-PPTMA composite thin films at different frequencies.

.

The figure 7.4.28 shows a slightly different behavior to that of the PPPy and PPTMA thin films. The value of ε' in PPPy-PPTMA bilayer thin films increases with temperature in all frequency region, whereas in PPPy thin films the values of ε' were found to be increased with temperature at lower frequency, but remained constant at higher frequency at all temperature. However, the increase in ε' with temperature is due to greater freedom of movement of dipole molecular chain of polymer films at high temperature. Since the dipoles are usually fixed in the dielectric rigidly, therefore the orientation of dipoles can not be changed even by the applied electric field at lower temperature. As the temperature increases, the dipoles comparatively become free and they respond to the applied electric field which causes an increase of polarization and consequently increase of ε' with the increase of temperature are observed [22].

7.4.2.2 Variation of Dielectric Loss Factor with Frequency and Temperature

Figure 7.4.30 shows the variation of the imaginary part of dielectric constant or loss factor ε'' with frequency at room temperature for PPPy-PPTMA bilayer composite thin films for all composition of thicknesses about 400, 450, 500, 525 and 550 nm respectively at room temperatures.

For all samples, the loss factor has higher value at low frequency which may be due to the free charge motion within the materials. However, with the increase of PPTMA in the bilayer structure, ε'' increases in the lower frequency region reflect the enhancement of mobility of charge carrier.

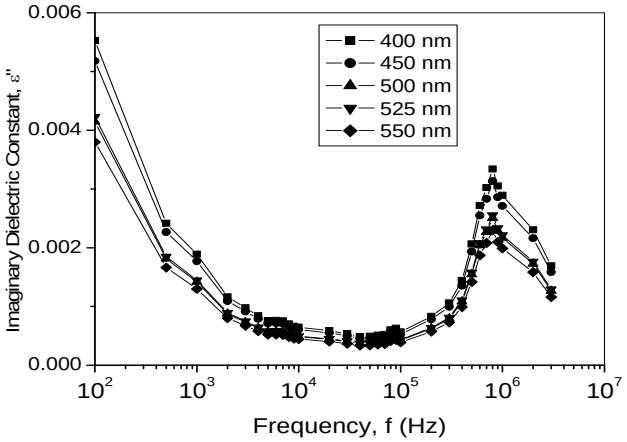

Figure 7.4.30 Variation of dielectric loss factor, ε'', as a function of frequency of the PPPy-PPTMA composite thin films of different thicknesses at room temperature.

The variation of dielectric loss factor ε'' with frequency for all the samples of PPPy-PPTMA bilayer thin films of thicknesses 400, 450, 500, 525 and 550 nm respectively at different temperatures are presented in Figure 7.4.31-7.4.35 respectively.

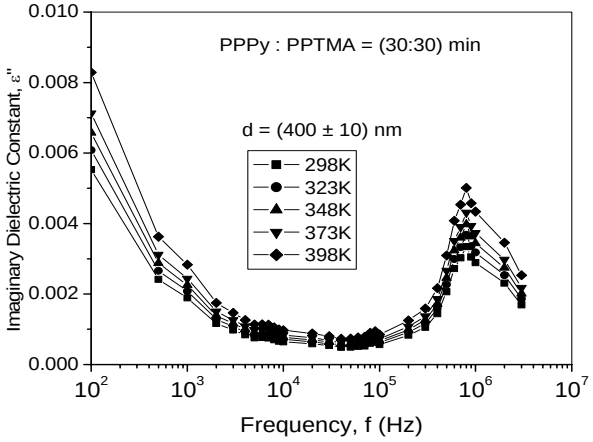

Figure 7.4.31 Variation of dielectric loss factor, ε'', as a function of frequency of the PPPy-PPTMA composite thin films of thickness 400 nm at different temperatures.

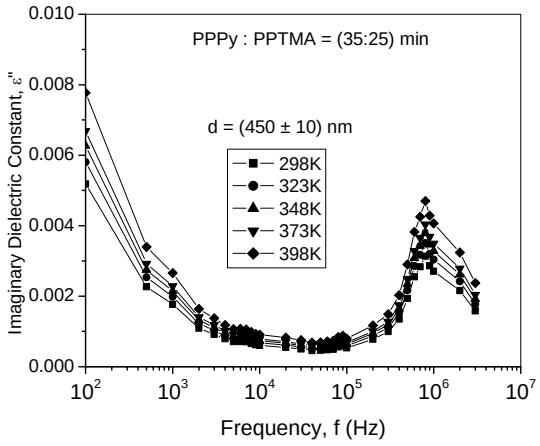

Figure 7.4.32 Variation of dielectric loss factor, ε'', as a function of frequency of the PPPy-PPTMA composite thin films of thickness 450 nm at different temperatures.

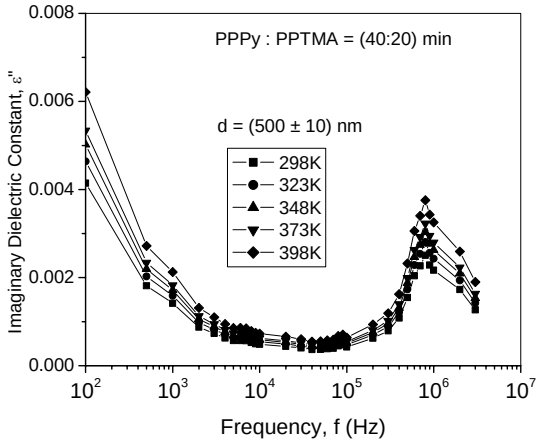

Figure 7.4.33 Variation of dielectric loss factor, ε'', as a function of frequency of the PPPy-PPTMA composite thin films of thickness 500 nm at different temperatures.

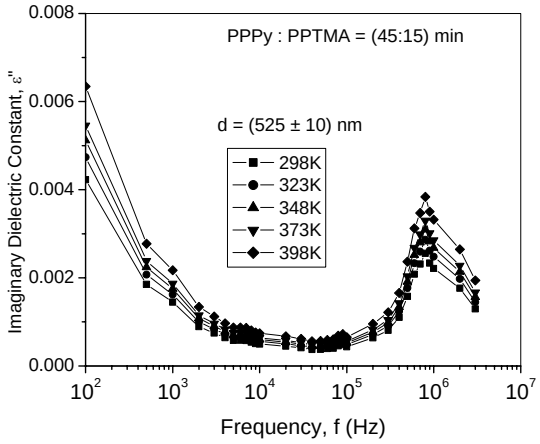

Figure 7.4.34 Variation of dielectric loss factor, ε'', as a function of frequency of the PPPy-PPTMA composite thin films of thickness 525 nm at different temperatures.

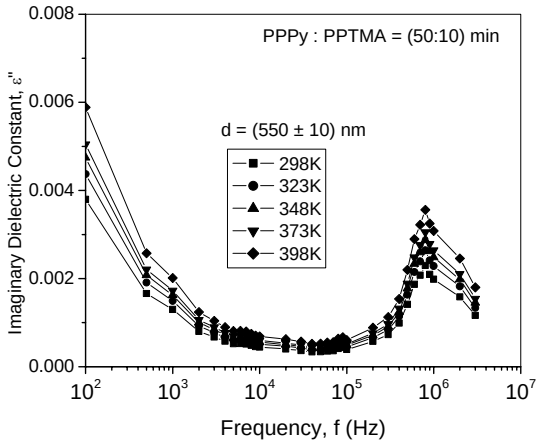

Figure 7.4.35 Variation of dielectric loss factor, ε'', as a function of frequency of the PPPy-PPTMA composite thin films of thickness 550 nm at different temperatures.

From the figures (Figures 7.4.31 - 35), it is observed that at all temperatures, ε'' initially decreases with increasing frequency until a loss minimum is observed and then rises with frequency up to a sharp peak in the loss spectra, and thereafter decreases sharply with the increase of frequency. Since the appearance of peak in the loss factor is attributed to the relaxation phenomena of polymer, therefore there seem to be two relaxations exist in the lower and higher frequencies. The lower one seems to be out of the range of the measurement frequency.

This type of behavior can be explained in terms of an equivalent circuit model proposed by Goswami and Goswami [11], and the behavior of ε'' is predicted by the equation (7.33). It is already discussed that an increase in ε'' with increasing applied frequency is dominated by resistive losses since the mobile charges contained in the film can not follow high-frequency electric fields. This loss of energy is associated with the degree of orientation of molecules in addition to the degree of internal friction of the films [25]. At higher frequencies, the very fast periodic reversal of the electric field occurs and no excess ion diffusion would become possible in the direction of the field. Above f_{max} the polar ionization decreases due to the charge accumulation results to a decrease in the value of the loss factor.

It is, however, is observed that the loss peaks have shifted towards the higher frequency side with the increase of temperature. The dielectric data is characterized by superposition of two processes: *(a)* conductivity contribution that produces an increase of both ε' and ε'' with the decreasing frequency which is not observed in these data; and *(b)* due to relaxation process exhibiting a maximum in ε'' that shifts higher frequency side with increase in temperature, which is usually attributed to dipolar orientation and these results are in agreement to this phenomenon.

Dielectric relaxation is a result of the reorientation process of dipoles in the polymer chains, which show a peak in ε'' spectra. For polymeric materials the movement of ions from one

site to another will perturb the electric potential of the surroundings. Motion of the other charges in this region will be affected by perturb potential. Such a cooperative motion of ions will lead to non-exponential decay, or a conduction processes with distribution of relaxation time [24]. From the Figure of imaginary part of dielectric constant spectra, a relaxation peak is observed in the higher frequency range, suggests that charge motion and polymer segmental motions are strongly coupled manifesting as a single peak in the ε'' spectra.

Figure 7.4.36 shows the variation of dielectric loss factor ε'' with temperature for the samples of PPPy-PPTMA bilayer thin films of thickness 400 nm at different frequency.

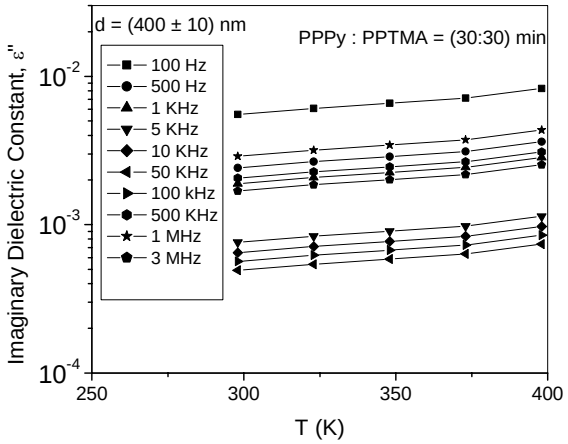

Figure 7.4.36 Variation of dielectric loss factor, ε'', with temperature of the PPPy-PPTMA composite thin films at different frequency.

An overall trend of increasing ε'' with temperature in all frequency range is observed from all the Figure 7.4.36. This result is slightly different than those of the component films, i.e., PPPy and PPTMA, since at very high frequency, the loss factor was found to be almost independent of temperature in those films. However, at lower frequencies the increase of loss factor with temperature can be attributed to the effective chain motion of polymer. At high frequencies, however, the increasing loss factor with increasing temperature might indicate that probably the orientational polarization due to chain motion of bilayer films is able to being in phase with the rapidly oscillating electric field. The increase in loss factor with temperature, however, is consistent with equation (7.33) as the ω^{-1} term becomes dominant because of the decreasing value of R with temperature.

7.4.2.3 Variation of ac Conductivity with Frequency and Temperature

Figure 7.4.37 represents the plot of the ac conductivity σ_{ac} as a function of the frequency for all the compositions for the PPPy-PPTMA composite thin films of thicknesses about 400, 450, 500, 525 and 550 nm respectively at room temperature.

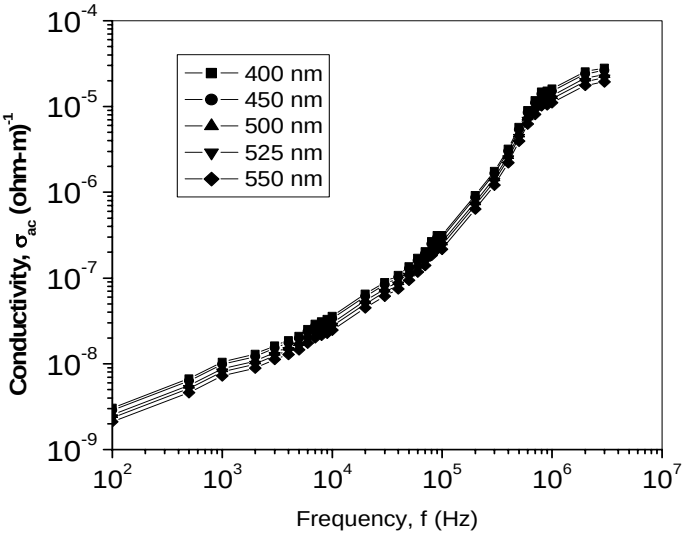

Figure 7.4.37 Plots of ac conductivity σ_{ac} as a function of frequency for the PPPy-PPTMA composite thin films of different thicknesses at room temperatures.

From the figure it is observed that σ_{ac} increases as the proportion of PPTMA in the bilayer structure, as well with the decrease of thickness of the films in the same frequency range. This is a similar behavior of dc conductivity σ_{dc}. In the previous chapter, we calculated the dc conductivity PPPy-PPTMA composite thin films of different compositions over a range of applied voltage and found that σ_{dc} is increased in the composite bilayer films of with the increase of PPTMA.

Figure 7.4.38 - Figure 7.4.42 show the variation of σ_{ac} with the frequency for all the compositions for the PPPy-PPTMA composite thin films of thicknesses about 400, 450, 500, 525 and 550 nm respectively at different temperatures 298, 323, 348, 373 and 398 K.

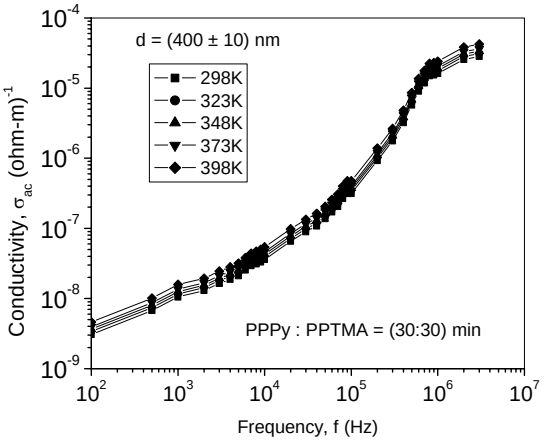

Figure 7.4.38 Plots of ac conductivity σ_{ac} as a function of the frequency for the PPPy-PPTMA composite thin films of thicknesses 400 nm at different temperatures.

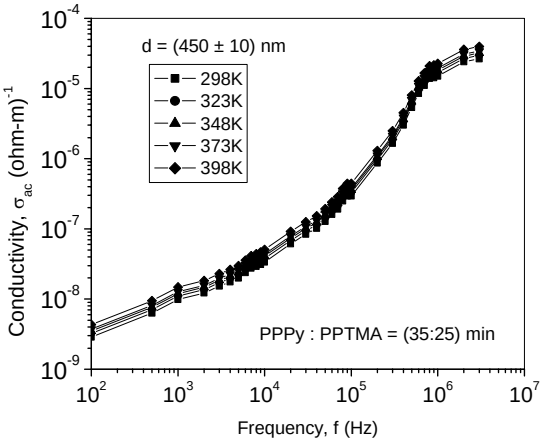

Figure 7.4.39 Plots of ac conductivity σ_{ac} as a function of the frequency for the PPPy-PPTMA composite thin films of thicknesses 450 nm at different temperatures.

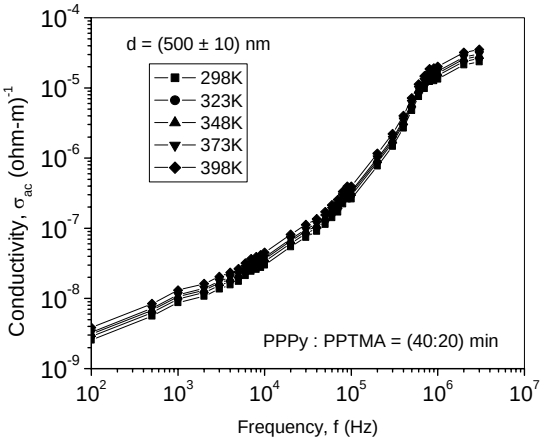

Figure 7.4.40 Plots of ac conductivity σ_{ac} as a function of the frequency for the PPPy-PPTMA composite thin films of thicknesses 500 nm at different temperatures.

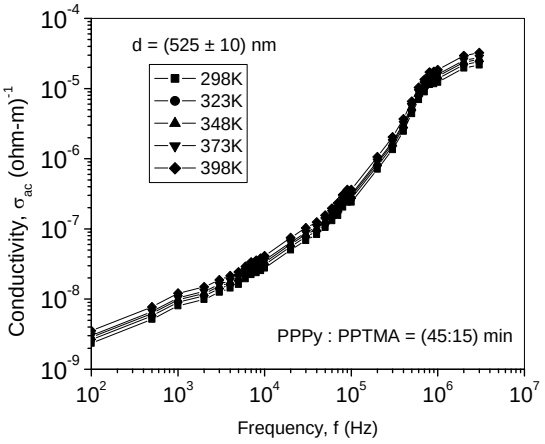

Figure 7.4.41 Plots of ac conductivity σ_{ac} as a function of the frequency for the PPPy-PPTMA composite thin films of thicknesses 525 nm at different temperatures.

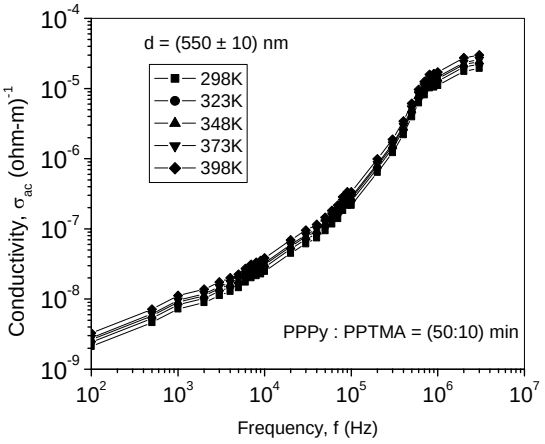

Figure 7.4.42 Plots of ac conductivity σ_{ac} as a function of the frequency for the PPPy-PPTMA composite thin films of thicknesses 550 nm at different temperatures.

All the figures (Figure 7.4.38 - Figure 7.4.42) show a common behavior that the ac conductivity σ_{ac} is linear function of the frequency; and like PPPy and PPTMA thin films, an increase of σ_{ac} is observed with increasing frequency. The dependence of ac conductivity, σ_{ac}, on frequency may be described by the power law [8]:

$$\sigma_{ac}(\omega) = A\omega^{n} \qquad (7.12)$$

where A is a proportonality constant and ω (=2 πf, f is the linear frequency) is the angular frequency and n is the exponent, which generally takes the value less than or equal to unity for Debye type mechanism and is used to understand the conduction/relaxation mechanism in amorphous materials.

For physical convenience, the values of *n* are usually between 0.4 and 0.8 [13]. The values of n, however, for all the samples for all temperature and frequency ranges have been found to lie in between 0.726 to 0.938, which is close to the values of physical convenience. The types of results are usually attributed to the dielectric relaxations caused by the motion of charges or atoms. Such motion can involve hopping or tunneling between equilibrium sites [27]. By analyzing the observed behavior of the σ_{ac} –frequency relationship it can therefore be concluded that, the ac conduction mechanism may be due to the hopping of electrons between pairs of localized states at the Fermi level.

However, from the σ_{ac} – frequency figures, it could be noticed that, σ_{ac} increases up to a certain frequency, say f_{max} (~100 kHz), and then becomes constant or sometimes decreases, i.e., for the applied frequency $f > f_{max}$ the conductivity seems to be not affected by the applied external field. This means that the applied frequency is higher than the f_{max} and thus it does not affected the hopping conduction mechanism i.e. for $f > f_{max}$ the applied field obstruct the hopping mechanism and consequently the conductivity remains unaffected or decreases with increasing frequency. It can be therefore concluded that for $f<f_{max}$ the applied field accelerates the charge carriers and the conductivity increases.

The variation of the ac conductivity σ_{ac} with the temperature at different frequency of the sample of thickness at about 400 nm is presented in Figure 7.4.43 and a weak dependence of σ_{ac} on temperature in the both (high and low) frequency range is observed..

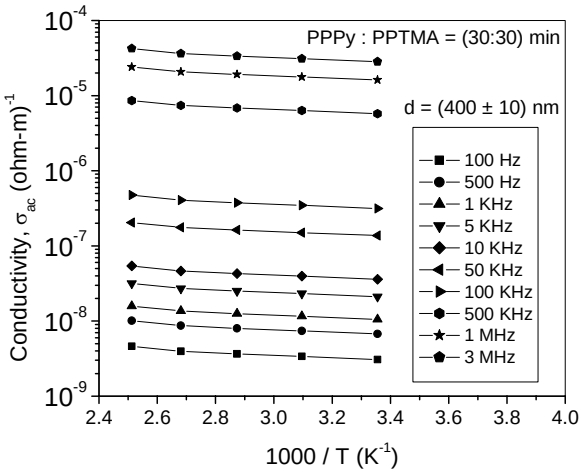

Figure 7.4.43 Variation of ac conductivity σ_{ac} with temperature of the PPPy-PPTMA composite thin films at different frequency.

The ac conductivity σ_{ac} can be explained in terms of the hopping of electrons between pairs of localized states at the Fermi level. The frequency-dependent σ_{ac} can usually be expressed as the sum of two different conduction mechanisms [28]:

$$\sigma_{ac} = \sigma_{ac}(f) + \sigma_{ac}(s) \qquad (7.37)$$

where $\sigma_{ac}(f)$ represents the relatively weak temperature dependence mechanism which has been interpreted as being due to hopping between localized states at the Fermi level, and $\sigma_{ac}(s)$ represents the stronger temperature dependence component of ac conductivity. Since, in our study, the σ_{ac} is found to be weakly dependent on temperature, therefore $\sigma_{ac}(s)$ can be neglected and only $\sigma_{ac}(f)$ is activated which allow us to interpret the ac conduction mechanism as the hopping between localized states at the Fermi level.

7.4.2.4 Comparative Study of Dielectric Properties and ac Conductivity

For a comparative study, the dielectric constant, ε', as a function of the frequency for the, PPPy, PPTMA and PPPy-PPTMA bilayer composite thin films of thickness about 450 nm at room temperature are presented in Figure 7.4.44. It is seen from the figure that the PPPy-PPTMA bilayer thin films have much higher value of ε' compared to those of its component thin films.

It is known that a low-ε' dielectric has low ability to polarize and hold charge, a high-ε' dielectric, on the other hand, has a high permittivity and is good at holding charge. Generally, substances with high dielectric constants break down more easily when subjected

to intense electric fields, than do materials with low dielectric constants. From the comparative study, it can thus be concluded that the PPPy-PPTMA bilayer thin films has higher ability to polarize and hold charge than that of its component thin films, and therefore the bilayer films could be more preferable dielectric for capacitors or for memory cells that store digital data in the form of charge.

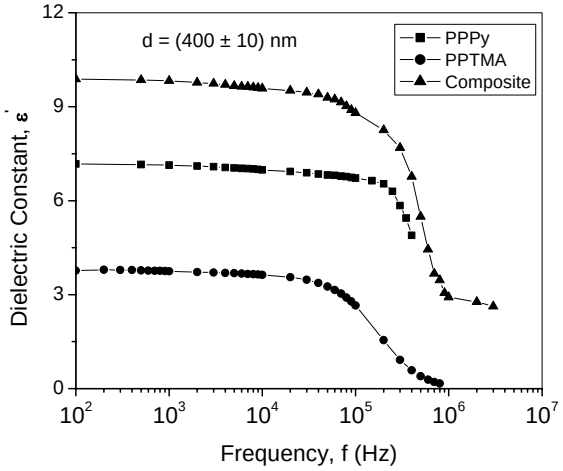

Figure 7.4.44 The dielectric constant, ε', as a function of the frequency for the, PPPy, PPTMA and PPPy-PPTMA composite thin films of thickness about 450 nm at room temperature.

In Figure 7.4.45, the dielectric loss factor, ε'', as a function of the frequency for the, PPPy, PPTMA and PPPy-PPTMA composite bilayer thin films of thickness about 450 nm at room temperature has been plotted.

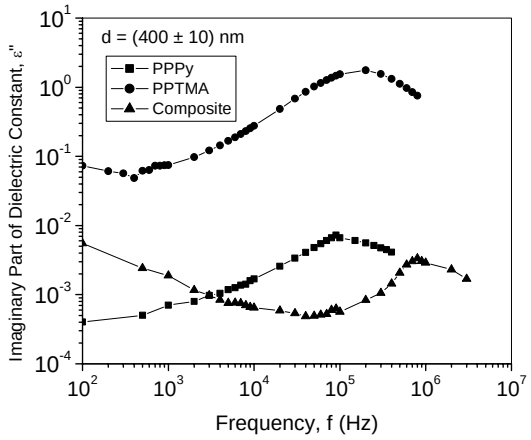

Figure 7.4.45 The dielectric loss factor, ε'', as a function of the frequency for the, PPPy, PPTMA and PPPy-PPTMA composite thin films of thickness about 450 nm at room temperature.

Comparing Figures 7.4.44 and 7.4.45, it could be seen that PPTMA thin film has lower values of ε' but higher values of ε'' compared to other thin films at any particular frequency.

PPPy-PPTMA bilayer thin film, on the other hand, show opposite character, i.e., bilayer film has higher values of ε' but lower values of ε''. Since ε' is a measurement of energy stored per cycle and ε'' is the energy dissipated per cycle, therefore from this observation it could be concluded that in the bilayer thin films more energy is stored but rate of energy dissipation is lower than that of its component thin films.

The loss spectra characterized by peak appearing at a characteristic frequency for all the samples suggest the presence of relaxing dipoles in all the samples. The strength and frequency of relaxation depend on characteristic property of dipolar relaxation. It is seen that the high frequency relaxation peak shifts to the higher frequency, and at the lower frequency side, a relaxation peak seems to appear just below the lowest frequency used in this study. Thus it can be concluded that both the loss peaks shift to the high frequency in the bilayer composite thin films compared to its components. The shifting of loss peaks towards the higher frequency is an indication of reducing the relaxation time in the bilayer thin films. This behavior may be due to an increase in the amorphous content in the bilayer structure.

In the amorphous regions, the chains are irregular and entangled, whereas they are arranged regularly in the crystalline regions. Hence, it is much easier to move the molecular chains in the amorphous state than in the crystalline state. The molecular packing in the amorphous state is weak and so the density is lower than it is in crystalline regions. Thus, the chains in the amorphous phase are more flexible and are capable of orienting themselves relatively easily and rapidly. The dipoles in the side chain of the polymer orient themselves with certain frequencies governed by the elastic restoring force which binds the dipoles to their equilibrium positions and the rotational frictional forces exerted by neighboring dipoles. In the amorphous phase, dipolar molecules should be able to orient from one equilibrium position to another relatively easily, and contribute to absorption over a wide frequency or temperature range [30].

Figure 7.4.46 shows the ac conductivity σ_{ac} as a function of the frequency for the, PPPy, PPTMA and PPPy-PPTMA bilayer composite thin films of thickness about 450 nm at room temperature. It is seen that the bilayer thin film has lower σ_{ac} than those of its component films over whole frequency range. This is a similar behavior of dc conductivity σ_{dc}. In the chapter 6, it is discussed that PPPy-PPTMA composite thin films have lower values of σ_{dc} than that of its component films for a certain thickness.

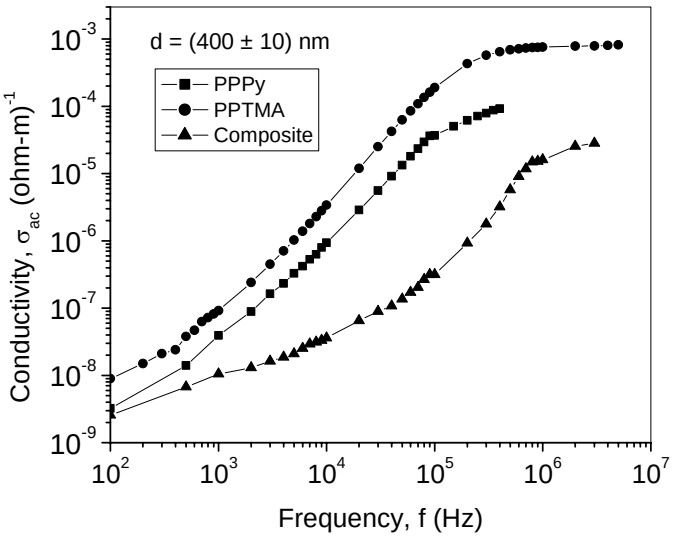

Figure 7.4.46 The ac conductivity σ_{ac} as a function of the frequency for the, PPPy, PPTMA and PPPy-PPTMA composite thin films of thickness about 450 nm at room temperature.

The total conductivity of the composite thin films, however, may depend on the microscopic and macroscopic conductivities. The microscopic conductivity depends upon the doping level, conjugation length or chain length etc, whereas the macroscopic conductivity depends on the inhomogeneities in the composites, compactness of pellets, orientation of microparticles etc. In the present system, the individual thin films were deposited one over the other to prepare the PPPy-PPTMA bilayer thin films, which may give rise to a system with polymer-polymer complex interface, i.e., the interface between the PPPy and PPTMA thin films may not be homogeneous and therefore there are some possibilities of presence of irregularities in the interface. It should be noted that in most inhomogeneous polymeric systems, the electronic conductivity is affected by this interface. So the microscopic conductivities remain almost the same but the physical (macroscopic) properties viz. compactness and molecular orientations, may significantly vary due to the complex polymer interface. This disorderness decreases the compactness and molecular orientations leading to a decrease in resultant conductivity.

7.5 Conclusions

From the behavioral characteristics of the ε' as a function of frequency for PPPy, PPTMA and PPPy-PPTMA bilayer composite thin films, it is observed that at the low frequencies, the dielectric constant for all the samples are almost independent of frequency, but at high frequencies the decrease in ε' is very prominent. The decrease of ε' with frequency is usually attributed to the electrical relaxation processes and multi-component contribution of

polarizability of the polar materials. The observed frequency dependence of the dielectric constant in this study is probably due to the interfacial or space charge polarization, which is usually observed in sandwich type configurations. The other relaxation processes can also be superimposed with this polarization; e.g. the orientational polarization of molecular chains. Since the orientation polarization depends upon the molecular arrangement of dielectric and at higher frequencies, the rotational motion of the polar molecules of dielectric is not sufficiently rapid for the attainment of equilibrium with the field. The orientational polarization is therefore decreased with increasing frequencies which in turns results in a decrease of dielectric constant with increasing frequency.

However, the ε' shows a temperature dependence and the rate of variation is found to be different at different frequencies. It is observed that at high frequencies, ε' remains almost constant with increasing temperature, but at low frequencies it increases with increasing temperature. The strong temperature dependence of ε' at higher temperature and lower frequencies is attributed to the thermally activated electron hopping mechanism.

It is observed that the ε'' increases with the frequency up to a characteristics frequency f_{max} with a sharp peak and after that decreases. The loss spectra characterized by peak appearing at a characteristic frequency for all the samples suggest the presence of relaxing dipoles in all the samples and the behavior has been attributed to structural rearrangement of the molecule, the α-relaxation process, connected with segment motion in polymers

The temperature dependence of the ε'' at different frequencies has shown an increasing trend of the ε'' with temperature, especially at low frequency region. At very high frequency, the loss factor is almost independent of temperature. At lower frequencies the increase of loss factor with temperature may be due to more effective chain motion of polymer,

The variation of the σ_{ac} with the frequency show a common pattern of linear behavior, i.e. the ac conductivity σ_{ac} is linear function of the frequency. The results have been attributed to the relaxations caused by the motion of electrons or atoms, which could involve hopping or tunneling between equilibrium sites. By analyzing the observed behavior of the σ_{ac}–f relationship it has been therefore concluded that, the ac conduction mechanism may be due to hopping.

In a comparative study of the dielectric properties PPPy, PPTMA and PPPy-PPTMA bilayer composite thin films of nearly same thickness of about 450 nm it is seen that the bilayer thin film has higher value of ε' compared to those of its component thin films. This result implies that bilayer thin films has higher ability to polarize and hold charge than those of its component thin films, and therefore the bilayer films could be more preferable dielectric for

capacitors or for memory cells that store digital data in the form of charge. Moreover, since bilayer film has higher values of ε' but lower values of ε'' at a particular frequency, therefore it has been concluded that in the bilayer thin films more energy is stored but rate of energy dissipation is lower than that of its component thin films. It is also observed that the dielectric loss peaks of bilayer thin films shift towards the higher frequency, which is an indication of reducing the relaxation time. This behavior may be due to an increase in the amorphous content in the bilayer structure.

The σ_{ac} of the bilayer thin film has been found to have lower values than those of its component films over whole frequency range, which is a similar behavior of σ_{dc}. During the formation of bilayer thin films by plasma polymerization, a system with polymer-polymer complex interface might br grown up in between the PPPy and PPTMA thin films. This interface may not be homogeneous and therefore there are some possibilities of presence of irregularities in the interface and in most inhomogeneous polymeric systems, the electronic conductivity is affected by this interface. It is known that the total conductivity of the composite thin films, however, may depend on both the microscopic and macroscopic conductivities. The microscopic conductivity depends upon the doping level, conjugation length or chain length, etc. whereas the macroscopic conductivity depends on the inhomogeneities in the composites, compactness of pellets, orientation of microparticles etc. Therefore in this system the resultant conductivity may significantly vary due to the complex polymer-polymer interface, and the disorderness of the interface may cause a decrease in the conductivity of the bilayer thin films.

References

[1] Elliott, S. R., *A theory of A.C. conductivity in chalcogenide glasses*, Philosophical Magazine, 36, 1291–1304, 1977.

[2] Yasuda, H., *Plasma Polymerization*, Academic Press, New York, 1985.

[3] Debye, P., *Polar Molecules*, Dover Publications, New York, 1929.

[4] Sultan, P. M., J. Am. Ceram. Soc., 47, 188, 1964.

[5] Mahalingam, T., Radhakrishna, M., Balasubrahmanian, C., Thin Solid Films 59, 231, 1979.

[6] Serghei, A., Tress, M., and Kremer, F., Macromolecules, 39, 9385, 2006.

[7] Donth, E., Huth, H., and Beiner, M., J. Phys.: Condens. Matter, 13, 451, 2001.

[8] Mott, N. F., and. Davis, E. A, *Electronic Processes in Non-Crystalline Materials*, Clarendon Press, Oxford, 1979.

[9] Blythe, A. R., *Electrical Properties of Polymers*, Cambridge University, Press, Cambridge, London, 1979

[10] Cole, K. S., and Cole, R. H., J. Chem. Phys., 9, 341, 1949.

[11] Goswami, A., and Goswami, A. P., Thin Solid Films 16, 175, 1973.

[12] Havriliak, S., and Negami, S. J., Polym. Sci. C, 14, 99, 1966.

[13] Boltzmann, L., *Akad. Wissenschaft, Wien.* 1874.

[14] Hopkinson, J., *Original Papers*. Cambridge University Press, Cambridge, 1901.

[151] Liang, T., Makita, Y., Kimura, S., *Effect of film thickness on the electrical properties of polyimide thin films*, Polymer 42, 4867- 4872, 2001.

[16] Despotopoulou, A. M., Miller, R. D., Rabolt, J. F., Frank, C. W., J. Polym. Sci. Part B 34, 2335, 1996.

[17] Smyth, C. P., *Dielectric behavior and Structure*, McGraw Hill, New York, 1955.

[18] M. Barsoum, *Fundamentals of Ceramics*, Mc Graw-Hill, New York 1977.

[19] Dutta, C. R., and Barua, K., Thin Solid Films, 100, 149, 1983.

[20] Long A. R., and Hogg, W. R., J .of Non-Cryst. Solids; 59-60, 1095, 1983.

[21] Tareev, B., *Physics of Dielectric Materials*, MIR Publications, Moscow, 1979.

[22] Frohlick, H., *Theory of Dielectrics*, Oxford University press, Oxford, 1956.

[23] Nakagawa, K ., and Ishida. Y., J. Polym. Sci., Polym. Phys. Ed., 11, 1503, 1973.

[24] Fu, Y., Pathmanathan, K., and Steven, J. R., J. Chem. Phys. 94, 6326, 1991.

[25] Biloiu, C., Biloiu, I. A., Sakai, Y., Sugawara, H., Ohta, A.., J. Vac. Sci. Technol., A 22, 1158, 2004.

[26] Phadke, S. D., Thin Solid Films 48, 319, 1978.

[27] Elliott, S. R., Adv. Phys., 36 (2), 135, 1987.

[28] Rockstad, H. K., J. Non-Cryst. Solids 8-10, 621, 1972.

[29] Chowdhury, F.-U.Z., and Bhuiyan, A. H., *Dielectric properties of plasma polymerized diphenyl thin films*, Thin Solid Films 370, 78-84, 2000.

[30] Rastogi, R. C., Chopra, K. L., Thin Solid Films 27, 311, 1975.

Chapter 8

Conclusions

This chapter summarizes the experimental results
that have been found during the characterization of plasma polymerized thin films
and includes the suggestion for the future research work.

8.1 Conclusions

A parallel plate capacitively coupled glow discharge reactor was used to prepare PPPy, PPTMA and PPPy-PPTMA bilayer composite thin films at room temperature onto glass substrates. To deposit the PPPy-PPTMA bilayer composite thin films, pyrrole-monomer has been used as the parent-material and TMA monomer has been deposited in different deposition time ratio after the pyrrole thin films were grown. The deposition time-ratios of (PPPy : PPTMA) were (50min :10min), (45min :15min), (40min :20min), (35min : 25min) and (30min : 30min). Different time-ratios of the monomer have produced the bilayer composite thin films with different thicknesses.

The FTIR spectra of pyrrole monomer and PPPy have indicated that the monomer has undergone the re-organization during the plasma polymerization. It is reported that the PPTMA film does not exactly resemble to that of the TMA structure. Finally, comparison between PPPy, PPTMA and PPPy-PPTMA has shown that the bilayer composite thin films contain the characteristics of both the monomers.

From the DTA and TGA traces it is observed that PPPy, PPTMA and PPPy-PPTMA lose approximately 23%, 28% and 40% of their initial mass at 550, 650 and 450 C. The weight loss in PPPy-PPTMA is much higher than those of its components even at relatively lower temperature. This behavior suggests that less breakdown thermal energy is needed for PPPy-PPTMA than those of its components. The significant loss in the mass in PPPy-PPTMA bilayer thin films suggests that in the bilayer structure the bonds require less thermal energy to be dissociated in comparison to the bonds formed among the PPPy and PPTMA chains, which need greater thermal energy to dissociate the bonds.

From the optical characterization it is observed that the absorption peak intensity increases and broadens with increasing thickness of all types of thin films. A red shift of about 20 nm for PPPy is observed with respect to the pyrrole monomer and a red shift of about 79 nm for PPTMA with respect to the TMA monomer is reported, which indicate the presence of an increased degree of conjugation in the resulting films.

The absorption coefficient, α, show a general trend that the thin films of lower thickness have higher values of α, which indicates that in the films of lower thickness the intensity of light is reduced more. A similar trend is observed in the plots of extinction co-efficient, k, as a function of $h\nu$. It was seen that the film of lower thickness has higher value of k, which indicates that the light is more attenuated in the films of lower thicknesses than that of the

films of higher thicknesses and the probability of raising the electron transfers across the mobility gap with the photon energy is higher in the films of lower thicknesses. From the comparative study of PPPy, PPTMA and PPPy-PPTMA bilayer thin films of same thickness, it is however observed that the PPTMA thin film have higher values of both α and k than those of the PPPy and PPPy-PPTMA bilayer thin films. This result indicates that intensity of light is more reduced and more attenuated in PPTMA films those of other films, even if the thickness of the different types of films remains same. Moreover, the probability of raising the electron transfers across the mobility gap with particular photon energy is higher in PPTMA thin films than that of other films, which might cause higher conductivity PPTMA thin films than that of both PPPy and PPPy-PPTMA bilayer composite thin films.

Another important result is that both the E_{qd} and E_{qi} are observed to be decreased with the decrease of the thicknesses for all types of films, which is an indication of increasing the conductivity of the film of lower thickness. It is also observed that the energy gaps of the PPPy-PPTMA bilayer films are higher compared to those of the PPPy and PPTMA thin films which indicates a lower conductivity of the bilayer composite thin films that those of its component films. The change in the conductivity suggests a probable change in physical properties during the formation of the plasma polymerized thin films. In this system there may give rise to a system with polymer–polymer complex interface during the formation of bilayer composite structure which might be inhomogeneous and irregular in nature. This inhomogeneity of the interface may give rise to a higher resistivity in bilayer composite thin films. Moreover, during the subsequent formation of the films by plasma polymerization, there might be adsorbed and/or trapped oxygen of the interface in between the PPPy and PPTMA thin film layers, which is indicated in the FTIR spectra of the films. The oxidation of the interface of the bilayer might affect the physical properties of the bilayer thin films. The increase of optical band gap may be due to this reason.

The *J-V* characteristics of PPPy, PPTMA and PPPy-PPTMA bilayer thin films have shown a general trend that the current conduction is higher in the films of lower thickness than that of the higher-thickness films at the same voltage. This difference in the conductivity for different thicknesses suggests a probable change in physical properties during the formation of the plasma polymerized thin films. The most probable reason of this behavior may be due to better morphological characteristics of the films of lower thickness. The film morphology is highly thickness dependent, and better morphology (lower roughness) is usually observed for smaller thickness, which causes increased charge mobility. Thinner films present more structural order due to more homogeneous surfaces, decreased grain size and improve interchain conduction, and as a result, an increased conductivity could be observed.

The J-V characteristics were characterized by two different slopes in the lower and higher voltage regions. The slopes at lower voltage region indicated a probable Ohmic conduction, while at higher voltages a non-ohmic conduction was observed. This complex conduction behavior was explained in terms Schottky–Richardson mechanism, Poole–Frenkel mechanism, tunneling or Fowler–Nordheim mechanism and space charge limited conduction mechanism, and it was found that the current conduction in PPPy, PPTMA and PPPy-PPTMA bilayer thin films follow a SCL conduction mechanism.

The free charge carriers' density N, the trap density, N_t and the mobility of the charge carriers μ, were calculated from the conduction data and it was observed that all the calculated quantities had higher values for lower thickness and gradually decreased with the increase of the thicknesses. The higher values of N and μ for lower thicknesses confirm our observation that the conductivity of the films with lower thickness is higher than that of the films of higher thickness.

From the J-V characteristics of PPPy-PPTMA bilayer thin films, it is observed that the current conduction is increased with an increased proportion of PPTMA in the bilayer structure. The conductivity of PPPy, PPTMA and PPPy-PPTMA bilayer composite thin films of nearly same thickness is also calculated to compare the conduction nature of these films and is observed that the conductivity of PPTMA films are higher than that of the PPPy thin films, but the conductivity in PPPy-PPTMA films is found to be lower than those of its component thin films. This result also suggests an increase in the resistivity of the PPPy-PPTMA films during the formation, which might be an effect of inhomogeneous complex interface between the PPPy and PPTMA film in the bilayer structure. This result is consistent with the optical properties of bilayer thin films.

It is seen from this study that both the optical and electrical properties of the PPPy-PPTMA bilayer composite thin films show a clear departure from the ideal bilayer behavior. It is already mentioned that the reports on the plasma polymerized bilayer thin films are less abundant in the literature. Only few reports are available and in all reports it is seen that the conductivity of the bilayer thin films is higher than those of its component thin films, which is discussed in the literature review of this study. Our result, in contrast to the reported results, is different. To explain this result and to compare the experimental results of the bilayer composite thin films with an ideal bilayer structure a model has been developed and two new equations (equation 5.19 and equation 6.44) have been proposed in this study. These equations have provided theoretical explanations of the departure of the experimental results from that of the ideal nature of the bilayer composite structure.

In the study of temperature dependence of current, a trend of decreasing activation energy with decreasing temperature is observed, which indicates a gradual transition to the hopping regime. However, the change in activation energy at higher temperature in comparison to that at lower temperature could be attributed to a considerable temperature-dependence of SCLC mechanism.

The ac electrical properties the ε' of PPPy, PPTMA and PPPy-PPTMA bilayer composite thin films is found to be almost independent of frequency at the low frequency region whereas at the high frequencies the very prominent decrease in ε' with frequency is observed. The decrease of ε' with frequency is attributed to the electrical relaxation processes and multi-component contribution of polarizability of the polar materials; e.g. interfacial or space charge polarization, which is usually observed in sandwich type configurations and orientational polarization of molecular chains which is decreased with increasing frequencies due to the lack of proper response with the field for the attainment of equilibrium. However, the ε', showed a temperature dependence and the rate of variation is found to be different at different frequencies. It is observed that at high frequencies, ε' remains almost constant with increasing temperature, but at low frequencies it increases with increasing temperature. The strong temperature dependence of ε' at higher temperature and lower frequencies is attributed to the electronic polarization and to the thermally activated electron hopping mechanism.

It is observed that the dielectric loss factor ε'' first decreases with rise in frequency in low frequency region followed by a peak in the loss spectra and then increases with the frequency up to a characteristics frequency f_{max} with a sharp peak and after that decreases again. The loss spectra characterized by peak appearing at a characteristic frequency for all the samples suggest the presence of relaxing dipoles in all the samples and the behavior was attributed to structural rearrangement of the molecule, the α-relaxation process, connected with segment motion in polymers

The variation of the ac conductivity σ_{ac} with the frequency has shown a common linear behavior, i.e., an increase of σ_{ac} is observed with increasing frequency. The results are attributed to the relaxations caused by the motion of electrons or atoms, which could involve hopping between equilibrium sites.

In a comparative study of the dielectric properties PPPy, PPTMA and PPPy-PPTMA bilayer composite thin films of nearly same thickness, it is seen that the bilayer thin films have much higher value of ε' compared to those of its component thin films. This result indicates that the bilayer thin films has higher ability to polarize and hold charges than those of its

component thin films, and therefore the bilayer films could be more preferable dielectric for capacitors or for memory cells that store digital data in the form of charge. Moreover, since bilayer film has higher values of ε' but lower values of ε'' at a particular frequency than those of the component films, therefore it is concluded that in the bilayer thin films more energy is stored but rate of energy dissipation is lower than that of its component thin films. It is also observed that the loss peaks of bilayer thin films shift towards the higher frequency, which is an indication of reducing the relaxation time. This behavior might be due to an increase in the amorphous content in the bilayer structure.

The ac conductivity σ_{ac} of the bilayer thin film is found to have lower values than those of its component films over whole frequency range, which is a similar behavior of dc conductivity σ_{dc}. The complex, inhomogeneous and irregular interface between the component thin films, which has been grown during the formation of bilayer thin films by plasma polymerization, might affect the electrical conductivity. Moreover, the disorderness of the interface might cause a decrease in the compactness and molecular orientations leading to a decrease in the resultant conductivity of the bilayer composite thin films.

Finally, it is seen from the summarized findings of the structural, optical and electrical investigations on the bilayer composite thin films that the polymer-polymer complex interface between the component thin films in the bilayer structure played a vital role in determining the physical characteristics of the bilayer composite thin films. This interface may be inhomogeneous and irregular. The probable inhomogeneities, irregularities and disorderness of the interface might have affected the optical band gaps as well as the electrical conductivity of the bilayer composite thin films. Thus these observations are new additions to the present knowledge of the scientists and researchers in this field of research. It could be mentioned that the interpretation about the behavior of the polymer-polymer complex interface is not clearly understood, and therefore there is still a scope to explore the mysterious character of the polymer-polymer complex interface in such composite systems.

8.2 Suggestions for Future work

In this work an attempt is made to investigate the structural, optical and the electrical properties of PPPy, PPTMA and PPPy-PPTMA bilayer composite thin films. It is observed that both the optical and electrical properties are thickness dependent. An intimately arising question from this observation is: how to describe the thickness dependence of these physical processes in thin polymer films? Our result is explained by using existing theories, but the reports on thickness-dependent optical and electrical properties are found to be less abundant in literature. To study the thickness dependence more precisely the FTIR spectra

could be taken and analyzed for the films of different thickness separately to know the probable structural change due to the change of the thickness. The XRD analysis could also be done for each thickness to get information about the chemical structure of the materials. The XPS investigation which provides quantitative information of the element present could be carried on to study the bonding of different functionalities and chemical states in the thin films of different thickness. The SEM analysis could provide information about the morphological change with the change of the thickness. The electron spin resonance (ESR) study may also be carried out to see the nature and source of radicals in this material. All the results of the above analysis could then be correlated with the thickness dependent optical and electrical properties of the thin films of different thickness.

Another important result is found from the study of this work is that the PPPy-PPTMA bilayer composite thin films have higher band gaps and consequently the lower electrical conductivity than that of its component thin films. The results are explained by assuming a complex polymer-polymer interface effect which might be inhomogeneous and irregular by nature. But we did not have precise information about the structural change in the interface of the bilayer composite thin films for the different compositions. To get a very important interpretation about the behavior of the polymer-polymer interface which is almost absent in the literature, the FTIR, XRD, XPS, SEM and ESR analyses could be carried on to explore the change in the structural and elemental properties for each of the composition of the bilayer thin films and then these results could be correlated with the optical and electrical properties of the bilayer thin films in terms of the mysterious polymer-polymer complex interfacial character.